MicroRNA-196a in Human Adipose Tissue

Catriona Hilton

Oriel College

Oxford Centre for Diabetes, Endocrinology and Metabolism
Radcliffe Department of Medicine
University of Oxford

DPhil Thesis

Trinity term 2015

Acknowledgements

Firstly, thank you to the MRC and Novo Nordisk UK Research Foundation who sponsored the work contained in this thesis. I would like to recognise all the participants in the OBB, without whom experiments like these would not have been possible.

I can't imagine a better two supervisors than Matt and Fredrik. I have learnt and grown so during this fellowship and that is in no small part thanks to your mentorship. Thank you for all of your help, support and guidance.

I have been very fortunate to have been based in the OXLIP group in OCDEM for the past 4 years. The group has supported me, challenged me and taught me. Most importantly, I have made some amazing friends. Thank you to Maja and Katherine for being such a joy to share the endless Pt2 differentiation time-courses with, to the nurses downstairs for all their help, and to everyone in the lab that has spent time teaching me techniques and advising me on experiments.

To my parents; this is as much your achievement as mine. Thank you for giving me the opportunities and the self-believe to go out and do what I wanted to in life.

Harry, this DPhil quite genuinely would have been impossible without your unwavering support. The last 4 years has been gruelling, fun, exhausting and exhilarating and I'm so glad that we did it together. Finally to my children, thanks for giving me another reason to be up at 2am apart from writing a thesis. You are without a doubt what makes me proudest from the last 4 years.

Abstract: MicroRNA-196a in human Adipose Tissue.

Catriona Hilton, Oriel College, University of Oxford.

Submitted for degree of Doctor of Philosophy, Trinity 2015.

MicroRNAs are small non-coding RNAs that have been shown to play a role in adipose tissue biology. Adipose tissue depots differ in terms of the metabolic risk that they confer. Therefore, I aimed to identify microRNAs which regulate body fat distribution. An initial microarray screen of abdominal subcutaneous and gluteal adipose tissue, with validatory qPCR, identified microRNA-196a as being more highly expressed in gluteal adipose tissue. These expression patterns were retained in primary and immortalised pre-adipocytes from abdominal subcutaneous and gluteal adipose tissue. The precursor of miR-196a contains a single nucleotide polymorphism, rs11614913. Genotyping was performed on 5,823 individuals from the Oxford Biobank and combined with detailed information on body composition by DXA scanning and miR-196a expression determination in fat biopsies. This revealed that the rs11614913 TT genotype was associated with a 32% reduction in miR-196a expression in abdominal subcutaneous adipose tissue ($p=0.002$), an expansion in waist-to-hip ratio and an increase in mean adipocyte size in abdominal subcutaneous adipose tissue in males. RS11614913 was also found to be associated with bone mineral density, and the relationship between bone mineral density and body fat distribution was explored using the Oxford Biobank. To establish a functional role for miR-196a, the Pt2 abdominal and gluteal cell lines were validated as models for pre-adipocyte proliferation and adipogenesis. MiR-196aKO pre-adipocyte cell lines were generated. MiR-196aKO was found to reduce proliferation in abdominal subcutaneous ($p=0.002$) and gluteal ($p=0.002$) pre-adipocytes, with no effect in adipogenesis. In addition, transcriptomic profiling of miR-196aKO pre-adipocytes revealed enrichment for GO term clusters related to extracellular matrix and angiogenesis, suggesting a mechanism by which miR-196a might regulate regional adipose tissue expansion.

Declaration

The work presented in this thesis is the original work of the author. Experiments were carried out at the Oxford Centre for Diabetes Endocrinology and Metabolism, University of Oxford, under the supervision of Dr Fredrik Karpe and Dr Matt Neville. The work was funded by a MRC and Novo Nordisk UK Research Foundation Clinical Fellowship.

Where data has been generated as part of a collaboration this is stated in the chapter. Sections of the text in this thesis have been previously published (Biochim Biophys Acta. 2015;1851(5):686-696 and Int J Obes. 2013;37(3):325-32). The text is the original work of the author and permission for reproduction was granted by the journals.

I hereby state that no part of this thesis has been submitted for any other degree at this or any other university.

This thesis is approximately 45,000 words.

Abbreviations

ASAT	Abdominal subcutaneous adipose tissue
AT	Adipose tissue
ASO	Antisense-oligonucleotide
BMI	Body mass index
BMD	Bone mineral density
BAT	Brown adipose tissue
cDNA	Complementary DNA
CRP	C-reactive protein
DXA	Dual-energy x-ray absorptiometry
DMEM	Dulbecco's eagle's medium nutrient mixture
eQTL	Expression quantitative trait loci
ECM	Extracellular matrix
FGF	Fibroblast growth factor
FCS	Foetal calf serum
GO term	Gene ontology term
GWAS	Genome-wide association study
GSAT	Gluteal subcutaneous adipose tissue
HBSS	Hank's buffered salt solution
HDL	High density lipoprotein
HOX	Homeobox gene family
HOMA-IR	Homeostatic model assessment of insulin resistance
hASC	Human adipose-derived stem cells
HEK293	Human embryonic kidney 293 cell line
hTERT	Human telomerase reverse transcriptase
Pt2 Abdo	Immortalised cell line derived from abdominal subcutaneous preadipocytes
Pt2 AbdoCon	Immortalised cell line derived from abdominal subcutaneous preadipocytes and stably expressing control vector
Pt2 Abdo miR-196aKO	Immortalised cell line derived from abdominal subcutaneous preadipocytes and stably expressing mir-196a inhibitor
Pt2 Glut	Immortalised cell line derived from gluteal preadipocytes
Pt2 GlutCon	Immortalised cell line derived from gluteal subcutaneous preadipocytes and stably expressing control vector
Pt2 Glut miR-196aKO	Immortalised cell line derived from gluteal subcutaneous preadipocytes and stably expressing mir-196a inhibitor
LD	Linkage disequilibrium
LDL	Low density lipoprotein
miRNA/miR-	Mature microRNA
mESC	Mesenchymal embryonic stem cells
MSCs	Mesenchymal stem cells
MHO panel	Metabolically healthy obese panel
OBB	Oxford Biobank
PBS	Phosphate buffered saline

pre-miRNA/pre-miR	Precursor microRNA
pri-miRNA/pri-miR	Primary microRNA
qPCR	Quantitative polymerase chain reaction
RT	Reverse transcription
RISC	RNA-induced silencing complex
SNP	Single nucleotide polymorphism
SD	Standard deviation
SEM	Standard error of the mean
SVF	Stromal vascular fraction
SAT	Subcutaneous adipose tissue
T2DM	Type 2 diabetes mellitus
TLR4	Toll-like receptor 4
TAG	Triacylglycerol
T3	Triiodo-L-thyronine
WHR	Waist-to-hip ratio
WAT	White adipose tissue

Publications, abstracts and prizes arising from this thesis

PUBLICATIONS

Hilton, C, Karpe, F, Pinnick, KE. Role of developmental transcription factors in white, brown and beige adipose tissues. Biochim Biophys Acta. 2015;1851(5):686-696.

Hilton C, Karpe F. Circulating MicroRNAs: What Is Their Relevance? Clin Chem 2013;59(5):729-31.

Hilton C, Neville MJ, Karpe F. MicroRNAs in adipose tissue: their role in adipogenesis and obesity. Int J Obes. 2012.

MANUSCRIPTS IN PREPARATION

'MicroRNA-196a regulates human body fat distribution'.

'The Pt2 cell lines: novel paired pre-adipocyte cell lines from abdominal subcutaneous and gluteal adipose tissue'.

'A common polymorphism rs11614913 in pre-miR-196a-2 is associated with bone mineral density'.

'Human body fat distribution shows sexual dimorphism in its association with bone mineral density'.

PRESENTATIONS

Podcast recording for Clinical Chemistry Journal: "Circulating microRNAs; what is their relevance?" (May 2013)

Catriona Hilton, Matt Neville, Katherine E Pinnick, Katherine Mackay, Fredrik Karpe. MicroRNA-196a is a candidate for regulation of body- fat distribution in human beings. *Poster presentation at Academy of Medical Sciences Spring Meeting, 2013. Abstract published in the Lancet.*

Catriona Hilton, Matt Neville, Katherine Pinnick, Katherine Mackay, Fredrik Karpe. MicroRNA-196a is a potential regulator of body fat distribution in humans. *Poster presentation at EASD, Barcelona, September 2013.*

Catriona Hilton, Matt Neville, Katherine Pinnick, Katherine Mackay, Fredrik Karpe. MicroRNA-196a as a potential regulator of Homeobox (HOX) gene expression in human adipose tissue. *Poster presentation at the Adipose Tissue Discussion Group Annual Meeting, Bath, 2012.*

Neville MJ, **Hilton C**, Karpe F. The role of microRNA 146b in human adipose tissue in modulating inflammation. *Poster presentation at the Adipose Tissue Discussion Group Annual Meeting, Cambridge, 2011.*

PRIZES

2013 Runner up in Elsevier/OCDEM Young Clinician Scientist Competition

Table of contents

Table of figures

Table of tables

1 Introduction

Obesity and its associated metabolic disease represent an escalating public health burden [1]. At present many individuals remain refractory to weight loss by diet and exercise and existing pharmacological interventions. The obese transition leads to a deviation away from the main function of adipose tissue (AT); that of effective and appropriately controlled fat storage and release, and AT dysfunction in obesity predisposes to the metabolic consequences of obesity, such as insulin resistance, diabetes and cardiovascular disease. A greater understanding of the molecular mechanisms underlying AT function and dysfunction will be required if we are to identify novel therapeutic targets.

1.1 Adipose tissue structure and function

AT is a heterogeneous multi-depot organ comprising the energy-storing white AT (WAT) and the thermogenic brown AT (BAT) [2]. In addition, a third class of adipocyte can be found within certain WAT depots, the so called “brite” or “beige” adipocytes, which appear functionally similar to classical brown adipocytes [3, 4].

1.1.1 White adipose tissue

The major WAT depots in humans are located intra-abdominally (omental, mesenteric and perirenal; jointly referred to as visceral) and subcutaneously (abdominal, gluteal and femoral). Smaller WAT depots are found throughout the human body including in the pericardial region, the retro-orbital space, within the bone marrow and on the face [5, 6]. The predominant function of WAT is energy storage and release, but WAT is also now recognised as an important metabolic and endocrine organ that releases adipokines and cytokines [7]. WAT is composed mainly of white adipocytes that accumulate lipid in a large unilocular droplet [6], but also found within WAT are other cell types such as pre-

adipocytes and mesenchymal stem cells [8] (MSCs) and immune cells including macrophages [9], neutrophils [10] and lymphocytes [11, 12].

1.1.2 Brown adipose tissue

BAT is a thermogenic organ important for non-shivering temperature maintenance in infants and also present and metabolically active in adults [13]. BAT is mostly located in the neck and supraclavicular regions of adult humans [14]. Adipocytes found in the well demarcated BAT depots are characterised by multilocular lipid droplets, high UCP1 expression and the presence of numerous mitochondria, consistent with the thermogenic properties of these tissues [13, 15]. In adults BAT mass is inversely associated with BMI [16, 17], fasting plasma glucose [18] and type 2 diabetes status [17]. BAT induction occurs in humans in response to exposure to cold [19, 20] and is associated with increased energy expenditure and a reduction in overall body fat [20], suggesting that BAT recruitment may pose an important anti-obesity target.

1.1.3 Beige adipocytes

'Browning' is the process by which clusters of beige adipocytes emerge within certain WAT depots [21]. This is inducible by various stimuli including prolonged cold exposure and beta-adrenergic agonists. Beige adipocytes, in common with brown adipocytes, are UCP1 positive thermogenic cells with multilocular lipid droplets [22]. Despite sharing common properties it remains unclear whether beige adipocytes perform the same role as brown adipocytes [23] and whether there are sufficient numbers of beige adipocytes to influence metabolic health. There is some preliminary evidence to suggest that this may be the case, at least in mice [24, 25]. Whilst in rodents BAT is a well-defined entity that is clearly

distinct from WAT and beige fat it has been suggested that BAT depots in adult humans are comprised primarily of beige adipocytes [22, 26].

1.2 Summary of the different white adipose tissue depots

1.2.1 Embryological origin

The various WAT depots are heterogeneous in terms of their developmental origins [27]. With the exception of facial AT, which derives from the ectoderm [28], AT is generally considered to derive from the mesoderm, with different anatomical regions thought to give rise to localised depots [29]. Lineage tracing studies in mice have recently lent support to this view, demonstrating that visceral WAT develops from Wilms' tumour gene (Wt1)-expressing cells found specifically in the lateral plate mesoderm. By comparison, Wt1-expressing cells make no contribution to subcutaneous WAT leaving the exact embryological origins of this depot unknown [30]. Furthermore, there is heterogeneity amongst individual visceral depots with regards to the contribution of Wt1 cells, demonstrating the complexity of AT as a multi-depot organ.

Several groups have investigated the mRNA expression profiles of different AT depots using genome-wide transcriptomic approaches. These studies have consistently noted distinct transcriptional signatures, not only between BAT and WAT [31-33], but also between separate WAT depots (visceral, abdominal subcutaneous AT, gluteal) [34-40]. Interestingly, many of the genes identified are known to play a role in embryological development and body patterning. The role of developmental and body patterning genes in AT formation and function is discussed in more detail in 4.1.4.

1.2.2 Anatomy and histology

Although white adipocytes from different anatomical regions may appear superficially similar, upon closer inspection depot-specific differences can be observed relating to their histological arrangement [6, 41]. There are differences in adipocyte size between AT depots, for example visceral adipose tissue (VAT) adipocytes are often reported to be smaller than subcutaneous adipocytes [42-44] although not all findings are in agreement which likely reflects differences in techniques and participants [45, 46]. Subcutaneous WAT depots are also structurally diverse. In general, abdominal subcutaneous adipose tissue (ASAT) is characterised by larger adipocytes, a limited network of blood vessel and a scant and poorly developed collagenic network [47]. Gluteal subcutaneous adipose tissue (GSAT) is generally composed of smaller adipocytes, has more developed stromal tissue and is well vascularised [47]. The ASAT depot is further divided by Scarpa's fascia into the deep subcutaneous and superficial subcutaneous AT layers [48, 49]. Histologically, the deep subcutaneous AT layer contains a larger proportion of small adipocytes [49], higher expression of inflammatory genes and increased macrophage infiltration [50].

1.2.3 Functional properties

Both *in vivo* and *in vitro* studies have shown that WAT depots display functional differences in terms of fatty acid handling, adipokine production and capacity for pre-adipocyte proliferation and adipogenesis.

The expression and secretion of a number of adipokines differs between VAT and subcutaneous AT (SAT). For example, adiponectin, which exerts insulin-sensitizing actions [51], is expressed at significantly lower levels in VAT compared to SAT in humans [52], whereas the pro-inflammatory cytokine, interleukin-6, is secreted at higher levels from adipocytes from the visceral depot compared to those from the subcutaneous depot [53].

The adipokine secretory profiles of GSAT and ASAT also differ. Using *in vivo* arterio-venous sampling to measure adipokine release from gluteofemoral AT our group has shown that lower-body AT displays a more "protective" adipokine secretory profile releasing higher amounts of insulin-sensitising palmitoleate (16:1n-7) and lower amounts of the pro-inflammatory cytokine interleukin-6 [40, 54].

Lipolysis is greater in upper body than in GSAT *in vivo* [55-57] and *in vitro* [58], with VAT having greater lipolytic activity than SAT [59]. Conversely, uptake of meal-derived fatty acids occurs more readily in upper-body fat compared with lower-body fat [60]. Furthermore, the fatty acid compositions of upper and lower fat differ [54, 61] with lower body fat containing a lower proportion of saturated fatty acids. Overall, it would seem that the upper-body depots play a more active role in the storage and mobilisation of diet-derived lipids whilst lower-body depots turnover more slowly and provide stable long-term fat storage [62, 63]. In line with this, GSAT has lower blood flow when compared with ASAT *in vivo* [56, 57].

GSAT mass is independently inversely correlated with insulin [64] and *in vitro* studies have demonstrated that differentiated pre-adipocytes derived from GSAT are more insulin sensitive than those derived from ASAT [65, 66].

AT expansion can occur by hypertrophy of existing adipocytes or recruitment and differentiation of precursors (hyperplasia). Pre-adipocytes isolated from the visceral compartment are less functional than those isolated from ASAT and have a lower capacity for proliferation and differentiation [67, 68]. It has been suggested that in response to overfeeding ASAT expands by hypertrophy whilst GSAT expands by hyperplasia [69] although in individuals from a range of different BMI groups ASAT and GSAT adipocytes were observed to be of similar size [70]. *In vitro,* pre-adipocytes isolated from GSAT are

confirmed to have higher rates of replication than those from ASAT [54]. Upper body fat stores are mobilised more readily than lower body stores during weight loss [55].

1.2.4 The relationship between fat distribution and metabolic health

Obesity is an important risk factor for a myriad of health problems including type 2 diabetes, cardiovascular disease and certain cancers [71]. However, approximately 10-30% of obese individuals do not exhibit the typical features of obesity-associated metabolic disease such as insulin resistance, hypertension and dyslipidaemia [72]. This subgroup has been labelled the "metabolically healthy obese" and would seem to imply that it is not the absolute amount of AT that determines metabolic health. Furthermore, not all fat depots confer equal metabolic risk. Indeed, waist-to-hip ratio (WHR), as a proxy measure of body fat distribution, is a better indicator of myocardial infarction risk than body mass index (BMI) [73]. Polycystic ovary syndrome is associated with an android body fat distribution [74, 75] and a reduction in gluteofemoral AT mass [76]. WHR has been postulated to be more closely linked with ASAT mass than VAT mass, a relationship that strengthens with increasing BMI [77]. Both ASAT mass and VAT mass correlate positively with fasting insulin [78] and the so-called metabolic syndrome [77, 79], with VAT having a stronger association. Indeed, the relative proportion of VAT to SAT is a predictor of metabolic risk independent of both overall adiposity and VAT mass [80], although a causative relationship between VAT and metabolic health has not been proven [81].

Importantly, the associations between metabolic risk and upper- or lower-body adiposity differ not just in terms of the strength of association but also in directionality. For this reason it is proposed that the GSAT depot exerts a protective effect, which may reflect the distinct underlying traits of these depots [82, 83]. There are also differences between abdominal deep and superficial SAT with the depth of the deep layer correlating with

insulin resistance and cardiovascular risk [49]. Ectopic deposition of fat (pericardial, hepatic and inter-muscular) is also associated with increased cardio-metabolic risk, although because of the close relationship between VAT and ectopic fat deposition it becomes difficult to dissect the individual contribution of these fat depots [84].

1.2.5 Factors influencing adipose tissue distribution

The genetic predisposition to body shape is relatively strong, with heritability estimates for waist-to-hip ratio falling in the range of 40% -70% [85, 86]. Despite this the precise genetic mechanisms determining body fat distribution remain poorly understood. The study of rare monogenic forms of partial lipodystrophy have identified a limited set of genes which, when perturbed, result in the selective loss of certain WAT depots (*CIDEC, PLIN1, AKT2, PPARG, LMNA*) [87]. These genes all appear to play important roles in adipocyte function [88], although it is sometimes unclear how they exert a regional phenotype. In addition, over 20 genetic loci have now been associated with body fat distribution through genome-wide association studies (GWAS) using anthropometric measures or computed tomography [89, 90]. Perhaps rather disappointingly these loci explain only a small proportion of the variation in body fat distribution (less than 5%) and, since most are located outside exonic regions, it remains an ongoing challenge to identify the causative genes and to understand their biological relevance. Common polymorphisms associated with body fat distribution have also been identified using a candidate approach to screen genes with known mechanistic roles in adipocyte biology. Polymorphisms have been identified in genes relating to catecholamine action (the adrenergic receptors) [91] and adipogenesis (*PPARG*) [92] and also in genes involved in steroid hormone metabolism and action such as *NR3C1* (the glucocorticoid receptor) [93] and *ESR1* (the oestrogen receptor a) [94]. Overall our understanding of the genetic causes

of AT distribution is limited and it would seem likely that there are further genetic determinants of body fat distribution which remain to be uncovered.

There are also other mediators that can influence body fat distribution. The powerful effects steroid hormones exert on fat distribution have been widely reported [95]. Body shape exhibits striking sexual dimorphism. In general, men have less total body fat than women of the same BMI, whilst being more prone to upper-body fat deposition [96]. Furthermore, sex hormones have been shown to directly alter body composition and fat distribution in prospective measurements of transsexuals receiving hormone treatment [97]. The contribution that glucocorticoids make to body fat distribution is evident in individuals exhibiting the clinical condition of Cushing's syndrome in which elevated cortisol levels are accompanied by increased central adiposity and a diminution of peripheral AT depots [98]. Changes in body fat distribution are also associated with the ageing process. Typically, an increase in total adiposity is apparent, with a specific increase in VAT but a relative loss of SAT, particularly in the gluteofemoral depot [99]. Notably in females an increase in visceral adiposity is associated with post-menopausal oestrogen deficiency [100]. Body fat distribution can also be influenced by environmental factors, for example, by drugs such as antiretroviral therapies [101].

1.3 Isolated pre-adipocytes retain 'memory' of their depot of origin

Growing evidence suggests the functional characteristics of various fat depots are determined by intrinsic mechanisms rather than simply being a function of their anatomical locations. Although WAT depots found in rodents are not directly comparable to those found in humans, studies in rodents have shed some light on WAT depot-specific properties. For instance, the transplantation of SAT into the visceral compartment of mice leads to improved insulin sensitivity, glucose tolerance and adiposity. By comparison, the

transplantation of VAT is without effect suggesting that the metabolic improvements exerted by SAT are the result of intrinsic properties of this tissue [102, 103]. Depot-specific differences in WAT adipocyte function are often maintained when cells are removed from their native tissues and cultured *in vitro* [67], suggesting that depot-specific features are determined by intrinsic mechanisms rather than the influence of the local milieu. At the cellular level, pre-adipocytes isolated from their native WAT depots retain many of the functional features of that depot *in vitro* including depot-specific lipolytic activity [104], adipokine secretion [104, 105] and fatty acid handling [54, 106]. Regional differences are also apparent in the propensities of pre-adipocytes to undergo apoptosis [107], proliferation and adipogenesis, both in humans [36, 68] and in rodents [38].

The depot-of-origin memory exhibited by pre-adipocytes is consistent with the view that different AT depots comprise of distinct pre-adipocyte subpopulations. Uncovering what might be responsible for determining the intrinsic differences between regional pre-adipocytes will be an important step in understanding the mechanisms by which the different fat depots contribute to metabolic risk. Ultimately this knowledge will be vital to developing new therapeutic strategies for targeting AT dysfunction.

1.4 MicroRNAs

1.4.1 Overview

MicroRNAs (miRNAs) are a group of small (approximately 22 nucleotide) non-coding RNAs that have emerged as important regulators of mRNA expression. MiRNAs are predicted to act on multiple targets [108] and quantitatively alter the expression of their target genes and proteins. MiRNAs therefore represent promising targets for modulating complex

pathways, and indeed the correct expression and function of miRNAs is known to be vital to a variety of biological processes and disease states [109, 110].

In 2005 it became possible to manipulate miRNAs in vivo by the injection of 'antagomirs' into the peripheral blood [111]. More technologies have emerged that potently antagonise miRNAs *in vivo* [112] and cause effective restoration of miRNA expression [113]. Clinical trials of miRNA manipulation in humans are now underway [113].

1.4.2 MiRNA structure, synthesis and action

MiRNAs are found in all multicellular organisms from plants to humans. In many instances they are highly conserved through evolution and therefore likely to be important for normal cellular function. Indeed, completely disrupting miRNA processing is lethal [114].

MiRNA biogenesis has been well reviewed elsewhere [115, 116]. Briefly, a primary miRNA (pri-miRNA), which may be several thousands of bases long, is cleaved by a protein complex containing the enzyme Drosha to give a precursor miRNA (pre-miRNA) of around 70 nucleotides in a stem-loop structure [117]. This is then transported out of the nucleus into the cytoplasm and further processed by the enzyme Dicer to give a short double stranded miRNA complex, which contains the mature miRNA strand and a passenger strand which is normally degraded, but which can be functional [118]. Traditionally it was thought that the -5p miRNA is functional within the cell, whilst the -3p miRNA is degraded (also referred to as the miR* strand in older nomenclature), but more recent studies have shown that this balance varies depending on the miRNA and the cell type [119]. The mature miRNA is incorporated with the Argonaute sub-family of proteins into the RNA-induced silencing complex (RISC). The miRNA then guides the RISC complex to a target mRNA, often by virtue of complementarity between the miRNA seed sequence and the 3'UTR of the target mRNA, although functional miRNA targeting can occur in other areas

of the mRNA [120, 121]. Base pairing between the miRNA and its target is often imperfect causing repression of translation to protein, although highly complementary pairing may cause cleavage of the target mRNA. Translational activation by miRNAs has also been described [122].

MiRNAs are likely to predominantly be fine tuners of gene expression [123, 124], but there is some evidence that on reaching a critical threshold they may highly repress protein production and in so doing act as 'off switches' [125] and that in other cases they may act as a safeguard against excessive mRNA expression [126]. Each miRNA may fine tune the expression of hundreds or even thousands of proteins [123, 127], and it is estimated that over 60% of mammalian mRNAs encode conserved targets of miRNAs [108]. Additionally, each mRNA may be targeted by many miRNAs [108]. This system therefore has potentially enormous regulatory capacity, but also possesses a complexity that can make it difficult to untangle.

1.4.3 The role of microRNAs in adipose tissue function

Support for an integral role of miRNA in AT formation and function has come from studies demonstrating that inhibition of Drosha and Dicer in MSCs inhibited differentiation into adipocytes [128] and that inhibition of Drosha in the murine 3T3-L1 cell line inhibited adipogenesis [129]. Mice engineered to have loss of Dicer in post-differentiation adipocytes have severely depleted WAT with reduced lipogenesis and adipogenesis associated transcripts and were also noted to have normal brown adipose tissue but with reduced expression of genes involved in thermoregulation [130]. It should be noted, however, that disrupting Drosha and Dicer is a non-specific model that will have a global impact on miRNA expression.

In vivo studies of miRNAs in drosophila have shown that animals with miR-14 deleted have increased levels of triacylglycerol and diacylglycerol, with the converse effect being observed with increased miR-14 [131]. MiR-278 null drosophila have higher circulating insulin and glucose and are lean [132] and drosophila with miR-8 knocked out have smaller body size and defective insulin signalling in the fat compartment (drosophila do not have a liver; their fat compartment is the equivalent of human WAT and liver) [133]. Although these miRNAs do not have human homologues these studies lend support to the importance of miRNA within fat. Since their discovery miRNAs have attracted considerable interest and the volume of research into them is growing exponentially. Numerous studies examining miRNA expression and the effect of miRNA modulation *in vivo* and *in vitro* have demonstrated active roles for miRNAs in AT biology (see Table 1.1). MicroRNA signatures, both locally within AT [134] and circulating in blood and exosomes [135] have been associated with complications of obesity in the form of the 'metabolic syndrome'.

MiRNAs represent an elegant network of regulation, both fine-tuning and dramatically altering the expression of genes involved in adipose tissue formation and function. MiRNA profiling has revealed changing miRNA expression in adipose tissue and functional studies have attributed roles to some of these miRNAs within adipogenesis, insulin resistance and inflammation.

1.4.1 MicroRNAs and adipose tissue distribution

To date a number of descriptive studies have used genome wide miRNA profiling to investigate miRNA expression patterns within human WAT (Table 1.2). I have concentrated here on studies conducted in humans rather than in rodents. Whilst rodent models can be invaluable for elucidating the function of miRNAs *in vivo,* rodent AT depots cannot be considered analogous to our own and so findings relating to fat distribution are

unlikely to be directly translatable to humans. Despite significant overlap between the murine and human genomes [136] a recent study found that mRNA expression profiles were significant divergence between the two species and that this was more pronounced for non-coding transcripts [137]. This is in line with my own review of the literature where I have found several miRNAs to have opposite expression profiles or functional effects reported in murine and human AT (Table 1.1).

Several authors have observed associations between body fat distribution and the expression of miRNAs within WAT [138, 139] and circulating blood [140, 141] but to date a causal role for miRNAs in AT distribution has not been demonstrated.

1.5 Summary

Human AT is a complex organ with functions extending far beyond energy storage. The various regional AT depots are heterogeneous in terms of their form, function and relationship with metabolic phenotype. Indeed, AT distribution is an independent risk factor for metabolic disease, with upper and lower body AT displaying opposite relationships with cardiovascular and diabetes risk. Gaining a greater understanding of the molecular mechanisms that underlie regional AT function will be key to developing new therapeutic targets with which to counteract the growing health burden of obesity-related disease. MiRNAs are non-coding RNAs which form an elegant network of transcriptional regulation and which are known to have key roles in adipocyte biology. As such they represent promising candidates for modulating adipose tissue function. Although exciting data are emerging implicating numerous miRNA in AT form and function to date little is known about their role in human AT distribution.

Table 1.1: miRNAs identified as differentially regulated in white adipose tissue and in adipogenesis and their functional characterisation.

miRNA	Expression in adipose tissue	Expression during adipogenesis	Functional work
let-7c	↑in obesity in humans [142]	↑in murine [143, 144] and human [145] adipogenesis	Inhibits clonal expansion and differentiation [143]
miR-103	↓in obesity in mice [146]	↑in murine adipogenesis [143, 146, 147] ↓in murine adipogenesis [144] No change in human adipogenesis [142, 148]	Enhances murine adipogenesis [146] Silencing improves insulin sensitivity in mice [149]
miR-125a	↑in rat model of Type 2 diabetes [150] ↑in obesity in humans [151]	↑in adipogenesis of human bone marrow derived multipotent cells [128] ↑in porcine adipogenesis [152]	Inhibits porcine adipogenesis [152]
miR-125b	↓in murine obesity [146] ↓in human obesity [142]	↓in murine adipogenesis [146]	
miR-132	↑in human omental fat in obesity [141]	↑in murine adipogenesis [153]	Inhibits murine pre-adipocyte clonal expansion and adipogenesis [153]
miR-135a		↓in murine adipogenesis [154]	Inhibits murine adipogenesis [154]
miR-138		↓human adipogenesis [155]	Inhibits differentiation in hASCs [155]
miR-139-5p		↑in human adipogenesis [156]	Inhibits clonal expansion and differentiation [156]
miR-143	↓ in obesity in humans [157, 158] ↓[146]↑[159] in obesity in mice	↑in human adipogenesis [145] ↑in murine adipogenesis [143, 144, 146, 157]	Enhances differentiation [145, 146]
miR-145		↑in porcine adipogenesis [160]	Inhibits porcine adipogenesis [160] Inhibits lipolysis [161]
miR-146b	↑in ASAT and VAT in human obesity [162] ↑in obesity in mice [163]	↑murine adipogenesis [146, 164] ↑human adipogenesis [162]	Inhibits proliferation and enhances adipogenesis of visceral pre-adipocytes [162] Enhances murine adipogenesis [164]
miR-148a	↓in obesity in mice [146] ↑in human obesity [165]	↑in murine [146] and human [165] adipogenesis	Enhances adipogenesis [165]
miR-15a		↑in murine adipogenesis [144]	Overexpression decreases number but increases size of murine adipocytes [166]
miR-17-92 cluster	↑in human omental fat in obesity (miR-17-p) [141]	↑in murine adipogenesis [129]	Enhances adipogenesis [129]
miR-193		↑in murine adipogenesis [143]	Increases adiponectin production from WAT [167]

miRNA	Expression in adipose tissue	Expression during adipogenesis	Functional work
miR-195a		↓in murine adipogenesis [168]	Inhibits adipogenesis [168]
miR-21	↑in obesity in humans [157] ↑in obesity in mice [163]	↑ (murine) [146] ↑in early differentiation of hASCs [169]	Inhibits proliferation of hASCs [170] Enhances adipogenesis [169]
miR-204		↑in human adipogenesis [171]	Enhances adipogenesis [171]
miR-210		↓(human) [142] ↑in murine adipogenesis [143]	Promotes adipogenesis [172]
miR-221	↑in obesity in mice [146] ↑in obesity in humans [173]	↓(human)[142] ↓in murine adipogenesis [146]	
miR-222	↑in obesity in mice [146, 163] ↑in rat model of Type 2 diabetes [174] ↑in VAT in gestational diabetes [175]	↓in murine adipogenesis [146]	Inhibits insulin-stimulated glucose uptake in 3T3-L1 cells [175]
miR-26	↓ in VAT in obesity in mice and humans [176]	↑in human adipogenesis [177]	Enhances human adipogenesis [177] Enhances insulin mediated glucose uptake [176]
miR-27	↑in obesity in mice [178] ↓ in obesity in mice [179] ↑in rat model of Type 2 diabetes [174]	↓in murine adipogenesis [178, 179] ↓in adipogenesis of hASCs [180]	Inhibits adipogenesis [178-181] Inhibits mitochondrial biogenesis [181]
miR-29	↑in mouse model of type 2 diabetes [150, 182]		Transfection leads to insulin resistance[182]
miR-30a-e	↓in obesity in mice [146, 163]	↑in human [142, 183] and murine [146] adipogenesis	Enhances adipogenesis [183, 184]
miR-320		↑in insulin resistant murine adipocytes [185]	Improves insulin sensitivity [185]
miR-335	↑in obesity in mice [186]	↑in murine adipogenesis [186]	
miR-378	↑in obesity in mice [187]	↑in human adipogenesis [142, 183] ↑in murine adipogenesis [187]	Enhances lipid accumulation in adipocytes [147, 187, 188] Overexpression increases catecholamine driven lipolysis [189] Inhibits adiponectin release [190]
miR-422	↓in murine obesity [146]	↑in murine adipogenesis [146]	
miR-519d	↑in human obesity [191]		Enhances adipogenesis [191]

Abbreviations: hASCs=human adipose-derived stem cells.

Table 1.2: Published studies investigating genome wide miRNA profiles of human white adipose tissue.

Year	Study	Conditions	Population	Methodology	Main findings
2009	Kloting *et al.*[192]	Paired omental AT and ASAT biopsies	n=15 obese and overweight subjects (M=8, F=7; T2DM=6, NGT=9)	Screening for 155 miRNAs using qPCR	Identified several miRNAs with expression associated with depot, T2DM or correlated with anthropometric variables or histology. Results did not stand up to correction for multiple testing.
2010	Ortego *et al.*[142]	ASAT biopsies	n=28 (F=28. lean=6, obese with T2DM=9, obese without T2DM=13).	Microarray with validatory qPCR	11 miRNA were differently expressed with obesity, 1 miRNA was differently expressed with T2DM. Also produced miRNA expression data from lean and obese cell lines through adipogenesis.
2010	Martinelli *et al.*[191]	ASAT biopsies	n=28 (morbidly obese=20, non-obese=8. M=13, F=15).	Microarray. Expression of 3 miRNAs validated by qPCR.	Expression of 42 miRNAs was different between obese and non-obese ASAT biopsies. Expression of 6 miRNAs was related to sex.
2011	Heneghan *et al.*[141]	Paired omental AT and ASAT biopsies	n=5 (3=morbidly obese, 2=lean). Replicated in n=29 (19=morbidly obese, 10=lean).	Microarray in n=5. qPCR in replication study.	In n=5 there was a low correlation between miRNA expression in ASAT and omental AT. No miRNAs were different with obesity in ASAT, 5 miRNAs changed with obesity in omental AT. Two of these were replicated in n=29.
2011	Rantalainen *et al.*[134]	Paired ASAT and GSAT biopsies	n=70 (M=40, F=30. Healthy control = 41, metabolic syndrome = 29). Replicated in n=40 (M=20, F=20. Healthy controls = 28, metabolic syndrome = 12).	Microarray	136 miRNAs were differently expressed between ASAT and GSAT; 59 of these were also different in the replication study. 14 miRNAs in ASAT were associated with metabolic syndrome; 3 replicated. Correlated miRNA expression with genotyping data and mRNA expression data.
2012	Parts *et al.*[138]	ASAT biopsies	n=131 females from TWINS UK cohort	Next generation sequencing	Identified miRNAs that correlated with anthropometric and metabolic traits. Correlated miRNA expression with genotyping data and mRNA expression data.
2013	Civelek *et al.*[139]	ASAT biopsies	n=200 men characterised for metabolic traits	Next generation sequencing	Identified 24 miRNAs with expression correlating with anthropometric and metabolic traits. Correlated miRNA expression with genotyping data and mRNA expression data.
2013	Meerson *et al.*[173]	ASAT biopsies	n=29. Replicated in n=80.	Microarray with qPCR validation in separate cohort of n=80.	Expression of three miRNAs was associated with obesity.

Abbreviations: AT=adipose tissue. VAT=visceral adipose tissue. ASAT=abdominal subcutaneous adipose tissue. GSAT=gluteal subcutaneous adipose tissue. N=number. M=male. F=female. T2DM=type 2 diabetes mellitus.

1.6 Aims of thesis

In this thesis I hypothesise that miRNAs have a regulatory role in human WAT distribution and in determining depot-specific function.

The overall aim of this thesis is to describe miRNA expression in human ASAT and GSAT and to understand their potential role in fat distribution and determining the different properties of the tissues. Specifically;

- I aim to describe miRNA expression patterns in human ASAT and GSAT according to gender, obesity and AT depot (Chapter 3).
- Having identified miR-196a as being strongly differentially expressed between ASAT and GSAT, I aim to characterise its expression pattern within human WAT and through pre-adipocyte differentiation *in vitro* (Chapter 4).
- To determine the expression of putative *HOX* gene targets of miR-196a in AT in relation to miR-196a expression, in order to investigate whether it might be acting through their regulation.
- The precursor of miR-196a contains a SNP, rs11614913. I aim to use this as a genomic tool to dissect miR-196a function *in vivo* by genotyping cohorts of individuals and then determining miR-196a expression in ASAT and GSAT, body fat distribution by detailed DXA scanning and adipocyte size (Chapter 5).
- In light of the common mesenchymal origins of AT and bone and the literature relating miR-196a to bone metabolism, I aim to identify a role for miR-196a in determining bone mineral density (BMD) through rs11614913 genotyping (Chapter 6).

- To further understand the relationship between miR-196a and BMD I perform a detailed analysis of the associations between body fat distribution and BMD in the OBB cohort (Chapter 6).
- I aim to characterise the Pt2 abdominal subcutaneous and gluteal immortalised pre-adipocyte cell lines and determine their appropriateness for functional experiments (Chapter 7).
- I aim to use miR-196a inhibition to determine the effect of miR-196a on pre-adipocyte phenotype by investigating pre-adipocyte proliferation, adipogenesis and transcriptomic profile (Chapter 7).

2 Overview of methods

2.1 Subject cohorts and tissue panels

2.1.1 Oxford Biobank (OBB)

The Oxford Biobank (OBB) is a cohort of more than 7,500 population-based men and women aged between 30 and 50 who live in Oxfordshire. Individuals with T2DM, cardiovascular disease or any other significant chronic illness and pregnant women are excluded. All of the volunteers in the OBB have undergone a comprehensive anthropomorphic and metabolic characterisation. Height, weight, waist, hip, blood pressure and skinfold measurements are available for all subjects and detailed dual-energy X-ray absorptiometry (DXA) scans are currently available for more than 4,000 individuals. All subjects have had fasting blood samples taken for measurement of insulin, glucose, C-reactive protein (CRP), cholesterol, triglycerides (TAG) and non-esterified fatty acids (NEFA) concentrations. DNA is extracted from whole blood and all volunteers are consented for subsequent genotyping. This includes custom genotyping as required in addition to Illumina Infinium Exome chip data (www.illumina.com) on 5,500 volunteers. In addition, paired whole fat biopsies from ASAT and GSAT are available for a subset of individuals (n=220). The combination of detailed characterisation of subjects and genotyping information allows for recruitment according to phenotype or by genotype for further studies. Ethical approval was granted by Oxfordshire Clinical Research Ethics Committee (08/H0606/107) and all study participants have given written informed consent.

Whole-body DXA scans were performed using a Lunar iDXA (GE Healthcare) and images were processed using enCORE v14.1 software (GE Healthcare). Details about how the various AT and bone compartments were defined are given in 5.2.2. Plasma glucose, CRP, TAG and HDL

concentrations were measured enzymatically using commercially available kits on an ILab 650 clinical analyzer (Instrumentation Laboratory, UK). Plasma insulin concentrations were measured by radioimmunoassay (Millipore UK Ltd.) and insulin resistance was calculated using the homeostatic model assessment of insulin resistance (HOMA-IR) [193]. AT biopsies were taken under local anaesthesia (1% lignocaine) using a 12-gauge needle aspiration technique under aseptic conditions. Biopsies were washed in 0.9% saline solution and homogenized with Tri-Reagent (Invitrogen, UK) in an automated homogeniser (Retsch-MM301, Retsch, Germany) prior to storage in a -80 freezer for analysis at a later date.

Phenotypic characteristics of subsets of the OBB used for analysis in this thesis are described in the relevant chapters.

2.1.2 Paired omental AT and ASAT from metabolically healthy obese and metabolically unhealthy obese (MHO panel)

Samples were kindly provided by Dr Vidya Mohamed-Ali (University College London). Paired omental AT and ASAT surgical biopsies were available for sixteen women who were undergoing bariatric surgery. All participants had been characterised as either metabolic healthy or metabolically unhealthy.

2.2 Cell culture and description of cell lines

2.2.1 Isolation and culture of primary pre-adipocytes

AT biopsies were taken from OBB participants as described above. ASAT biopsies were taken from the abdominal wall 2 inches lateral to the umbilicus and GSAT biopsies were taken from the upper outer quadrant of the buttock. Biopsies were transported immediately on ice for

pre-adipocyte isolation. AT was mechanically minced using sterile scissors, washed twice with Hank's buffered salt solution (HBSS) to remove blood, then incubated with 1mg/ ml collagenase (Roche, Burgess Hill, UK) in HBSS in a shaking water bath (60 rpm) at 37 °C for 45 minutes. The digested AT was centrifuged at 1000xg for 5 minutes at 4 °C in order to pellet the pre-adipocyte containing stromal-vascular fraction. The mature adipocytes and supernatant were removed and the pellet re-suspended in growth medium (Dulbecco's Eagle's Medium Nutrient Mixture (DMEM)/F12 HAM (v/v, 1:1), 10% foetal calf serum (FCS) (Invitrogen, Paisley, UK), 1 µl/100 ml fibroblast growth factor (FGF), 100 U/ ml penicillin and 0.1 mg/ ml streptomycin). The re-suspended cells were filtered twice, through 250 µm nylon mesh and then through 100 µm nylon mesh (SEFAR, Bury, UK), in order to remove non-dispersed cells. The filtered cells were centrifuged again as above and the supernatant removed. The cell pellet was re-suspended in 5 mls growth medium and cells were seeded in a T25 tissue culture flask. The following day the adherent pre-adipocytes were washed with phosphate buffered saline (PBS, Sigma Aldrich, Gillingham, UK) to remove contaminating red blood cells and cell debris and fresh growth medium was added. Pre-adipocytes were passaged when they reached 80% confluency by washing twice with PBS and then adding trypsin-EDTA (Sigma, UK) to cover the base of the flasks. Once cells had separated from the base of the flask growth medium was added to quench trypsin activity and medium containing pre-adipocytes was collected and sedimented by centrifugation as above. The resultant pre-adipocyte pellet was then re-suspended in growth medium and cells re-plated at approximately half the initial concentration. All cell cultures were incubated at 37 °C with

5% CO_2. Pre-adipocyte cultures were expanded and passaged until an appropriate number of pre-adipocytes were available for experiments.

To differentiate pre-adipocytes, cells were grown until confluent and then growth media were replaced with differentiation media (DMEM/F12 HAM (1:1) containing 2 mM glutamine, 17 µM pantothenate, 100 nM human insulin, 1 nM triiodo-L-thyronine (T3), 33 µM biotin, 10 µg/ml transferrin and 1 µM dexamethasone). 3-Isobutyl-1-methylxanthine (IBMX) (250 µM) and troglitazone (4 µM) were added for the first 4 days and culture media exchanged every other day. Cells were cultured in differentiation media for 14 days by which time lipid droplets were visible by light microscopy.

2.2.2 Pt2 cell lines

The Pt2 cell lines were developed by post-doctoral fellows from Takeda, Japan, during placements within the OXLIP group in OCDEM. Pre-adipocyte cell lines were generated from paired ASAT and GSAT biopsies from a 50 year old male participant in the OBB. He was characterised at the time of biopsy as follows: BMI=24.4kg/m^2, height=183cm, WHR=0.93, glucose=5.28 mmol/l, insulin=12.6mU/l, HOMA-IR=2.96, TAG=0.78 mmol/l, total cholesterol=5.78 mmol/l, HDL=1.75 mmol/l, calculated LDL=3.68 mmol/l, CRP=0.43mg/l.

Immortalised pre-adipocyte cell lines (referred to hereafter as 'Pt2 cell lines') were generated using a method based on that described by Darimont *et al*. [194]. Human telomerase reverse transcriptase (hTERT) and human papillomavirus type 16 E7 oncoprotein (HPV16-E7) were sub-cloned from the pBABE-neo-hTERT and pGEX2T E7 plasmids (Addgene, USA) into the pLenti6.3/V5-DEST lentiviral expression vector (Invitrogen, UK). 293FT producer cells were used to generate hTERT and HPV16-E7 lentiviral particles using the ViraPower HiPerform

Lentiviral Expression System (Invitrogen, UK). Pre-adipocytes were isolated from ASAT and GSAT needle biopsies from the subject and were pre-treated with hexadimethrine bromide (6µg/ ml) and transduced initially with hTERT lentiviral particles. Cells were cultured in the presence of blasticidin (2µg/ ml) until blasticidin-resistant, and therefore stably transduced, cells were selected. Blasticidin-resistant pre-adipocytes were then co-transduced with HPV16-E7 lentiviral particles. Constitutive protein expression of both hTERT and HPV16-E7 was confirmed by Western blot and telomerase activity was confirmed using the Trapeze Telomerase Detection kit (Merck Millipore, UK).

Pt2 pre-adipocytes were cultured and differentiated as described for primary pre-adipocytes.

2.2.3 HEK293 cell line

Human Embryonic Kidney 293 (HEK293) cell lines were cultured in growth media consisting of DMEM with 4500 mg/l glucose, 10% FCS, 2 mM glutamine, 100 U/ ml penicillin and 0.1 mg/ ml streptomycin. Cells were passaged at sub-confluency using the same method as that used for pre-adipocyte passage.

2.3 Molecular biology techniques

2.3.1 Genotyping

OBB genomic DNA was extracted from whole blood by LGC Genomics (Hoddesdon, UK). DNA was diluted in nuclease-free water to a concentration of 5ng/µl and 10ng of each sample was plated in 386-well plates (4titude, Wotten, UK) along with non-template controls and at least 3 sample duplications for quality control. Plates were dried by incubation at 80 °C for 10 minutes. Genotyping was performed using KASP On Demand custom designed and validated

primers for rs11614913 and rs736825 (LGC Genomics, Hoddesdon, UK). The assays consisted of 2 forward primers, corresponding to the 2 alleles, and a common reverse primer. The region of genomic DNA of interest is amplified during the genotyping reaction; the master mix contains fluorescent labels (VIC/FAM) that bind to a sequence within the allele-specific forward probes. 4 µl of reaction mix was added to each well of dried down genomic DNA: 2 µl genotyping Mastermix (containing polymerase and dNTPs, LGC Genomics, Hoddesdon, UK), 1.95 µl nuclease-free water and 0.05 µl of SNP specific assay. After brief centrifugation, samples were heated to 94 °C for 15 minutes (polymerase activation) and underwent 10 cycles of a touchdown thermo-cycling protocol, comprising 94 °C for 20 seconds (DNA melting) and 61 °C for 60 seconds, dropping by 0.6 °C per cycle, followed by a further 26 cycles of 94 °C for 10 seconds and 55 °C for 60 seconds (combined annealing and extension step). Plates were then briefly centrifuged and allelic discrimination performed on the ABI Prism 7900 HT Real-Time PCR System (Life Technologies, UK) using SDSv2.3 software (Life Technologies, UK). Genotypes were checked visually to ensure that they had been assigned appropriately and were reassigned if necessary. After assignment of identifier IDs duplicates were checked for genotyping accuracy.

2.3.2 RNA methods

2.3.2.1 RNA isolation

Freshly taken whole AT samples were either snap-frozen in liquid nitrogen immediately and then stored at -80 °C or immediately homogenised in Tri-reagent (Life Technologies, UK). In the latter case samples were transferred to 2 ml Eppendorf tubes containing 1 ml of Tri-reagent and a coneball ball bearing (Retsch, UK). Tissues were homogenized at a frequency of

25 Hz for 1.5 minutes on a Mixer Mill MM 400 free standing homogenizer (Retsch, UK). Lysate was then transferred to a clean 1.5 ml RNase-free tube (Life Technologies, UK) and centrifuged at 12,000xg for 20 minutes at 4˚C to remove released lipids. The homogenate fraction was removed by pipetting through the resultant lipid layer. It was then transferred into a clean 1.5 ml RNase-free tube for storage or RNA extraction.

For cell culture, media were removed and cells were washed twice in PBS. 500µl Tri-reagent was then added to each well of the 6-well plate and wells were scraped vigorously with a scraper (Sarstedt, UK). Tri-reagent was then collected and stored at -80 °C until required for RNA extraction.

2.3.2.2 RNA extraction

RNA from samples for different studies was extracted using the methods outlined in Table 1.3.

Table 1.3: Methods of RNA isolation and extraction for the studies included in this thesis

Study	Sample type	Extraction method
Microarray studies	Whole AT / cell culture	Modified mirVana column method
OBB lean/obese	Whole AT needle biopsy	Modified mirVana column method
MHO panel	Surgical whole AT biopsy	Tri-reagent total RNA
rs11614913 eQTL studies	Whole AT needle biopsy	Modified mirVana column method
Cell culture studies	Pre-adipocytes/differentiated pre-adipocytes/HEK293 cells	Tri-reagent total RNA

2.3.2.2.1 MirVana column method

MirVana columns allow for extraction of the whole RNA fraction, including miRNA. A modified method was used in which cells or tissues were first scraped or homogenized in Tri-reagent. This was because mirVana lysis buffer foamed when homogenised. MirVana miRNA isolation kits were purchased from Life Technologies. 100 µl chloroform was added per 0.5 ml of Tri-reagent and shaken vigorously by hand for 15 seconds before incubation at room temperature for 5 minutes. Phase separation was completed by centrifugation at 12,000xg for 15 minutes at 4˚C. The aqueous phase was transferred to an RNase-free tube and combined with an equal volume of the mirVana kit lysis buffer. This was then combined with 1.25 times volume of 100% ethanol to the total volume of the aqueous phase and lysis buffer and filtered through the columns according to the manufacturer's protocol. The RNA contained within the columns was then washed twice with the supplied wash solutions. RNA was eluted in 100µl of elution solution heated to 95˚C followed by a second elution with 60ul. To concentrate the RNA the eluent was precipitated by the addition of 15µl of sodium acetate and 150µl isopropanol. Samples were stored overnight at -30 °C or for at least 1 hour at -80 °C. Samples were then centrifuged at 12,000xg for 15 minutes at 4˚C to pellet RNA. The pellet was washed twice in 1 ml 80% ethanol (Sigma Aldrich, Gillingham, UK), briefly air dried and then re-suspended in 12-20µl of RNA storage solution (Life Technologies, UK), depending on the size of the pellet.

2.3.2.2.2 Tri-reagent total RNA method

100 µl chloroform was added per 0.5 ml of Tri-reagent and shaken vigorously by hand for 15 seconds before incubation at room temperature for 5 minutes. Phase separation was

completed by centrifugation at 12,000xg for 15 minutes at 4˚C. The aqueous phase was transferred to an RNase-free tube and combined with an equal volume of isopropanol (Fisher Scientific, Loughborough, UK). The samples were stored overnight at -30 °C or for at least 1 hour at -80 °C. RNA was then pelleted, washed and re-suspended as above.

2.3.2.3 RNA quantification

Re-suspended RNA was left to equilibrate overnight and then quantified by spectrophotometry using the Nanodrop NDV1000 Spectrophotometer (ThermoScientific, UK) according to the manufacturer's instructions. The 260/280 and 230/260 nm ratios were checked for each sample to ensure that they were close to 2.0 to ensure adequate purity.

2.3.2.4 cDNA synthesis

Single stranded cDNA for qPCR reactions was synthesised and transcript expression quantified using a number of different technologies in different experiments. More information on the advantages and disadvantages of the different technologies and how RT and qPCR reaction volumes were optimised is given in Chapter 3.

To summarise, in early experiments cDNA was synthesised using the Taqman Megaplex primer pool, or individual miRNA reverse transcription (RT) primers for those not found in the pool, with or without a cDNA amplification step. Full methods for these experiments are described in 3.2.2.2. For the experiments in which the Pt2 cell line was validated (7.3.1.2), cDNA was generated using the High Capacity cDNA Reverse Transcription Kit (Life Technologies, UK). This is not designed for amplification of small RNA species and would not give sensitive or proportional miRNA amplification; therefore, this methodology was only

used for detection of mRNA transcripts. Methods for this are described in full in 7.2.1.2. In other experiments, cDNA synthesis and detection of miRNAs were performed using Qiagen miScript RT kit and assays; this is described below (p.53).

The general design of qPCR experiments, detection of transcripts using Taqman assays and Qiagen cDNA synthesis and qPCR are described in full below.

2.3.2.5 Standard curve and cDNA dilution

For each experiment a standard curve comprising dilutions of a pool of cDNA from all samples in the experiment was produced. Five serial dilutions of pooled cDNA in pH8 0.01M TRIS buffer were used, ranging from 1/25 to 1/400. To determine the optimum cDNA dilution for each experiment a test run of standards was performed on the Corbett Rotor gene 6000 (Qiagen, UK) using an assay for a low-moderate expression transcript. Sample cDNA dilutions were typically in the range of 1/40-1/100; occasionally a 1/10 dilution was required for detection of pre-miRNA. Details of individual experiments are provided in the relevant chapters. All samples and standards were plated in triplicate. The standard curve was included alongside samples for every assay to allow for calculation of the efficiency of the reaction. Negative controls (water and non-template water controls from the RT reaction) were also plated.

2.3.2.6 qPCR using Taqman assays

Taqman Gene Expression assays were used to detect miRNA following Taqman RT synthesis and to detect mRNA in all experiments. Where possible, assays were selected that spanned an exon-exon boundary in order to avoid non-specific amplification of contaminating genomic

DNA. Reactions were performed in a final volume of 6 µl comprising 2.7 µl of diluted cDNA, 0.3 µl of assay and 3 µl of either Taqman Gene Expression Mastermix (Life Technologies) or Kapa Probe Fast Mastermix (Kapa Biosystems). Thermal cycling and fluorescence detection was performed on the ABI Prism 7900HT. Where the reaction mix contained Taqman Gene Expression Mastermix the following amplification programme was used: 95 °C for 10 minutes followed by 40 cycles of 95 °C for 15 seconds and 60 °C for 1 minute. For Kapa Probe Fast Mastermix samples were heated to 95 °C for 3 minutes followed for 40 cycles of 95 °C for 3 seconds and 60 °C for 20 seconds. During every cycle a fluorescence reading was taken as a measure of the quantity of amplified template cDNA present.

2.3.2.6.1 Qiagen cDNA synthesis and qPCR

In the majority of experiments in this thesis cDNA was generated using the Qiagen miScript I kit or Qiagen miScript II kit. RNA concentrations for samples were normalised to give 300-500ng of RNA in 10 µl of nuclease-free water. The RT reaction mix was prepared on ice in accordance with the manufacturer's instructions and was combined with the normalised RNA to give a 20 µl final reaction volume. The reaction mix was warmed to 37 °C for 60 minutes to generate the cDNA and then to 95 °C for 5 minutes to denature the miScript enzyme.

For detection of mRNA transcripts Taqman assays were used using the same methods as described above.

For detection of miRNA cDNA generated using the Qiagen miScript I or II kits Qiagen miScript primer assays were used with the QuantiTect SYBR Green PCR Kit (Qiagen, UK). Mastermixes were reconstituted according to the manufacturer's instructions. An 8 µl final volume reaction was performed to include 2.4 µl of cDNA dilution. Thermo-cycling was again

performed on the ABI Prism 7900HT with fluorescence detection with every cycle, using the following parameters: 15 minutes at 95 °C followed by 40 cycles of 94 °C for 4 seconds, 55 °C for 30 seconds and 72 °C for 30 seconds.

2.3.2.7 Reference gene selection

To correct for small differences in RNA quality and impurities, cDNA synthesis efficiency and technical quantification variability, gene expression was quantified using "relative quantification". In this method, expression of the gene of interest is presented relative to a selection of appropriate invariant endogenous reference transcripts [195]. Any biological variation in the expression of reference genes would result in a false estimate of the abundance of the transcript of interest. Therefore, reference genes were carefully selected to be stably expressed in AT and pre-adipocytes [148]. mRNA was quantified relative to the average expression of peptidylprolyl isomerase A (*PPIA*) and phosphoglycerate kinase 1 (*PGK1*). miRNA and pre-miRNA abundance was quantified relative to the average of miR-103, miR-24 and miR-331. For each experiment reference genes expression was examined to ensure that it was stable and was not unexpectedly regulated by experimental conditions.

2.3.2.8 Analysis of qPCR data

Readings of fluorescence detected during the qPCR reaction on the ABI 7900HT were analysed using SDSv2.3 software (Life Technologies, UK). A threshold (CT) was selected manually at a level at which fluorescence levels for all samples were increasing exponentially. A transcript was deemed not to be detected if no amplification was detected within 35 qPCR cycles.

Relative transcript expression was calculated using the ddCt (ΔΔCt) relative quantification method [195]. The SDSv2.3 results containing the number of cycles at which the fluorescence for each sample crossed the CT and the slope of the standard curve were exported to a text file and then imported into Microsoft Excel for analysis. The average value of triplicate CT values for each sample was calculated. These were then recalibrated to the minimum CT value of all the samples to give the ΔCT using the formula:

$$\Delta CT = Assay\ efficiency^{(min\ CT - Sample\ CT)}$$

Where assay efficiency = $10^{(-1/slope)}$ and the slope refers to the gradient of a line plotting CT (x-axis) against log(dilution) of the standards (y-axis).

The resulting ΔCT was normalized by dividing it by the geometric mean of the ΔCTs of the reference genes. The resulting ΔΔCT value was used for all further analysis.

2.3.3 Protein extraction and Western blotting

2.3.3.1 Protein extraction from Tri-reagent

Attempts were made to optimise protein extraction from Tri-reagent in order to measure HOXC8 in whole AT samples from the OBB panel and the rs11416913 eQTL panel. Protein was extracted using the protocol supplied by Life Technologies. 0.15 mls of 100% ethanol was added to 0.5 mls of Tri-reagent homogenate. The tubes were mixed by inversion and centrifuged at 2000xg for 5 minutes and 4 °C. The organic phase was removed, combined in a clean Eppendorf with 0.75 mls isopropanol and incubated at room temperature for 10 minutes. It was then centrifuged at 12000g for 10 minutes at 4 °C. The resulting protein pellet was washed three times in 0.3M guanidine HCL and once in 100% ethanol before being briefly air dried and re-suspended in 200ul of 1% SDS.

This method produced protein of reasonable yield and quality (as assessed by Commassie blue stain) but HOXC8 failed to be detected by a number of antibodies using the Western blot methods detailed below. A second method of protein extraction was trialled in which the organic phase was combined with 0.9 mls of acetone instead of isopropanol and 2.5% glycerol was added to the wash steps. This made no difference to protein yield, purity or the ability to detect HOXC8 protein on Western blotting. Attempts to detect HOXC8 in whole AT Tri-reagent homogenate were therefore abandoned.

2.3.3.2 Lysis of cultured cells and protein quantification

Before lysing cultured cells for protein extraction cells were washed twice in PBS. 150µl of lysis buffer (50 mM Tris pH8.0, 250 mM NaCl, 5 mM EDTA, 0.5% and Igepal CA-630) was added to each well of a 6-well plate before incubation of ice for 5 minutes. Cells were then scraped as for RNA extraction and whole cell lysates transferred into a clean Eppendorf tube with protease inhibitors (Complete EDTA-free, Roche). Protein samples were sonicated and quantified using DC Protein Assay (Bio-Rad) according to the manufacturer's instructions. Samples were quantified in duplicate against a standard curve of known concentrations of bovine serum albumin. Absorbances were read using the VersaMAX microplate reader set to 750nm and protein concentrations were calculated by SoftMaxPro software. Protein samples were then diluted in lysis buffer and Laem mli 4x sample buffer (Bio-Rad) to give a final concentration of 30ng protein in 25µl.

2.3.3.3 Western blotting

Normalised protein samples were resolved on a Criterion Stain-Free precast gel (Bio-Rad, UK). Following electrophoresis the gel was imaged on the ChemiDoc MP system (Bio-Rad, UK) to visualise separation. Protein transfer onto a polyvinylidene fluoride (PVDF) membrane was performed using the Trans-Blot Turbo system (Bio-Rad, UK). The membrane was visualised again with the ChemiDoc MP to ensure adequate transfer of protein. The resultant image allowed for quantification of total protein in each lane. The membrane was blocked in a solution of 1X TBS, 0.1% Tween-20 and 5% powdered milk for 1 hour at room temperate with agitation. It was then probed with HOXC8 rabbit polyclonal antibody (ab86236 Abcam) at a 1:1000 dilution in 1X TBS, 0.1% Tween-20, 5% powdered milk for 1 hour at room temperature. After washing, the membrane was incubated under the same conditions with 1:1000 goat anti-rabbit IgG horseradish peroxidase (HRP)-conjugated secondary antibodies (DAKO). An enhanced chemiluminescence (ECL) reaction was performed using Clarity ECL substrate (Bio-Rad, UK) and was visualised using both the ChemiDoc MP and imaging film. The protein of interest was quantified and normalised to total protein using Image Lab software (Bio-Rad, UK).

2.4 Microscopy

For light microscopy a Nikon Eclipse TS100 microscope coupled to a Nikon E4500 camera was used to detect and acquire images. For fluorescence microscopy an Olympus BH2 microscope coupled to a Canon EOS700D was used.

2.5 Statistical analysis

All statistical analyses were performed in SPSS 20.0 unless otherwise stated. The statistical tests used are outlined in each chapter. Data were checked for normality visually and using Wilks-Shapiro or Kolmogorov-Smirnov tests and parametric or non-parametric tests used as appropriate. P-values are 2-sided and a p-value of <0.05 was deemed statistically significant for all tests unless otherwise stated.

3 MicroRNA expression profiles in human adipose tissue

3.1 Introduction

As discussed in 1.4.3 there is compelling evidence that appropriate miRNA regulation is necessary for the formation and function of healthy AT. Whilst the body of research into miRNA profiles and regulatory networks in AT has grown exponentially in recent years, their role in the determination of WAT depot-differences remains an under-researched area. Table 2.2 in Chapter 1 outlines publications that have investigated genome-wide miRNA expression in WAT; only one of these studies [134], published after the microarray part of this project had been completed, investigated differences in miRNA expression between ASAT and GSAT. Given the rapidly increasing prevalence of overweight and obesity and their associated morbidities worldwide [196] a fuller understanding of the mechanisms that regulate WAT depot-associated risk is urgently needed.

In this chapter I describe global miRNA expression in human whole ASAT and GSAT. The aim of this work is to identify and characterise miRNAs related to the depot-specific function of ASAT and GSAT. Therefore, in order to identify a candidate miRNA for further study, whole ASAT and GSAT were screened by a global microarray platform to identify miRNAs exhibiting a depot-related difference in expression. Subsequent to the global microarray search for differentially expressed miRNAs, a number of candidate miRNAs were selected and validated by qPCR. Firstly, this provided a technical replication using a different methodology with a high specificity [197]. Secondly, this represented an experimental replication of the microarray results, as the panel of individuals recruited for the microarray experiment was substantially expanded for the qPCR validation.

The qPCR validation panel (referred to hereafter as the OBB ASAT/GSAT panel) was designed to include paired ASAT and GSAT samples from 40 individuals. It was composed of 20 men and 20 women, half of whom were lean and half obese. The inclusion of individuals of different sex and BMI allowed for investigation into whether miRNA differences between ASAT and GSAT were attenuated or enhanced by obesity or according to sex. Additionally, it allowed for a comprehensive description of WAT miRNA profiles in order that miRNAs regulated by sex or obesity could be identified and investigated in other future projects.

3.1.1 Aims

1. To identify miRNAs with depot-specific expression in ASAT and GSAT.

2. To identify miRNAs associated with obesity.

3. To identify miRNAs with different expression in AT according to sex.

3.2 Materials and Methods

3.2.1 Microarray experiments

RNA extraction, microarray experimental work and microarray analysis were performed by Dr Neville.

3.2.1.1 Sample selection

RNA extraction from whole AT biopsies using Tri-reagent is described in Chapter 2. Twenty-three samples were interrogated with microarrays, with one array per sample. Samples consisted of ASAT biopsies from 15 men (8 lean and 7 obese) and paired GSAT biopsies from 8 of the men (5 lean and 3 obese). In the initial microarray screen only men were recruited; the

study was later expanded to include women to enable investigation of sex specific differences in AT depot-related miRNA profiles.

3.2.1.2 Experimental technique

Agilent Human microRNA Microarrays v2.0 (Agilent Technologies, Santa Clara, USA) were used to identify miRNAs expressed in whole ASAT and GSAT samples. This technology was selected because at the time of the experiment it was considered a leading technology and it had been optimised within the university so there was technical support available. For each sample 100ng of total RNA was hybridised to the array. MicroRNA labelling, hybridization and washing were carried out according to the manufacturer's instructions. The DNA microarray scanner (Agilent G2565BA) was used to scan hybridized microarrays and features were extracted using the Agilent Feature Extraction image analysis tool (version 9.5.1) with default protocols and settings.

3.2.1.3 Data analysis

Data were background corrected and quantile normalised in R [198] using the Bioconductor AgiMicroRna package [199]. Differential expression analysis was performed in Genesifter (Geospiza, Seattle, USA). One way ANOVA was used to determine which miRNAs were differently expressed between conditions. Benjami-Hochberg correction was used to take account of multiple testing and a corrected p-value of 0.05 was taken to be significant. A minimum fold-change of 20% was selected to identify clinically important differences in expression.

3.2.2 qPCR

3.2.2.1 Selection of qPCR validation panel

To validate the results of the microarray experiment a panel of 40 individuals from the OBB was assembled (the OBB ASAT/GSAT panel). This included those individuals who had been included in the initial microarray experiment. The panel was composed of paired ASAT and GSAT biopsies from 20 lean (BMI<25) and 20 obese (BMI>25) individuals, with equal numbers of men and women in each group. The anthropometric and biochemical characteristics of the panel are shown in Table 3.1. RNA extracted from needle biopsies in Tri-reagent (described in 2.3.2.2.2) was already available for all participants.

Table 3.1: Characteristics of individuals in the OBB ASAT/GSAT panel assembled for qPCR validation. Paired ASAT and GSAT biopsies were available for all participants. Values represent means, standard deviations are provided in brackets.

	Lean Mean (SD)				Obese Mean (SD)				Lean vs obese
	Men		Women		Men		Women		p-value
BMI (kg/m2)	24.4	(0.5)	22.5	(1.4)	35.1	(6.3)	32.2	(3.7)	
Waist circumference (cm)	89.3	(5.2)	76.6	(4.0)	117.4	(14.0)	102.9	(9.9)	<0.001
Hip circumference (cm)	98.6	(2.4)	96.6	(4.5)	116.7	(10.3)	114.1	(8.2)	<0.001
WHR	0.9	(0.1)	0.8	(0.0)	1.0	(0.1)	0.9	(0.1)	<0.001
Plasma glucose (mmol/l)	5.3	(0.5)	4.8	(0.5)	5.5	(0.5)	5.3	(0.7)	0.147
Plasma insulin (mU/l)	8.7	(3.8)	8.2	(1.6)	21.8	(9.5)	12.6	(4.2)	<0.001
Plasma Triglycerides (mmol/l)	1.6	(1.5)	0.7	(0.2)	2.1	(0.9)	1.4	(0.4)	<0.001
Plasma HDL cholesterol (mmol/l)	1.2	(0.3)	1.5	(0.3)	1.0	(0.1)	1.2	(0.3)	0.013

3.2.2.2 qPCR methods

Fort-one miRNAs were validated by qPCR. These included 3 reference genes and 23 miRNAs that were different according to depot or with obesity on microarray screening with a fold-change of greater than 20%. This was selected as an arbitrary cut off in an attempt to identify miRNAs with clinical, as well as statistical, significance. It was considered that miRNAs that were different by less than 20% were unlikely to have a measurable effect on AT biology. In addition, 15 microRNAs were selected for qPCR that were not coded for on the microarray or were not significantly different between conditions, but which were of interest because of literature implicating them in AT related function.

Three separate qPCR technologies were used in these experiments as at this time miRNA quantitation techniques were still being established and optimised. All methodologies have their own advantages and disadvantages.

The use of the Megaplex pool (#4399966, Life Technologies, UK) means that multiple miRNAs can be reverse-transcribed in a single cDNA synthesis reaction. Reference controls are also contained within the pool, making relative quantitation more reliable.

Taqman assays are considered more specific than Qiagen assays. Taqman qPCR probes generate a fluorescent signal that is sequence-specific. Qiagen qPCR reactions use SYBR green dye which is incorporated into any double stranded DNA that has been amplified during the PCR reaction. SYBR green dye will therefore also detect primer-dimers (primers than have hybridised to each other because of complimentary sequences), which can compete for the PCR reaction and interfere with quantification. Specificity of the SYBR green qPCR reaction

can be confirmed by checking a dissociation curve to ensure a single PCR product is present at the end of the reaction.

Aside from this limitation, the Qiagen miScript technology has several advantages. Taqman methodologies require the synthesis of miRNA and mRNA cDNA pools in separate reactions and the user must either perform a separate cDNA synthesis for each miRNA or is limited to examining those miRNAs with primers contained within the Taqman Megaplex pool. The miScript RT-kit synthesises one cDNA pool containing copies of all RNAs of all lengths. During the RT step miRNA are polyadenylated and transcribed using primers with a universal 3' tag attached. This then allows for amplification cDNA synthesis of both the miRNA and mRNA content. The synthesis of a global cDNA pool allows for more accurate comparison of expression of miRNAs and mRNAs from the same sample as error introduced from repeated RNA dilutions and RT reactions is eliminated. In addition, mRNA can be quantified from cDNA synthesised with the miScript kit using either Qiagen Sybr green or Taqman chemistries.

Table 3.2 indicates the technologies used for quantification of each miRNA. Reference miRNAs were quantified on the panel using all technologies; in addition several other miRNAs were quantified using more than one technology to allow for assessment of agreement between techniques. Where this is the case the data used in the final analysis was generated using Taqman Megaplex with pre-amplification.

Table 3.2: qPCR technologies used for quantification of miRNAs

MiRNA	Taqman Megaplex without preamplification	Taqman Megaplex with preamplification	Taqman Individual assay	Qiagen miScript assay
miR-103	X	X	X	X
miR-24	X	X	X	X
miR-331	X	X	X	X
Let-7a		X		
Let-7b		X		
Let-7c		X		
Let-7g		X		
miR-10b		X		
miR-1225-5p			X	
miR-122a		X		
miR-125b		X		
miR-132	X			
miR-134	X			
miR-143		X		
miR-145		X		
miR-146a		X		X
miR-146b		X		X
miR-15b	X	X		
miR-195		X		
miR-196a			X	
miR-196b				X
miR-204		X		
miR-21		X		
miR-210		X		
miR-221	X	X		X
miR-223		X		X
miR-23b		X		
miR-25		X		
miR-26b		X		
miR-27a	X			
miR-27b	X			
miR-28-3p		X		
miR-320		X		
miR-335	X			
miR-378			X	
miR-424		X		
miR-486		X		
miR-572			X	
miR-575				X
miR-638		X		
miR-939				X

3.2.2.2.1 Taqman Megaplex without pre-amplification

Synthesis of cDNA using the Taqman Megaplex pool (Life Technologies, UK) was performed by Dr Neville. Taqman Megaplex pools contain multiple RT stem-loop primers to allow for simultaneous cDNA synthesis for multiple mature miRNAs. Megaplex primer pool A (version 1) was used, which contained primers for 384 miRNAs. Synthesis of cDNA took place according to manufacturer's instructions. Each 7.5µl reaction contained 320ng of template RNA diluted in 3.2µl of RNase free water along with:

Megaplex RT Primers (10X)	0.80µl
dNTPs with dTTP (100 mM)	0.20µl
MultiScribe Reverse Transcriptase (50 U/µL)	1.50µl
10X RT Buffer	0.80µl
MgCl2 (25 mM)	0.90µl
RNase Inhibitor (20 U/µL)	0.10µl

Reactions were performed using the PTCV225 Peltier Thermal-Cycler (MJ Research, Waltham, Massachusetts, USA) using the following conditions: 16 °C for 2 minutes, 42 °C for 1 minute then 50 °C for 1 second (repeated for 40 cycles) followed by 85 °C for 5 minutes. A standard curve of the cDNA pool was generated as described in 2.3.2.5 to determine the appropriate cDNA dilution for qPCR. In this case cDNA was diluted 1:60 in 10 mM pH8 TRIS. Diluted cDNA was plated in 384 well plates with 2.7ul of cDNA in a well.

qPCR was performed using Taqman miRNA assays (Life Technologies, UK). The qPCR reaction was scaled down from a 20µl reaction to a 6µl final volume reaction. This was optimised by Dr Neville and shown to give results that were consistent with the larger scale reaction. To each

well of diluted cDNA template 3µl of Taqman Gene Expression Mastermix (Life Technologies, UK) and 0.3µl of assay were added. Thermal cycling and fluorescence detection was performed on the ABI Prism 7900HT. The following amplification programme was used: 95 °C for 10 minutes followed by 40 cycles of 95 °C for 15 seconds and 60 °C for 1 minute. During every cycle a fluorescence reading was taken as a measure of the quantity of amplified template cDNA present.

3.2.2.2.2 Taqman Megaplex with pre-amplification

The protocol for Taqman Megaplex pools recommends that between 350ng-1,000ng of template RNA is used for each reaction. Because the amount of RNA available to us was less than this in some cases, the addition of a pre-amplification step was tested to determine whether this would improve sensitivity. Taqman Megaplex pre-amplification primers (Life Technologies, UK) are a pool of forward and reverse primers that amplify the miRNA cDNA by PCR. In optimisation experiments I tested a half-volume pre-amplification reaction and found that it gave equivalent results to a full volume reaction. Therefore the reaction was performed as follows:

cDNA product from Megaplex RT reaction	1.25µl
Taqman pre-amplification Mastermix (2x)	6.25µl
Megaplex pre-amplification primers (10x)	1.25µl
Nuclease free water	3.75µl

The reactants were combined in a 96-well plate and were cycled as follows: 95 °C for 10 minutes, 55 °C for 2 minutes, 72 °C for 2 minutes, followed by 12 cycles of 95 °C for 15 seconds and 60 °C for 4 minutes.

The resultant cDNA was diluted 1:100 in 10 mM pH8 TRIS and plated in triplicate in 384-well plates with 2.7ul of cDNA in a well. qPCR was performed as above.

3.2.2.2.3 Taqman individual assays

Primers for a number of miRNAs were not included within the Megaplex pool A. An individual cDNA synthesis reaction was carried out for each of these. Again, a half volume RT reaction was tested and found to give equivalent results to a full volume reaction. Therefore, each reaction included the following:

RNA template (100ng/µl)	2.5 µl
Primer	1.5µl
dNTPs with dTTP (100 mM)	0.075µl
MultiScribe Reverse Transcriptase (50 U/µL)	0.50µl
10x RT Buffer	0.75µl
RNase Inhibitor (20 U/µL)	0.095µl
Water	2.08µl

The reaction was thermo-cycled using the following parameters: 16 °C for 30 minutes, 42 °C for 30 minutes, 5 °C for 85 minutes. The qPCR reaction used a 1/50 cDNA dilution and was carried out as previously.

3.2.2.2.4 Qiagen miScript assays

In contrast with the Taqman technologies, the Qiagen miScript technology allows for generation of a cDNA pool containing cDNA copies of all transcripts contained in the template RNA. This allows for quantification of miRNA and mRNA from a single RT reaction. Because of this advantage Qiagen miScript technology was adopted for use in the rest of the project. A

number of miRNAs to be validated were quantified using this method. Methods for synthesising cDNA with the Qiagen miScript kit and for performing qPCR with miScript assays are described in 2.3.2.6.1. The qPCR reaction was scaled down to an 8ul final reaction volume. This had been validated in-house to give equivalent results to the recommended 10ul reaction. For this experiment a 1/25 cDNA dilution was used.

3.2.3 Statistical analysis of qPCR data

Methods for normalising raw CT values to give ΔΔCT values are outlined in 2.3.2.8.

Data were checked for normal distribution by visually inspecting plotted data and by using Shapiro-Wilk tests and checking kurtosis and skew statistics. For comparison of depot-differences paired fold-changes were calculated (i.e. the mean of individual fold-changes). In order to identify clinically significant changes data were filtered so that only miRNAs with a fold-change of greater than 20% were considered different between conditions. Paired T-tests or Wilcoxon signed rank tests were used as appropriate. All other variables were tested in each depot separately. BMI and gender were coded as categorical variables and differences in miRNA expression were assessed using independent T-tests or Mann-Whitney U tests. Again, only data displaying a difference of greater than 20% between conditions were considered clinically significant. Where indicated analyses were performed separately on men and women. Pearson's correlation was used to assess agreement between continuous variables. In order to assess correlation between miRNA expression and circulating insulin with correction for BMI, the reciprocal of BMI and miRNA expression were used (in order that the data fitted a normal distribution) in a partial correlation model.

Uncorrected p-values are presented in this chapter. The main aim of the experiments presented here was to identify candidate miRNAs that were regulated in AT according to depot or obesity for further study. It was considered that a miRNA that was regulated across several conditions might be of particular interest. Additionally, the intention was to confirm that a candidate miRNA was important in AT using functional experiments. Therefore, it was considered that avoiding type 1 error was preferable even at the risk of increasing type 2 error. Full data with p-values are presented in the Appendix (Table 9.1-9.4). Here, miRNAs that would remain significant using a Bonferroni adjusted p-value (p=0.00125) are indicated in bold.

3.3 Results

3.3.1 Microarray data

Probe sets for 798 miRNAs were present on the microarrays: of these, 161 miRNAs were expressed in AT and 79 reached significance (uncorrected p-value <0.05) for differential expression in at least one condition.

Figure 3.1 shows a heat map illustrating which miRNAs were different between depot and between lean and obese WAT in each depot. Figure 3.2 depicts the 26 miRNAs that were significantly different with a greater than 20% fold-change between ASAT and GSAT.

Figure 3.1: Heatmap showing the 79 significantly different miRNAs between abdominal and gluteal subcutaneous adipose tissue in lean and obese men with a fold-change of greater than 20%.

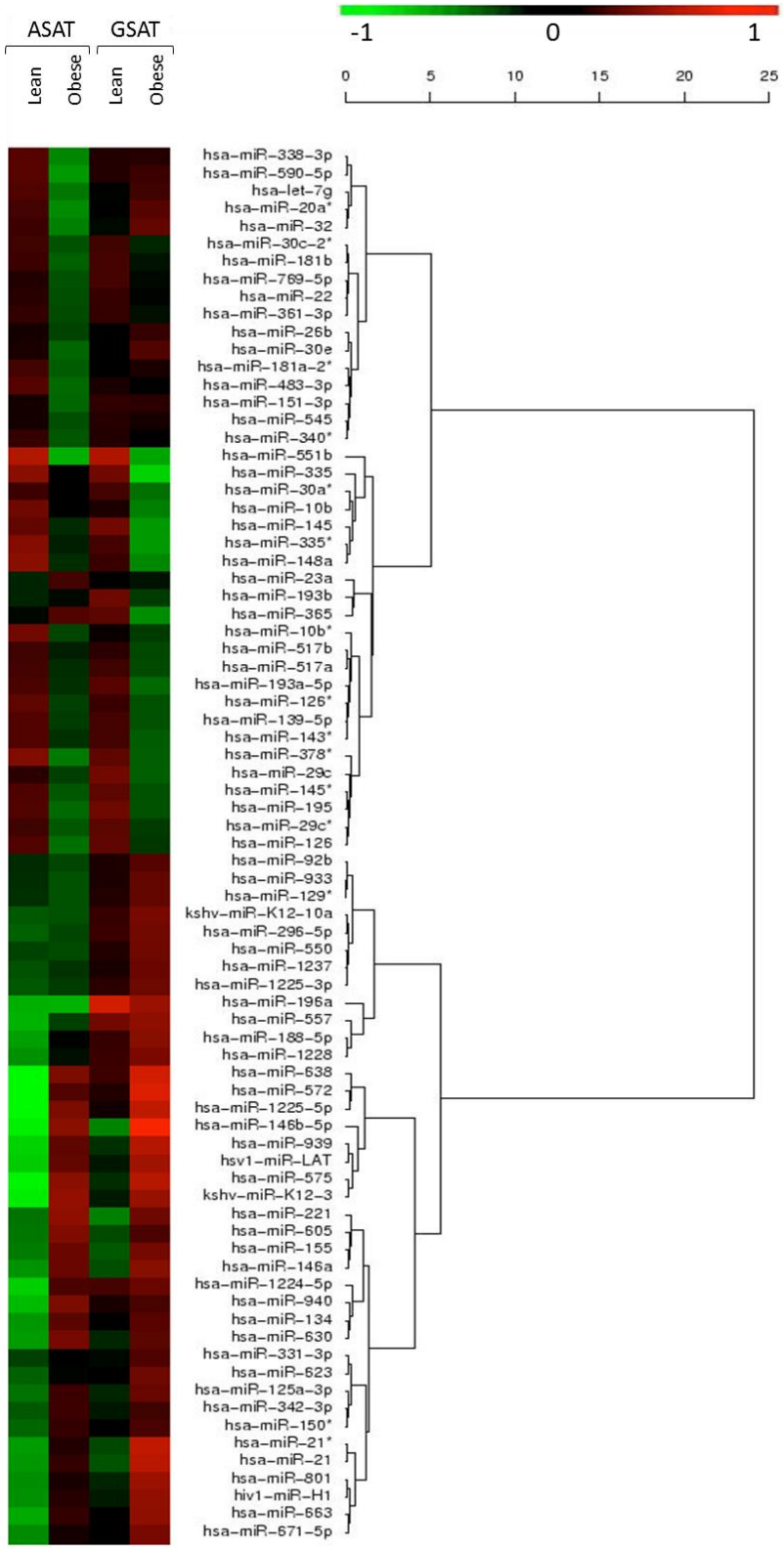

Figure 3.2: Heatmap showing the 26 miRNAs with significantly different expression in ASAT and GSAT and a fold-change of greater than 20%.

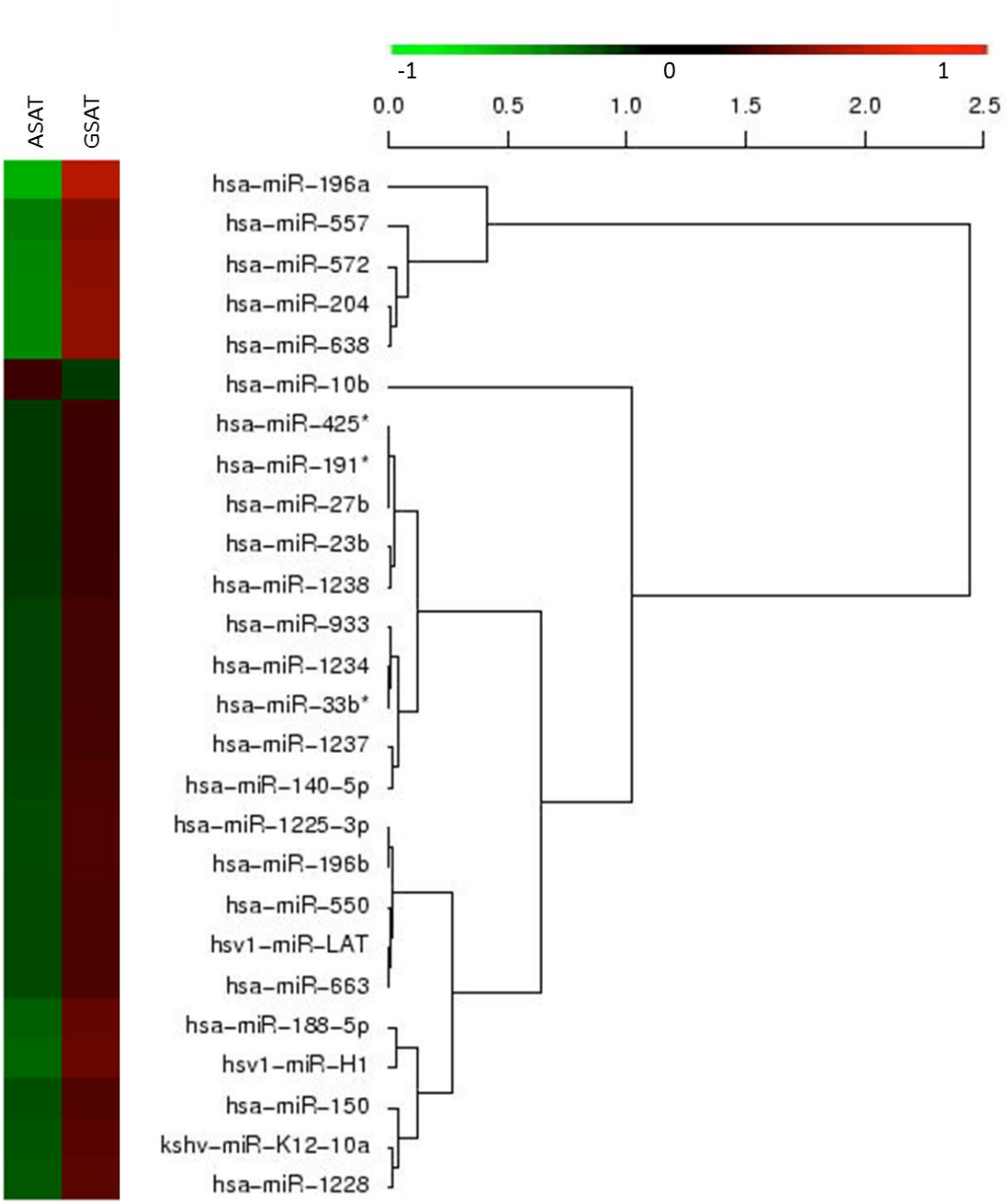

3.3.2 Confirmatory qPCR

3.3.2.1 Agreement between microarray and qPCR results

Figure 3.3 shows the correlation between fold-changes in miRNA expression between GSAT and ASAT as detected by microarray and by qPCR. Of 23 miRNAs that were detected by microarray to be differently expressed between ASAT and GSAT with a fold-change of 20%, 13 were also significant on qPCR, although for only 7 of these did the fold-change exceed 20%. It should be noted that the correlation between the microarray and qPCR data represents not only the sensitivity and specificity of the two methods, but also the replication of findings from the smaller panel of men used for the microarray experiment to the expanded panel of men and women used for qPCR validation.

Figure 3.3: Correlation between fold-changes in microRNA expression between ASAT and GSAT as detected by microarray and qPCR.

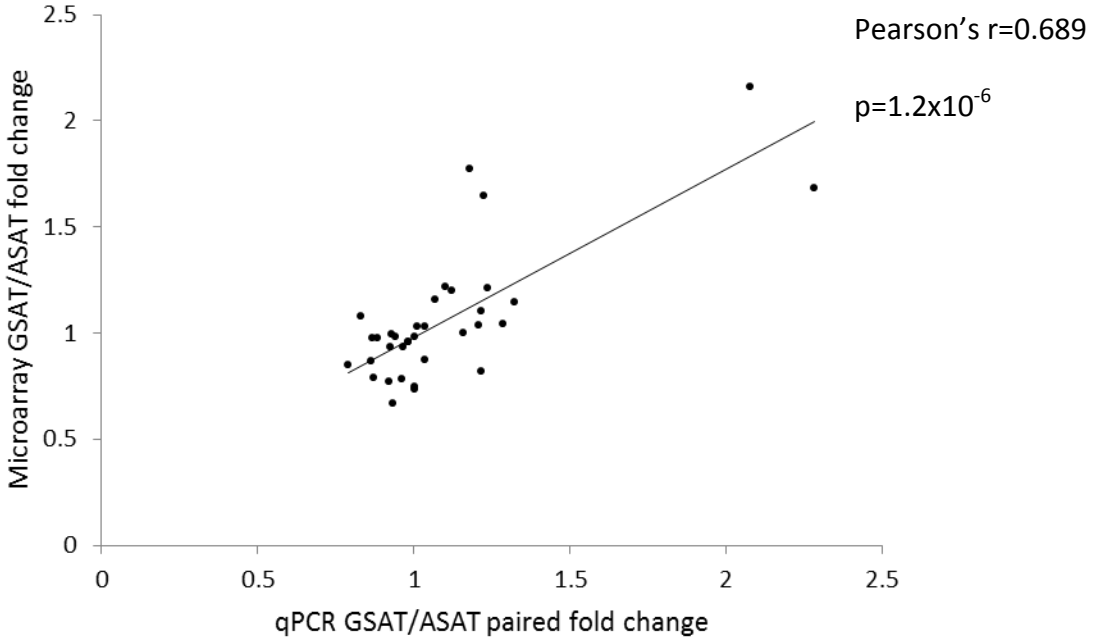

3.3.2.2 Agreement between qPCR technologies

Expression of 41 miRNAs was validated by qPCR (Table 3.2). As discussed in 3.2.2.2 a number of qPCR methodologies were used and a selection of miRNAs were validated using more than one qPCR technology. Fold-changes calculated using qPCR data from the different technologies correlated well with one another (Figure 3.4). It should be noted that observed variations between technologies could be introduced during RNA dilution, cDNA synthesis, cDNA dilution and the qPCR reaction, as well as due to different primer or probe specificities and reaction efficiencies.

Figure 3.4: Agreement between different technologies used for validatory qPCR. Graphs illustrate the agreement between paired fold-changes between ASAT and GSAT as calculated using different qPCR technologies.

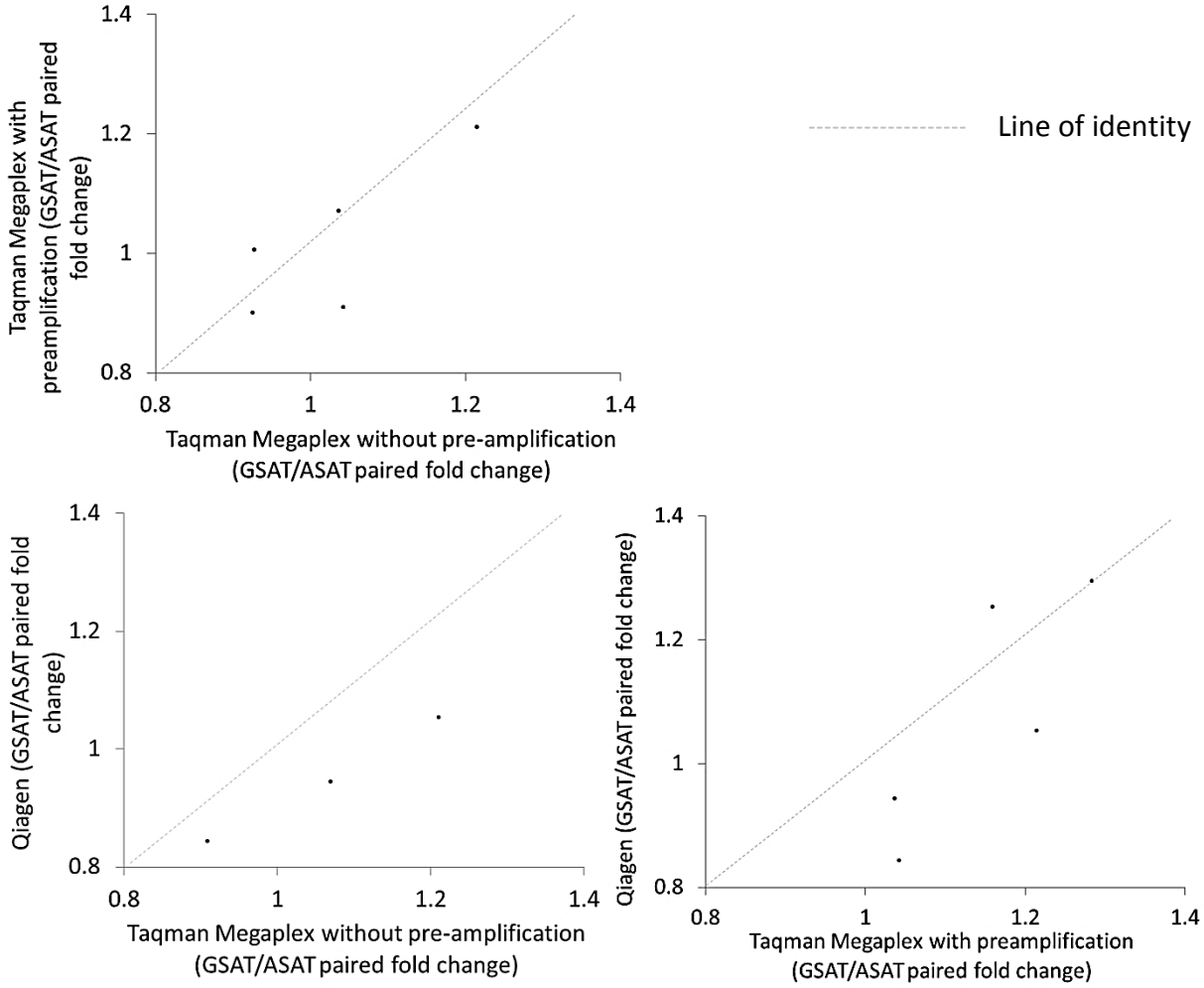

3.3.2.3 MicroRNA expression in subcutaneous abdominal and gluteal adipose tissue

Of the 41 miRNAs validated by qPCR 12 were significantly different by at least 20% between ASAT and GSAT (Figure 3.5). Interestingly, all of these were more highly expressed in GSAT. When lean or obese subjects were considered separately 8 miRNAs remained significantly different between ASAT and GSAT in either lean or obese subjects or both (Figure 3.6). Two miRNAs, miR-320 and miR-335, were significantly higher in ASAT than GSAT, but with a fold change of less than 20% (miR-320: -13%, p=0.009; miR-335: -16%, p=0.012). MiR-424 was significantly higher in GSAT in obese individuals but not when all BMIs were considered together. There was a tendency for depot-differences for the majority of miRNAs to be more significant in obese participants.

There is sexual dimorphism in body shape and body fat distribution is influenced by sex hormones [97]. Therefore depot-differences in miRNA expression were considered separately for men and women (Figure 3.7) In addition to the miRNAs identified in Figure 3.5, miR-335, let-7b and let-7c all had lower expression in GSAT compared with ASAT in women only. MiR-196b and miR-146b both had markedly different depot-specific expression patterns in men and women.

MiR-196a and miR-204 consistently displayed higher expression in GSAT than ASAT (approximately 2.1-fold and 2.3-fold respectively) in both men and women and in lean and obese individuals.

Figure 3.5: Significantly different miRNAs between abdominal subcutaneous and gluteal adipose tissue. Bars represent standard errors of paired fold-changes.

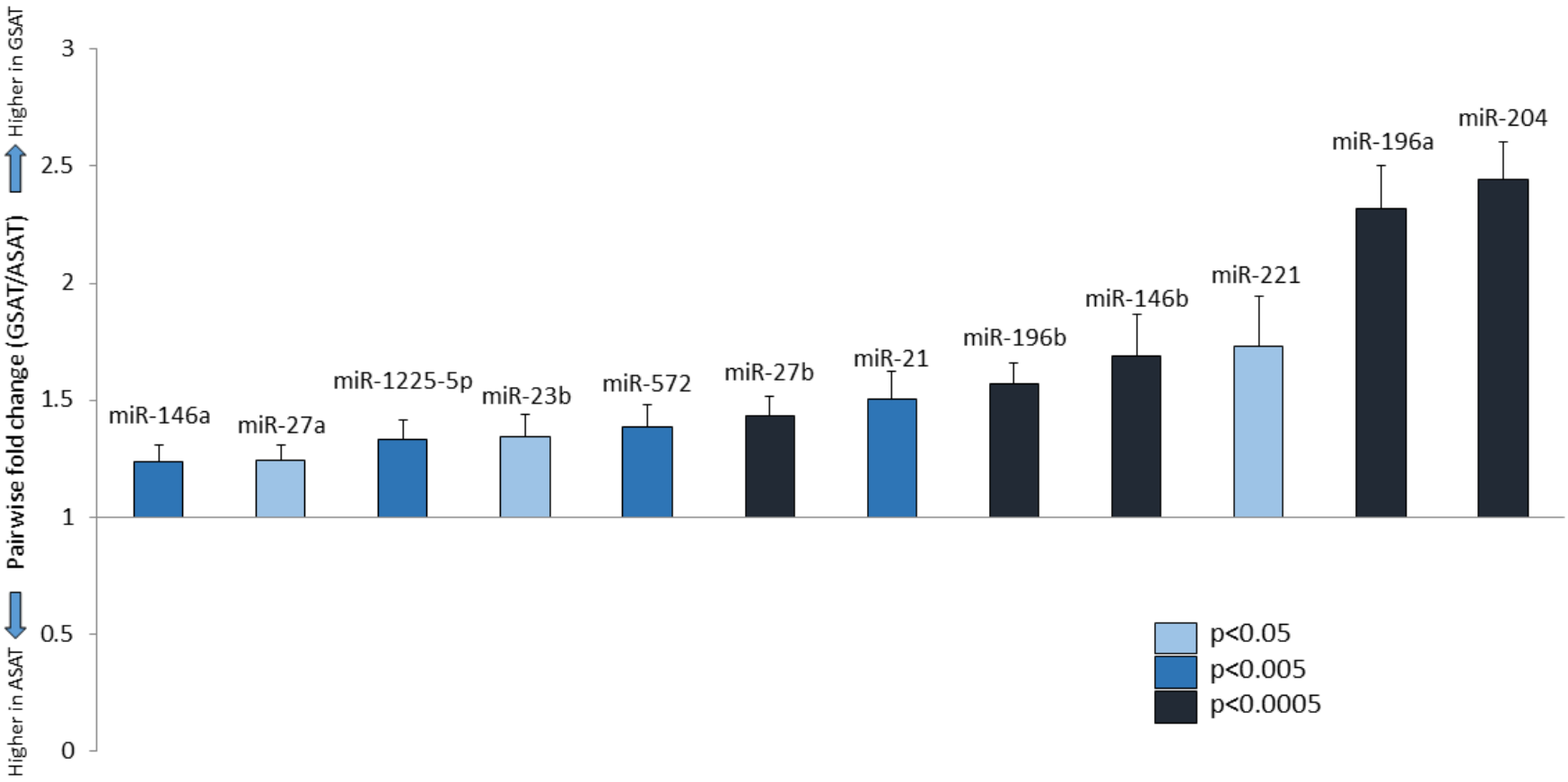

Figure 3.6: Significantly different miRNAs between abdominal subcutaneous and gluteal adipose tissue according to obesity status. Bars represent standard errors of paired fold-changes.

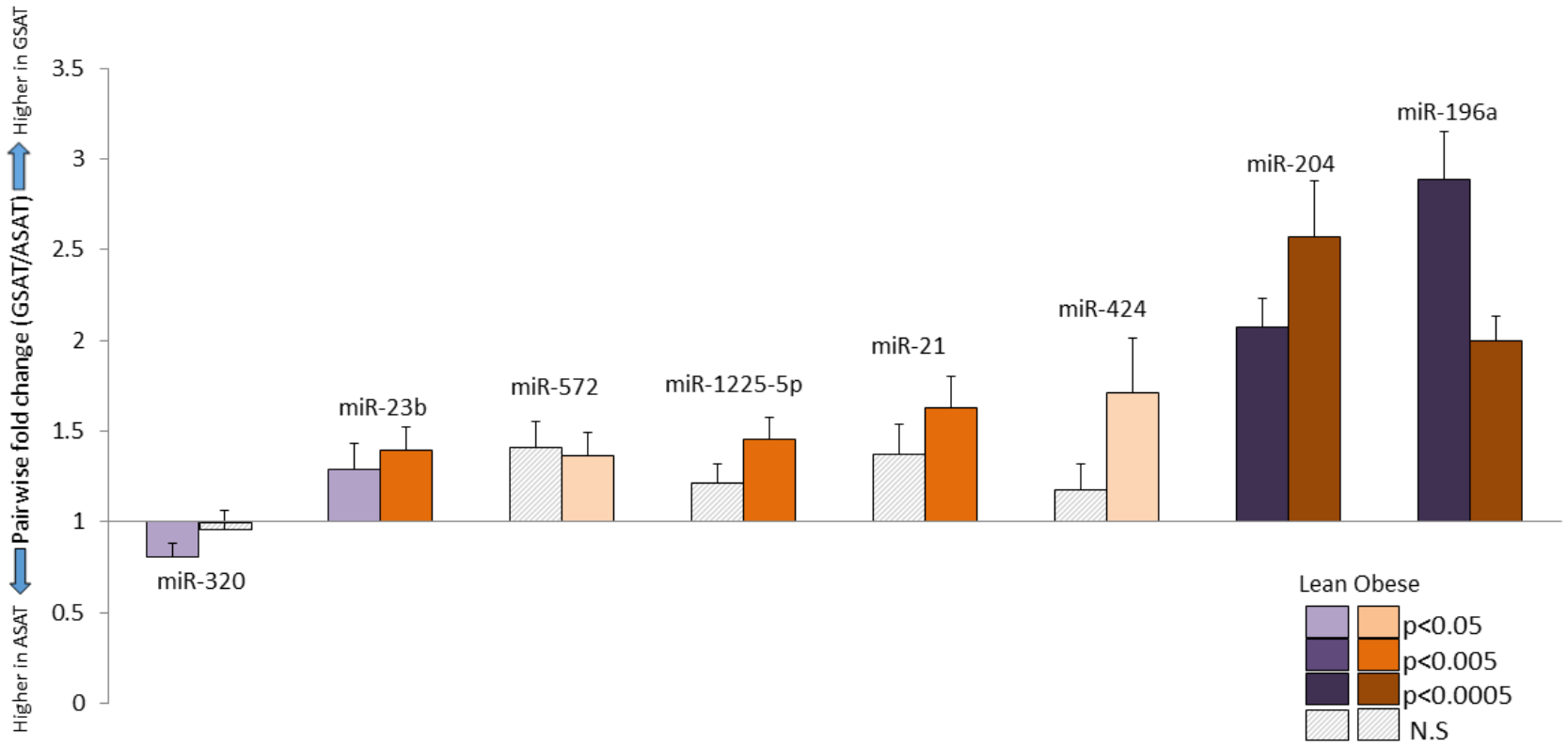

Figure 3.7: Significantly different miRNAs between abdominal subcutaneous and gluteal adipose tissue according to sex. Bars represent standard errors of paired fold-changes.

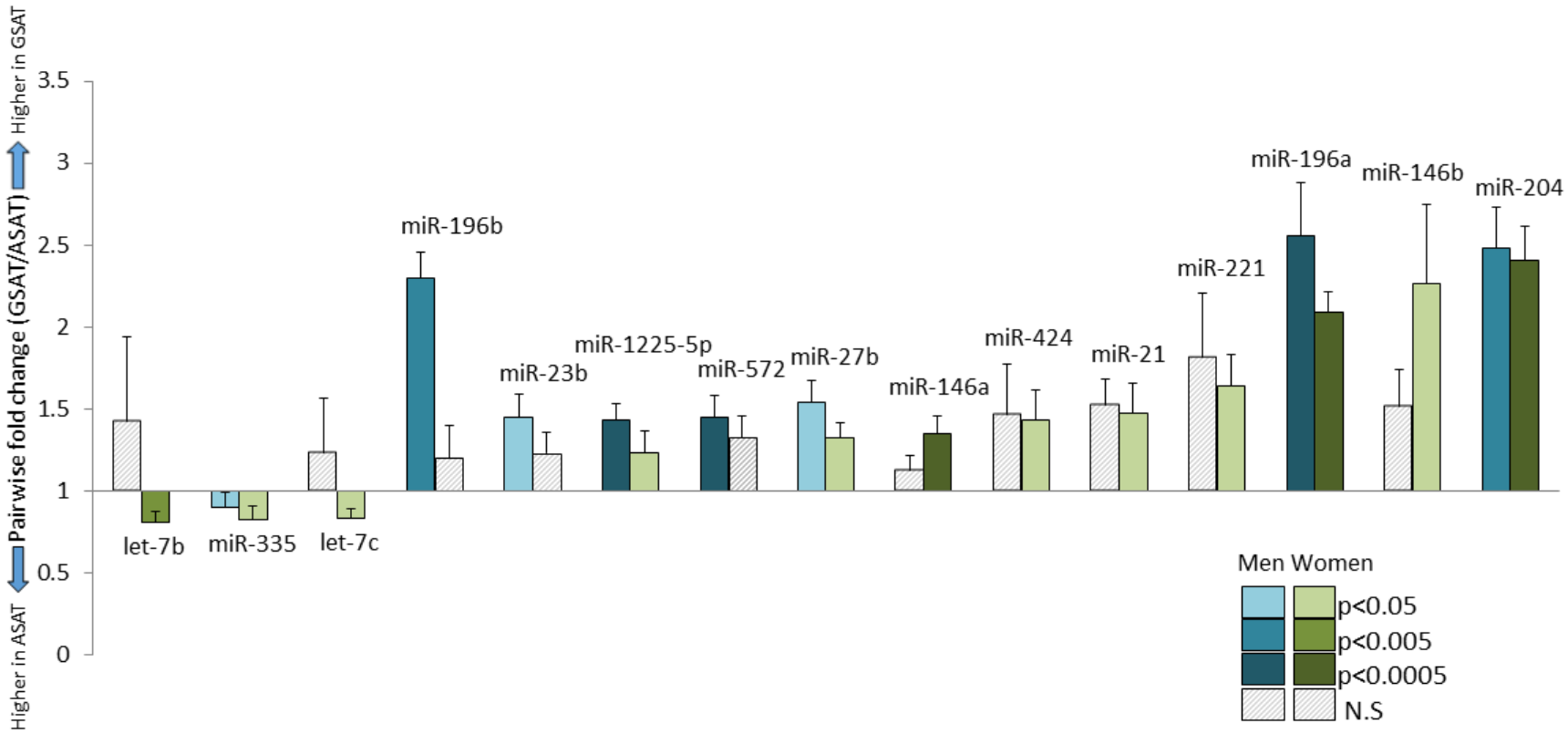

3.3.2.4 Adipose tissue microRNAs in lean and obese subjects

MiR-335, miR-144, miR-23b and miR-145 were all detected at lower levels in both GSAT and ASAT in obesity, whilst miR-378, miR-221, miR-21 and miR-146b detected at higher levels with obesity in both depots (Figure 3.8). A number of miRNAs were lower or higher with obesity in ASAT only. MiR-551b and miR-1225-5p were both significantly lower in GSAT only in obese subjects.

MicroRNA-146b was the most strongly up-regulated miRNA in obesity. Although it appeared to be similarly up-regulated in both ASAT and GSAT further interrogation of the data revealed a sex and depot related discordance in change in miR-146b expression with obesity (Figure 3.9). Obese men and women both had 2.3-fold higher miR-146b expression in GSAT than lean men and women. However, in ASAT from obese men miR-146b was only 1.4-fold higher than in lean men, whilst obese women had 5.6-fold higher miR-146b expression in ASAT than lean women.

A number of studies have suggested that AT miRNAs might be regulated by, or regulate, insulin resistance [149, 150, 174, 200]. Therefore, correlation with serum fasting insulin was calculated for those miRNAs that were differently expressed with obesity (Table 3.3 and Table 3.4). Within GSAT miR-551b was the only miRNA to correlate with insulin after correction for BMI. Interestingly expression of several obesity-related miRNAs within ASAT correlated with fasting insulin even after correction for BMI (Table 3.4).

Figure 3.8: MiRNAs within abdominal subcutaneous or gluteal adipose tissue that are significantly different between lean and obese individuals.

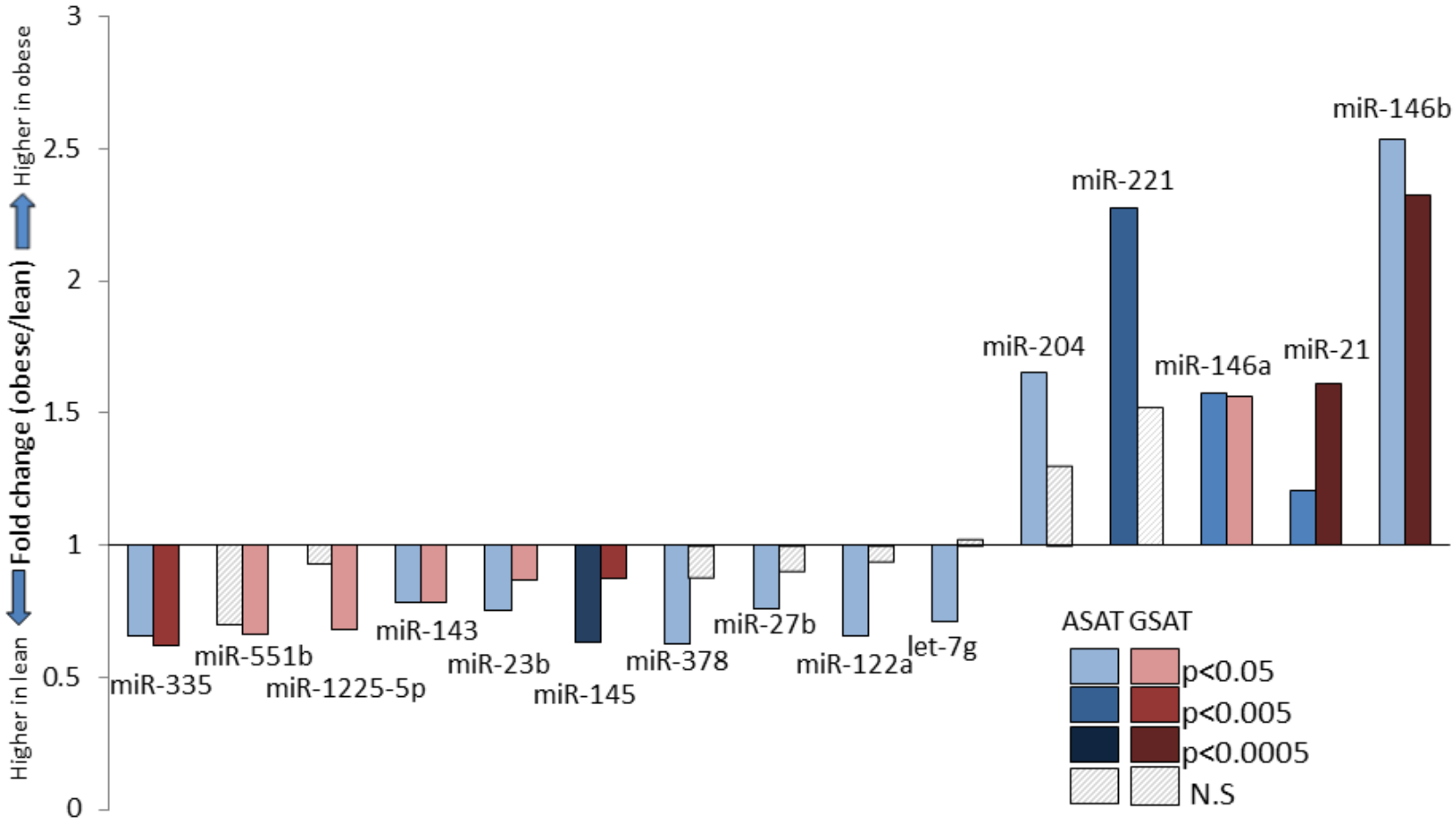

Figure 3.9: Sex and depot discordance in miR-146b expression in obese compared with lean individuals. Significance refers to miR-146b expression in obese versus lean individuals.

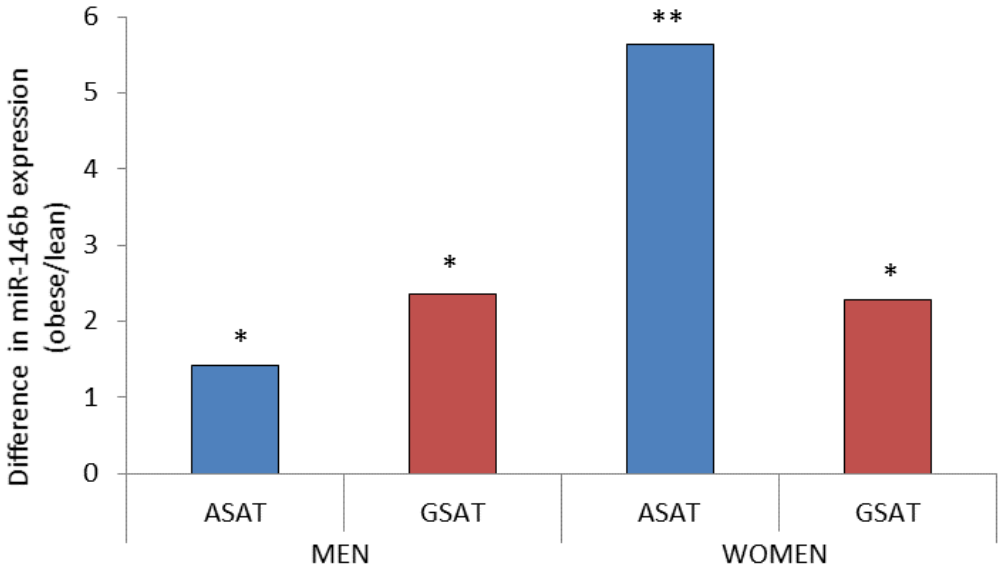

Table 3.3: Correlations between miRNA expression and insulin in GSAT, with and without correction for BMI, for miRNAs differentially expressed with obesity in GSAT.

	miRNA correlation with insulin			miRNA correlation with insulin, corrected for BMI		
miRNA	**Correlation**	**r^2**	**p-value**	**Correlation**	**r^2**	**p-value**
mir-551b	-0.49	0.24	0.001	-0.38	0.14	0.018
mir-335	-0.47	0.22	0.002	-0.25	0.06	0.119
mir-145	-0.43	0.18	0.006	-0.13	0.02	0.442
mir-143	-0.35	0.12	0.029	-0.31	0.10	0.056
miR-1225-5p	0.19	0.04	0.24	-0.08	0.006	0.64
miR-378	0.21	0.04	0.19	-0.05	0.003	0.75
miR-23b	0.28	0.08	0.08	0.18	0.03	0.28
mir-21	0.29	0.09	0.067	-0.12	0.01	0.480
mir-146b	0.48	0.23	0.002	0.30	0.09	0.066

Table 3.4: Correlations between miRNA expression and insulin in ASAT, with and without correction for BMI, for miRNAs differentially expressed with obesity in ASAT.

	miRNA correlation with insulin			miRNA correlation with insulin, corrected for BMI		
miRNA	**Correlation**	**r^2**	**p-value**	**Correlation**	**r^2**	**p-value**
mir-145	-0.62	0.38	<0.001	-0.39	0.15	0.014
mir-335	-0.53	0.28	<0.001	-0.38	0.14	0.019
mir-27b	-0.51	0.26	0.001	-0.42	0.18	0.007
mir-23b	-0.50	0.25	0.001	-0.37	0.14	0.022
mir-143	-0.50	0.25	0.001	-0.36	0.13	0.025
mir-378	-0.36	0.13	0.021	-0.15	0.02	0.369
let-7g	-0.33	0.11	0.036	-0.17	0.03	0.314
mir-122a	-0.30	0.09	0.063	-0.17	0.03	0.298
mir-21	0.22	0.05	0.183	0.03	0.00	0.85
mir-204	0.28	0.08	0.082	0.99	0.99	0.997
mir-221	0.33	0.11	0.038	0.07	0.01	0.521
mir-146b	0.50	0.25	0.001	0.34	0.11	0.035
mir-146a	0.53	0.29	<0.001	0.31	0.10	0.053

3.3.2.5 Adipose tissue microRNAs and sex

Sexual dimorphism in miRNA expression has been described [201, 202] and has been postulated to be influence the differences in prevalence and severity observed for a number of human diseases [203-205]. In total twenty-two AT miRNAs exhibited at least a 20% difference in expression between men and women. Although sex-discordance in miRNA expression was often only significant in either ASAT or GSAT, expression patterns tended to display the same non-significant trends in the other depot (Figure 3.9). A greater number of miRNAs were highly expressed in male rather than female AT, with a tendency for the difference in expression to be stronger and more consistent in ASAT. MiR-424 was highly significantly different between men and women in both ASAT and GSAT.

Figure 3.10: MiRNAs within abdominal subcutaneous or gluteal adipose tissue that are significantly different between men and women.

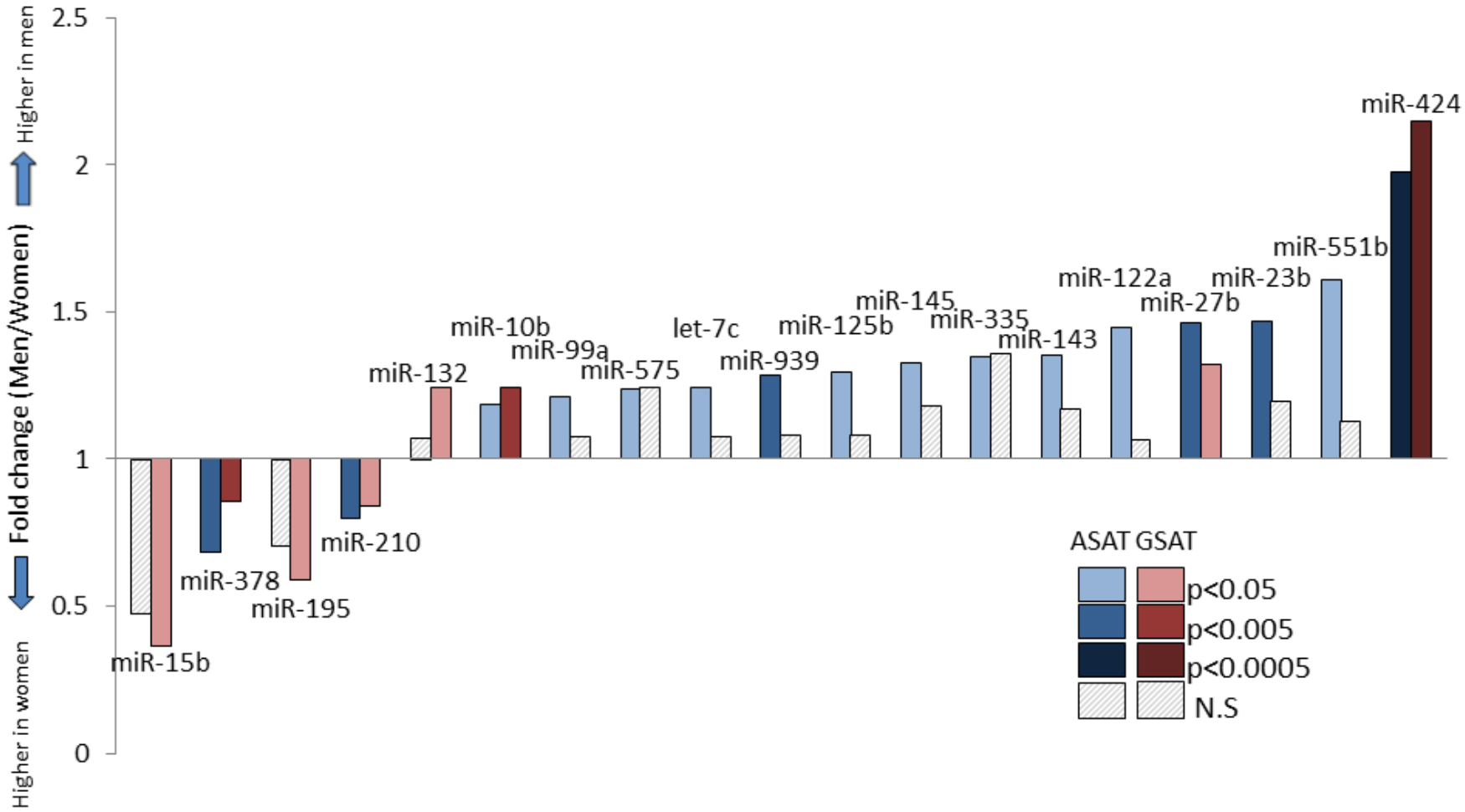

3.3.2.6 MicroRNA processing

A tendency was observed for a greater number of miRNAs to display higher expression in GSAT than in ASAT, and in men than in women. Expression of *DROSHA* and *DICER* (both integral parts of the small RNA processing machinery) were therefore examined by qPCR to explore whether there was a more general regulation of miRNA processing. Neither *DROSHA* nor *DICER* was significantly different according to sex or AT depot. There was a small but significant down-regulation in *DROSHA* mRNA in obese individuals in both ASAT (fold-change= -1.175, p=0.004) and GSAT (fold-change= -1.097, p=0.025). There was no relationship between BMI and *DICER*.

Expression of the miRNA precursors pre-miR-146b, pre-miR-196a-2, pre-miR-221 and pre-miR-223 was determined by qPCR on the OBB ASAT/GSAT panel. Fold-changes of the precursor and mature miRNAs were compared for lean vs obese, GSAT vs ASAT and men vs women comparisons. There was good agreement between the pre-miR and mature miRNA fold-changes (Figure 3.11), suggesting that miRNA processing machinery was unlikely to be responsible for global changes in miRNA expression.

Figure 3.11: Agreement in fold-changes in expression of miRs and pre-miRs. Comparison of fold-changes in expression with obesity, sex and depot (GSAT vs ASAT) for pre-miR-146b, pre-miR-196a-2, pre-miR-221 and pre-miR-223 and the -5p mature miRNA derived from each precursor.

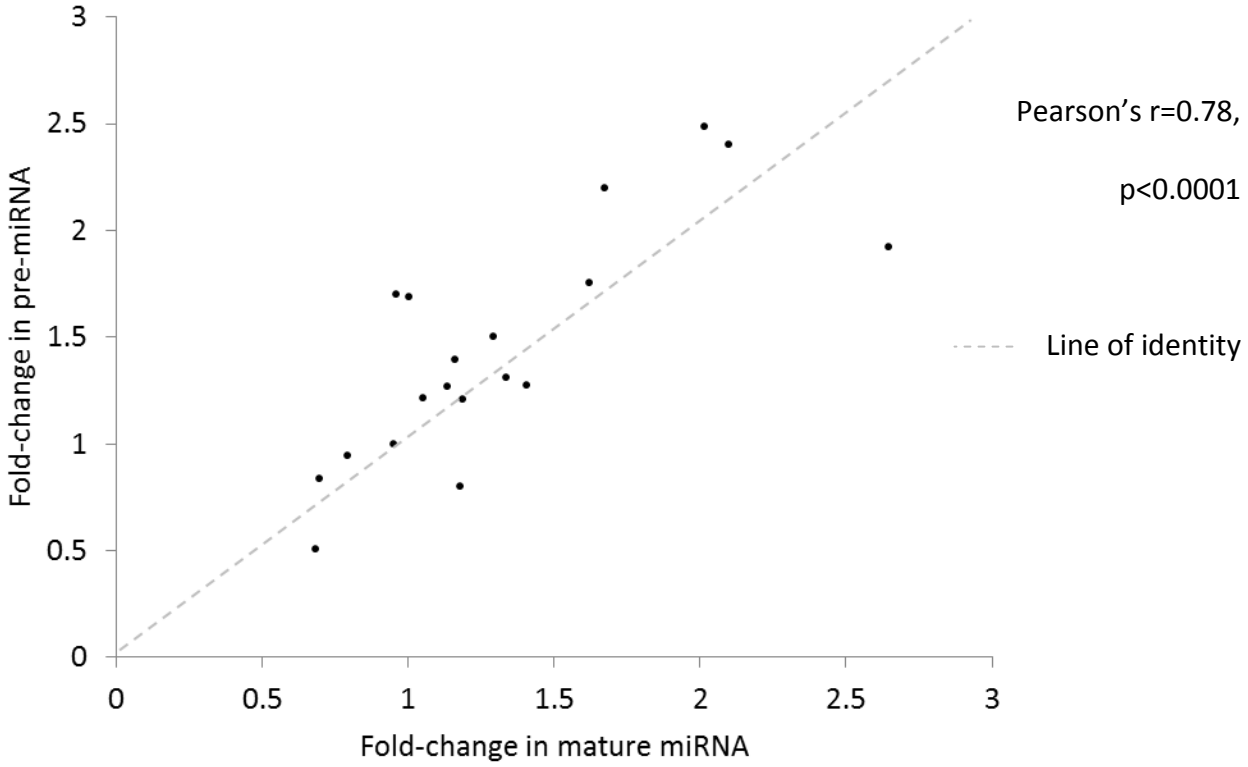

3.4 Discussion

In this chapter I have used a genome-wide approach to identify patterns of miRNA expression in SAT according to depot (ASAT or GSAT), BMI and sex. At the time that this project was conducted this was the only study to have compared miRNA expression in ASAT and GSAT. One perhaps surprising observation is the consistency of miRNA expression in AT and the comparatively small number of miRNAs that appear to be regulated. This is consistent with other studies of genome wide miRNA expression in AT [134, 139, 141, 142, 173, 191]. Indeed, in this study only a handful of miRNAs were significantly regulated with a fold-change of greater than 50%. It is proposed that the regulated miRNAs have a significant biological function in AT.

MiR-196a and miR-204 were the most differently expressed miRNAs between GSAT and ASAT. A number of studies have implicated miR-196a in WAT biology [206-208] but its relationship with the different WAT depots has never been studied. MiR-196a is expressed from within the *HOX* gene clusters and is predicted to target several of the *HOX* genes. In turn, there is a body of literature to suggest that the HOX proteins have WAT depot-specific expression and function. The literature on miR-196a and the *HOX* genes is discussed in detail in the next chapter. Uniquely amongst the candidate miRNAs identified in this study, miR-196a has another feature that made it attractive for further study: the presence of a common SNP within its precursor. For these reasons, miR-196a was felt to be the most promising candidate and the role of miR-196a in human body fat distribution became the primary focus of this thesis.

MiR-204 displayed higher expression in GSAT and was also up-regulated in obese individuals specifically within ASAT. MiR-204 promotes adipogenesis by suppressing the Wnt/β-catenin signaling pathway [209] and by targeting *RUNX2* [210], a key regulator of the osteogenic vs adipogenic cell lineages. The expression patterns observed in our study suggests that miR-204 may have a role in ASAT expansion in obesity.

A study by Rantalainen *et al.* [134], published after this project began, examined differential miRNA expression in ASAT and GSAT. They identified 59 microRNAs with depot-specific expression patterns, reflecting the different experimental and statistical methodologies between our studies. Rantalainen *et al.* [134] performed an initial microarray analysis using a different technical platform in a cohort of seventy subjects. They then validated significant miRNAs by microarray analysis of ASAT and GSAT from independent cohort of 40 individuals. Our study aimed to identify miRNAs with substantially regulated expression in AT as we reasoned that these were most likely to have an important biological role. Therefore, only miRNAs that were different by at least 20% between conditions were deemed to be differently expressed, restricting the number of miRNAs identified in our study. Seven of the 12 miRNAs identified to be higher in GSAT in our study were also identified by Rantalainen *et al.* [134]. In our experiment only two miRNAs, miR-320 and miR-335, were higher in ASAT than GSAT, both with nominal un-corrected p-values and with modest fold changes. Both of these miRNAs have been implicated in adipocyte biology [185, 186, 211, 212]. However, neither of these were found to have a depot-specific expression pattern by Rantalainen *et al.* [134] raising caution that these may be false-positives.

GSAT can be considered a relatively quiescent tissues with reduced fatty acid storage following a meal [60] and lower overall fatty acid mobilisation [55-57] when compared with ASAT. There was a tendency for miRNAs to be more highly expressed in GSAT, therefore I speculated that significantly regulated miRNAs might be working concordantly to regulate common pathways in AT. DIANA miRPath v2 [213] (http://diana.imis.athena-innovation.gr) is a web-based algorithm that identifies enriched target pathways that include proven or predicted miRNA targets for a user specified list of miRNAs. Target transcripts were filtered to include only those expressed in AT (16,839 annotated genes expressed in AT in a previous microarray experiment, data courtesy of Dr Neville). Despite this, the transcriptional networks predicted to be targeted by the miRNAs regulated by SAT depot or with obesity were difficult to interpret biologically. Outputs tended to be for cancer or non-adipose disease related pathways. Interestingly, Godard *et al*. [214] recently reported that pathway analysis of this type tends to be biased towards cancer-related pathways, perhaps reflecting the over-representation of cancer related research in the microRNA field compared to other clinical disciplines. A more sophisticated pathway prediction technique, entailing the incorporation of whole genome mRNA and miRNA datasets, was used in another study to speculate on the roles of miRNAs in ASAT and GSAT [134]. It found that only a minority of miRNAs were significantly and inversely correlated with their predicted conserved target mRNAs [134]. The authors reported that these mRNAs were enriched for KEGG terms related to AT biology, suggesting that repression by these miRNAs is likely to be functionally relevant. As the correlation between mRNA and protein repression is imperfect, future studies might shed more light on this area by combining proteomic and transcriptomic data in AT.

A number of trends in miRNA expression were observed in this study. The majority of miRNAs with a depot-specific expression pattern were more highly expressed in GSAT (Figure 3.5) and differences tended to be more marked in obese subjects (Figure 3.6). Sex-discordant microRNAs tended to have higher expression in male AT, particularly in the ASAT depot (Figure 3.9). Disruption of *DICER* leads to altered fat distribution in mice and has been observed in human HIV-related lipodystrophy [215]. I therefore investigated whether there was a more general difference in miRNA processing machinery between SAT depots or with gender obesity. Although there was a small difference in mRNA expression of *DROSHA* with obesity no other relationships were observed. Furthermore, fold-changes in pre-miRs and miRs were well correlated, suggesting that changes in miRNA expression are miRNA-specific and not caused by more general changes in miRNA maturation or degradation.

A number of studies have explored genome-wide miRNA expression in obesity (See Table 2.2). In agreement with our data miR-143 [157], miR-221 [142] and miR-146b [162] have been observed to be differently expressed according to BMI in humans and miR-21 [157] was differently expressed in a murine model of obesity. Data from mouse models of obesity is not always consistent with human data. For example, miR-27 has been described to be both up- and down-regulated in murine obesity [178, 179] miR-335, which was strongly downregulated in human obesity in our data, was increased in a murine model of obesity [186]. A number of miRNAs identified in our study have previously been implicated in AT biology (miR-143 [145], miR-146b [146], miR-335 [186], miR-378 [142, 183], miR-221 [142] and miR-27 [178-180]).

We identified miR-146b as the most strongly up-regulated miRNA in obese vs lean participants. Mir146b is up-regulated in response to inflammation and TLR4 ligands *in vitro*

[216, 217]. The toll-like receptor 4 (TLR4) signalling pathway is an innate immune pathway which is active in adipose tissue and which is postulated to have a key role in AT inflammation and its associated complications [218, 219]. Furthermore, mir146b appears to negatively regulate NF-kB, a component of the TRL4 signalling pathway, via inhibition of *TRAF6* and *IRAK1*, leading to suppression of NFkB dependent genes such as *TNFα*, *IL-6* and *IL-8* [216, 217, 220, 221]. Therefore, it has been suggested that mir146b acts as a negative feedback mechanism within the toll-like pathway, dampening the innate immune response. Interestingly, miR-146b expression was discordant between men and women in ASAT only. The role of miR-146b in human obesity should be an area for future research. Some preliminary experiments investigating miR-146b were performed early in this project. It was hypothesised that miR-146b would be upregulated in response to lipopolysaccharide stimulation of pre-adipocytes, adipocytes or THP-1 cells, but in my experiments this was not demonstrated. Unpublished work from within our group has demonstrated a 2.4-fold up-regulation of miR-146b in ASAT in men following a 14 day course of rosiglitazone ($p<0.001$). I was unable to replicate this up-regulation in response to rosiglitazone in pre-adipocytes or adipocytes *in vitro*. At this point experiments focussed on miR-196a were yielding promising results, and so investigations into miR-146b were abandoned.

Expression of a number of miRNAs in ASAT was correlated with circulating fasting insulin. Within GSAT only miR-146b had a borderline significant correlation with insulin. This may reflect the different properties of the depots, although it is unclear whether regulation of any of these miRNAs cause altered insulin sensitivity in AT, are regulated by insulin, or whether expression of the miRNA and insulin concentrations are both confounders for other factors.

Associations between all miRNAs and insulin were attenuated by adjustment for BMI, suggesting that at least in part promotion of these miRNAs is obesity-dependent and not just related to insulin sensitivity or exposure.

MiR-27b emerged from this experiment as the miRNA most significantly correlated with circulating insulin. MiR-27 is a negative regulator of adipogenesis [178, 179] and has altered expression in murine obesity [178]. Additionally, miR-27 is more highly expressed in AT in rodent models of diabetes [150, 182] and in 3T3-L1 cells exposed to increasing concentrations of glucose [174, 182]. Furthermore, transfection of miR-27 into 3T3-L1 cells led to increased insulin resistance [182]. In contrast to the rodent data I observed miR-27b to be inversely correlated with insulin, suggesting that its mechanisms of promotion or action might be different between mouse and man, or that its relationship with insulin is complex.

Despite the importance of sex on AT distribution the relationship between AT miRNA expression and sex has been largely ignored. In this study a number of miRNAs had discordant expression between men and women (Figure 3.9). It is interestingly to note that the miRNA that was most strongly up-regulated in male AT, miR-424, is X-linked. Whilst the majority of X-linked genes have equivalent expression in men and women, a minority do display sex-related expression differences (and can be higher in either sex) [222, 223]. It remains to be seen whether this is relevant to the sex-difference observed in miR-424 expression in WAT. A number of miRNAs identified in this study have also been reported to regulate adipocyte biology (miR-378 [147, 187-190], miR-196 [168], miR-210 [172], miR-132 [153], let-7c [143], miR-145 [160, 161], miR-143 [145, 146] and miR-27b [178-181]). The role of AT sex-specific WAT miRNA expression in determining the different WAT distribution phenotypes in men and

women remains virtually un-researched and these data suggest some promising candidates for further study.

The methodology used in this chapter had a number of limitations. These experiments used human whole SAT samples and so the data generated reflects the whole-tissue transcriptional network. The cellular composition of SAT is influenced by site [50] and obesity [9] and the observed differences in miRNA expression may reflect this. Microarray analysis was selected for the initial screen for expressed and regulated miRNAs. This limited the screen to annotated miRNAs. The most recent release of miRBase (miRBase 21) includes 2,588 mature miRNA sequences; the microarray used in this study covered 723 human miRNAs. Therefore, although the microarray screen gave good coverage it was far from comprehensive. Validation of microarray data with qPCR is a widely accepted method and qPCR has been shown to have a high specificity for miRNA quantitation [197]. The use of qPCR as a 'gold standard' compared to microarray quantitation has, however, been challenged. It has been noted that for a small proportion of miRNAs qPCR quantitation does not agree with quantitation by a number of different microarray platforms [224, 225], although it has been suggested that this disparity is due to different methods of sample preparation [225]. The high degree of agreement between fold-changes calculated using microarray and qPCR data in this study is therefore reassuring, especially given that these also used different cohorts of participants.

During this initial study several different qPCR technologies were used as the project evolved and as different technologies were compared and optimised. Reassuringly, there was a high degree of correlation between different qPCR technologies. Data were normalised to three

internal reference controls for each qPCR technology. Therefore, fold-changes in miRNA expression can be directly compared between technologies despite differences in the amount of input RNA, RT efficiency and cDNA dilution.

This chapter has presented a reference atlas of miRNA expression in human whole SAT. This study facilitated the identification of the most strongly regulated miRNAs, and therefore the miRNAs most likely to have a biological role in human SAT. In the rest of this thesis I investigate miR-196a, one of the most strongly different miRNAs between ASAT and GSAT, and aim to determine whether it has a causative role in human body fat distribution and ASAT vs GSAT specific function.

4 Expression profiling of miR-196a

4.1 Introduction

MicroRNA-196a emerged from global miRNA profiling of human AT as one of the most strongly differently regulated miRNAs between ASAT and GSAT. In this chapter I discuss the literature relating miR-196a and *HOX* genes to AT biology and fat distribution. In the context of this background, and because a common SNP in pre-miR-196a-2 offered a potential tool for studying its role *in vivo*, I selected miR-196a as the focus for this thesis. I began by profiling the expression of miR-196a in human WAT and its cellular components.

4.1.1 MicroRNA-196a

Three paralogues of the mir-196 gene exist. As shown in Figure 4.1 the mir-196a-1 gene is located on chromosome 17 between the *HOXB9* and *HOXB10* genes and the mir-196a-2 gene is located between the *HOXC10* and *HOXC9* genes on chromosome 12. The mir-196b gene is located on chromosome 7 between the *HOXA9* and *HOXA10* genes. Mir-196a-1 and 2 transcribe the same mature miRNA, whilst the mature miRNA sequence transcribed by mir-196b differs by 1 nucleotide (Figure 4.2). As well as being expressed from within the HOX gene clusters miR-196a is predicted bioinformatically and experimentally to target *HOXA5* [226]*, HOXB8* [227, 228] and *HOXC8* [207, 229] (Figure 4.1). The relevance of the HOX protein family to AT biology is discussed in detail in 4.1.5.3.

The mir-196 genes are not found within invertebrates and their appearance is predicted to be linked to the evolution of vertebrates, in whom they are well conserved [230]. The advent of the mir-196 gene paralogues is hypothesized to be linked with the duplication of the *HOX* gene clusters [230]. It is possible that the presence of three mir-196 paralogues, which are

likely to target the same mRNAs due to homology of their 5'-ends, permits for tissue- and time-specific expression patterns and therefore allows for enhanced spatial and temporal fine tuning of the HOX proteins. This hypothesis has been given weight by the observation that the miR-196 paralogues are expressed at different times and in subtly different regions within the developing zebrafish embryo [231]. It has also been noted that, despite their near-identical sequences, miR-196a and miR-196b have different mRNA target affinities [232].

Figure 4.1: Location of the mir-196 genes in relation to their predicted HOX gene targets

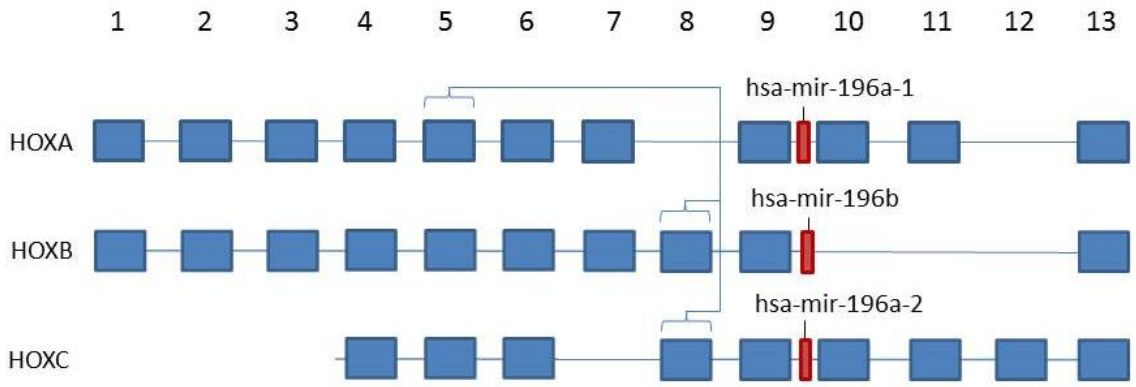

Figure 4.2: Sequences of mature hsa-miR-196a and hsa-miR-196b

MiR-196a; 3-GGGUUGUUGUACUUUGAUGGAU-5

MiR-196b: 3-GGGUUGUUGUCCUUUGAUGGAU-5

Figure 4.3: The number of publications relating to miR-196a.
http://www.ncbi.nlm.nih.gov/pubmed was searched on 11.02.2015 using the terms 'mir-196a OR micro RNA 196a OR mir196a'. Searches dates are to January of each year.

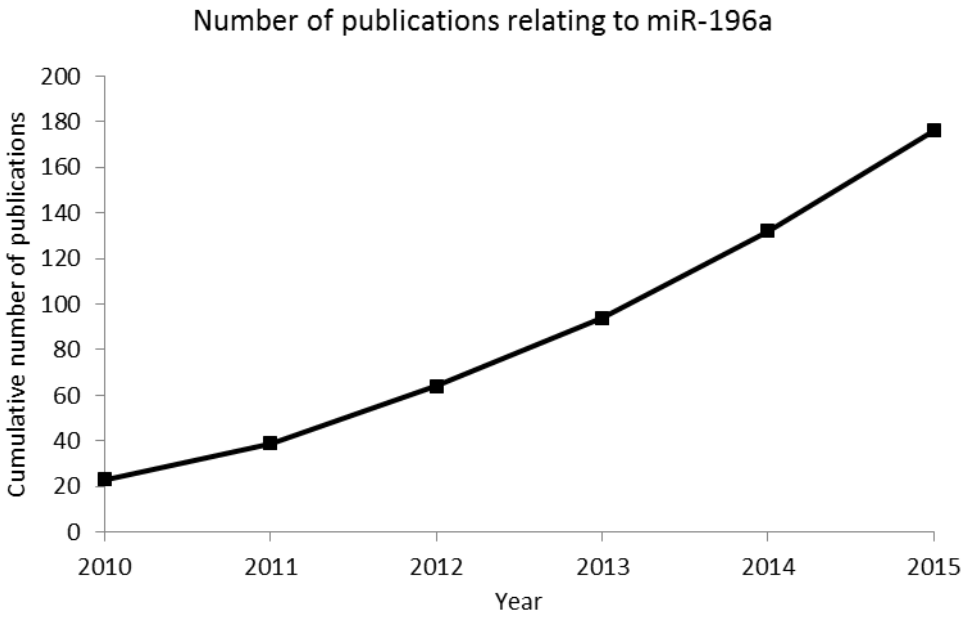

4.1.2 miR-196a in development and pathophysiology

Since this project was first conceived the number of publications on miR-196a has increased dramatically (Figure 4.3). Much of the literature consists of descriptive papers of miRNA expression in various disease states in which miR-196a has been identified along with numerous other candidates as being up- or down-regulated. Considerable effort has also been made to functionally characterise miR-196a, and I will summarise that literature here.

The location of the mir-196 genes within the HOX gene clusters, along with their suggested role as regulators of HOX protein expression, has led researchers to hypothesise that they might be important to normal embryogenesis. Within the developing embryo miR-196a expression is highest within the posterior trunk [227, 233]. MiR-196a appears to be important for development of the axial skeleton; miR-196a inhibition in the chick embryo caused posterior homeotic transformation of the last cervical vertebra [234] and in the zebrafish

embryo led to an expansion of the axial skeleton along the A-P axis [231]. Correct miR-196a expression appears to be crucial to normal hindlimb development, as evidenced by the ability of miR-196a to prevent retinoic acid mediated development of mesoderm into the hindlimb by protecting against inappropriate *HOXB8* expression [126]. Ectopic overexpression of miR-196a in the anterior embryo of *Xenopus laevis* (African clawed frog) caused dose-dependent abnormalities in eye development [233]. Taken together these findings are consistent with the idea that regional and appropriately timed miR-196a expression is important for normal embryogenesis. Due to the low mutation rate of miRNAs and the inability to perform these types of interventional studies in humans the precise role of miR-196a in human embryogenesis remains uncertain, but it is reasonable to postulate that it may play an important role.

There is considerable evidence that miR-196a also has a regulatory role in cells from a number of different lineages. miR-196a has been shown experimentally to negatively regulate proliferation of fibroblasts [235], cervical cancer cell lines [236-238], keratinocytes [239] and human osteosarcoma cell lines [240]. Other studies have identified it as an enhancer of proliferation in cells from glioblastoma multiforme [241], non-small cell lung cancer [226] and cell lines derived from pancreatic cancer [242, 243] and gastric cancer samples [244] via its actions on targets such as *HOXA5* [226] and *p27 (kip1)* [244]. MiR-196a appears to have no effect on the proliferation capacity of some other cell lines [245, 246]. MiR-196a has also been proposed to have a role in the differentiation of cells of several lineages [247] and in apoptosis [243].

From the above observations it seems likely that miR-196a plays an integral role in controlling tissue growth and that its effect are cell lineage, and therefore tissue, specific. It is perhaps unsurprising therefore that dysregulated miR-196a expression has been observed in a number of cancers. Indeed, miR-196a has been considered by some investigators to be a pro-oncogenic miRNA. miR-196a expression has been reported to be up-regulated in gastrointestinal stromal tumours [244, 248], pancreatic cancer [249], colorectal cancer [250], hepatocellular cancer [251] and in subgroups of acute myeloid and lymphatic leukaemias [252, 253]. MiR-196a overexpression in Barrett's oesophagus is predictive of progression to adenocarcinoma [254]. Circulating miR-196a expression is also raised in some malignancies, reflecting increased expression in the tumour, and so miR-196a may hold potential as a biomarker for cancer occurrence or progression [255-257]. In addition a SNP in the precursor in miR-196a-2, rs11614913, is linked with the incidence and severity of several different cancers. This is discussed in detail in Chapter 5.1. MiR-196a has been postulated to act by increasing invasiveness and migratory capacity of malignant cells [246, 258] and reducing apoptosis [241] as well as through its effects on proliferation. *In vivo* studies examining miR-196a modulation in murine models of colorectal cancer [245] and glioblastoma multiforme [241] have confirmed pro-oncogenic effects.

In keeping with the concept that miR-196a may have tissue-specific actions is the observation that in other cancers miR-196a has a tumour suppressive effect. Its expression is down-regulated in melanoma [229, 259] and endometrial cancer [260]. In *in vitro* and *in vivo* experiments, ectopic expression of miR-196a in melanoma cells reduced their invasiveness and appeared to reduce their oncogenic potential when implanted into mice [229]. Enforced

expression miR-196a and miR-196b also reduced the incidence of spontaneous metastases in a murine model of breast cancer [261].

MiR-196a dysregulation has been noted in other human diseases including scleroderma [262, 263] and keloid scarring [264]. Functional studies have shown that miR-196a inhibits production of type I [262-264] and type III collagen [264]. MiR-196a is up-regulated in the prefrontal cortex of patients with Huntington's disease [265] and its overexpression in transgenic mouse reduced accumulation of huntingtin protein aggregates and improved disease course [266]. Interestingly there is a miR-196a binding site within the hepatitis C virus (HCV) RNA genome [267]. MiR-196a is induced in hepatocytes in response to interferon-β treatment in a dose-dependent manner [267, 268] and represses HCV replication [267, 269]. MiR-196a and b expression are associated with Crohn's disease severity [270]. Brest *et al.* observed that a genetic polymorphism in *IRGM* disrupts a miR-196 binding site and therefore prevents miR-196 mediated suppression of *IRGM*, providing a mechanism for the increase in disease severity seen with the risk allele [270]. MiR-196a has also been linked with endothelial cell function with enforced miR-196a expression causing reduced angiogenesis through its targeting of Annexin-1 [271].

MiR-196a may hold promise as a therapeutic agent for spinal and bulbar muscular atrophy (SBMA). Mice with a rodent model of spinal and bulbar muscular atrophy (SBMA) were injected intramuscularly with a viral vector causing widespread ectopic miR-196a expression [272]. Mice treated with miR-196a had an improved disease course and life expectancy compared to mice treated with the control vector. Progression of SBMA is characterised by loss of muscle mass and weight loss and so although an AT phenotype was not reported in

this study it would be difficult to separate the effects of miR-196a treatment on AT from that on disease progression.

4.1.3 miR-196a in adipose tissue

The literature regarding the actions of miR-196a in AT is conflicted. Mori *et al.* recently proposed that miR-196a may function as an important regulator of the WAT lineage by inhibiting brown adipogenesis [207]. They noted that HOXC8 expression fell during brown adipogenesis of white precursors at the protein level, but not the mRNA level. Using *in vitro* culture of human WAT-derived pre-adipocytes overexpressing miR-196a and a murine model with AT-specific miR-196a overexpression they demonstrated that miR-196a regulates 'browning' specifically in WAT via its targeting of *HOXC8* which in turns regulates *CEBPβ* [207]. The transgenic miR-196a expressing mice exhibited improved glucose tolerance, resistance to obesity and increased energy expenditure, indicating that the induced beige adipocytes were functional.

One study observed no difference in white adipogenesis of hASCs with enforced miR-196a overexpression [206] whilst another group reported that it enhanced white adipogenesis in the murine 3T3-L1 cell line [273]. In a conference abstract, miR-196a was purported to enhance white adipogenesis of hASCs and was proposed to act by targeting *HOXC8* [208]. Interestingly, in the same abstract it was reported that forced *HOXC8* expression had no effect on osteogenic differentiation or differentiation of chondroblasts from hASCs [208]. Two conflicting studies both observed enhanced osteogenesis of hASCs with miR-196a expression [206, 274]. Down-regulation of *HOXC8* in hASCs due to miR-196a overexpression was associated with decreased proliferation [206] and negative correlation was found between

miR-196a expression in bone marrow-derived MSCs and markers of proliferation [275]. *HOXB7* was confirmed as a direct target of miR-196a and massive *HOXB7* overexpression led to increased proliferation and osteogenesis of bone marrow derived MSCs. However, forced *HOXB7* expression was also associated with a reduction in miR-196a expression, and so it is difficult to extrapolate a functional role for miR-196a from this study.

4.1.4 Developmental and patterning genes in adipose tissue

As mentioned in 1.2.1, genome-wide transcriptomic studies have reported distinct transcriptional signatures between BAT and WAT [31-33] and between VAT, ASAT and GSAT [34-40]. Many of the genes identified are involved in embryological development and body patterning. In one study, developmental genes accounted for 18.4% of the gene transcripts differing between depots, and 24.7% in undifferentiated pre-adipocytes [37]. Notably, depot-specific developmental gene signatures are retained *in vitro*, both in primary pre-adipocytes [35, 39, 40] and in immortalised pre-adipocyte cell lines after multiple rounds of cell division [37, 40]. Furthermore, a large number of these differentially expressed developmental genes are up-regulated during adipogenesis in mouse embryonic stem cells indicating that they may play important roles in adipocyte development [276]. This begs the question of whether differential expression of developmental genes could be responsible for some of the functional differences seen between depots, rather than just being markers of their embryological origin.

4.1.5 The *HOX* gene family

4.1.5.1 The HOX genes as developmental patterning genes

The *HOX* gene family are a group of related transcription factors that are important in determining body patterning along the anterior-posterior (A-P) axis during embryogenesis. Within humans the 39 *HOX* genes are organised in 4 clusters on 4 separate chromosomes [277], each containing up to 13 paralogous genes [278]. All HOX proteins contain a 61 amino acid homeodomain which enables them to regulate transcription by binding to a wide range of binding sites. They display co-linearity, that is, their chromosomal arrangement in general mirrors their expression along the A-P axis. In general, 3' *HOX* genes are expressed more anteriorly and earlier in the developing embryo and 5' (posterior) *HOX* genes are dominant over 3' *HOX* genes (so called 'posterior prevalence') [279]. *HOX* genes are present in all bilateral animals and mutations in *HOX* genes tend to produce defects in a predictable body segment relating to their expression profile. In simple organisms in whom there is only a single *HOX* gene corresponding to each body segment loss-of-function mutations in *HOX* genes can cause loss of a body segment whilst gain-of-function mutations may lead to duplication of body segments or homeotic transformations, that is, one body segment mutates to resemble another (generally posterior) segment [280]. Vertebrates have paralogues of each *HOX* gene. This allows for some degree of redundancy such that mutation of only one *HOX* gene paralogue tends to cause a more subtle phenotype [281, 282]. Moreover, *HOX* gene mutations in vertebrates often fail to conform to the posterior prevalence model displayed in simple organisms [283]. Murine knock-out studies have demonstrated that most *HOX* genes are important for normal skeletal development with a

number of *HOX* genes also being necessary for normal development and function across a range of organs and tissues [284].

4.1.5.2 The HOX genes in human health and disease

Human *HOX* gene mutations have been identified that cause congenital disorders involving the nervous, cardiovascular, haemotological, gastrointestinal and urogenital systems, the limbs, skeleton and face (as reviewed in [284]). Numerous studies have identified aberrant *HOX* gene expression in neoplastic tissue [285-287] and some functional experiments have shown that abnormal *HOX* gene expression can increase tumour proliferation [288], invasiveness [289] and metastatic potential [289]. Normal *HOX* gene expression has been shown to vital to normal cell proliferation [290], differentiation [290], adhesion [291], migration [292] and apoptosis [293]. The effect of a given HOX protein can be different, or even opposite, in different tissues, in keeping with the tissue or body segment specific phenotypes observed in knock-out mutants. Indeed, the transcriptional networks regulated by HOX proteins appear to be specific to different tissues [294] and to different timings during development [295].

4.1.5.3 The HOX genes in adipose tissue

HOX have been identified in several studies as amongst the most differentially expressed mRNAs between AT depots (see below [31-33, 35, 36, 296]). *HOX* genes display striking expression patterns between VAT and SAT [35, 38], as well as between individual visceral (omental, mesenteric, perirenal) [37] and subcutaneous (abdominal, gluteal) depots [36, 39, 40]. Evidence is accumulating to suggest that the *HOX* gene family, rather than just being anatomical markers, have an active role in dictating regional AT structure and function.

Over the last decade GWAS have revolutionised the hunt for common variants that predispose to disease phenotypes. Several GWAS have focused on finding causative genes which influence obesity and body fat distribution. These studies identified a loci near *HOXA11* [90] *HOXC13* [90, 297] as associated with WHR, and both *HOXC13* and *HOXB5* as risk alleles for childhood obesity [298]. The AT expression of several *HOX* genes has also been linked with obesity, body fat distribution and changes in nutritional status. *HOXA5,* for example, appears to be a marker of upper-body WAT, being more highly expressed in VAT [35] and ASAT [39, 40]. Of particular interest is the observation that *HOXA5* expression is positively associated with BMI and WHR in humans [35], suggesting this gene could be involved in the expansion of regional WAT depots in obesity, although an opposite relationship is seen in mice [32]. In response to fasting, expression of *Hoxc9* specifically in the mesenteric AT of obese mice is markedly increased while *Hoxc8* expression decreases in both visceral and subcutaneous depots, and *Hoxa5* expression is unchanged [32]. Although it is important to note the differences observed between humans and rodents, which are likely due to the comparison of dissimilar depots, these observations make it tempting to speculate that the *HOX* network may have a functional role in determining WAT expansion. This hypothesis has been given further weight by Dankel *et al.* who demonstrated up-regulation of *HOX* genes (including *HOXA5, HOXA9, HOXB5, HOXC6*) in human AT following extreme weight loss after bariatric surgery [299]. The authors of this study also carried out promoter analysis of the genes that were differently expressed before and after weight loss. They found that 48% of the differentially expressed genes contained at least one potential HOX binding site in their promoter regions [299]. However, not all studies have observed associations between the

expression of *HOX* network genes and obesity [39]. In addition, depot-specific expression of homeobox-domain containing genes (e.g. *SHOX2*) [32] and *HOX* gene cofactors (e.g. *PBX1, PBX3, MEIS1, MEIS2*) has also been reported [39, 300]. There are also differences in HOX gene expression between WAT and BAT: *Hoxc8* and *Hoxc9* appear to be WAT-specific being more highly expressed in WAT and beige adipocytes compared to BAT [301, 302].

Using *in vitro* models, temporal changes in the expression of specific *HOX* genes have been observed during adipogenesis of 3T3-L1 cells (*Hoxa4, Hoxa7, Hoxd4)* [303] and primary human pre-adipocytes (*HOXA10, HOXB8*) [39]. However, evidence supporting a functional role for these genes in adipocyte biology remains limited. As discussed above, *HOXC8* may function as an important regulator of the WAT lineage by inhibiting brown adipogenesis [207]. By comparison, treatment of WAT adipocytes with rosiglitazone induces expression of *Hoxc9* [3].

The homeobox-domain containing gene *Shox2* displays dramatically higher expression in ASAT than in the visceral depot in both rodents and humans [304] and is more highly expressed in gluteal pre-adipocytes compared to abdominal subcutaneous [40]. The AT-specific ablation of *Shox2* in mice is reported to protect against diet-induced obesity (particularly of the subcutaneous depot) however, this was not accompanied by protection from insulin resistance [304]. The reduction in adipocyte cell size in *Shox2*-deficient mice was accompanied by markedly higher rates of lipolytic activity and increased expression of the β3 adrenergic receptor (*Adrb3*) [304]. Lee *et al.* went on to demonstrate that *Shox2* directly interacts with *CEBPa* to repress its activation of *Adrb3*. *HOX* cofactors include the *PBX* and *MEIS* gene classes that appear to enhance *HOX* gene DNA-binding specificity [305, 306]. *Pbx1*-

deficient MSC derived from mouse embryos are unable to generate adipocytes [307]. Conversely, the opposite results are seen in human post-natal hASCs, where knock-down reduced proliferation and enhanced adipogenesis. The authors propose that *Pbx1* plays a complex role in the generation and maintenance of pre-adipocytes [307]. Interestingly, *Pbx1* has also been shown to attenuate osteogenesis in MSC by binding to *Pbx* sites in the promoters of osteoblast-related genes and impairing their transcriptional activation by *Hoxa10* [308]. Thus the *PBX* genes would appear to play important roles in cell fate determination. Transcriptional network analysis has identified *PBX1* and the related HOX cofactor, *MEIS1,* as two transcription factors which are up-regulated during mesenchymal embryonic stem cell (mESC) adipogenesis [276]. Furthermore, *in silico* prediction of transcription factor binding sites amongst genes co-expressed during mESC adipogenesis identified an over-representation of the *MEIS1* binding motif [276]. The MEIS family appear to regulate Hox protein-DNA binding specificity by forming heterotrimeric complexes with the *Hox* and *Pbx* genes [305]. A mechanism of action for *Meis1* and *Meis2* has not yet been determined in AT however knock-down of another family member, *Prep1,* has been shown to have an inhibitory effect on adipogenesis [309]. These findings demonstrate the potential for Homeobox genes to regulate regional AT function and thus contribute to body fat distribution.

4.1.6 miR-196a and the HOX genes

Interestingly, whilst *HOX* expression is turned on or off to dictate body pattern in simple organisms, it is thought that quantitative differences in *HOX* expression are important for development of the complex tissues found in higher order species [310, 311], a mechanism

that could be performed by miRNA regulation. Indeed, miRNAs expressed from within the *HOX* clusters have been bioinformatically predicted to preferentially target *HOX* gene encoded mRNAs located in the 3' direction above other mRNA targets [312]. For these reasons the genomic location of the mir-196 paralogues makes it an attractive candidate for further study.

4.1.7 Hypotheses and aims

In this thesis I hypothesise that miRNAs are important for regulating AT depot-specific deposition and function, and that it may be acting through regulation of HOX protein family. I aim to identify and characterise the regulatory role of miR-196a in human WAT. Having established miR-196a to be differently expressed between ASAT and GSAT I aimed to further characterise its expression patterns. Specifically, in this chapter, I aim:

1. To determine the relative expression of miR-196a across a range of human tissues.
2. To measure the expression of miR-196a in human whole ASAT, GSAT and VAT and in the component fractions of WAT.
3. To investigate the relative expression of the miR-196 paralogues in WAT.
4. To use pre-adipocyte isolation and culture to determine whether miR-196a expression is intrinsic to cells or regulated by the in vivo environment.
5. To determine expression of *HOX* targets of miR-196a in AT and pre-adipocytes to investigate whether it may be acting via *HOX* gene regulation.
6. To use *HOXC*-locus expression profiling to investigate whether miR-196a is likely to be co-regulated with surrounding *HOX* genes.

4.2 Materials and methods

4.2.1 miR-196a expression in fractions of adipose tissue

4.2.1.1 RNA extraction from adipocytes and stromovascular fraction

A whole ASAT needle biopsy was separated into mature adipocytes and SVF as follows. The biopsy was taken as per usual protocol (see 2.1.1), washed in HBSS and then incubated with 1mg/ ml collagenase in HBSS in a shaking water bath (60 rpm) at 37 °C for 45 minutes. The digested AT was centrifuged at 1000xg for 5 minutes at 4 °C. The digest was then separated into a layer of oil on the surface, a layer of adipocytes, supernatant and the SVF pellet. The oil was discarded and the adipocyte layer collected and washed by centrifugation in HBSS. The SVF pellet was isolated and red blood cells lysed with lysis buffer (155 mM ammonium chloride, 10 mM potassium bicarbonate, 0.1 mM EDTA). Tri-reagent was added to the isolated adipocyte layer and SVF for subsequent RNA extraction.

4.2.1.2 THP-1 cell line

The THP-1 cell line (ATCC, Teddington, UK) is a human monocyte cell line derived from the blood of a one year old boy with acute monocytic leukaemia [313]. Cells were cultured in suspension with RPMI-1640 (Sigma, UK) with 2 mM L-glutamine and 10% FBS and were sub-cultured to maintain them at a density of less than $1x10^6$ cells/ ml. For differentiation THP-1 cells were plated in 6-well plates with 100ng/ ml of phorbol myristate acetate (PMA) in usual culture media for 24 hours, followed by 48 hours in usual culture media.

4.2.1.3 cDNA synthesis and qPCR

RNA from adipocytes and SVF was isolated using the Tri-reagent total RNA method (described in 2.3.2.2.2). cDNA was synthesised using the Qiagen miScript kit and Qiagen miScript primers were used for measurement of transcripts. In adipocytes and SVF miR-196a was normalised to the average expression of the reference transcripts as described in 2.3.2.8 (miR-103, miR-24 and miR-331).

4.2.2 Summary of adipose tissue panels

The MHO panel is described in 2.1.2. cDNA was synthesised using Qiagen miScript kit and miR-196a was quantified using the miScript assay (as in Chapter 2). The OBB ASAT/GSAT panel is described in 3.2.2.1; RT-qPCR was performed using Taqman individual primer and assay as described in 2.3.2.6.

4.2.3 Pre-adipocyte differentiation time-courses

Abdominal and gluteal Pt2 pre-adipocyte cell lines at passages 6 to 8 were plated in 6-well plates at a density of $2x10^5$ cells/well. The day after plating, growth media were exchanged for differentiation media according to usual protocol: this is referred to as day 0. Cells were harvested in 500µl Tri-reagent and RNA was extracted using the Tri-reagent total RNA method described in Chapter 2. cDNA synthesis and qPCR were performed using the Qiagen miScript kit and Qiagen miScript primer assays (described in 2.3.2.6.1).

Primary pre-adipocytes differentiation time-courses and RNA isolation were performed by Dr Marijana Todorcevic. Pre-adipocytes were isolated from paired ASAT and GSAT needle biopsies from 3 male and 3 female volunteers in the OBB using the methods described in 2.2.1. Cells were seeded at low density and wells were harvested during proliferation. Growth

media were replaced with differentiation media when cells reached confluence. Differentiation time-courses, RNA extraction, cDNA synthesis and qPCR were as described above.

4.2.4 Bioinformatic miR-196a target prediction

Computational prediction of mRNAs targeted by miR-196a was performed using DIANA-microT-CDS (http://diana.imis.athena-innovation.gr) [314], TargetScan 6.2 (http://www.targetscan.org/) [315] and PicTar (http://pictar.mdc-berlin.de) [316]. Default settings were used. Lists of target predictions reaching significance for the three programmes were compared for overlap. MiRTarbase 4.5 [317] (http://mirtarbase.mbc.nctu.edu.tw/) was searched for experimentally verified miR-196a targets.

4.2.5 Statistical methods

For paired samples where two AT biopsies were obtained from the same subject but from different AT depots the mean of paired-fold-changes was calculated and paired t-Tests or Mann-Whitney U tests were used as appropriate to determine statistical significance.

To assess correlations between miR-196a expression and anthropometric and biochemical traits data were LN-transformed and partial correlations performed with adjustment for BMI. Correlations between paralogues of miR-196 were calculated using Pearson's correlations.

4.3 Results

4.3.1 Relative expression of miR-196a in different human tissues

A literature search was conducted to find studies examining genome-wide miRNA expression across a range of different human tissues (including AT). Two studies were identified that

made normalised miRNA expression profiling available in the supplementary materials. Parts *et al.* [138] performed small RNA sequencing on 131 women from TWINSUK who were included in the MuTHER consortium. They compared relative miRNA expression levels in AT to publically available small RNA sequencing data for a number of other human tissues. As shown in Figure 4.4 miR-196a is highly expressed in AT, muscle and kidney. This mirrors the findings of Liang *et al.* [318] who used qPCR to determine expression of 345 miRNAs across 40 human tissues (Figure 4.5). Figure 4.5 also demonstrates the different tissue-wide expression profiles of miR-196a and miR-196b.

Figure 4.4: log_2-normalised miR-196a in human tissues. Graphical representation of analysis by Parts *et al.*[138].

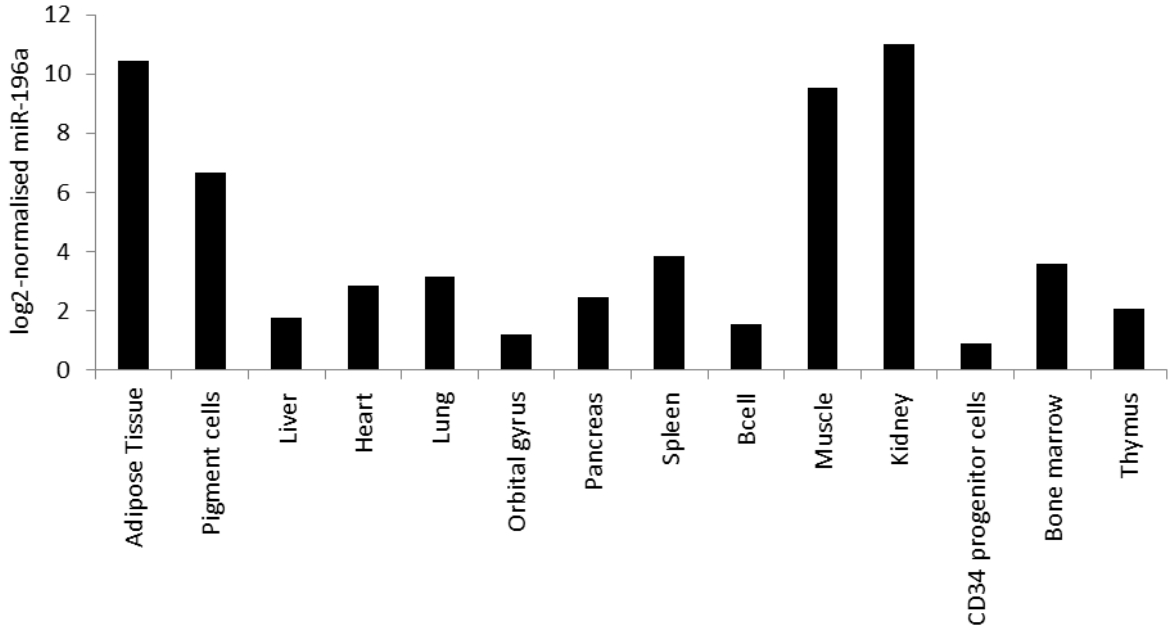

Figure 4.5: Expression of miR-196a and miR-196b in human tissues. Graphical representation of supplementary data from Liang *et al.*[318].

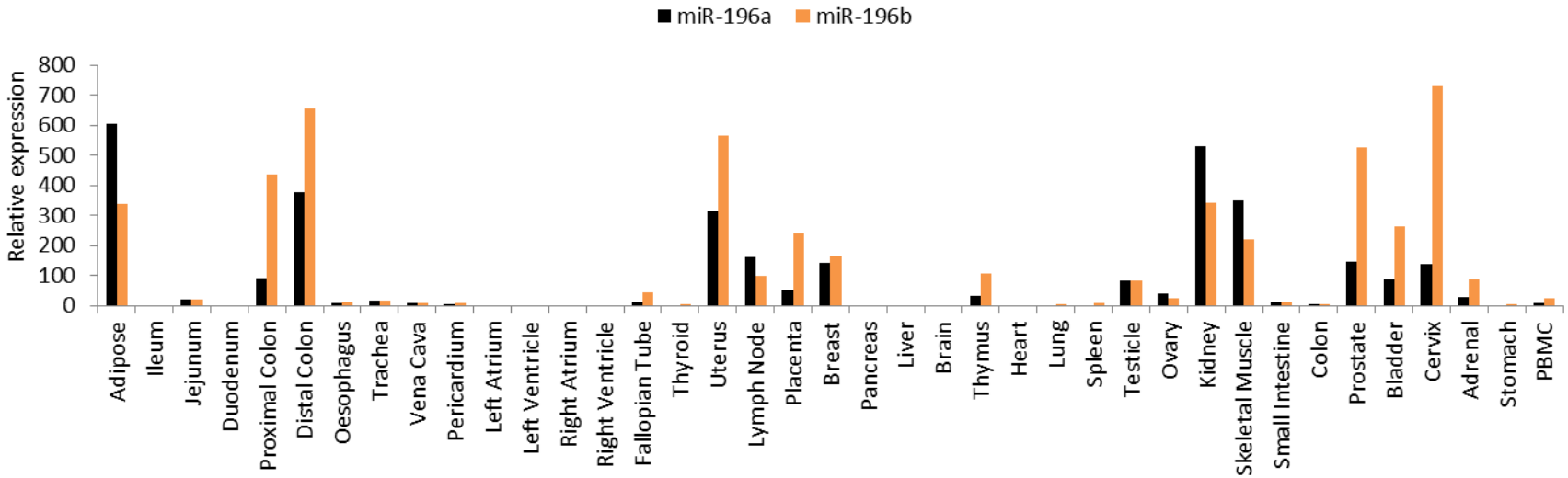

4.3.2 Expression of miR-196a in the component fractions of adipose tissue

Whole AT is a complex tissue composed of heterogeneous cells, including pre-adipocytes, adipocytes and macrophages. It was important to determine the relative expression of miR-196a in the component cell fractions of AT in order to determine which cell type should primarily be studied in functional experiments.

As discussed on page 129, *in vitro* differentiation time-courses demonstrated rising expression of miR-196a through adipogenesis (Figure 4.15). The expanded *in vitro* 'pre-adipocyte' population of both primary cells and the Pt2 cell lines would in fact represent a mixed population of fibroblasts, MSC and pre-adipocytes, with only those cells committed to an adipocyte lineage undergoing adipogenesis. Fractionation of one whole ASAT biopsy confirmed higher expression of miR-196a in the isolated adipocyte fraction than in the SVF (Figure 4.6).

SVF contains macrophages along with pre-adipocytes, MSC, fibroblasts and other immune cell types. AT can contain a large number of macrophages, particularly in obesity [9]. Therefore, I also quantified miR-196a expression in the THP-1 cell line. This is a human monocyte cell line that had been differentiated *in vitro* to have a macrophage-like phenotype. Macrophage miR-196a could not be compared directly with whole AT or pre-adipocyte RNA because different reference genes were used for normalisation. Relative abundance was estimated by synthesising cDNA for the different cell types in parallel using equal input RNA quantities and selecting a common CT threshold. This method revealed that the average CT for expanded pre-adipocytes isolated from ASAT was 30.7 vs 32.0 for THP-1 cell line. Thus, pre-adipocytes appear to have higher intrinsic miR-196a expression, especially when it is considered that CT values are on a logarithmic scale.

Figure 4.6: miR-196a expression in the SVF and adipocyte fractions of ASAT (n=1).

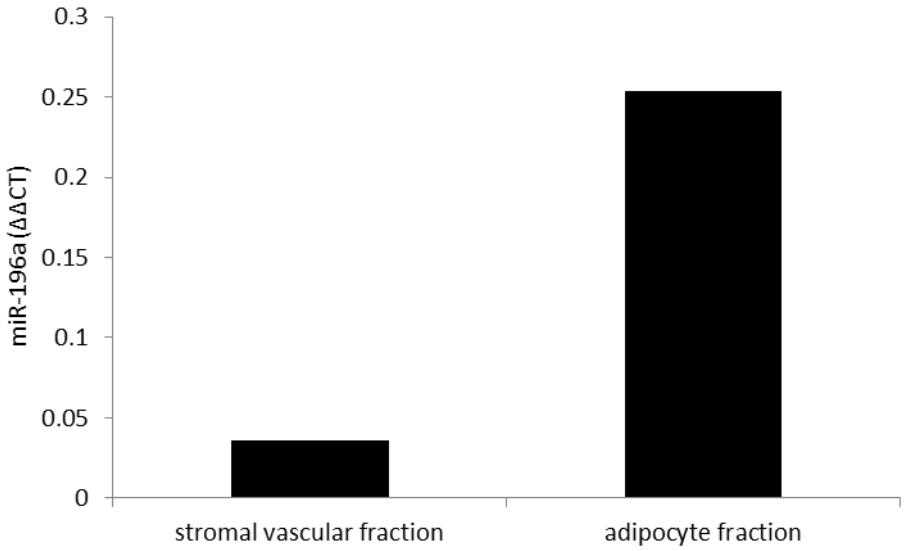

4.3.3 Expression patterns of miR-196a in human adipose tissue depots

4.3.3.1 Mature miR-196a

Table 4.1 summarises the expression of miR-196a in paired ASAT and GSAT, and in paired ASAT and VAT. The compositions of the panels are described on page 112.

MicroRNA-196a expression was confirmed by qPCR to be 2.34-fold higher in GSAT than in ASAT ($p<0.001$). There was no evidence that miR-196a was regulated according to BMI or gender. Although there was a degree of correlation between miR-196a in ASAT and GSAT this was not statistically significant, suggesting different regulation in the two depots (Figure 4.7).

Expression of miR-196a was significantly lower in VAT than in SAT. Within VAT expression of miR-196a was low but detectable (average CT in the MHO panel of 31.2). The MHO cohort comprised 8 obese females with metabolic complications of obesity and 8 metabolically healthy obese women; depot-difference in miR-196a expression was consistent in both groups and did not differ according to the metabolic profile (ASAT: $p=0.49$; VAT: $p=0.61$).

4.3.3.2 Correlations of miR-196a with metabolic and anthropometric parameters

There was significant positive correlation between miR-196a expression in GSAT, but not ASAT, and WHR after adjustment for BMI (Figure 4.8.A). This was driven by a positive correlation between GSAT miR-196a expression and waist circumference, but not hip circumference (Figure 4.8.B and C). In line with this, positive correlations were observed between miR-196a and TAG and cholesterol, with the latter apparently mediated through LDL cholesterol. These did not retain statistical significance after correction for WHR. Circulating glucose and insulin concentrations were not correlated with AT miR-196a expression.

Table 4.1: mRNA expression profiling of miR-196a using q-PCR.

Panel	Comparison	N	Paired fold-change	p-value
OBB lean/obese	GSAT/ASAT	40 paired ASAT and GSAT	2.34 (higher in GSAT)	p<0.001
	BMI	20 lean, 20 obese	0.96	p=0.62
	Gender	20 M, 20 F	1.18 (higher in M)	p=0.065
MHO	VAT/ASAT	16 paired ASAT and VAT	0.04 (higher in ASAT)	p<0.001

Figure 4.7: Correlation between miR-196a in ASAT and GSAT from the same individuals (n=40).

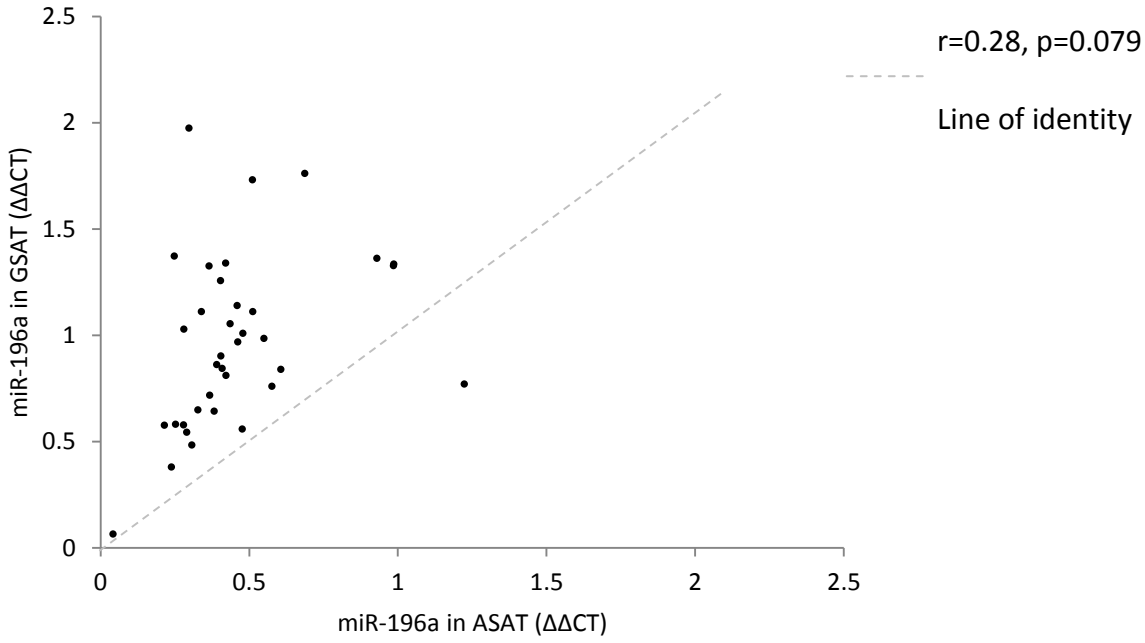

Figure 4.8: Correlations between miR-196a expression in both ASAT and GSAT and anthropometric and biochemical variables. Based on data from paired ASAT and GSAT biopsies from 40 individuals in the OBB lean/obese panel. Figures represent the correlations between miR-196a expression in both ASAT and GSAT with: A. WHR . B. Waist circumference C. Hip circumference D. Total cholesterol E. LDL cholesterol F. HDL cholesterol G. Triglycerides (TAG) H. Glucose I. Insulin. Statistics are for partial correlations adjusted for BMI.

A.

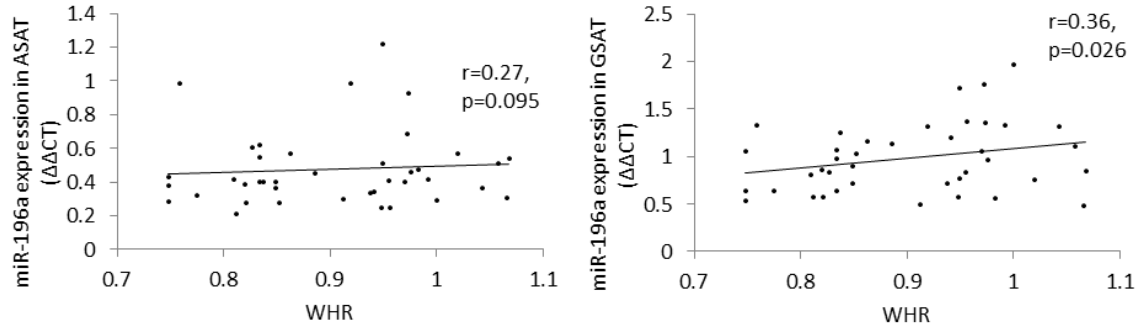

B.

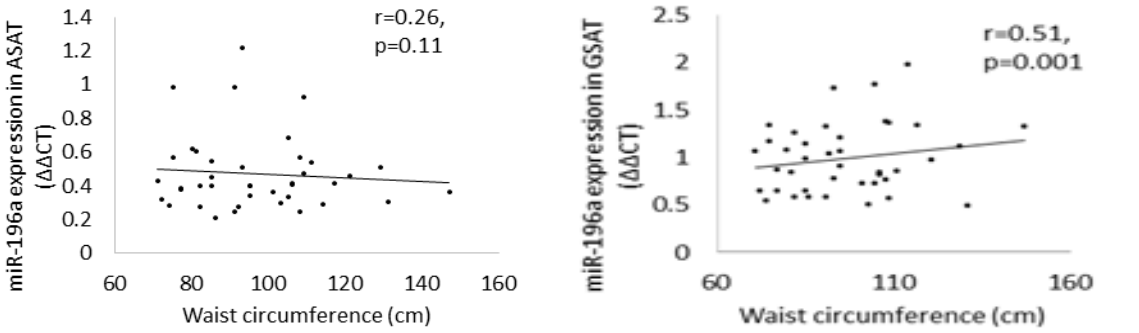

C.

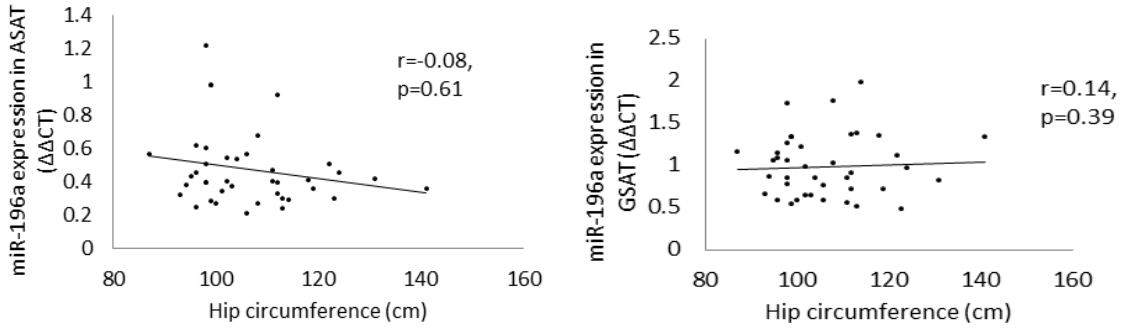

D.

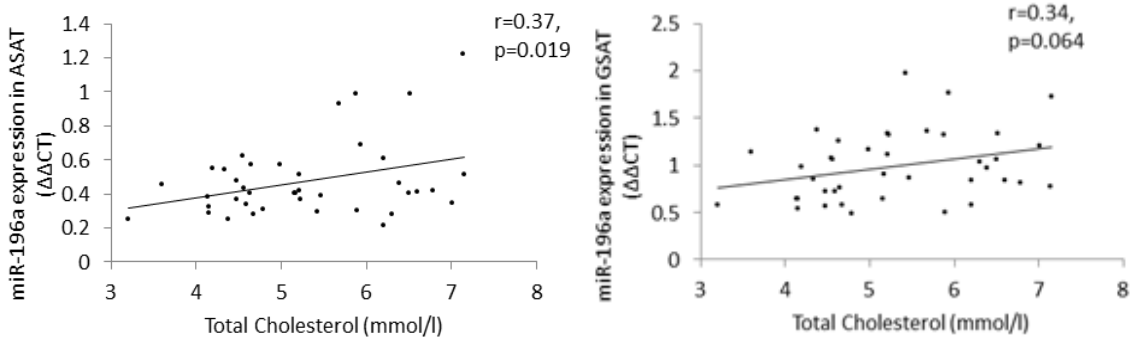

E.

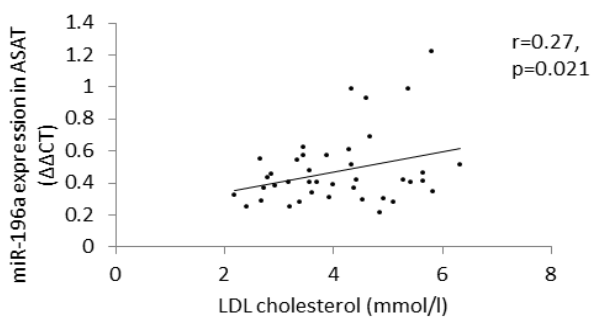
miR-196a expression in ASAT (ΔΔCT)
r=0.27,
p=0.021
LDL cholesterol (mmol/l)

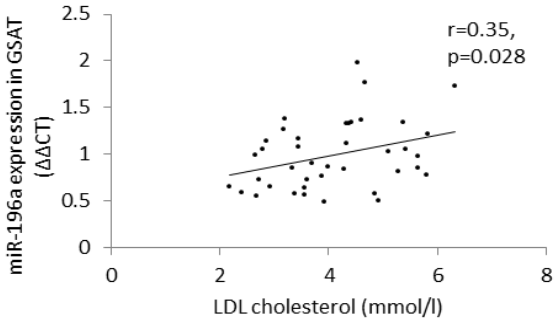
miR-196a expression in GSAT (ΔΔCT)
r=0.35,
p=0.028
LDL cholesterol (mmol/l)

F.

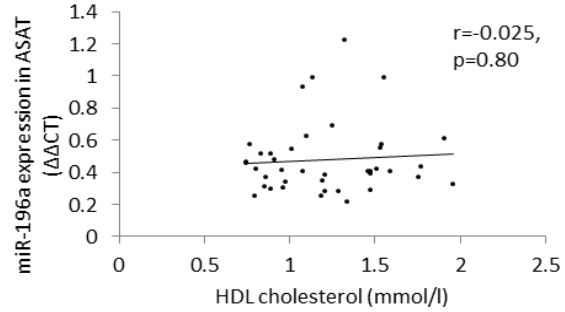
miR-196a expression in ASAT (ΔΔCT)
r=-0.025,
p=0.80
HDL cholesterol (mmol/l)

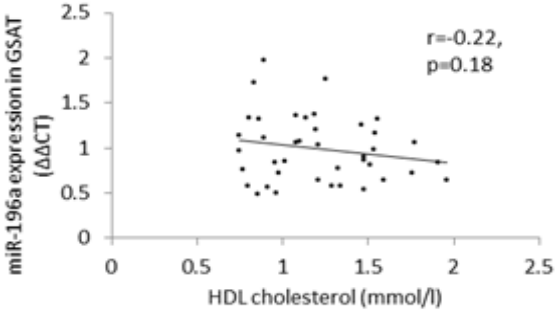
miR-196a expression in GSAT (ΔΔCT)
r=-0.22,
p=0.18
HDL cholesterol (mmol/l)

G.

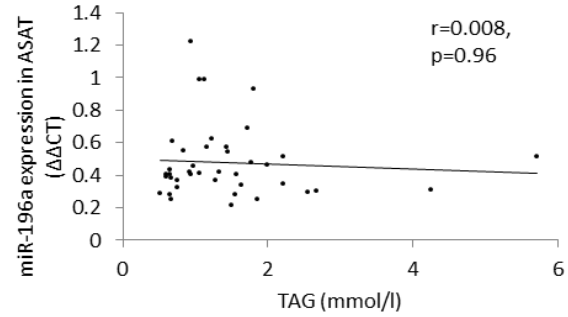
miR-196a expression in ASAT (ΔΔCT)
r=0.008,
p=0.96
TAG (mmol/l)

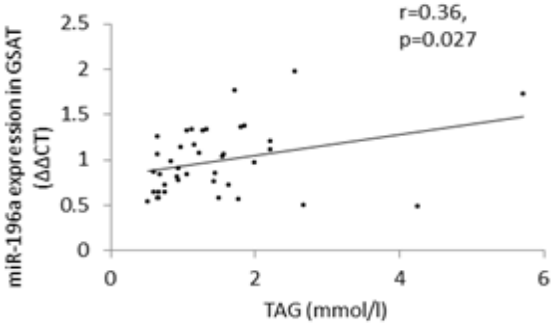
miR-196a expression in GSAT (ΔΔCT)
r=0.36,
p=0.027
TAG (mmol/l)

H.

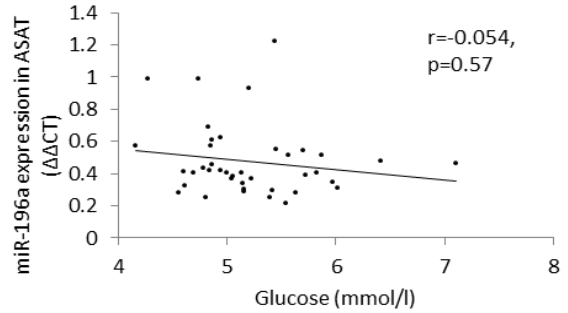
miR-196a expression in ASAT (ΔΔCT)
r=-0.054,
p=0.57
Glucose (mmol/l)

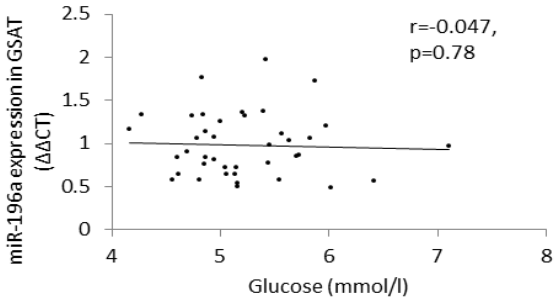
miR-196a expression in GSAT (ΔΔCT)
r=-0.047,
p=0.78
Glucose (mmol/l)

.

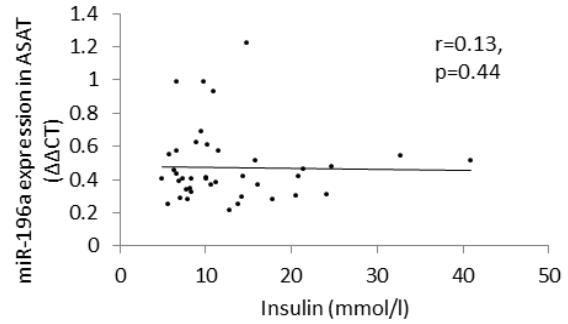
miR-196a expression in ASAT (ΔΔCT)
r=0.13,
p=0.44
Insulin (mmol/l)

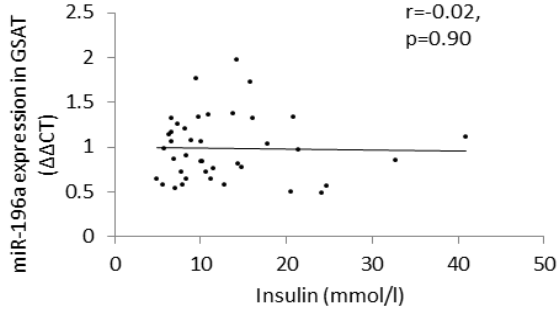
miR-196a expression in GSAT (ΔΔCT)
r=-0.02,
p=0.90
Insulin (mmol/l)

4.3.3.3 Relative expression of miR-196a-5p, miR-196a-3p and miR-196b

Data from qPCR experiments were used to estimate the relative expression of the miR-196 paralogues miR-196a-5p, miR-196a-3p and miR-196b. miR-196a-5p is the dominant strand and is referred to simply as miR-196a throughout this thesis. MiR-196a-3p is the complementary strand derived from the opposite arm of the precursor. Replicate plates of cDNA were used and assay efficiency was checked to ensure it was comparable for the different assays. A common threshold was selected for the analysis of plates.

Using a common threshold the mean CT of miR-196a-5p was 28.3 (SE 0.3) in whole ASAT and 27.3 (SE 0.5) in GSAT, whilst mean CTs of miR-196a-3p in ASAT and GSAT respectively were 32.2 (SE 0.2) and 32.4 (SE 0.2). This indicates that the expression of miR-196a-3p is around 10 to 15-fold lower than that of miR-196a-5p. Similarly, using whole ASAT from the MHO panel mir-196b was detectable at an average CT of 31.9 (SE 0.9) compared to an average CT of 28.4 (SE 0.8) for miR-196a, suggesting that miR-196b expression is around 25-fold lower than miR-196a.

Within the Pt2 pre-adipocyte cell line differences in expression were more marked: miR-196a was detected at a mean CT of 23.8 (SE 1.4) and 22.8 (SE 1.1) in abdominal and gluteal Pt2 cell lines respectively, whilst miR-196b was detected at a mean CT of 29.6 (SE 0.6) in the abdominal line and 29.3 (SE 0.7) in the gluteal line. This represents a 60-fold difference in expression. These data suggest that the pre-adipocyte and adipocyte cell populations make a greater contribution to whole AT miR-196a expression than to miR-196b expression.

Publically available qPCR and sequencing data were accessed to confirm these findings [138, 318, 319]. Liang *et al.* [318] and Mestadgh *et al.* [319] reported the expression of miR-196b in human AT to be 2- and 4-fold lower than miR-196a, whilst Parts *et al.* [138]

reported that the paralogues had similar expression. MiR-196a-3p expression was reported to be several hundred-fold lower [138, 319]. Despite some discrepancies in the magnitude of the fold-changes these data support the conclusions that the expression of miR-196b is lower or similar to that of miR-196a whilst that of miR-196a-3p is negligible.

4.3.3.4 Pre-miR-196a-1 and pre-miR-196a-2

The mature miR-196a paralogues produced from the mir-196a-1 and mir-196a-2 genes are identical in sequence and as such cannot be distinguished by qPCR. However, the sequences of pre-miR-196a-1 and pre-miR-196a-2 are unique. Precursor expression was assessed by qPCR in the OBB panel and in the Pt2 cell lines in order to estimate which paralogue was dominantly expressed.

Pre-mir-196a-1 was not detected in whole AT from the OBB ASAT/GSAT panel. As shown in Figure 4.9 pre-miR-196a-2 demonstrated a depot specific expression pattern mirroring that seen with mature miR-196a (2.4-fold higher in gluteal fat, p=0.006). Both paralogues were expressed in the Pt2 pre-adipocyte cell line and again pre-miR-196a-2 was more highly expressed than miR-196a-1 (Ct=31.3 vs 33.4 using common threshold).

Relative quantitation of miRNAs performed in this way only allows for estimation of the relative amounts of transcript present. Additionally, correlation between expression of precursor and mature microRNA is variable [320]. With these limitations in mind these results suggest that miR-196a-2 is the paralogue predominantly expressed in human AT.

Figure 4.9: Expression of A. miR-196a and B. pre-miR-196a-2 in the OBB panel.

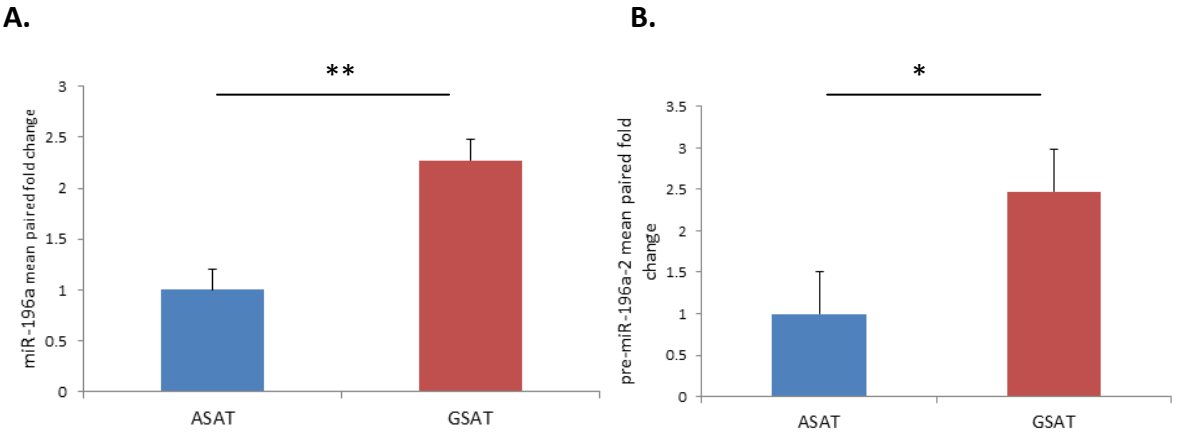

Figure 4.10: Expression of A. pre-miR-196a-1 and B. pre-miR-196a-2 in the Pt2 abdominal and gluteal pre-adipocyte cell lines

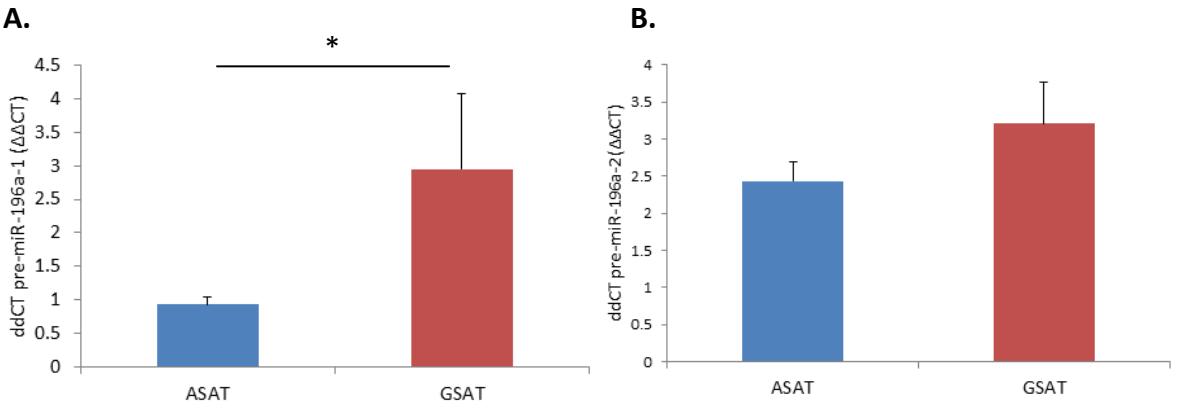

4.3.4 Targets of miR-196a

4.3.4.1 Bioinformatic prediction of putative miR-196a targets

There are a multitude of free web-based programs available for predicting miRNA-mRNA interactions. To predict mRNA targets of miR-196a I selected three well evaluated programs that use different algorithms. DIANA-microT-CDS [314] (http://diana.imis.athena-innovation.gr) and TargetScan 6.2 [315] (http://www.targetscan.org/) were selected because recent experimental evaluation found them to have greater sensitivity than a number of other softwares [321], whilst PicTar [316](http://pictar.mdc-berlin.de) was found to have the highest specificity [321].

All three methods consider free energy of the miRNA-mRNA duplex. TargetScan also takes into account the AU content (the concentration of A and U bases flanking the mRNA target site, which is correlated with more effective miRNA repression [322]). DIANA-microT-CDS identifies miRNA recognition elements within both the 3'UTR and the coding region (CDS) and is the only one to look for complementarity at multiple sites in the mRNA. Common miRNA-mRNA interactions are defined as 6-mer, 7-mer and 8-mer: 6-mer refers to a perfect match between 6 nucleotides of the miRNA seed sequence and the mRNA, 7-mer refers to a 6 nucleotide match with a miRNA-mRNA match at nucleotide 8 (7-mer m8) or an additional adenine at position 1 (7-merA1). Finally, 8-mer site comprises the seed match with both the m8 and the A1 nucleotide matches. Seed matches are illustrated in Figure 4.11. TargetScan looks for conserved 7mer and 8mer sites in the mRNA that are complementary to the seed sequence. PicTar searches just for 7mer sites.

Figure 4.11: A. 7-mer-A1, B. 7mer-m8 and C. 8mer miRNA-mRNA seed matched sites. Reproduced from Bartel et al. [323] with permission.

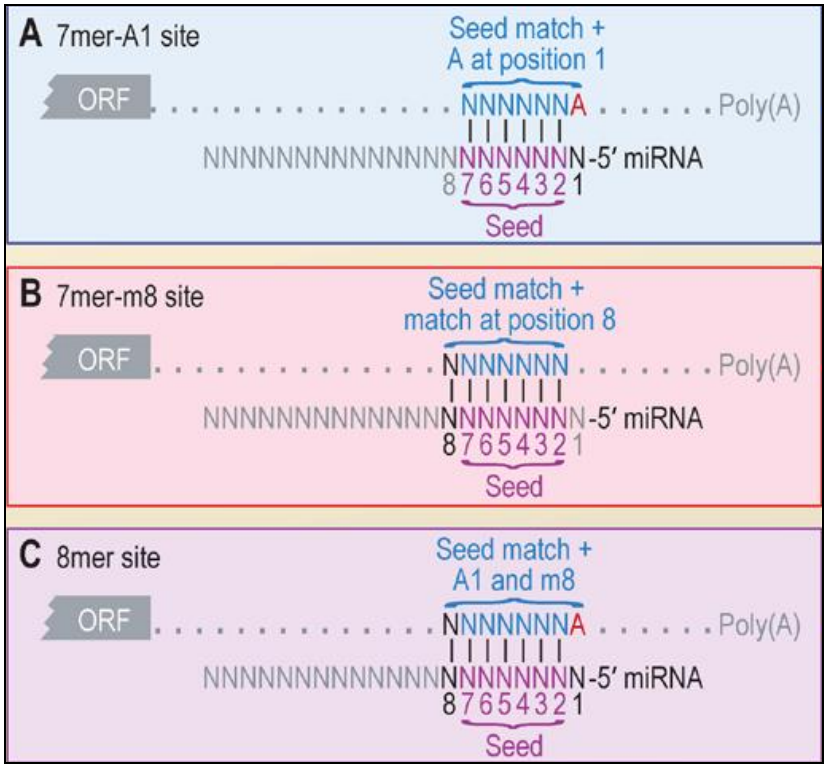

miRTarbase 4.5 [317] (http://mirtarbase.mbc.nctu.edu.tw/) is a curated database of over 50,000 miRNA targets with supporting experimental evidence. It currently represents the most extensive database of its kind. Evidence is considered strong or less strong depending on the validation method used. Strong evidence includes luciferase or green fluorescent protein (GFP) reporter assay, qPCR and Western blot, whilst less strong evidence includes microarray, high-throughput sequencing and pulsed stable-isotope labelling by amino acids in cultured cells (pSILAC).

A total of 502 target mRNAs were predicted by DIANA-microT-CDS, 295 by TargetScan and 125 by PicTar. Figure 4.12 demonstrates the degree of overlap between target transcripts predicted by the three algorithms. Table 4.2 lists transcripts that were predicted to be targeted by miR-196a by all three or by any 2 of the programmes. Transcripts with 'strong evidence' of miR-196a reported on miRTarbase are indicated by underlining in Table 4.2.

Figure 4.12: Venn diagram showing the degree of overlap in target prediction for miR-196a between DIANA-microT-CDS, TargetScan and PicTar. Diagram produced using Venny (http://bioinfogp.cnb.csic.es/tools/venny/).

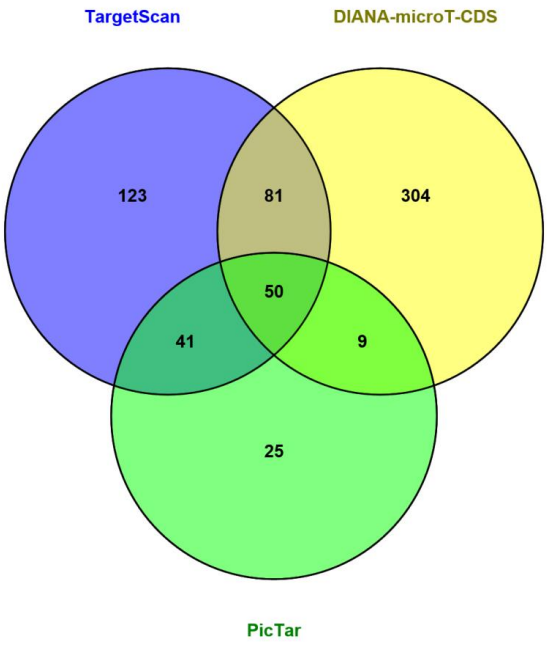

Table 4.2: Overlapping mRNA targets predicted by DIANA-microT-CDS, TargetScan and PicTar. Targets with strong supportive evidence recorded on miRTarbase 4.5 (reporter assay, qPCR or Western blot) are underlined.

mRNAs predicted to be targeted by miR-196a by all three prediction programs
AQP4, BACH1, CALM1, CALM3, CBFA2T3, CCDC47, CCNJ, CDKN1B, CDYL, CECR6, COL1A2, COL24A1, COL3A1, CPD, EPHA7, EPS15, ERG, EYA4, FAM55C, GAN, GAS7, GATA6, GPCPD1, HAND1, HOXA5, HOXB6, HOXB7, HOXC8, ING5, LCOR, LIN28A, LRP1B, MAP4K3, MGAT4A, NRAS, NRXN1, PBX3, PDGFRA, PPP1R15B, RSPO2, SETD8, SLC9A6, SMAD6, SMARCC1, SNX16, SSR1, TSPAN12, UHRF2, ZDHHC21, ZMYND11
mRNAs predicted to be targeted by miR-196a by two out of the three prediction programs
ABCB9, ABL1, ACSL6, ADCY9, AFF2, ARHGAP28, BCAT1, BIRC6, C20ORF160, CALM2, CASK, CDV3, CELF2, CEP350, CLCN5, COL1A1, CPM, CREBL2, CTPS, DCAF15, DCDC2, DDX19A, DDX19B, DICER1, DIP2A, DIRC2, DOC2A, DOCK3, E2F7, EEA1, ELF4, EPC2, EPHA3, ERLIN2, EXOC5, EXOC8, FAM127B, FAM19A5, FLRT1, GALC, GCNT4, GLTP, GSPT1, HABP4, HDX, HMGA1, HMGA2, HOXA7, HOXA9, HP1BP3, IGDCC4, IGF2BP1, IGF2BP3, IMPAD1, KCNJ2, KCNQ5, KCTD21, KIAA1274, KLHL23, LARP4, LCORL, LIN28B, LOR, LRIG2, LRRTM3, MAP3K1, MBNL2, MECP2, MRS2, NAP1L1, NEDD4L, NME4, NRK, NTN4, OPCML, OSMR, OTUD6B, OTX1, PACRGL, PAPOLG, PARD6B, PAX7, PBX1, PHF20, PLDN, POLR3D, PPAPDC2, PPP1R16B, PRTG, PTPRG, RAD23B, RANBP10, RANBP2, RAPGEF5, RASGRP1, RAVER2, RCC2, RGL2, RIOK3, RNF5, RPGRIP1L, RXFP2, SAPS2, SCHIP1, SDCBP, SEMA3A, SFMBT1, SLC31A1, SLC35D2, SMCR7L, SMCR8, SNTB2, SOCS4, SORCS1, SOX11, SOX12, SPRED1, STEAP2, SYNCRIP, SYT9, TMEM143, TMEM194A, TOX3, TRERF1, USP15, VSNL1, WDR37, YOD1, ZBTB26, ZNF507, ZNF710

4.3.4.2 Expression of the HOX genes

miR-196a is predicted computationally and experimentally to target the HOX genes *HOXA5* [226], *HOXB8* [227, 228] and *HOXC8* [207, 229]. The mRNA expression of these genes was investigated by qPCR in the OBB ASAT/GSAT and MHO panels (Figure 4.14) and in the primary and immortalised pre-adipocyte differentiation time-courses (Figure 4.15). Expression of miR-196a was higher in GSAT than ASAT, whilst expression of its proposed *HOX* targets was lower in GSAT than ASAT, consistent with possible regulation by miR-196a. However, when comparing VAT and ASAT the picture was less convincing. MiR-196a is expressed at low levels in VAT compared with ASAT. Expression of *HOXA5* and *HOXB8* was non-significantly higher in VAT than in ASAT, whereas expression of *HOXC8* mRNA mirrored that of miR-196a. Moreover, when examining individual samples there was no

clear correlation between miR-196a expression and mRNA expression of the *HOX* genes in individual SAT depots (Figure 4.13). Whilst protein expression was not examined, the lack of an inverse association suggests that miR-196a regulation is not directly responsible for depot-differences in *HOX* expression.

4.3.5 Depot specific expression of miR-196a and the *HOX* genes is maintained *in vitro*

The depot-specific expression patterns of miR-196a and *HOXA5 and HOXB8* were replicated in both primary pre-adipocytes derived from paired ASAT and GSAT and in immortalised pre-adipocyte cell lines, suggesting their expression is intrinsic to pre-adipocytes rather than being a function of their environment. Isolated pre-adipocytes did not exhibit a marked depot difference in *HOXC8* mRNA expression, perhaps suggesting that other cellular components of AT are responsible for whole AT regional expression differences in *HOXC8.* Again, there was no negative correlation between miR-196a and *HOXA5, HOXB8* and *HOXC8* mRNA.

Figure 4.13: Correlation between miR-196a in A. ASAT and B. GSAT and *HOXC8* mRNA in 40 individuals in the OBB ASAT/GSAT panel. Similar correlations were observed for *HOXA5* and *HOXB8*.

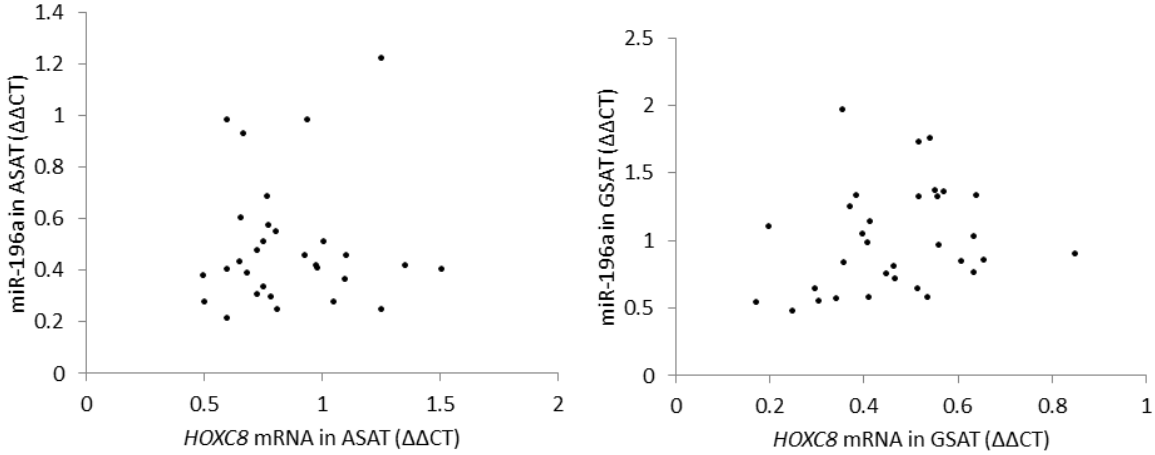

Figure 4.14: Expression of miR-196a and its HOX gene targets in human AT depots. Paired fold-changes are calculated relative to expression in ASAT and statistical significance refers to comparison in expression between either VAT or GSAT and ASAT.

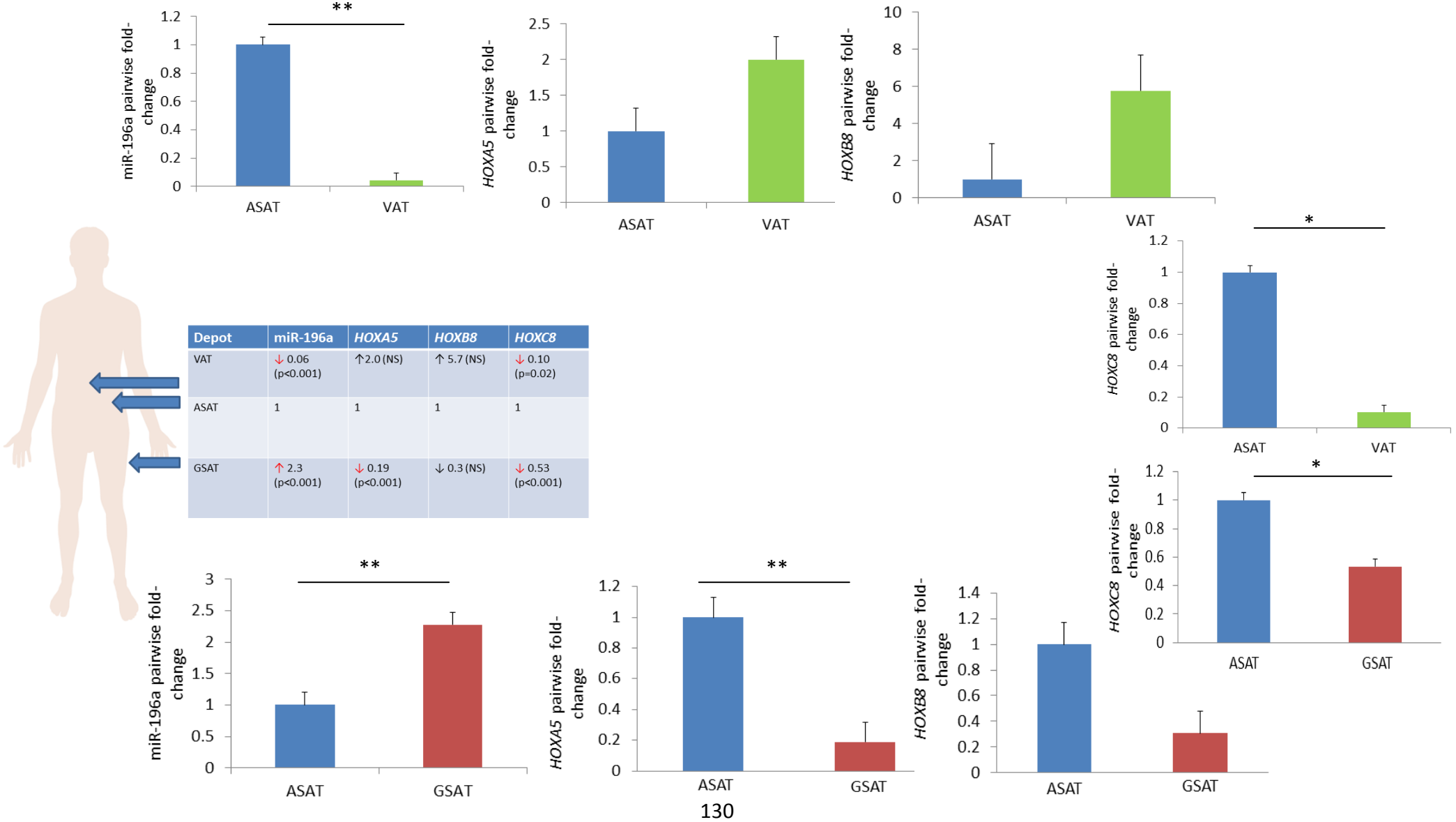

Figure 4.15: Expression of miR-196a and *HOXA5, HOXB8* and *HOXC8* through proliferation and adipogenic differentiation of primary pre-adipocytes (LEFT) and through adipogenic differentiation of immortalised Pt2 cell lines (RIGHT).

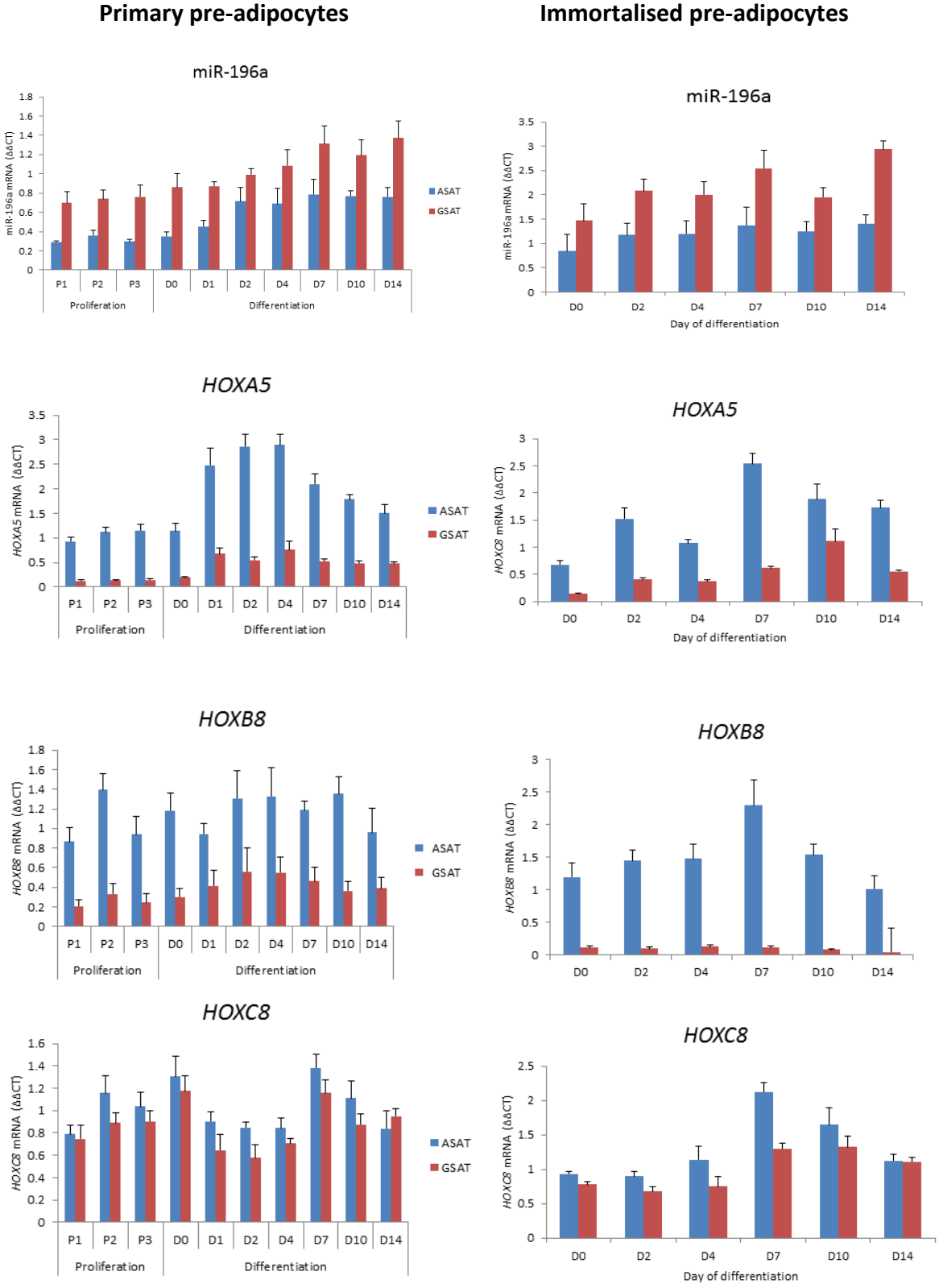

4.3.6 Expression patterns of the genes neighbouring miR-196a-2 on chromosome 12

Little is known about the promotion of miR-196a-2. In order to investigate whether miR-196a is co-expressed along with its neighbouring *HOX* genes the expression of the *HOX* genes located adjacent to miR-196a-2 was determined by qPCR in the OBB ASAT/GSAT panel (Figure 4.16). Although miR-196a had similar depot-specific expression patterns to *HOXC10* there was no correlation between expression of miR-196a and either *HOXC9* or *HOXC10,* suggesting independent regulation (Figure 4.17). Similar patterns were observed in ASAT.

Figure 4.16 Expression patterns of miR-196a-2 and its neighbouring *HOX* genes on chromosome 12. Expression was assessed by qPCR in the OBB lean/obese panel. Paired GSAT/ASAT fold-changes are shown.

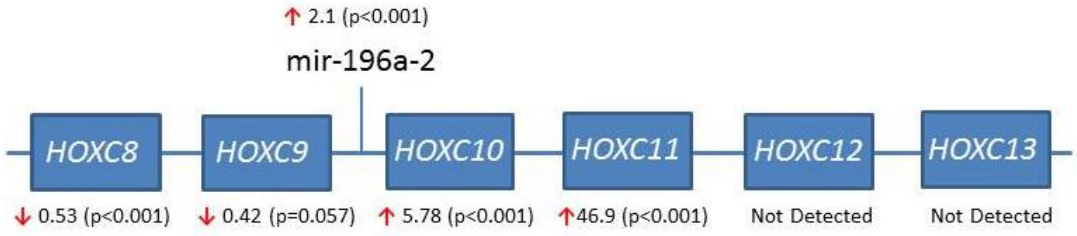

Figure 4.17: Correlation between miR-196a expression and A. *HOXC9* and B. *HOXC10* expression in GSAT.

A. **B.**

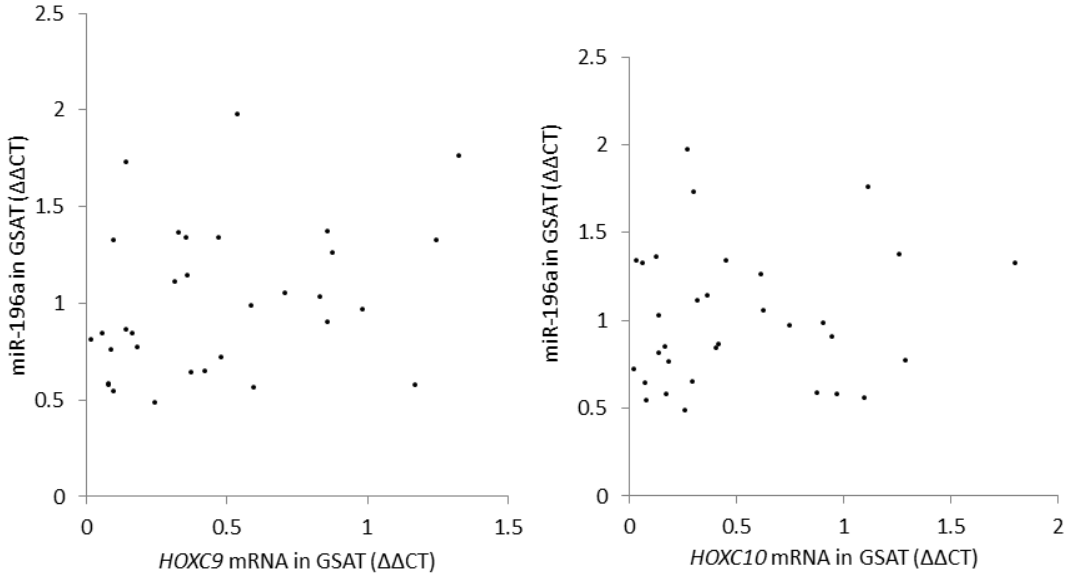

4.4 Discussion

The experiments in this chapter have demonstrated the following:

- miR-196a expression in AT is high in comparison to other human tissues.
- Within AT, miR-196a is most highly expressed in the mature adipocyte fraction.
- miR-196a is differentially expressed between AT-depots.
- miR-196a-5p is highly expressed in AT and pre-adipocyte cell lines compared to miR-196a-3p and miR-196b.
- miR-196a is predicted to target a large number of mRNAs, including members of the *HOX* gene family.
- Depot-specific expression of miR-196a and several of the *HOX* genes is maintained *in vitro* in differentiating pre-adipocytes.
- There is no negative correlation between miR-196a and *HOXA5, HOXB8* or *HOXC8*, suggesting that their inverse expression patterns may not be the result of direct targeting.

Relative expression levels of a transcript can provide a clue as to what the role of that transcript is and which tissue or cell type it is functional in. Publically available data revealed that miR-196a is most highly expressed in AT, kidney and muscle. This suggests that miR-196a may play an important functional role in these tissues. It should be noted that these tissues are all of mesenchymal origin. Therefore, miR-196a expression may reflect their developmental origins, or may equally be an active functional regulator of cells of mesenchymal lineage. The observation that miR-196a is more highly expressed in the mature adipocyte fraction of AT than in the SVF (Figure 4.6) has important implications for determining which cell type functional experiments should be conducted in.

Experiments in this chapter confirmed depot-specific expression of miR-196a in ASAT and GSAT and demonstrated that miR-196a expression within VAT is low by comparison (Table 4.1). Future work should aim to clarify the significance of low miR-196a expression in VAT. This may reflect their distinct cellular or extracellular compositions [47], the more inflammatory environment within VAT [324] or the distinct functional properties of VAT with regards to fatty acid handling and adipogenesis, as discussed in 1.2.3. Previous attempts within the group to generate paired ASAT and VAT pre-adipocyte cell lines have been unsuccessful, and the invasive nature of obtaining VAT samples precluded further investigations into this question in this project.

Previous studies have shown that miR-196a expression is regulated according to the position of the tissue within the body, with increasing expression moving distally along the A-P axis. This has been observed in mouse [227], frog [233] and chicken [126] embryos and in the human gastrointestinal tract [248]. The *HOX* genes in which the miR-196 paralogues are embedded display co-linearity, in other words their expression along the A-P axis mirrors their chromosomal organisation. Therefore the following chapters of this thesis will aim to clarify whether miR-196a is a functional regulator of AT function or a marker of body patterning.

The positive correlation observed between GSAT miR-196a expression and waist circumference, but not hip circumference, appears counterintuitive. However, a possible mechanism for this might be that miR-196a has a suppressive effect on GSAT expansion, leading to increased fat deposition in ASAT or VAT. In this way an inhibitory effect of miR-196a in GSAT might lead to 'overflow' storage to other depots in much the same way as is seen in the partial lipodystrophy syndromes.

In silico prediction of mRNA targeting by miRNA is an imprecise tool. The three bioinformatics algorithms used to predict mRNAs regulated by miRNA identified 633 putative targets between them, but only 50 of these were predicted by all 3 programs. Indeed, *HOXB8*, which is well established as a direct target with near-perfect complementarity to miR-196a [227, 228], was only predicted by TargetScan. Micro-196a is predicted to target a large number of mRNAs and a number of the *HOX* genes are amongst its predicted verified targets. Indeed, a previous study suggested that a sizeable percentage of predicted miR-196 targets are *HOX* genes [312]. It is tempting to speculate that regulation of the HOX proteins in AT might be caused by depot-specific miR-196a expression; however, the lack of inverse correlation between miR-196a and *HOXA5, HOXB8* and *HOXC8* does not support this. However, the degree of correlation between expression of target mRNA and its corresponding protein is imperfect [123, 134]. It is possible that the putative *HOX* targets of miR-196a are only regulated post-translationally. Expression of *HOXC8* protein with modulation of miR-196a is discussed in Chapter 7. Attempts to recover protein from whole AT biopsies homogenised in Tri-reagent were unsuccessful, as discussed in 2.3.3.1.

Profiling of *HOXC* mRNA revealed miR-196a, *HOXC10* and *HOXC11* were all more highly expressed within GSAT whilst *HOXC8* and *HOXC9* were expressed at higher levels in ASAT. This is in line with a previous study that observed correlation between the expression of miR-196a and *HOXC10* and *HOXC11* [248]. The authors proposed that enrichment for methylation sites led to concurrent up-regulation of this region [248]. In the mouse embryo miR-196a expression is similar to that of the *HOX-9* paralogues, but with different anterior limits of expression, suggesting that they are not simply co-regulated [227]. Indeed, in our data there was no significant correlation between miR-196a and *HOXC10* or

HOXC11 for individual samples in either ASAT or GSAT. It will be important for future work to clarify the mechanisms of promotion of miR-196a-2 and the *HOXC* genes. Moreover, whilst we characterised miR-196a expression spatially in AT it will also be important for future studies to investigate its temporal expression in relation to the *HOXC* genes.

This chapter has described the expression patterns of miR-196a in human AT. Building on this, the following chapters will attempt to characterise miR-196a functionally using an *in vivo* model based on genetic variation in pre-miR-196a-2 and an *in vitro* pre-adipocyte model.

5 Investigating the function of miR-196a using rs11614913, a SNP in the precursor of miR-196a-2

5.1 Introduction

Genetic variation in the form of single nucleotide polymorphisms (SNPs) is important for determining diversity of phenotype. The advent of GWAS has enabled researchers to identify loci associated with a vast range of complex human traits. A great deal of work has concentrated on uncovering the functional effects of these. Efforts have focussed on protein coding genes, despite the fact that the majority of disease related variants fall within non-coding regions [325, 326]. Several miRNA and pre-miRNA genes have been found to contain SNPs, although interestingly there is less genetic variation within miRNAs than would be predicted, suggesting that they are actively conserved [138, 139]. Indeed, miRNAs which are conserved between species contain fewer SNPs than those which are not conserved [327, 328]. SNPs that alter mature miRNA sequence can influence targeting specificity and affinity [328], whilst genetic variation within the pre-miRNA or in the genomic region flanking it may alter miRNA expression or maturation [328, 329] and determination of the dominant strand [330].

5.1.1 Genetic variability in hsa-pre-mir-196a-1 and hsa-pre-mir-196a-2

As illustrated in Figure 5.1 several SNPs have been identified within pre-mir-196a-1 and pre-mir-196a-2. With the exception of rs11614913, genetic variants in both precursors are rare (minor allele frequency (MAF) <0.0002). We have access to DNA and anthropometric data for approximately 5,500 individuals from the OBB. This sample size would be too small to detect effects of such rare variants. The GIANT consortium [90, 331] conducted a large meta-analysis of body composition GWAS studies including more than 140,000 individuals, but their analysis did not cover any of the other variants other than rs11614913. RS11614913 is a common variant with a MAF of 0.405 within the OBB.

Therefore, the OBB contained good numbers of all genotype groups allowing for investigation of body fat distribution with genotype, and for recruit-by-genotype studies.

Whilst there is a body of literature relating rs11614913 to phenotypes of several tissues (discussed in detail in 5.1.3) there is no literature associating the other variants with a functional phenotype. Crucially, rs11614913 falls within the precursor of mir-196a-2, which was shown in 4.3.3.4 to be the predominant paralogue expressed in human WAT. For these reasons rs11614913 was selected as a tool for interrogation of miR-196a related phenotypes in AT.

Figure 5.1: Genetic variation in hsa-pre-mir-196a-1 and hsa-pre-mir-196a-2.
SNPs falling within hsa-mir-196a-1 (A.) and hsa-mir-196a-2 (B.) are indicated by red rectangles. rs11614913 is highlighted by the red circle. Images were obtained from http://www.ncbi.nlm.nih.gov/projects/SNP [9] on 12.03.2015.

A. hsa-pre-mir-196a-1

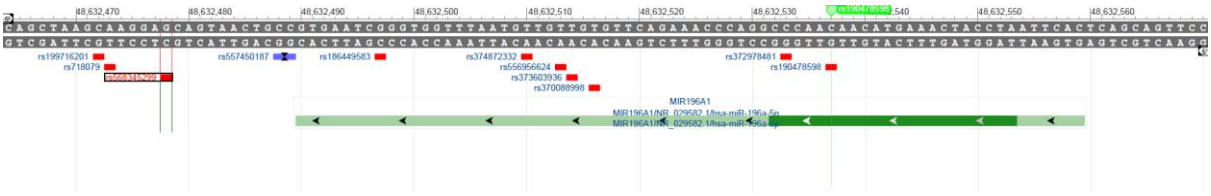

B. hsa-pre-mir-196a-2

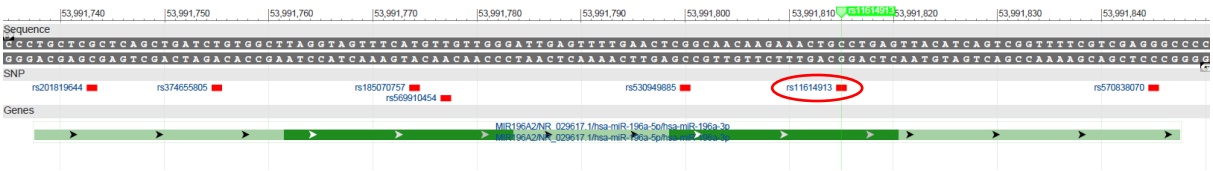

5.1.2 Genomic location of rs11614913

Pre-mir-196a-2 contains the SNP rs11614913, which causes a cytosine to thymine (C to T) transition. The allele frequency differs by population: within Caucasian populations the frequency of the C allele is around 68%, whilst in Asian populations it is 45% [332]. rs11614913 lies 5 ntds from the 3' end of miR-196a-2-3p (Figure 5.1). Given the low

expression of miR-196a-3p within human WAT and the fact that rs11614913 does not alter the seed sequence it is unlikely to affect mRNA targeting to a biologically relevant extent.

5.1.3 Overview of literature relating to rs11614913

rs11614913 has been associated with incidence of cancer of the stomach [333], lung [332], breast [334] and liver [335], with the T allele being protective in the majority of malignancies but detrimental in some [336].

The allele frequency differs between ethnic groups and indeed the T allele appears to confer different, and sometimes opposite, risks not only between different cancers but also to individuals of different ethnicities. For example, in Caucasian populations the TT genotype has been associated with an increased risk of lung cancer, whilst in Asian populations the converse is true [332]. This suggests a complex association influenced by differing genetic background and environment. The reasons for rs11614913 apparently different associations according to tissue type or ethnicity have not been explored. It should be remembered that miRNA regulate a multitude of complex transcriptional networks and so it is perhaps unsurprising that miRNA would have different regulatory effects depending on which mRNA targets are expressed or active.

Studies of a number of tissues have reported that mature miR-196a expression is related to rs11614913 genotype, with higher expression associated with the C allele [336-338]. Conversely, one study looking at 83 individuals with head and neck cancers found no association of genotype with expression, either in malignant or healthy tissues [339].

Several groups have investigated the extent to which expression quantitative trait loci (eQTL) are tissue specific [340-342]. In a review of published studies McKenzie *et al.*[342] found the percentage overlap in eQTL between blood and brain tissue to be in the range of 13-23%. eQTL status varies similarly between T-cells, lymphoblastic cell lines and

fibroblasts from the same individual [343] and between haemopoietic cell types dependent on their lineage and stage of differentiation [340]. This highlights the need to investigate potential regulatory variants in multiple tissues rather than assuming that data from another cell lineage or tissue can be taken as proxy evidence of an effect.

Lower mature miR-196a expression was confirmed in MCF7 cells (a human breast adenocarcinoma cell line) after transfection of a vector expressing the rs11614913 T allele versus wild-type [338]. As illustrated in Figure 5.1 rs11614913 alters the sequence of mature miR-196a-3p and in line with this one study noted an effect of the SNP on binding of miR-196a-3p to specific mRNA targets [336]. However, this is unlikely to be of biological relevance to WAT given the low expression of miR-196a-3p in this tissue (discussed in 4.3.3.3).

5.1.4 Pre-miRNA secondary structure and miRNA processing

RS11614913 alters the sequence of pre-miR-196a-2. In this chapter I consider how this might affect precursor structure or processing.

The secondary structure of small RNA molecules is determined by local interactions between complimentary regions. RNA will theoretically tend to assume the folding configuration in which it is most energetically stable. For a given RNA sequence, a lower free energy of binding (ΔG) corresponds with a more stable structure.

Figure 5.2: pre-miRNA cleavage by DICER. Reproduced with permission from an original article by from Gu *et al.* [344].

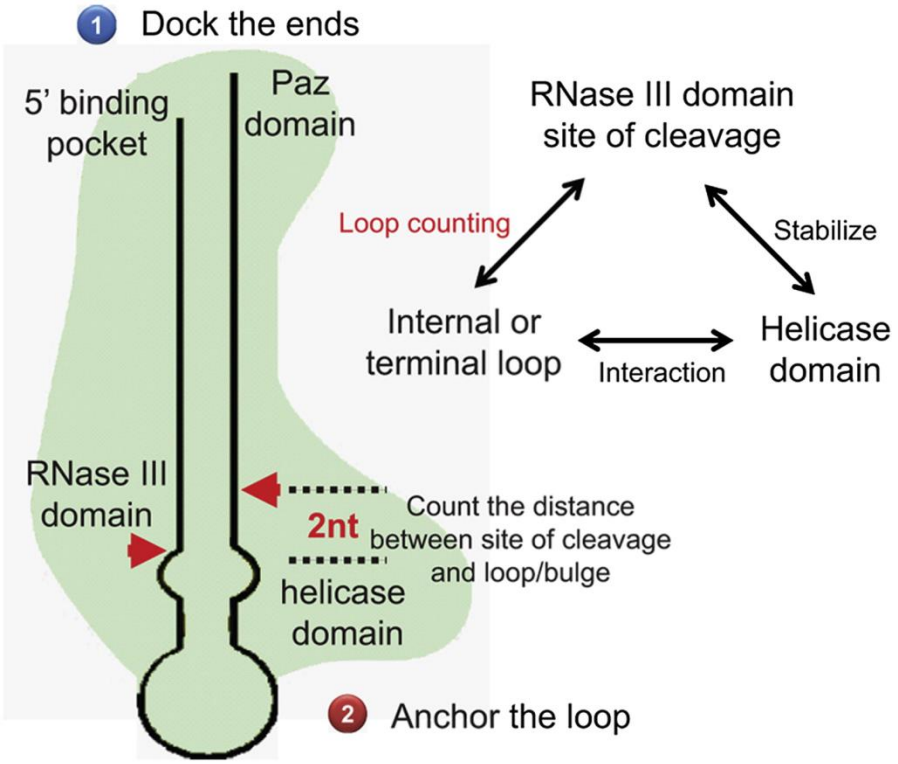

Correct folding of the pre-miRNA is necessary for its further processing into mature miRNA (Figure 5.2). The pre-miRNA is cleaved to give the mature miRNA and its complementary miRNA by Dicer, a ribonuclease (RNAase) III enzyme of ~220 kDa which displays specificity for double stranded RNA. Pre-miRNA hairpins are recognised for cleavage by the presence of a 2 nucleotides 3' overhang [345] by the Dicer PAZ (PIWI–AGO–ZWILLE) domain [346] and a terminal loop which interacts with the N-terminal helicase domain of Dicer [347, 348]. The distance between the PAZ and catalytic domains within Dicer is set such that most pre-miRNAs are cleaved ~22 nucleotides from the 3' end [346] (the so-called 3' counting rule). In mammals and flies Dicer also binds to the 5' terminus and cleaves at a 22 nucleotides distance (the 5' counting rule) in pre-miRNAs where the 5' end is thermodynamically unstable [349]. Specificity of Dicer cleavage sites in mammals is also

influenced by the position of the cleavage site relative to the terminal loop or bulges [350]. Soifer *et al.* [351] observed that the stability of the pre-miRNA stem was important for Dicer processing, with efficiency of processing diminishing as the thermodynamic stability of the hairpin reduced. Therefore, a SNP could alter pre-miR processing by affecting its stability, the sequence of cleavage sites or by changing the position of bulges in the precursor structure.

5.1.5 Hypotheses and aims

In this chapter I will make use of the fact that pre-miR196a-2 contains a common variant that may alter the functional properties of the mature microRNA. I use this to investigate the hypothesis that miR-196a regulates WAT accumulation in a depot-specific manner. Specifically:

1. To investigate whether WAT miR-196a expression is regulated by rs11614913 genotype.
2. To determine whether rs11614913 is associated with a body fat distribution phenotype.
3. To investigate whether rs11614913 is associated with adipocyte size *in vivo*.

5.2 Materials and methods

5.2.1 eQTL panel

Thirty individuals from the OBB of each rs11614913 genotype for whom RNA from whole ASAT and GSAT biopsies were available were selected. The three groups were matched for gender, age and BMI. General qPCR methods are outlined in 2.3.2.5. cDNA synthesis was performed using the Qiagen miScript kit (as described in 2.3.2.6.1) with 300ng of RNA for each sample. MiR-196a-5p and -3p expression were determined using a 1/50 cDNA dilution. Pre-miRNA expression was measured using a 1/10 cDNA dilution.

5.2.2 Genotype and phenotype data for the OBB cohort

Genotype data was obtained as described in 2.3.1.

Characterisation of participants in the OBB is described in 2.1.1. DXA scans were performed using the Lunar iDXA (GE Healthcare) and images were processed using enCORE v14.1 software (GE Healthcare). The android and gynoid AT regions are calculated based on bony landmarks (Figure 5.3). The android region is defined by the iliac crest at the lower boundary and the upper boundary is calculated as 20% of the distance between the neck and the iliac crest. The gynoid region includes the upper thighs and hips but does not overlap with the umbilicus. It is twice the height of the android region with the upper boundary located below the iliac crest by 1.5 times the height of the android region. VAT is calculated by the encore v14.1 software using a predefined algorithm. Android subcutaneous AT is calculated as total android AT - VAT.

Figure 5.3: A sample DXA scan showing the body regions as demarcated by enCORE v14.1 software.

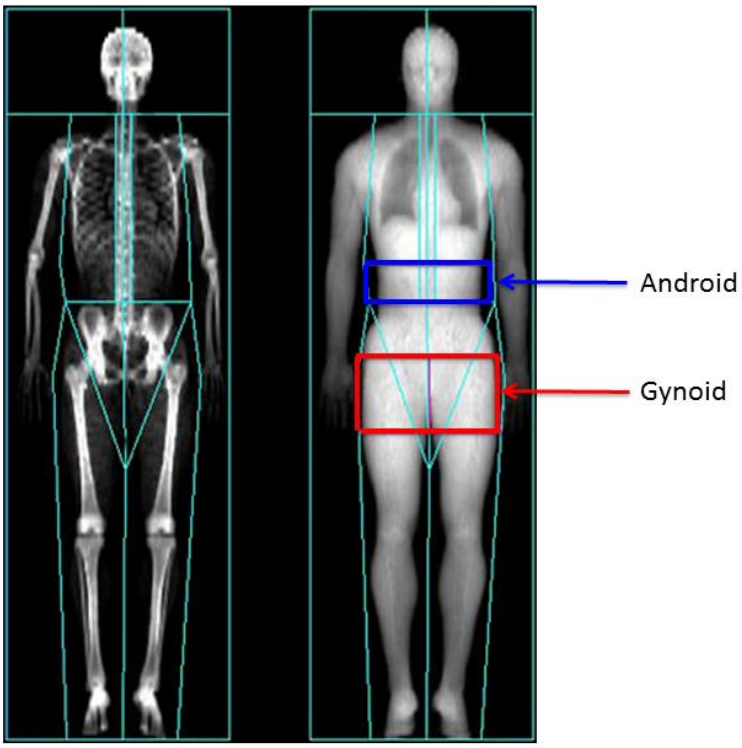

5.2.3 Cohorts used for replication studies

5.2.3.1 GIANT consortium

The **G**enetic **I**nvestigation of **AN**thropometric Traits (GIANT) consortium (http://www.broadinstitute.org/collaboration/giant) is an international collaboration between investigators that aims to identify genetic loci associated with human obesity, AT distribution and height through meta-analysis of GWAS data. Summary data from a number of GWAS meta-analyses have been made publically available.

5.2.3.2 MuTHER consortium

The Multiple Tissue Human Expression Resource (MuTHER) project was established by the Wellcome trust with the aim of creating a resource of genetic and genomic data from lymphocytes, subcutaneous AT, muscle and skin from 850 twins recruited from TWINSUK. This allows for investigation of the relationships between genomic variation, methylation status, mRNA expression and disease traits. All samples have been genome-wide expression profiled (Illumina HT-12v3 Chip) and genotyped (Illumina 610k or 1M chip) and the summary data from this is available at http://www.muther.ac.uk. Small RNA sequencing data for miR-196a and rs11614913 genotype information were obtained by private correspondence with Prof Cecilia Lindgren and TWINSUK respectively.

5.2.3.3 GeFOS Consortium

The GEnetic Factors for Osteoporosis (GeFOS) Consortium is an international collaborative effort to uncover the genetic variants underlying osteoporosis risk using meta-analysis of GWAS data [352]. Combined GWAS data for femoral neck (FN) and lumbar spine (LS) BMD were available for 19,195 individuals of Northern European descent from 5 separate studies (http://www.gefos.org/).

5.2.4 Adipocyte size according to rs11614913 genotype

The relationship between mean adipocyte size and rs11614913 genotype was investigated in collaboration with Professor Peter Arner (Karolinska Institute, Sweden). Mean adipocyte size data was provided by Professor Peter Arner. To generate these data needle ASAT biopsies were obtained from fasted obese and non-obese subjects. AT biopsies were minced and placed in Krebs-Ringer-phosphate buffer (KRP) containing 100 U/ ml collagenase and 4% albumin for 60 minutes at 37^{o}C in a shaking water bath. The digest was filtered and floating adipocytes were removed from undigested material and washed three times with KRP containing 0.1% albumin. Purity of the isolation was confirmed by light microscopy of 200 cells for each subject. Fat cell diameter was determined during direct microscopy of 100 cells for each individual. Adipocyte volume was calculated from cell diameter using formulas described by Hirsch and Gallian [353] and the mean adipocyte volume for each individual was then calculated.

Genomic DNA for the panel was provided by Professor Arner. Genotyping was performed as described in 2.3.1 using 30ng of genomic DNA for each individual. The relationship between mean adipocyte size and genotype was analysed in men and women separately using a linear regression model with correction for BMI and age.

5.2.5 Statistical methods

5.2.5.1 Genotype associations

Genetic association analysis of rs11614913 was performed using a linear regression model in SPSS 22.0 with covariates as outlined in the relevant results sections. Means for genotype groups were plotted and the pattern of data inspected visually: where there was a clear dose-response pattern (e.g. in Figure 5.7A) genotype groups were coded 1, 2, 3 and

were treated as scale numerical data; where the relationship between the independent variable and genotype did not indicate an additive model of inheritance (e.g.Figure 5.7.C) genotype groups were recoded as dummy variables and treated as two categorical variables. Residuals were checked for normal distribution. Standardised β values are presented.

5.2.5.2 Other statistical methods

For eQTL experiments data were analysed using a recessive model. Independent t-tests or Mann-Whitney U tests were used as appropriate.

5.3 Results

5.3.1 rs11614913 is predicted to change pre-miR-196a folding

Processing of pre-miRNA to mature miRNA is dependent on precursor stability and structure. I therefore investigated whether the rs11614913 nucleotide transition in pre-miR-196a-2 would alter its folding.

MFold is a web-based program that predicts the secondary structure of RNA by using on a thermodynamic model to calculate the energetically most stable folding. Outputs were generated in MFold 3.5 using default settings. As illustrated in Figure 5.4, the presence of rs11614913 was predicted to alter the folding of pre-miR-196a in such a way that would increase the free energy of binding of the secondary structure and so tend to destabilise it.

Figure 5.4: Folding and free energy of binding of miR-196a-2 containing the wild-type allele (top) and minor allele (bottom), as predicted in M fold.

rs11614913 is highlighted in yellow, mir-196a-5p is denoted by blue lettering and mir-196a-3p by red lettering.

Folding of wildtype hsa-pre-mir-196a-2.
Initial ΔG = -51.20.

```
UG-     - UC-        C--|                  A           A UG G
   CUCG C    AGCUGAU    UGUGGCUUAGGUAGUUUC UGUUGUUGGG U   A \
   GAGC G    UUGGCUG    ACAUUGAGUCCGUCAAAG ACAACGGCUC A   U U
CGG     U CUU        ACU^                  A           A GU U
```

Folding hsa-mir-196a-2 with rs11614913 C to T transition.
Initial ΔG = -46.60.

```
UG-     - UC-        C--|          GU      A           A UG G
   CUCG C    AGCUGAU    UGUGGCUUAG  AGUUUC UGUUGUUGGG U   A \
   GAGC G    UUGGCUG    ACAUUGAGUC  UCAAAG ACAACGGCUC A   U U
CGG     U CUU        ACU^          UG      A           A GU U
```

5.3.2 rs11614913 is an eQTL for miR-196a

5.3.2.1 rs11614913 is an eQTL for miR-196a in a panel recruited from the OBB

I next investigated whether rs11614913 genotype was associated with expression of miR-196a within WAT, and whether this association was depot specific. The expression of miR-196a-5p (referred to throughout this thesis as miR-196a), miR-196a-3p and pre-miR-196a-2 was determined by qPCR in paired ASAT and GSAT biopsies from 30 individuals of each genotype. The three groups were selected to be matched for gender, age and BMI (Table 5.1).

Table 5.1: Characteristics of the panel established to investigate miR-196a expression in ASAT and GSAT in relation to rs11614913 genotype.

Genotype	CC	CT	TT	Significance
N	30	30	30	
Gender	M=16, F=14	M=16, F=14	M=16, F=14	
Age (years)	44.9	44.4	44.8	p=0.813
BMI (kg/m^2)	25.60	25.73	25.61	p=0.967
WHR	0.88	0.88	0.88	p=0.983
Fat mass (kg)	19.38	19.84	19.52	p=0.988
Systolic bp (mmHg)	122.1	117.6	118.1	p=0.166
Diastolic bp (mmHg)	82.2	80.2	78.8	p=0.174
HOMA-IR	2.71	2.70	2.81	p=0.671
Total Cholesterol (mmol/l)	5.20	5.26	5.65	p=0.362
HDL-C (mmol/l)	1.27	1.33	1.32	p=0.907
LDL-C (mmol/l)	3.25	3.36	3.63	p=0.309
CRP (mg/l)	2.07	2.67	1.39	p=0.336

Figure 5.5: miR-196a expression with rs11614913 genotype in whole ASAT and GSAT. Individuals were matched for gender and BMI. n=90 (30 of each genotype). MAF=0.405. Bars represent standard errors. Graphs show expression of; A. miR-196a-5p. B. miR-196a-5p analysed using a recessive model. C. miR-196a-3p. D. pre-miR-196a-2.

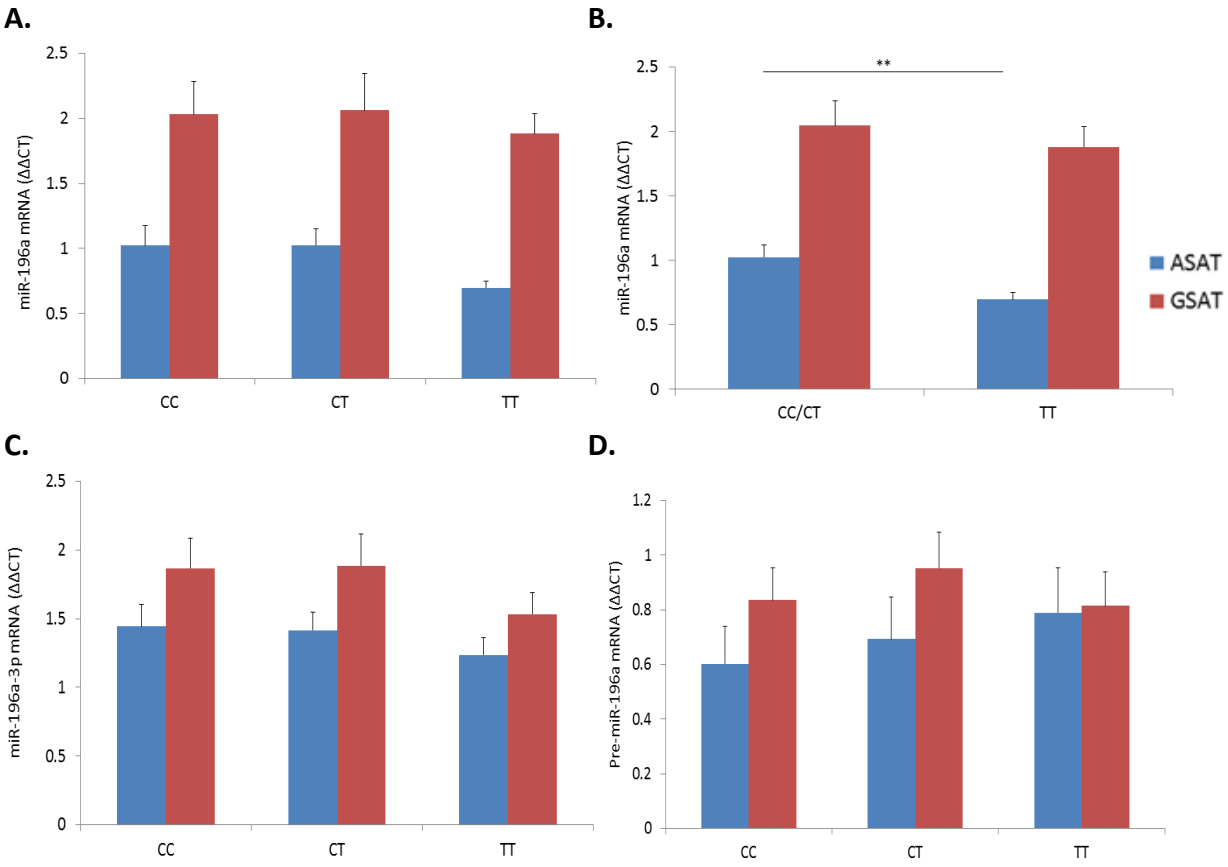

A recessive effect of rs11614913 on miR-196a-5p expression was observed (Figure 5.5.A) with the TT genotype associated with reduced expression of miR-196a in ASAT (-32%, p=0.005) and a non-significant trend towards reduced expression in GSAT (-8%, N.S.) (Figure 5.5.B). A similar non-significant trend was observed for miR-196a-3p (Figure 5.5.C). There was no effect of genotype on pre-miR-196a-2 expression (Figure 5.5.D), suggesting that the effect of the T allele is occurring post-transcriptionally on processing of the pre-miRNA into the mature miRNA.

The mRNA expression of *HOXA5, HOXB8* and *HOXC8* did not alter with rs11614913 genotype (data not shown). The *HOX* mRNAs are expressed at relatively low levels within

AT and the effect on mRNA levels of a 32% reduction in miRNA are likely to be modest. Therefore, it is likely that this study was not sufficiently powered to detect changes in target mRNA expression. Modulation of miRNA levels often has more measurable effects on protein than mRNA [123]. With this in mind efforts were made to isolate protein from these samples for Western blotting but as outlined in 2.3.3.1 this was unsuccessful. Although it was possible to isolate protein from biopsies homogenised in Tri-reagent, HOXC8 was not detectable using Western blot. In later experiments cultured cells were lysed using a lysis buffer. Using the same Western blotting technique and antibody it was then possible to detect HOXC8 (7.3.2.2).

5.3.2.2 Efforts to replicate eQTL data in the MuTHER consortium

5.3.2.2.1 HOXC8 expression

The MuTHER project has made cis-eQTL data publically available that covers mRNA, but not miRNA, expression. The size of this dataset made it possible that an effect of rs11614913 on regulating *HOX* expression, via modulation of miR-196a expression, might be detectable.

Publically available cis-eQTL data were accessed at http://www.muther.ac.uk/ on 02.12.2013. Data from the study by Grundberg *et al.* [354] were generated from ASAT biopsies from 856 female individuals (154 monozygotic twin pairs, 232 dizygotic twin pairs and 84 singletons) aged between 38 and 84 years. Data were analysed using the Genevar (GENe Expression VARiation) platform [355] using the preloaded algorithm.

rs11614913 TT genotype was associated with increased *HOXC8* expression (β=0.043, p=0.015). This direction of effect would be consistent with that expected if lower miR-

196a expression in TT-homozygotes was leading to reduced targeting of *HOXC8*. This eQTL was not present in lymphoblastic cell lines or skin from the same cohort.

5.3.2.3 miR-196a expression

miR-196a-1 and miR-196a-2 expression data was kindly provided by Professor Cecilia Lindgren by private correspondence. Normalised log_2-transformed small RNA sequencing data was available for whole ASAT biopsies for 119 women from the MuTHER cohort [138]. Corresponding rs11614913 genotype status was obtained by application to TWINSUK.

miR-196a-1 and miR-196a-2 have identical mature sequences. Within this dataset identical sequences arising from separate precursors had been mapped to loci by distinguishing unique flanking regions and by inferring relative proportions using SNPs such as rs11614913. Despite this the expression patterns of miR-196a-1 and miR-196a-2 were identical (Figure 5.6.A and B), suggesting that the analysis pipeline had not discriminated between them. For this reason both paralogues were combined for analysis (Figure 5.6.C). The same direction of effect was observed as in the OBB cohort but with a smaller effect size (-13.4% reduction in miR-196a-5p expression with TT homozygosity, N.S).

Figure 5.6: Expression of miR-196a by rs11614913 genotype in the MuTHER cohort.

Graphs show log_2 transformed small RNA sequencing data from 119 ASAT biopsies (CC=30, CT=70, TT=19) for miR-196a-1, miR-196a-2 and both paralogues combined. Bars represent standard errors.

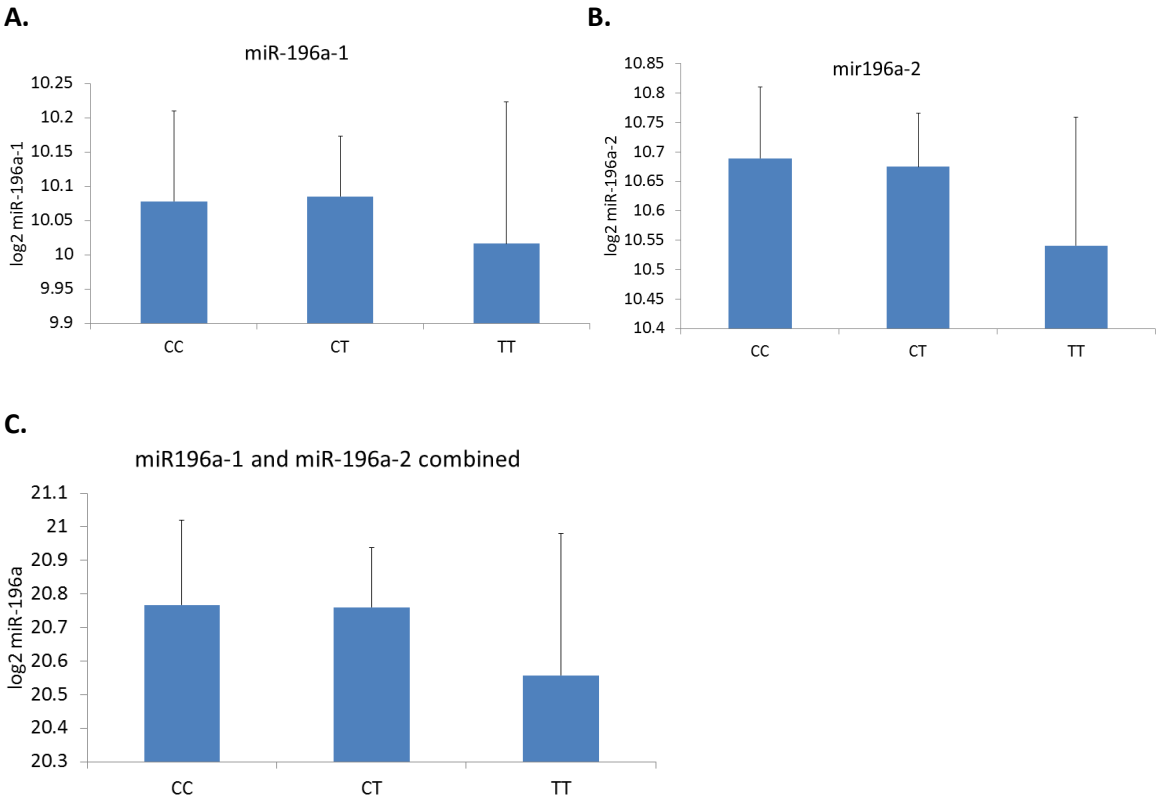

5.3.3 rs11614913 is associated with human body fat distribution

5.3.3.1 rs11614913 and body fat distribution in the OBB

The association between rs11614913 and miR-196a expression specifically within ASAT provided an *in vivo* model with which to test the hypothesis that miR-196a modulates human body fat distribution. Genotyping was performed on all participants in the OBB for whom genomic DNA was available (n=5,823). Characteristics of this panel are shown in Table 5.2. Genotypes were assigned for 99.7% of individuals and were in Hardy-Weinberg equilibrium (X^2=0.16, p=0.70).

The minor rs11614913 T allele was associated with an increase in WHR of 0.67% in men (p=0.027) and non-significant increase of 0.72% in women (p=0.37) after adjustment for

BMI and age (Figure 5.7.A). This was mediated by an expansion of waist circumference (0.75% increase in men; β=0.020 p=0.020, 1.68% in women; β=0.015 p=0.091) rather than by a decrease in hip circumference (men; β=0.001 p=0.939, women; β=0.006 p=0.45). Interrogation of DXA body composition data suggested that this effect was caused by an expansion of android SAT rather than VAT (Figure 5.7.B-C).

Whilst these results were encouraging the sample size of the OBB is relatively small, limiting the ability to detect subtle effects of variants. The associations observed were of borderline statistical significance and it was unclear whether they were due to chance or whether the OBB cohort was underpowered to detect a real effect. It was therefore important to validate these findings in a larger cohort.

Table 5.2: Characteristics of the OBB cohort for whom genomic DNA was available for genotyping.

	Mean	Standard Deviation
Number of participants	5823	
Number with DEXA data available	3515	
Gender	M=2562 F=3261	
Age	41.7	5.81
BMI	26.0	4.61
WHR	0.86	0.087

Figure 5.7: Associations between rs11614913 genotype and body fat distribution.
MAF=0.405. Data were analysed in SPSS 20.0 using a linear regression model. Data were adjusted for age and BMI. Standardised β values are presented. Bars represent standard errors. Graphs show A. WHR according to rs11614913 genotype B. Android SAT mass according to genotype C. VAT mass according to genotype.

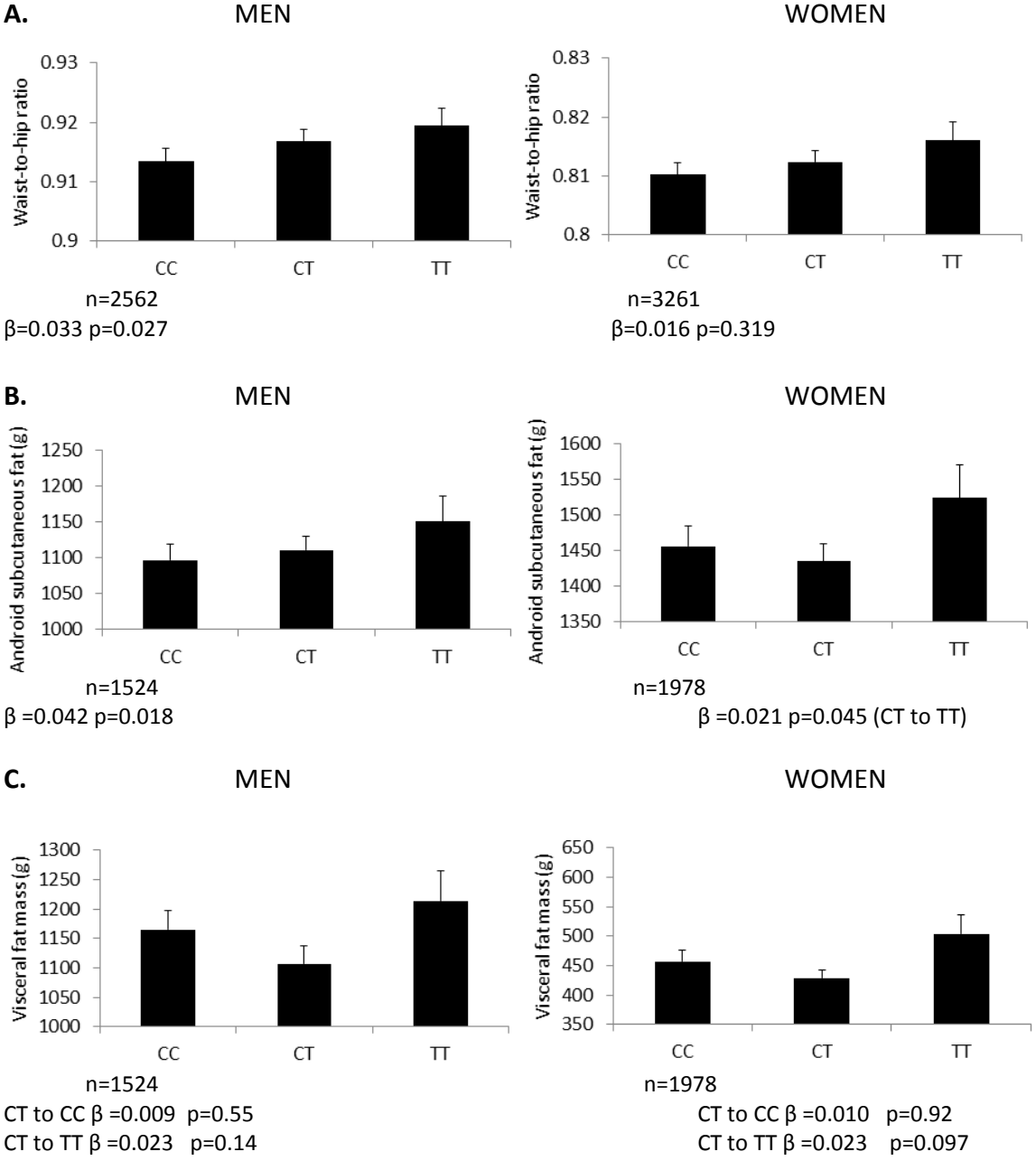

5.3.3.2 Validation of the relationship between rs11614913 in the GIANT consortium

The GIANT consortium has access to anthropometric and genotyping data for nearly 250,000 individuals. Shungin *et al.* [90] conducted a meta-analysis of waist and hip circumference measurement associations, adjusted for age, BMI and study specific co-variates, in individuals of European ancestry using data from 57 GWAS studies. The p-values were corrected using genomic control at the individual study level and again after meta-analysis.

In line with our data rs11614913 was associated with WHR after adjustment for BMI and age in both men ($2.7x10^{-5}$) and women ($1.1x10^{-7}$), with this effect being clearly driven by an expansion of waist circumference rather than a reduction in hip circumference (Table 5.3).

LocusZoom [356] is a free online program that can be used to plot regional association results from GWAS. The data from the meta-analysis by Shungin *et al.*[90] was not available for input into LocusZoom. However, it was possible to generate plots using data from an earlier meta-analysis of the GIANT consortium dataset containing 133,723 individuals [331]. Figure 5.8 shows plots for the region flanking pre-miR-196a-2 for both men (A.) and women (B.). Other SNPs in the region are discussed in more detail in 6.3.3.

Table 5.3: The relationship between rs11614913 and WHR adjusted for BMI in a European population.
Based on open access summaries of meta- analyses of GIANT consortium data by Shungin *et al.*[90]. MAF=0.433. For all conditions the T allele was the effect-increasing variant. All analyses are adjusted for BMI and age.

Gender	Number of participants	Measurement	β	Standard error	p-value
Men	55,920	WHR	0.028	0.0067	$2.7x10^{-5}$
	60,340	Waist circumference	0.032	0.0066	$1.2x10^{-6}$
	56,413	Hip circumference	0.0044	0.007	0.53
Women	85,629	WHR	0.029	0.0055	$1.1x10^{-7}$
	90,592	Waist circumference	0.029	0.0053	$6.8x10^{-8}$
	86,241	Hip circumference	-0.0016	0.0057	0.78
Combined	141,414	WHR	0.029	0.0044	$6.9x10^{-11}$
	150,738	Waist circumference	0.03	0.0044	$1.7x10^{-11}$
	142,467	Hip circumference	0.0003	0.0046	0.95

Figure 5.8: Plots showing GWAS associations for the region flanking pre-mir-196a-2 and WHR adjusted for BMI.
Plots of rs11614913 and the 200kb flanking region were generated with LocusZoom [356] using data from Randall *et al.*[331]. Negative log10 transformed p-values for association are shown. rs11614913 is represented by the purple diamond. The degree of linkage disequilibrium of each SNP with rs11614913 in the Hapmap CEU population is represented by colour coding.
Plots show: A. WHR adjusted for age and BMI in men. B. WHR adjusted for age and BMI in women.

A.

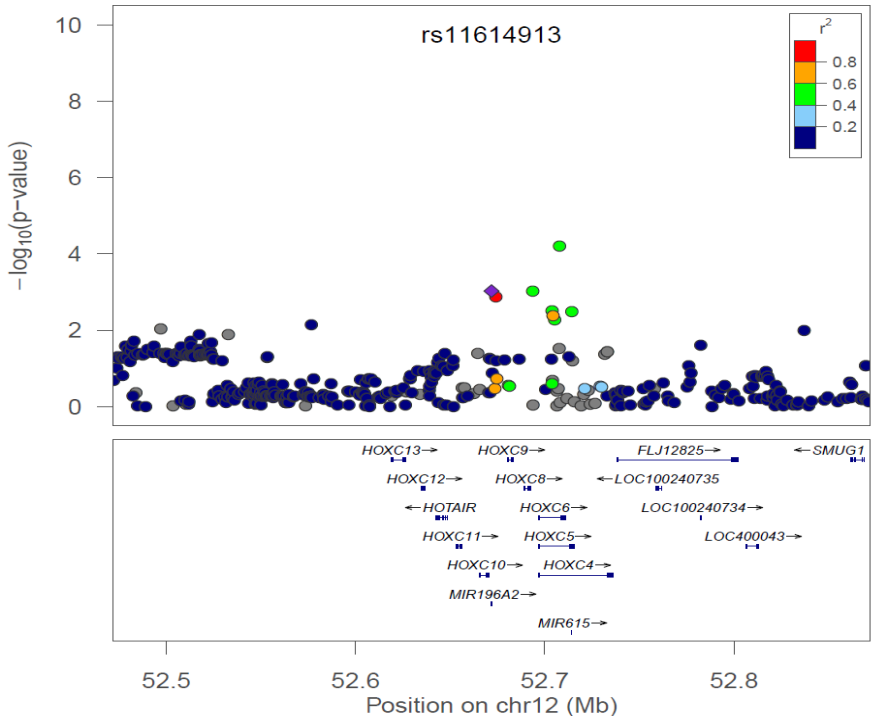

B.

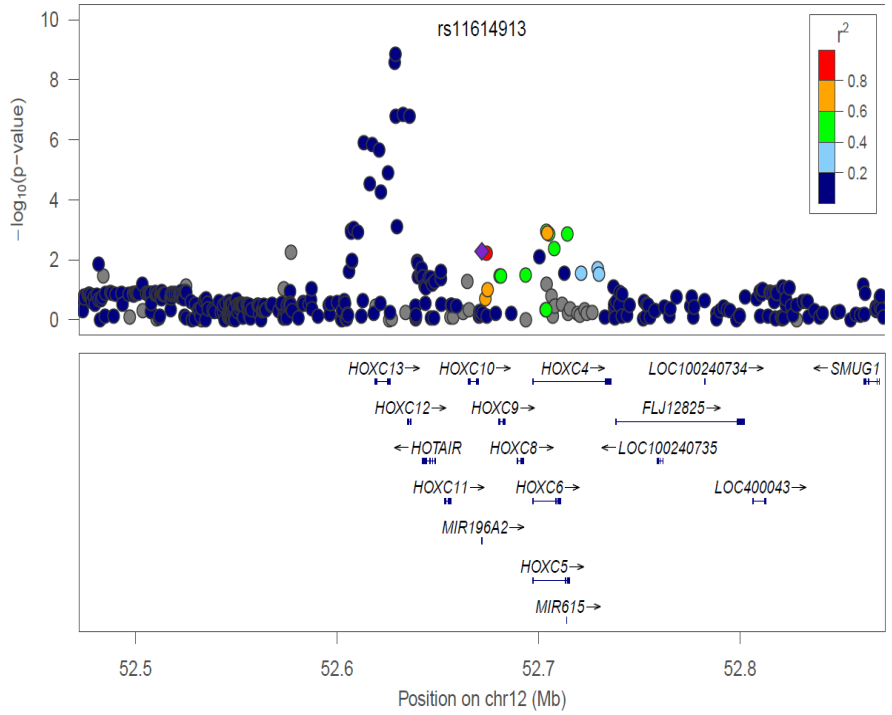

5.3.4 rs11614913 is associated with adipocyte size

A total of 234 women and 81 men were rs11614913 CC or TT homozygotes and were included in the analysis. The mean age of the panel was 39 years (SE=0.63) and the mean BMI was 32.1 (SE=0.48). Genotypes were in Hardy-Weinberg equilibrium (X^2=0.02, p=0.97). The TT genotype was significantly associated with larger mean adipocyte size in ASAT in men (CC to TT: β=0.15, p=0.019; CT to TT: β=0.08, p=0.23; Figure 5.9.A). In women there was no significant association between rs11614913 genotype and adipocyte size (CC to TT: β=0.018, p=0.64; CT to TT: β=0.005, p=0.90; Figure 5.9.B).

Figure 5.9: Mean adipocyte size according to rs11614913 genotype in A. men and B. women. Linear regression analyses were performed in men and women separately controlling for age and BMI.

A. Mean adipocyte size in men according to rs11614913 genotype. N=50 CC, 31 TT.

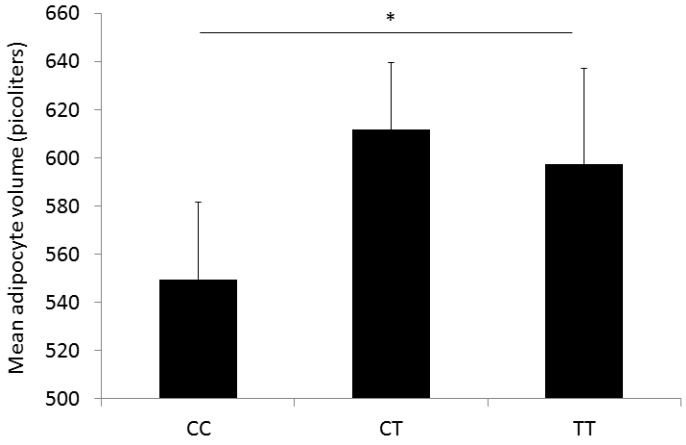

B. Mean adipocyte size in women according to rs11614913 genotype. N=139 CC, 93 TT.

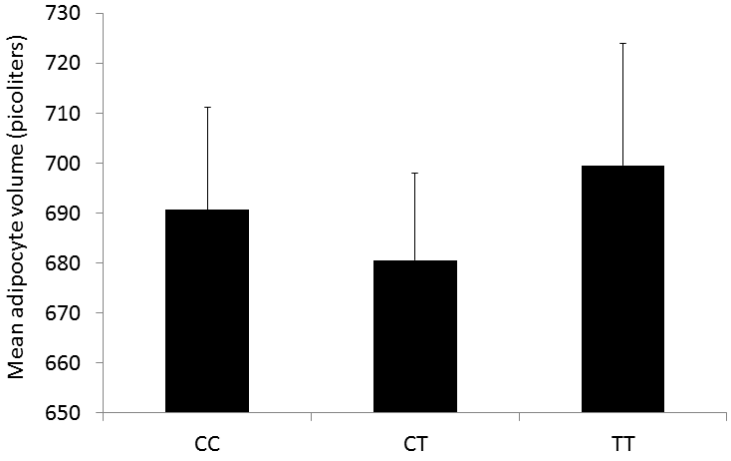

5.4 Discussion

The presence of a common genetic variant in the precursor of miR-196a provided a powerful genetic tool with which to interrogate the function of miR-196a *in vivo*. The rs11614913 TT genotype was associated with lower expression of miR-196a specifically within ASAT; in turn it is also associated with an increase in android WAT, suggesting a role for miR-196a in regional WAT expansion. To our knowledge this is the first proposed example of a miRNA eQTL modulating an AT phenotype. I will discuss other potentially causative variants in linkage disequilibrium with rs11614913 in 6.3.3.

The rs11614913 C to T transition was predicted to alter the secondary structure of pre-miR-196a-2 in such a way that would destabilise the precursor and so putatively affect the efficiency of its cleavage by Dicer. Consistent with this, expression of miR-196a was associated with rs11614913 genotype whilst expression of pre-miR-196a-2 was not. Further work would be required to establish whether this is the mechanism by which rs11614913 modulates miR-196a expression. One approach would be to separate the RNA secondary structures by non-denaturing gel electrophoresis. An alternative approach would be transfection with pri- or pre-miR-196a-2 WT or rs11614913 variant expressing vectors, followed by determination of miR-196a expression. Similarly, WT or variant pre-miR-196a-2 could be incubated with Dicer and processing efficiency assessed. These experiments would clarify whether rs11614913 alters processing, but would not elucidate a mechanism or prove that this would occur at physiological levels of pre-miR-196a-2 *in vivo*. It would, however, be interesting to see whether differentiated pre-adipocytes derived from ASAT or GSAT process the variant precursor differently.

Although the eQTL finding did not statistically replicate in the MuTHER cohort the same trend to lower expression of miR-196a with the TT genotype, particularly in ASAT, was

demonstrated. The ability to detect an eQTL for rs11614913 in the MuTHER cohort was limited by small numbers of the minor T-allele.

The reasons for this seemingly depot-specific effect are not clear. A number of eQTLs are tissue specific [341, 342]. Indeed, Parts *et al.* [138] investigated miRNA eQTLs in ASAT and GSAT and found them to be different in the two tissues. Moreover, the association observed in the OBB was in whole SAT which is a heterogeneous tissue with cellular composition that differs by region. Further research should isolate the component cell fractions of AT and ensure that miR-196a is regulated within pre-adipocytes and adipocytes.

Genotyping of the OBB cohort for rs11614913 suggests that the T allele is associated with an expansion of WHR caused by an increase in android WAT. WHR has been postulated to correlate more closely with ASAT mass than VAT mass [77] and in line with this our data suggest that the increase in android WAT mass is caused primarily through an expansion in android subcutaneous WAT. Consistent with this, in collaboration with Professor Arner's group I demonstrated that rs11614913 TT-genotype is also associated with larger mean cell size in ASAT, at least in men (Figure 5.9).

I was fortunate to have access to the OBB cohort that has detailed DXA characterisation of body composition for the majority of participants. It can be argued that genome-wide significance thresholds need not apply as genotyping for rs11614913 was approached with a pre-specified hypothesis. Despite this, the sample size of the OBB cohort is small for detecting subtle changes in body composition, and as a result the statistical significance of associations within the OBB cohort are nominal.

For these reasons it was vital to replicate these findings in a separate cohort. Interrogation of data from the GIANT consortium meta-analysis clearly shows an association between

the rs11614913 T allele and increased WHR. This was driven by an increase in waist circumference rather than a decrease in hip circumference. Future collaborations should aim to investigate the suggestion in our data that rs11614913 modulated WAT expansion is ASAT specific. It will also be important to study cohorts of different ages to clarify at what age these associations begin to emerge. This will help to establish whether miR-196a regulates AT-distribution early in development or in adult years.

There are a number of reasons why rs11614913 has not been identified in previous studies as associating the WHR. Many of the GWAS conducted looking for associations for WHR have used SNP-arrays, and many of these have not included rs11614913. Additionally the small effect size means that large populations are required to detect an association.

There are suggestions from the data that miR-196a might have, to some degree, sex specific effects. Firstly, in **Error! Reference source not found.** we saw that the GSAT/ASAT old change was somewhat more marked in men than in women. Within the OBB genotype-phenotype associations for body fat distribution tended to be more marked in men than in women, both in terms of magnitude and statistical significance, although this was not seen in the larger GIANT consortium cohort. Finally, an association with adipocyte size was only seen in male ASAT. This may represent a stronger regulatory role for miR-196a in male AT or it may be due to different mechanisms of action between the sexes. These observations informed the choice of pre-adipocytes derived from a male donor for the functional experiments in Chapter 7.

These data support the hypothesis that miR-196a acts in an AT depot specific manner to modulate human body fat distribution. In the next chapter I use rs11614913 as a genomic tool to investigate the effect of miR-196a on bone metabolism.

6 Investigating the role of miR-196a in bone metabolism using rs11614913

6.1 Introduction

6.1.1 Adipose tissue and bone share a common lineage

In the previous chapter I observed that rs11614913 TT-homozygosity was associated with lower expression of miR-196a in ASAT, expanded waist circumference and larger mean adipocyte size within ASAT. As discussed below, there is a complex relationship between AT and bone.

There are a number of plausible mechanisms by which altered adipokine and hormone levels relating to WAT mass and distribution might influence bone metabolism (reviewed here [357]). Genetic or molecular factors may also explain the associations between WAT and bone phenotypes. Adipocyte and bone progenitors are both of mesenchymal lineage. Moreover, MSCs, found in AT and bone marrow, are capable of differentiating into both mature adipocytes and osteocytes [358]. Indeed, variants which affect osteogenesis will often also affect adipogenesis [359, 360].

6.1.2 MiR-196a, the *HOX* genes and bone metabolism

MiR-196a and the *HOX* genes have been implicated in bone physiology. Disruption of several of the Hox proteins cause skeletal malformations [361-363]. Importantly, mice lacking all Hox-8 paralogues display an axial skeleton phenotype affecting the thoracic ribcage and thoracic and lumbar spine [364]. Similarly, mir-196a ablation in zebra fish caused an increase in the number of rib-bearing vertebrae [231]. miR-196a has been proposed to enhance osteogenic differentiation of hASCs *in vitro* through its targeting of *HOXC8* [206]. In experiments conducted by Kim *et al.*[206] lentiviral overexpression of miR-196a in hASCs enhanced osteogenesis and this effect was mimicked by inhibition of

HOXC8. Conversely, antisense-oligonucleotide (ASO) mediated inhibition of miR-196a inhibited osteogenesis of hASCs.

In view of the facts that 1. bone and AT are of common lineage and 2. the literature implicating miR-196a in bone metabolism, I hypothesised that miR-196a would be important for bone physiology and that this may be reflected in a relationship between rs11614913 genotype and bone mineral density (BMD).

6.1.3 The associations between body fat distribution and bone mineral density

In Chapter 5 I observed an association between rs11614913 and body fat distribution. To investigate a possible relationship between miR-196a and BMD it was important to understand the relationship between body fat distribution and BMD, in case the two relationships were confounding one another.

The literature on body composition and bone mineral density (BMD) varies considerably dependent on the population being studied. It is a consistent observation across a range of ages and ethnicities that lean mass and BMD are positively associated [365-368]. A number of groups have also reported that BMD increases with increased total AT mass [365, 366, 369]. However, it has also been suggested that the direction of association between AT mass and BMD is gender dependent [367] whilst other groups have reported no association [368].

With regards to body fat distribution, an inverse correlation between upper body fat deposition and BMD has been observed in older Korean men and women [370], in obese Chinese women (but not men) [371] and in Caucasian individuals [372]. A lack of association has also been described [373]. Conversely, a study of lean Indian adults found a negative association between leg AT-to-total AT mass and BMD [369] and a positive relationship between WHR and BMD has been described in both pre- and postmenopausal

women [374, 375]. Associations between body fat and BMD may be different in men and women, with a more detrimental effect conferred by central AT in women and limb AT in men [376]. Interestingly, one group assessed bone microarchitecture of trans-iliac bone biopsies from premenopausal women and found that increased trunk fat was associated with inferior bone quality and lower rates of bone formation (although the latter effect disappeared after correction for BMI) [377].

When attempting to further dissect the contribution of the individual WAT depots the literature is even more conflicted. George *et al.* noted a negative relationship between VAT mass and BMD in Black African and Asian Indian adults [367] and the same relationship has been observed in sedentary obese children and adolescents [378]. A lack of association between VAT and BMD has also been described [373, 379]. One group observed discordant relationship of VAT with age, with increasing VAT having a negative association with BMD in younger men and a positive association in older men [379]. Most studies investigating ASAT have failed to find a relationship with BMD [368, 373].

6.1.4 Hypotheses and aims

In light of the literature suggesting a role for miR-196a and the *HOX* genes in the formation and metabolism of bone, another tissue of mesenchymal origin, I hypothesise that miR-196a regulates bone metabolism as reflected by BMD. I use a common variant in pre-mir-196a-2, rs11614913, as a genomic tool to test this hypothesis. Specifically, I aim to:

1. To investigate whether rs11614913 is associated with regional BMD.

2. To characterise the relationship between AT distribution and BMD within the OBB cohort in order to separate the associations of rs11614913 with AT distribution and BMD

from one another.

6.2 Materials and methods

6.2.1 Genotype and phenotype data for the OBB cohort

The same rs11614913 genotyping information was used as in 5.3.3.1.

Characterisation of participants in the OBB is described in Chapter 2. DXA scans were performed using the Lunar iDXA (GE Healthcare) and images were processed using enCORE v14.1 software (GE Healthcare), as described in 5.2.2. BMD was determined in predefined regions (Figure 5.3) and calculated by enCORE v14.1 software. Bone mineral calibration and quality control were performed using a spine phantom according to the manufacturer's instructions.

6.2.2 GeFOS Consortium

The GEnetic Factors for Osteoporosis (GeFOS) Consortium is an international collaborative effort to uncover the genetic variants underlying osteoporosis risk using meta-analysis of GWAS data [352]. Combined GWAS data for femoral neck (FN) and lumbar spine (LS) BMD were available for 19,195 individuals of Northern European descent from 5 separate studies (http://www.gefos.org/).

6.2.3 Statistical methods

6.2.3.1 Genotype associations

For rs11614913 genotype analysis a linear regression model was performed in SPSS 22.0 using the same methods as described in 5.2.5.1, with covariates as outlined in the relevant results sections.

Statistical analyses for associations between other SNPs in the HOXC cluster and predetermined quantitative traits were performed using the PLINK program v.1.07 (http://pngu.mgh.harvard.edu/~purcell/plink/) [380]. Quantitative traits were log transformed and analysed using a linear regression model. Data were adjusted for age, gender and BMI. Significance is presented as empirical p-values (EMP) as calculated by the additional implementation of permutation procedures to the linear regression model. Permutation procedures were used because they are robust to changes in data distribution and Hardy Weinberg equilibrium.

6.2.3.2 Other statistical methods

To investigate the associations between AT distribution and BMD multivariate-adjusted linear regression was performed in SPSS 20.0. Separate analyses were performed for each sex because of the different patterns of AT distribution and BMD in men and women. For all regression analyses the BMD variable was the dependent variable. Associations with lean mass were adjusted for age at the time of study visit, weight and height (as a proxy for skeletal size). All regional AT quantitative traits were adjusted for age at study visit, height and total fat mass as estimated by DEXA, in order to isolate the associations with regional fat depots for that of total adiposity. For women, menopausal status and known use of hormone-releasing contraceptives were also added to the model as covariates. A backwards stepwise model was used and normality of the residuals was checked. Standardised β values are presented.

6.3 Results

6.3.1 rs11614913 is associated with human bone mineral density

6.3.1.1 rs11614913 and bone mineral density in the OBB

AT and bone are both primarily composed of cells of mesenchymal lineage, and the *HOX* proteins and miR-196a have been proposed to regulate osteogenesis. Therefore it was hypothesised that rs11614913 would also be associated with BMD.

Within the OBB cohort the T allele of rs11614913 was associated with reduced bone mineral density of the spine (Figure 6.1.A: Men; -2.36% p=0.002, women; -1.34%, p=0.046) and the pelvis (Figure 6.1.B: Men; -1.96% p=0.020, women; -1.25% p=0.072). The minor T-allele was associated with total BMD in men only (men; β=-0.053 p=0.025, women; β=-0.023 p=0.29). There was no significant association between rs11614913 and BMD of the arms or legs.

6.3.1.2 Validation of the relationship between rs11614913 and bone mineral density in the GEFOS consortium

Again, it was important to replicate these findings in an independent and, ideally, larger cohort. The GeFOS consortium has made public summary data for a meta-analysis of 5 separate GWAS of FN and LS BMD for 19,195 individuals [352]. All subjects were of Northern European descent aged between 18-96 years. In all studies the majority of participants were women (57-100%). As shown in Table 6.1 rs11614913 was significantly associated with BMD of the FN and LS in both men and women, with the same direction of effect as that in the OBB. Effect sizes were not available.

Figure 6.1: Bone mineral density by rs11614913 genotype in the OBB.
MAF=0.405. BMD is measured in g/cm^2. Data were analysed in SPSS 20.0 using a linear regression model. Data were adjusted for age and BMI. Standardised β values are presented. Bars represent standard errors. Graphs show: Spinal BMD in men (A) and women (B) according to rs11614913 genotype. Pelvic BMD in men (C) and women (D) according to rs11614913 genotype.

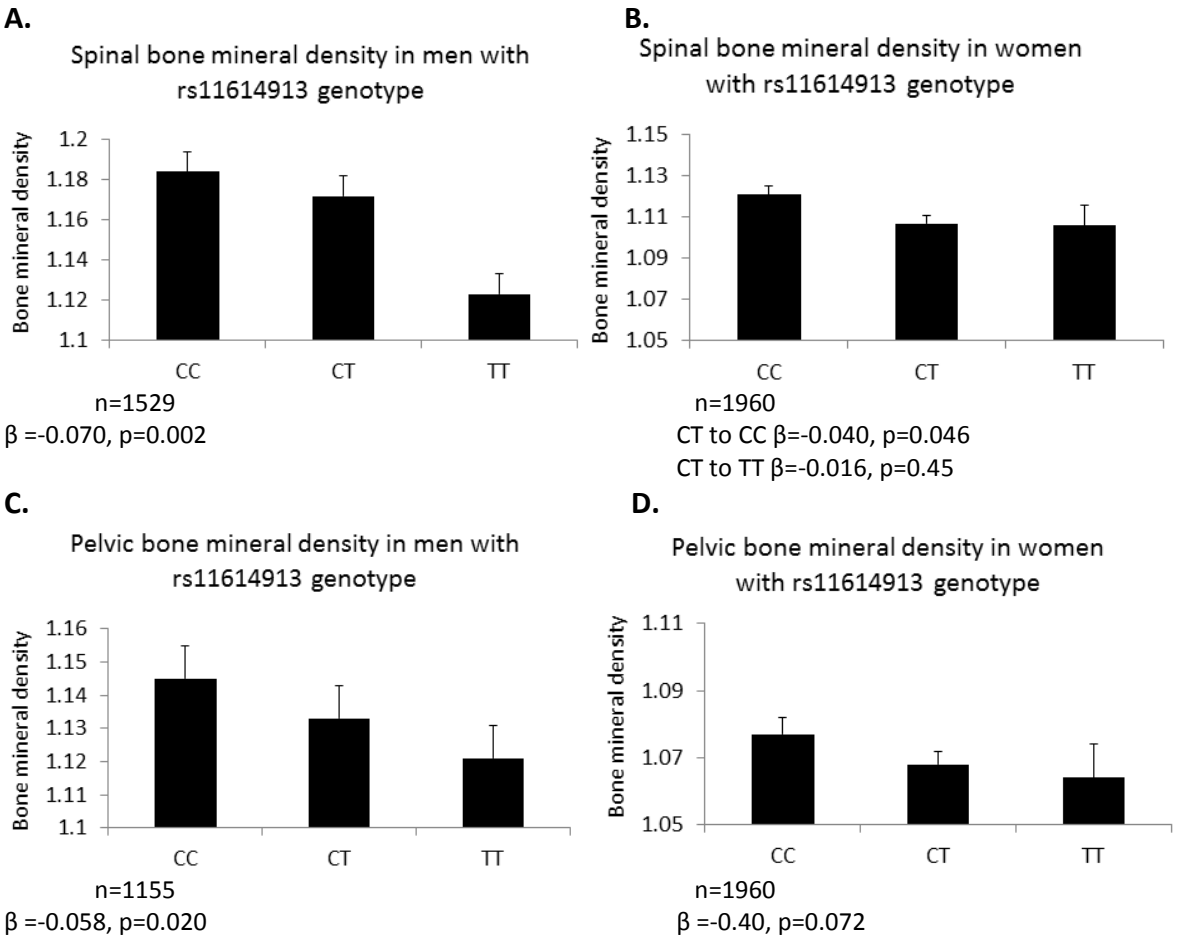

Table 6.1: Association of rs11614913 with bone mineral density in the GeFOS consortium
Statistical significance presented is from the meta-analysis by Estrada *et al.* [352] using regression coefficients and after correction for multiple testing both at the individual study level and after meta-analysis.

Site of BMD measurement	Gender	Direction of effect of T allele on BMD	p-value
Lumbar Spine	Men	Decreases	1.12×10^{-3}
	Women	Decreases	3.18×10^{-9}
	Combined	Decreases	8.92×10^{-10}
Femoral neck	Men	Decreases	4.66×10^{-3}
	Women	Decreases	1.27×10^{-4}
	Combined	Decreases	6.08×10^{-8}

6.3.2 The relationship between body fat distribution and bone mineral density in the OBB

AT and bone share a common lineage and AT is known to influence bone metabolism. Therefore, it was necessary to consider the possibility that the association of rs11614913 with both body fat distribution and BMD was due to confounding factors; in other words, that an increased WHR and decreased axial BMD might be directly correlated with one another. A literature search showed a lack of clear evidence that was directly applicable to the OBB (Caucasian, healthy 30-50 year olds) and conflicting evidence regarding other populations. For these reasons the OBB database was interrogated to determine the relationship between body fat distribution and BMD.

There are number of factors that are known to influence BMD. With this in mind, separate analyses were carried out for each gender. Age at the time of study visit and height (as a proxy for skeletal size) were included as covariates for all regression models. To isolate the associations with individual AT-depots, total AT mass was added as a covariate for these outcomes. Within the OBB 32.1% of women and 32.5% of men were current or ex–smokers. Smoking status was recoded as total pack-years. Self-reported weekly alcohol consumption (measured in units) was also available. Surprisingly, neither smoking nor alcohol intake were associated with BMD in either gender, perhaps because of the young healthy population in the OBB. Therefore, neither of these variables was included in the final model.

The women in the OBB were all below the age of 50 at the initial study visit. Menopause status (pre- or post-menopausal) was recorded for 74.3% of women. 7.1% of women were recorded to be post-menopausal. This was a significant predictor of reduced total BMD

(β=-0.080, p=6.4x10^{-5}). Menopause status (Post- vs pre-menopausal or missing data) was recoded as a dummy variable and included as a covariate.

Hormonal contraceptive use has been associated with lower BMD [381, 382]. The form of contraception used was recorded for 40.7% of women. Of those with data available: 32.4% took an oral contraceptive pill (OCP); 34.6% had a coil inserted; 3.7% had an implant; 2.1% had a depot injection and 28.2% did not use any of the above. Depot injections and implants release progestogens whilst intrauterine coils can be copper (non-hormonal) or progestogen releasing. Likewise, the OCP can contain progesterone only or more commonly progesterone combined with a synthetic oestrogen. No further information was available regarding which of these were used. Therefore, hormone-releasing contraceptives of any type were combined together. The intrauterine coil was excluded. Use of any hormone-releasing contraceptive was associated with BMD (β=-0.087, p=7.0x10^{-7}) and so this was added as a covariate to regression models for the female population.

Total fat mass was independently associated with BMD in both men and women (Table 6.2 and Table 6.3). Interestingly BMD of the arms was also associated with total fat mass (men; β=0.227 p=4.24x10^{-21}, women; β=0.241 p=1.29x10^{-31}) implying that this is not just a load bearing effect.

Obesity appears to attenuate the effects of AT mass on BMD (Table 6.2 and Table 6.3). In obese individuals (BMI>30), the positive association between BMD and total AT mass was lost both in men and in women. In contrast AT mass remained predictive of BMD in lean (BMI<30) men and women. As shown in Table 6.4 and Table 6.5 there was a strong positive relationship between lean body mass and BMD at all sites in both genders. Obesity did not substantially alter the associations between lean mass and BMD.

The ratio of android-to-gynoid AT was positively correlated with BMD of the spine in both men and women and with BMD of the pelvis in women, but not with total BMD. Importantly, the effect of regional AT distribution on BMD is gender specific. In women android SAT and VAT displayed opposite relationships to BMD, with android SAT being correlated with increased BMD whilst VAT was correlated with reduced BMD. These effects were reflected in the relationship of BMD and VAT-to-android SAT ratio. In contrast, there was no convincing relationship between regional android AT distribution and BMD at any site in men.

Gynoid AT mass did not correlate with total BMD in either gender, although interestingly there was a negative association between BMD of the spine and gynoid AT mass in both genders. We observed the same association between BMD of the spine and leg fat (men; β=-0.170 p=0.0030, women; β= -0.230 p=1.2x10^{-6}). The association between lower body fat mass and reduced spinal BMD has been reported by another group [383] who noted an inverse association between gynoid fat mass and BMD at the LS and femur after correction for age and body weight in elderly Italian women.

The associations between AT mass or distribution were not substantially altered by adjustment for HOMA, as a measure of insulin resistance, implying that insulin is unlikely to be the mediating mechanism (data shown in the Appendix, Table 9.5 and Table 9.6).

Table 6.2: The relationship between total BMD and lean mass or total AT mass in lean or obese men. Linear regression model adjusted for age and height.

	Whole cohort			Lean (BMI<30)			Obese (BMI>30)		
	N	Standardised β	p-value	N	Standardised β	p-value	N	Standardised β	p-value
Lean mass	1718	0.555	$3.3x10^{-100}$	1405	0.555	$4.2x10^{-70}$	131	0.427	$2.5x10^{-9}$
Total AT mass	1718	0.246	$1.0x10^{-25}$	1401	0.137	$2.5x10^{-7}$	311	-0.028	0.61

Table 6.3: The relationship between total BMD and lean mass or total AT mass in lean or obese women. Linear regression model adjusted for age, height, menopause status and use of hormonal contraceptives.

	Whole cohort			Lean (BMI<30)			Obese (BMI>30)		
	N	Standardised β	p-value	N	Standardised β	p-value	N	Standardised β	p-value
Lean mass	2275	0.444	$6.4x10^{-92}$	1891	0.423	$4.2x10^{-55}$	376	0.347	$2.5x10^{-8}$
Total AT mass	2275	0.254	$6.2x10^{-36}$	1891	0.154	$7.7x10^{-12}$	376	-0.027	p=0.62

Table 6.4: Associations between body fat distribution and BMD in men in the OBB cohort.

	Total BMD		LS BMD		Pelvic BMD		Arm BMD	
	Standardised β	p-value	Standardised β	p-value	Standardised β	p-value	Standardised β	p-value
Lean mass†	0.475	2.70×10^{-33}	0.395	1.2×10^{-23}	0.561	3.3×10^{-41}	0.347	1.8×10^{-16}
Android-to-gynoid AT ratio‡	0.018	0.58	0.104	0.001	0.052	0.13	-0.028	0.40
VAT mass‡	-0.017	0.12	0.036	0.47	0.009	0.86	-0.122	0.02
Android SAT mass‡	-0.038	0.41	-0.072	0.12	-0.055	0.25	-0.66	0.16
VAT-to-android SAT ratio‡	0.004	0.85	0.022	0.34	0.009	0.72	0.006	0.83
Gynoid AT mass‡	-0.139	0.068	-0.243	0.001	-0.111	0.16	-0.220	0.005

†Adjusted for age at study visit, weight and height
‡Adjusted for age at study visit, height and total body fat mass

Table 6.5: Associations between body fat distribution and BMD in women in the OBB cohort.

	Total BMD		Spine BMD		Pelvic BMD		Arm BMD	
	Standardised β	p-value	Standardised β	p-value	Standardised β	p-value	Standardised β	p-value
Lean mass†	0.398	$1.7x10^{-28}$	0.293	$9.6x10^{-17}$	0.474	$7.7x10^{-38}$	0.185	$8.3x10^{-7}$
Android-to-gynoid AT ratio‡	0.041	0.15	0.159	$1.7x10^{-8}$	0.106	$3.2x10^{-4}$	-0.037	0.21
VAT mass‡	-0.153	$2.7x10^{-5}$	-0.002	0.95	-0.059	0.18	-0.185	$4.7x10^{-7}$
Android SAT mass‡	0.263	$4.9x10^{-5}$	0.260	$4.2x10^{-5}$	0.290	$1.1x10^{-5}$	0.073	0.27
VAT-to-android SAT ratio §	-0.116	$5.2x10^{-8}$	-0.013	0.53	-0.090	$3.8x10^{-5}$	-0.089	$4.9x10^{-5}$
Gynoid AT mass‡	-0.109	0.07	-0.210	$3.7x10^{-4}$	-0.183	0.003	-0.022	0.72

†Adjusted for age at study visit, weight, height, use of hormonal contraceptives and menopause status.
‡Adjusted for age at study visit, height, total body fat mass, use of hormonal contraceptives and menopause status.
§Adjusted for age at study visit, height, weight, use of hormonal contraceptives and menopause status.

6.3.3 Investigation of other variants in linkage disequilibrium with rs11614913

The genotyping data suggest that the locus containing pre-mir-196a-2 has a role in the regulation of body fat distribution and bone metabolism, but do not prove that the causative gene is pre-mir-196a-2. I therefore investigated the likelihood that the observed phenotypes were driven by another variant in linkage disequilibrium (LD) with rs11614913.

The Hapmap project is an international collaboration set up to produce a haplotype map of common patterns of human genetic variation [384]. Hapmap data was accessed to assess LD blocks within the *HOXC* locus (Figure 6.2). As can be seen clearly in Figure 5.8 and Figure 6.2 rs11614913 is in low LD with the *HOXC13* locus variants that have previously been associated with WHR [90, 297]. Moreover, associations at the *HOXC13* locus show significant sexual dimorphism Figure 5.8 and [90, 297]) that is not observed with rs11614913.

The rs736825 polymorphism is located at 12q13.13 near *HOXC6*. It was identified by Estrada *et al.* as a secondary signal associating with BMD at the LS and FN that still achieved genome wide statistical significance after conditional analysis for the primary SNP [352]. HOXC6 has been implicated in development of the axial skeleton; mice homozygous for disruption of the *HOXC6* gene have a homeotic transformation of the second thoracic vertebra [385]. Interrogation of the Hapmap database revealed that there was a high degree of LD between rs736825 and rs11614913 (D'=0.94, r2=0.536, LOD=11.17). The MAF of rs736825 was reported to be 0.37 by the 1000 genomes project [386], making it likely that the r2 might be higher than that estimated by the Hapmap project. Therefore the OBB was genotyped for rs736825 and its associations with body fat distribution and BMD analysed. In addition, exome chip genotyping had been performed

on DNA from 5,741 individuals in the OBB (unpublished data, Prof. Karpe and Dr Neville). All other variants within the *HOXC* cluster for which genotype data were available were also analysed.

LD data was not available for rs78002127 (indicated by the red arrow in Figure 6.3). However, within the OBB its MAF=0.0008, suggesting that it cannot be driving the association between rs11614913 and WHR. Other SNPs associating with WHR and spine BMD are in low LD with rs11614913 according to the Hapmap CEU dataset. Whilst rs736825 was associated with WHR in men (EMP=0.021, additive model adjusted for BMI and age) it was only associated with spinal BMD in men (EMP= 0.018) and was not associated with pelvic BMD in either gender.

Figure 5.8 shows a variant located close to, and in high LD with, rs11614913. This is rs3803042 (indicated in Figure 5.8 by the red circle. MAF=0.41, 1000 genomes project) which was identified as a marker of WHR in the 2012 analysis of the GIANT consortium dataset [331]. rs3803042 remains significantly associated with WHR adjusted for BMI in the most recent analysis by Shungin *et al.*(n=141,125, β=0.027, p=1.5x10^{-9}). It is located within a non-coding region between pre-miR-196a and *HOXC9*. There is no literature suggesting a functional role for this variant. Another SNP that is significantly associated with WHR and is in moderate LD with rs11614913 is rs894737 (represented in Figure 5.8 by the orange circle in *HOXC4)*. This is located within the introns of *HOXC4, HOXC5* and *HOXC6*. Again, there is no further literature regarding this variant.

Figure 6.2: The LD block structure of the region surrounding pre-mir-196a-2 on chromosome 12.
The image was generated in Haploview 3.2 using the Hapmap CEU data (www.hapmap.org). Numbers within diamonds represent D' values for SNP pairs. This is represented visually with colour coding; red within the diamonds represents strong LD (>95%). rs11614913 is highlighted in the red box.

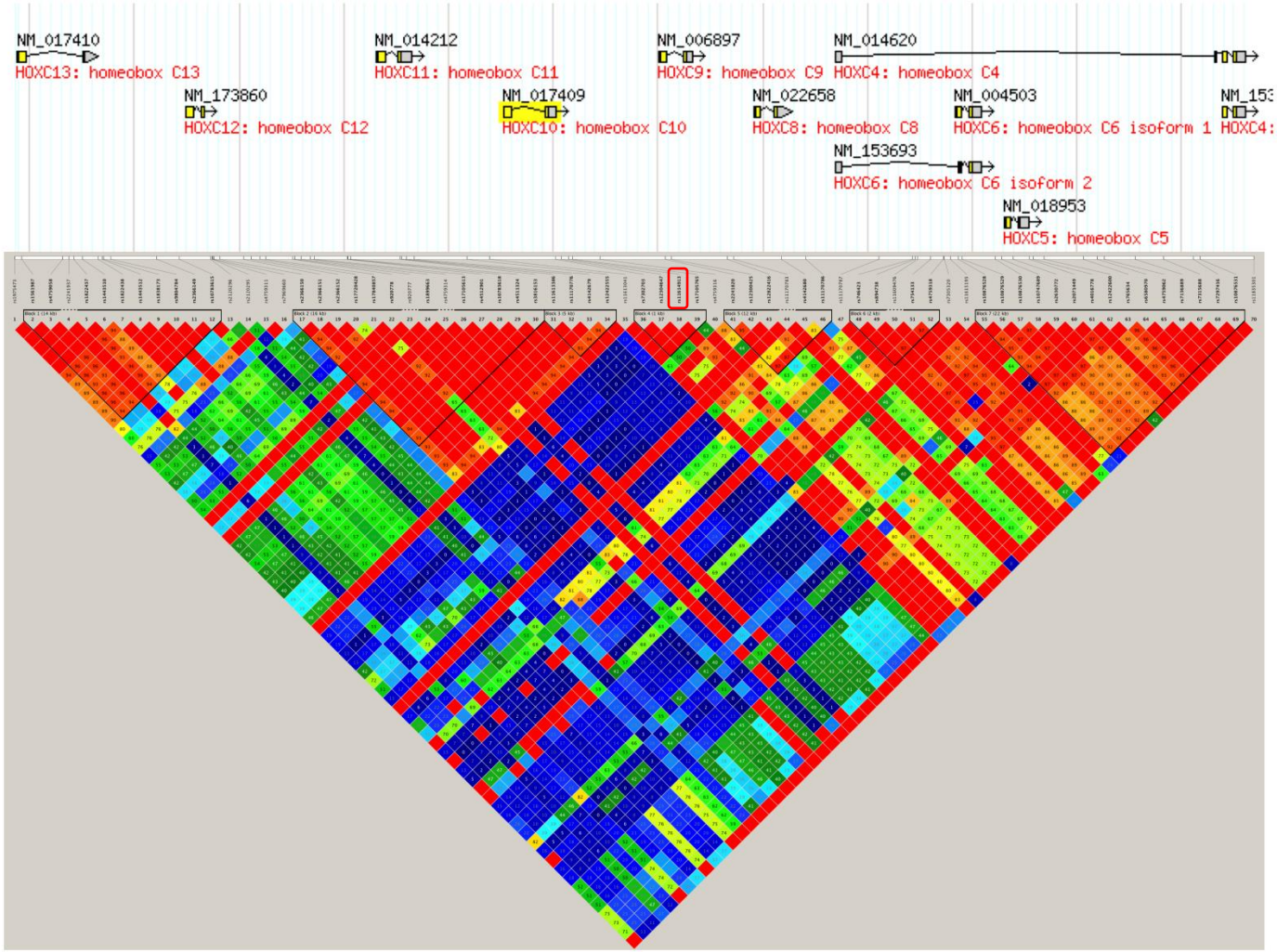

Figure 6.3: Regional plots of the *HOXC* gene cluster plotted in LocusZoom using data for subjects from the OBB.
LD data is imputed using Hapmap CEU data. The recombination rate overlay is based on HapMap CEU data. Gene positions are annotated based on hg19/1000 Genomes March 2012 release. RS11614913 is represented by the purple diamond. In these figures rs736825 is indicated by the green dot and rs78002127 by the red arrow. Plots for the relationships between pelvic BMD and variants in the HOXC cluster are similar to those for spinal BMD and are not shown.

A. WHR in men

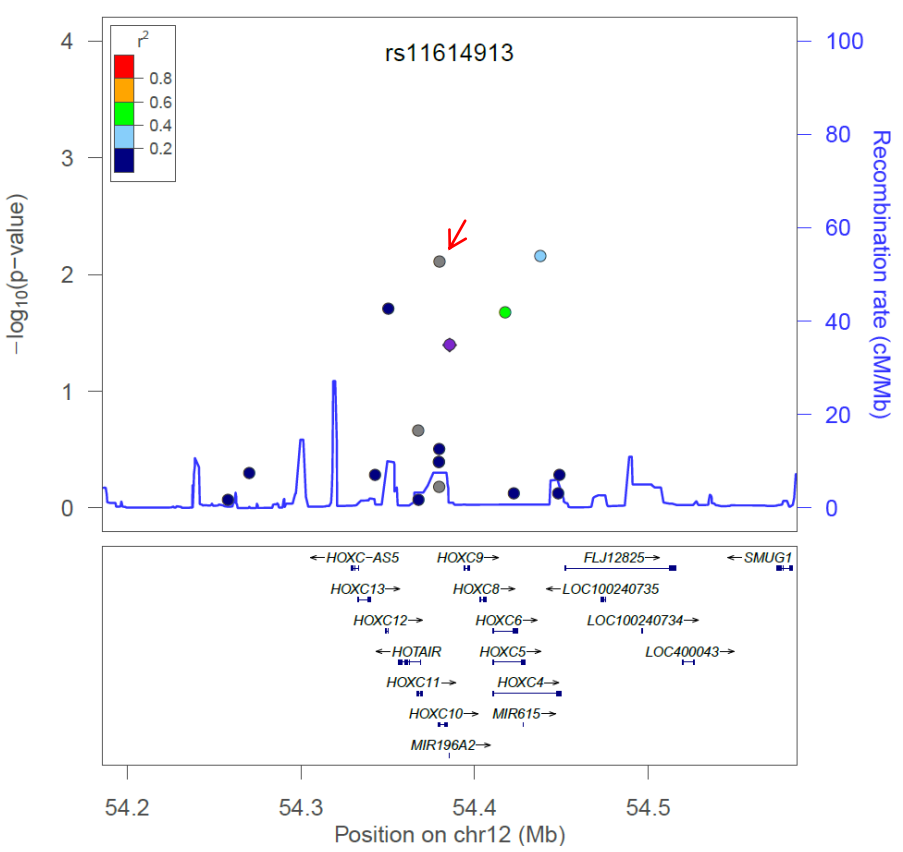

B. WHR in women

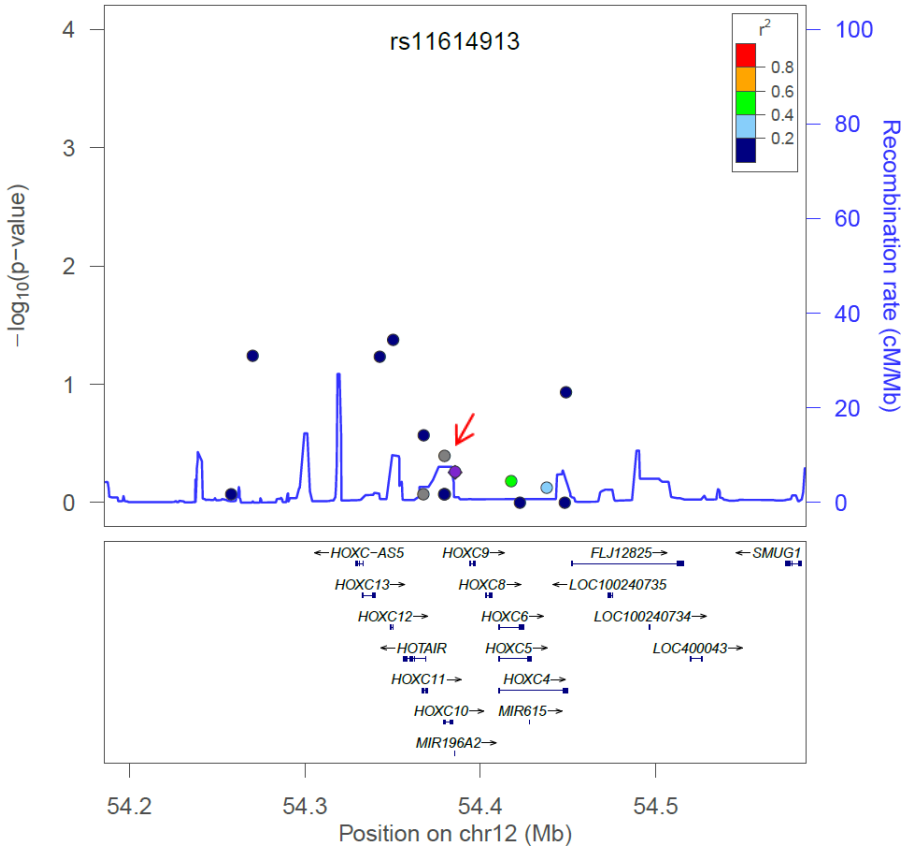

Figure 6.4: Regional plots of the *HOXC* gene cluster plotted in LocusZoom using data for subjects from the OBB.
LD data is imputed using Hapmap CEU data. The recombination rate overlay is based on HapMap CEU data. Gene positions are annotated based on hg19/1000 Genomes March 2012 release. RS11614913 is represented by the purple diamond. In these figures rs736825 is indicated by the green dot and rs78002127 by the red arrow. Plots for the relationships between pelvic BMD and variants in the HOXC cluster are similar to those for spinal BMD and are not shown.

C. Spinal BMD in men

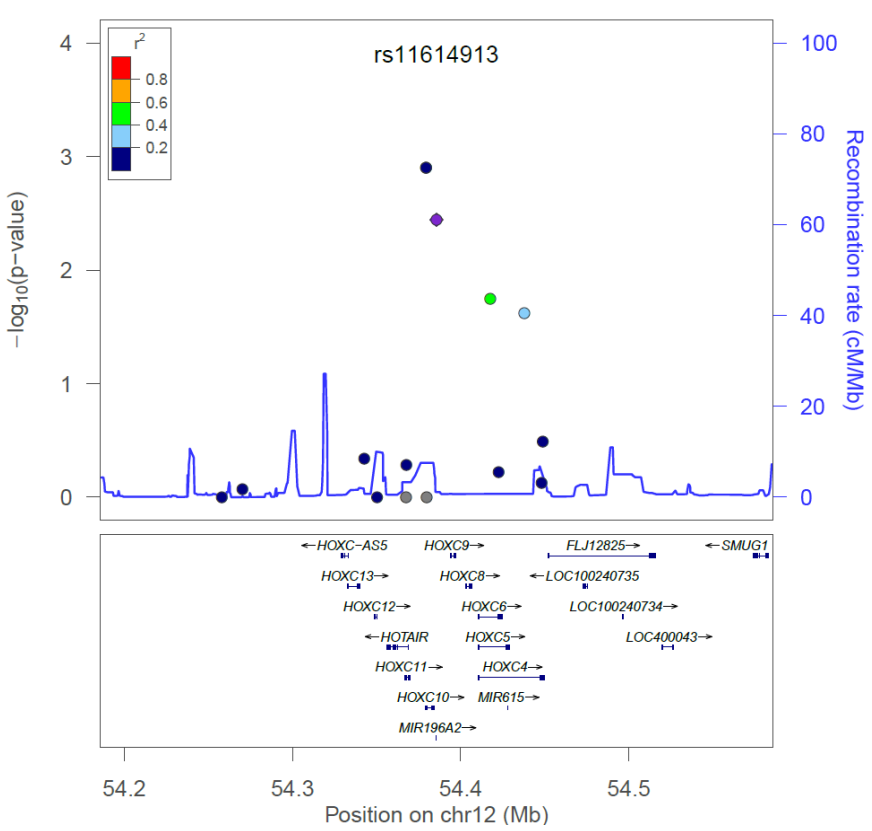

D. Spinal BMD in women

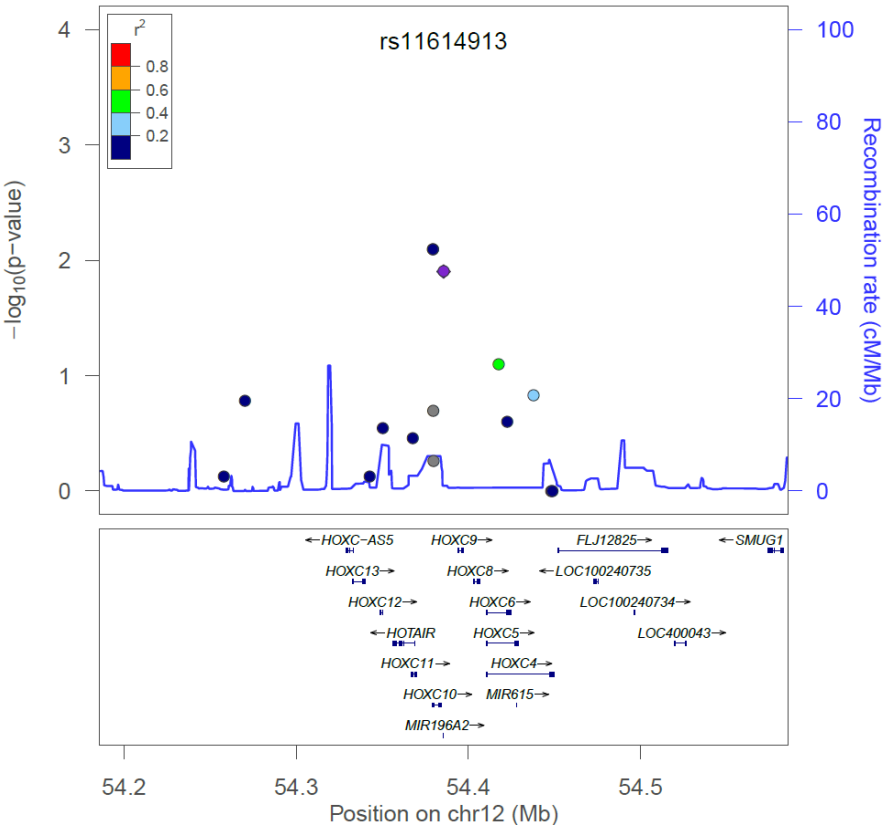

6.4 Discussion

Consistent with a previous study [366] we found that the positive association between increasing AT mass and BMD was attenuated in obesity. Bone mineralisation is positively modulated by AT through the direct effect of weight loading and indirectly through adipokines [357], circulating insulin [387] and increased aromatisation of androgens [388]. However, increased AT mass is also correlated with a more inflammatory profile of circulating cytokines [389] which in turn increases bone resorption [390]. It may be that in obesity the detrimental actions of AT on bone begin to outweigh its protective effects.

Within the OBB population there is a sexual dichotomy in the association between AT distribution and BMD. In women the abdominal AT depots (ASAT and VAT) have opposing associations with BMD; in men the evidence that regional abdominal AT deposition influences BMD is weaker. This may explain why some studies investigating BMD in male-only cohorts have failed to find associations with individual AT depots [42]. Importantly, our data show that the rs11614913 variant is associated with reduced BMD and with increased waist circumference which might be caused by an expansion in android SAT, whilst in our population as a whole there a modest positive association between android-to-gynoid AT ratio and a positive relationship between android ASAT and BMD in women. Therefore, the associations between rs11614913 and both BMD and body fat distribution phenotypes appear to be independent.

Associations tended to be strongest for BMD at the spine and pelvis, both in the genotype analysis and relating to body fat distribution. This may be a true biological effect or may be an artefact of the way in which BMD is measured, that is, BMD determination may be more accurate at these sites and small associations therefore more readily detected.

There are some limitations to the conclusions that can be drawn from genotype association studies. Firstly, causality cannot be inferred from association. Secondly, it is

not possible to distinguish between the effects of variants in LD. Investigation of other variants in the *HOXC* locus did not highlight another gene which was likely to be driving the observed associations, but neither did it rule this possibility out. Indeed, multiple causative variants may be present at a single locus [391].

If rs11614913 is an eQTL for miR-196a in bone, as in AT, then the observation that the rs11614913 T-allele is associated with reduced BMD is consistent with reports that miR-196a induces osteogenesis in vitro [206, 274]. It was beyond the scope of this project to investigate the relationship between miR-196a and BMD functionally. A review of publically available datasets revealed that miR-196a is expressed within bone marrow [138], albeit at ~115-fold lower levels than in AT ($p=0.001$). Bone marrow is a complex tissue composed of numerous cell types including mature and precursor haematoopoietic cells along with stromal cells (MSCs, fibroblasts, adipocytes, osteoblasts and osteoclasts, amongst others). To clarify the role of miR-196a in bone metabolism it will be necessary to determine its relative expression in osteocytes, osteoblasts and osteoclasts (responsible for bone homeostasis, production and resorption respectively). It will be important to determine whether expression is influenced by rs11614913 genotype. Finally, future experiments should functionally characterise the role of miR-196a in osteogenesis.

7 Functional studies

7.1 Introduction

7.1.1 Mechanisms of WAT expansion

In response to over-nutrition WAT expands to allow energy storage. The ability of WAT to appropriately store fat is crucial to metabolic health. The lack of adequate amounts of subcutaneous AT, or its inability to expand when needed, may lead to a failure of the subcutaneous AT to appropriately store lipids resulting in increased visceral and ectopic fat deposition [1]. Indeed, the necessity to maintain functional AT expansion, the so-called "adipose tissue expandability" hypothesis [2] is illustrated by the morbidly obese AdTG-ob/ob mouse which is genetically modified to possess an unlimited capacity for AT expansion and is markedly more insulin sensitive than ob/ob littermates [3]. As discussed in the introduction (1.2.4*)*, ASAT and GSAT have opposite associations with metabolic health and individuals display marked differences in their propensities to store fat in different AT depots.

7.1.2 Pre-adipocyte proliferation

WAT expansion can occur through adipocyte hyperplasia or hypertrophy. A study of monozygotic twin pairs concordant or discordant for obesity revealed that same-weight twin pairs had adipocytes of similar size and number, suggesting a degree of genetic influence [392]. In response to energy excess, the ability to expand WAT through adipocyte hyperplasia appears to differ between individuals, with some obese twins having an increase in adipocyte number and some having fewer adipocytes than their lean twins [392].

Spalding *et al.* [393] estimated that approximately 10% of white adipocytes turnover each year and interestingly this rate was reported not to be influenced by age or changes in energy balance. Indeed, adipocyte number has been reported to stay constant despite

marked weight reduction [393, 394] or gain [394]. However, on an individual level fat mass is proposed to be determined both by adipocyte size and number, with the latter being determined before adulthood is reached [393, 395], at least in individuals with early-onset obesity. Therefore, whilst there is some controversy over the role of pre-adipocyte proliferation in response to energy excess, it seems clear that adipocyte hyperplasia is important in determining fat mass early in life.

Pre-adipocytes derived from GSAT and ASAT have been described to have similar rates of proliferation *in vitro* [396], a finding in line with our own unpublished data. In comparison to VAT, SAT has a greater ability to increase pre-adipocyte number through proliferation in mice [397] and in humans [68].

7.1.3 Adipogenesis

Mesenchymal stem cells (MSC) give rise to cells of the adipocyte lineage through a process involving an early commitment step followed by terminal adipocyte differentiation. In humans the number of mature white adipocytes remains relatively constant throughout adult life, reflecting the fine balance between adipocyte death and adipogenesis. Terminal adipogenic differentiation sees the committed adipocyte precursors or "pre-adipocytes" acquire the functional characteristics of the mature adipocyte. The adipogenic differentiation of pre-adipocytes is tightly regulated by a well-defined transcription factor cascade [398] involving the transient expression of early transcriptional regulators (CEBPβ, CEBPδ) followed by the induction of critical adipogenic regulators (CEBPα, PPARγ) which co-ordinate the expression of many adipocyte genes. There are depot-specific differences in the regulation of adipogenesis. Treatment with PPARγ agonists enhanced *in vitro* adipogenesis of pre-adipocytes derived from the subcutaneous AT depots whilst pre-adipocytes derived from the omental depot were refractory to its effects[399]. Although the stages of terminal adipogenic differentiation have been well characterised [398] early

events in the commitment of MSC to the adipocyte lineage are less clear. Resident progenitors have been identified within the adipose stromal vascular fraction [400].

7.1.4 Extracellular matrix and angiogenesis

WAT is a complex organ with dynamic interplay between its structural and cellular components. Adipocytes are contained within a network of extracellular matrix (ECM) proteins, the structure of which varies between WAT depots [47]. ECM deposition is determined by the production of fibrillary proteins such as the collagens and fibrinogen and their degradation, for instance, by the matrix metalloproteinases. In addition to providing a structural matrix for WAT, ECM plays a role in determining the ability of WAT to expand [401]. Thus, appropriate ECM is necessary for *in vivo* adipogenesis [402], whilst excessive accumulation of ECM components can inhibit WAT expansion [401]. In mice, the extent of AT remodeling and ECM deposition in response to high-fat feeding is depot-specific [403] but experimental data on this in humans is lacking.

Appropriate angiogenesis appears to be a crucial factor in adipogenesis and WAT remodelling *in vivo.* In mice, adipogenesis was closely related to adipogenesis of cell clusters and inhibition of new blood vessel formation inhibited adipogenesis [404]. Furthermore, mice treated with antiangiogenic agents displayed fat mass reduction which was mediated through increased apoptosis [405]. Angiogenesis and ECM deposition are linked. It has been suggested that the inability of expanding AT to recruit sufficient new vasculature leads to AT hypoxia and AT fibrosis via the induction of HIF1α [406]. Equally, propensity for angiogenesis and the type of new vessels formed is dependent on ECM components and structure [407].

Other important cell types such as macrophages [408] and leukocytes [409] are involved in AT remodelling. However, expression profiling of miR-196a across tissues and in THP-1 cells (4.3.2) does not support this as being of crucial relevance to this project.

7.1.5 Tissue culture as a model for investigating the function of genes

Human AT is a multicellular, complex and dynamic organ. This complexity can make it difficult to understand the regulatory roles of single miRNAs. One way of trying to simplify the AT organ in order to dissect the mechanisms by which a gene is acting is to use *in vitro* culturing of its component cell fractions. This allows for controlled conditions in which one variable at a time can be altered and its effect observed, namely miR-196a expression in these experiments. Pre-adipocytes differentiated *in vitro* were chosen as the cell type in this model because adipocytes are the major component of AT and the component in which miR-196a was shown in to be most highly expressed (4.3.2). Having established that miR-196a exhibits AT-depot specific expression patterns and that its expression was associated with a human AT distribution phenotype I went on to develop an *in vitro* model with which to test the hypothesis that miR-196a regulated WAT accumulation in a depot-specific manner by regulating pre-adipocyte proliferation and/or adipogenesis.

7.1.6 Hypotheses and aims

In vivo experiments demonstrated that rs11614913 TT-genotype is associated with reduced miR-196a expression in ASAT. In addition, the minor T-allele is associated with increased WHR which may be regulated by expansion of ASAT. Further genotype analysis suggested that the TT genotype of rs11614913 is associated with increased adipocyte size within ASAT. In this chapter I knock down miR-196a to mirror the change in expression seen in rs11614913 TT-homozygotes and explore the effects of this on pre-adipocyte phenotype. Specifically, I investigate whether miR-196a has depot-specific effects on pre-adipocyte function.

Aims:

1. To determine whether the Pt2 cell lines are appropriate *in vitro* models for investigating pre-adipocyte function.

2. To establish a method of modulating miR-196a expression in pre-adipocytes *in vitro*.
3. To determine whether miR-196a regulates proliferation or adipogenesis of pre-adipocytes *in vitro* in a depot-specific manner.
4. To perform transcriptomic profiling of pre-adipocytes derived from both depots, with and without miR-196a inhibition, to identify biological pathways regulated by miR-196a.

7.2 Materials and methods

7.2.1 Validation of the Pt2 cell line

7.2.1.1 Proliferation of Pt2 cell lines

Proliferation rates of Pt2 cell lines were determined by Dr Goshi Nakamura (Takeda, Japan). Cells were plated density of 2,500 cells per flask in T25 flasks at passages between 9 and 11. Separate flasks were trypsinised and counted using haemocytometer for each time-point. Four counts were performed for each time-point and four separate experiments were performed.

7.2.1.2 Adipogenic differentiation of the Pt2 cell line

Experiments used primary cells from the Pt2 donor and immortalised pre-adipocytes derived from ASAT and GSAT biopsies from the Pt2 donor ('Pt2 Abdo' and 'Pt2 Glut'). Experiments were performed in both low and higher passage Pt2 cell lines. Pre-adipocytes were plated in 6-well plates at a density of $2x10^5$ cells/well. Table 7.1 outlines the experimental design. The day following pre-adipocyte plating growth media was exchanged for differentiation media according to the protocol outlined in 2.2; this is referred to as day 0. Cells were harvested in 500µl Trizol and RNA extraction was performed as described in Chapter 2.

For detection of miRNA cDNA synthesis and qPCR used the Qiagen method, described in 2.3.2.6.1. A 1/40 cDNA dilution was used.

For mRNA detection in this experiment only cDNA was generated using the High Capacity cDNA Reverse Transcription Kit (Life Technologies, UK). Briefly, RNA sample concentrations were normalised to give 500ng of RNA in 10 µl of nuclease-free water. This was combined on ice with 10 µl of RT master mix which was made up according to the manufacturer's instructions. Reactions were performed using the PTCV225 Peltier Thermal-Cycler (MJ Research, Waltham, Massachusetts, USA) and consisted of a 10 minute incubation at 25 °C (to anneal primers) followed by 37 °C for 120 minutes (to generate cDNA) and a 5 minute step at 85 °C (to denature the Multiscribe reverse transcriptase enzyme). Detection of transcripts using qPCR was performed using Taqman assays as described in Chapter 2 on a 1/40 cDNA dilution.

Table 7.1 Experimental design for assessing adipogenesis in the Pt2 cell lines and primary pre-adipocytes derived from Pt2 ASAT and GSAT.

Condition	Passages	Number of experimental replicates	Timepoints for cell harvesting
Primary pre-adipocytes derived from ASAT and GSAT biopsies from Pt2 donor	Passage 6x3 Passage 8x3	6	Days 0, 2, 4, 7, 10, 14
Pt2 Abdo and Pt2 Glut cell lines	Passage 8x3 Passage 9x3	6	Days 0, 2, 4, 7, 10, 14
Pt2 Abdo and Pt2 Glut cell lines	Passage 17 Passage 18x2 Passage 19 Passage 21	5	Days 0, 2, 4, 7, 10, 14

7.2.2 Transient transfection of miR-196a mimic and inhibitor

Cells were plated in 6-well plates at a density of $2x10^5$ cells/well in antibiotic free growth media. miScript miRNA miR-196a mimic (MSY0000226) and miR-196a inhibitor (MIN0000226) and AllStars Negative siRNA AF 488 control (#1027284) were obtained from Qiagen (UK). For each well of a 6-well plate 195ul of Opti-MEM Reduced Serum Media

(Invitrogen, UK) was combined with 5ul of Lipofectamine™ 2000 (Invitrogen, UK) and left at room temperate for 10 minutes. The miScript mimic or inhibitor or negative controls were combined with opti-MEM in a separate tube to give a total volume of 200ul at the required concentration. This was then added to the opti-MEM and Lipofectamine™ 2000 and the solution left at room temperature for a further 20 minutes to allow lysosomes containing the construct to form. 400ul of the combined solution was added to each well along with 1.6 mls of antibiotic free growth medium.

In order to perform transfection of pre-adipocytes on cover slips with AllStars negative siRNA control, pre-adipocytes were plated at a density of $2x10^5$ cells/well in 6-well plates containing glass cover slips. Cells were transfected with 10 nM mimic using the methods described above. At the desired time point cover slips were removed and washed gently with PBS before being fixed with 4% paraformaldehyde in PBS. Nuclei were stained using Vectashield mounting medium with DAPI (Vector laboratories, UK). Microscopy was performed as described in 2.4.

7.2.3 Lentiviral constructs and generation of stable pre-adipocyte cell lines

As discussed in 7.2.2 transient transfection was not satisfactory for experiments and so a stable cell lines were generated. MISSION custom hsa-mir-196a-5p inhibitor and ath-miR-416 negative control cloned into the TRC2-pLKO-puro vector were purchased from Sigma-Aldrich (USA) in the form of DNA plasmids. Plasmids were amplified in MAX Efficiency DH5α Competent E. Coli (Invitrogen, UK). Briefly, MAX Efficiency DH5α Competent cells were transformed with hsa-mir-196a-5p inhibitor or control plasmid by heat shock according to the manufacturer's instructions. Transformed bacteria were incubated on agar plates containing ampicillin at a final concentration of 100µg/ ml overnight at 37 °C, after which single colonies were picked and incubated in Lennox ezmix LB broth (Sigma-Aldrich, UK) containing 100µg/ ml ampicillin for 24 hours at 37 °C. Amplified plasmids

were isolated using the Midiprep plasmid kit (Qiagen, UK) according to manufacturer's instructions. DNA was quantified using the Nanodrop ND-1000 spectrophotometer.

Lentiviral particles were produced by co-transfection of HEK293 cells with the MISSION hsa-mir-196a-5p inhibitor or ath-miR-416 negative control vector along with packaging vectors (MISSION packaging mix, Sigma-Aldrich, UK). Packaging vectors (contained within packaging mix) encode viral packaging and envelope genes. Co-transfection of packing vectors and plasmid DNA into the HEK293 producer cells generates viral particles containing the specified transgene. HEK293 cells were cultured in T25 flasks according to usual protocol (see 2.2.3) but with antibiotic free media. Cells were transfected at 70-80% confluence by the addition of 1µg of plasmid DNA along with 10µl of packaging mix and 6µl of Fugene 6 (Promega, UK) in fresh antibiotic free HEK293 media. After sixteen hours media were discarded and replaced with complete HEK293 media. The following day media were collected and stored. Cells were then cultured with fresh complete media for a further 24 hours that was again collected and stored on day 3 of the protocol.

Next, stable HEK293 cell lines were generated to demonstrate effective infectivity of the lentiviral particles and function of the miR-196a inhibitor. Passage 12 HEK293 cells in T25 flasks at 50% confluence were cultured in 4 mls of complete HEK293 medium with the addition of hexadimethrine bromide at a final concentration of 8µg/ ml and 1 ml of miR-196a inhibitor or negative control lentiviral particles for 24 hours. From day 3 cells were cultured in the presence of 2µg/ ml puromycin in order to select transduced cells. This dose of puromycin has been confirmed in experiments conducted within the group to kill both pre-adipocytes and HEK293 cells not containing the puromycin resistance gene.

To generate stable pre-adipocyte cell lines, Pt2 Abdo and Pt2 Glut cell line pre-adipocytes at passage 8 were plated in T25 flasks at a density of $1.2x10^5$cells/flask in complete growth media. Cells were transduced and selected using the same protocol as for HEK293 cells.

Pre-adipocyte cell lines were cultured in the presence of puromycin during the proliferative phase but not after the addition of differentiation media. The stable cell lines generated here are referred to as AbdoCon, Abdo miR-196aKO, GlutCon and Glut miR-196aKO.

7.2.4 Adipogenesis of miR-196aKO or control pre-adipocytes

In six separate experiments AbdoCon, Ab miR-196aKO, GlutCon and Glut miR-196aKO Pt2 pre-adipocytes at passages 10-12 were seeded in 6-well plates at a density of $2x10^5$ cells/well. Differentiation media were added according to the protocol described in 2.2.1 from 24 hours after seeding. Cells were harvested by scraping in 500µl Trizol reagent on days 0 (i.e. immediately prior to the addition of differentiation media), 2, 4, 7, 10 and 14.

7.2.5 Proliferation of pre-adipocytes with miR-196aKO

AbdoCon, Ab miR-196aKO, GlutCon and Glut miR-196aKO Pt2 pre-adipocytes at passages 10-12 were plated in T75 flasks in equal numbers and triple counted manually using a haemocytometer. To minimise error, trypsinised cells were then re-plated in another T75 flask. In this way an underestimation in cell numbers during one count would lead to plating a larger than planned number of cells for the next experiment, and so small counting errors would be averaged out over successive counts. For each condition four independent aliquots of cells were plated and were passaged and counted at least 3 times. Doubling time was calculated as;

Doubling time = t2-t1 ((log(2)/log(q2/q1))

where t=time (days) and q=cell number.

Statistical significance was determined using paired t-tests.

7.2.6 Immunocytochemistry for detection of Caspase-3

Pt2 Glut miR-196aKO, GlutCon, Abdo miR-196aKO and AbdoCon pre-adipocytes were plated in 6-well plates containing glass coverslips at a density of 100,000 cells/well. Thirty-

six hours after plating cells were washed gently in PBS and fixed in 4% paraformaldehyde in PBS. Cover slips were removed from 6-well plates and transferred to a wet-chamber where they were washed twice in tris-buffered saline (TBS) and then incubated in 0.001% Triton X in TBS for 15 minutes to make the cell membranes permeable. The cover slips were washed twice more in TBS, incubated 1/20 swine serum in TBS for 20 minutes, before an overnight incubation with 1/100 dilution of anti-caspase 3 cell rabbit anti-human antibody (#9661S, Cell Signaling, USA) at 4 °C. The following day cover slips were washed three times and incubated for 30 minutes with 1/50 anti-rabbit biotin secondary antibody followed by 3 further washes and a 30 minute incubation with Streptavidin 485 at a 1/100 dilution. After three further washes in TBS cells were mounted on slides using Vectashield with DAPI. Microscopy was performed as outlined in 2.4.

7.2.7 Statistical methods

For experiments where paired cell lines are compared (e.g. Pt2 Abdo and Pt2 Glut, or AbdoCon and Ab miR-196aKO), paired T-tests or Wilcoxon signed rank tests were used, depending on the distribution of the data. Statistical methods for microarray analysis are described in the relevant sections.

7.2.8 Microarrays

Passage 10 Ab Con, Ab miR-196aKO, Gl Con and Glut miR-196aKO Pt2 pre-adipocytes were plated in 6-well plates at a density of 100,000 cells/well. This density was selected in the light of functional experiments demonstrating a negative effect of miR-196a on proliferation. At the time of harvesting pre-adipocytes were sub-confluent and therefore undergoing active proliferation. Pre-adipocytes were harvested 72 hours after plating by scraping in Tri-reagent. Duplicate wells were pooled to give a total volume of 1 ml Trizol. RNA was isolated using the mirVana miRNA Isolation Kit (Life Technologies) as described in

2.3.2.2.1. RNA concentration was assessed using the Nanodrop ND-1000 spectrophotometer and by RiboGreen® assay and samples were normalised to give 100ng RNA in a total volume of 11 µl. RNA quality was verified using the Agilent TapeStation (Agilent, Santa Clara, US) and the RNA integrity Number (RIN) value of all the samples was greater than 7. Microarray experimental work, data normalization and generation of significant gene lists were performed at the Wellcome Trust Centre for Human Genetics, Oxford. Six replicates of each condition were submitted for microarray experiments along with the Affymetrix RNA control sample at the same starting concentration. RNA samples were reverse transcribed using the Illumina TotalPrep-96 RNA Amplification Kit and then converted into labelled cDNA using the Illumina Whole-Genome Gene Expression Direct Hybridisation Assay. The labelled ss-cDNA was then hybridised to two HumanGene2.1 ST-16 Array Plates. The array was washed, stained and scanned using the Affymetrix GeneTitan platform. Raw data were Robust multi-array (RMA) normalised and checked for quality. Differential expression analysis was performed for:

1. GlutCon vs AbdoCon
2. Abdo miR-196aKO vs AbdoCon
3. Glut miR-196aKO vs GlutCon

Database for Annotation, Visualization, and Integrated Discovery (DAVID) is a free online software that provides gene ontology (GO) enrichment analysis and functional classification to user-defined gene lists (http://www.david.niaid.nih.gov/ [410, 411]). GO enrichment analysis was performed with the gene list from the Affymetrix HumanGene2.1 ST-16 array as background. EASE score (a modified Fisher's exact test) was used to calculate enrichment for GO classifications. The default functional annotation cluster function within DAVID was used to cluster redundant or closely related GO terms together. The enrichment score for each cluster is the geometric mean of the Bonferroni-corrected p-values for the cluster.

7.2.9 Confirmation of microarray results by qPCR

Sixteen transcripts from key enriched GO terms were selected for qPCR validation. Seven experimental replicates (including the original microarray experiment) of Pt2 pre-adipocytes with miR196aKO or control vectors were included in the validation experiment. RNA was extracted using the Tri-reagent method and reverse transcription and qPCR were performed using Qiagen miScript reagents as described in 2.3.2.6.1. Statistical significance was calculated using paired t-tests or Wilcoxon signed ranks tests depending on the distribution of the data.

7.3 Results

7.3.1 Assessing the validity of the Pt2 cell line for functional experiments

7.3.1.1 Proliferation

Data on proliferation of the Pt2 cell line was provided by Dr Goshi Nakamura (Takeda, Japan) who performed the experiments. Figure 7.1 demonstrates proliferation rates for Pt2 Abdo and Pt2 Glut cell lines compared to primary pre-adipocytes. As would be expected the immortalised pre-adipocytes proliferated more quickly than primary pre-adipocytes from the same donor, but in both primary and immortalised pre-adipocytes proliferation rates were equivalent for both depots.

7.3.1.2 Adipogenesis

The differentiation capacity of Pt2 cell lines was assessed by light microscopy and measurement of mRNA expression of *PPARγ* and *CEBPα*. Experiments were performed in primary pre-adipocytes from the Pt2 donor and in Pt2 Abdo and Pt2 Glut cell lines at low passage (passages 8-9) and high passage (passages 18-21). Differentiation capacity for low passage Pt2 Abdo and Pt2 Glut pre-adiocytes was similar to that of primary pre-adipocytes

from the Pt2 donor, both microscopically and in terms of mRNA expression, with pre-adipocytes derived from both ASAT and GSAT showing similar propensities for adipogenesis (Figure 7.2). By contrast, Pt2 cells at passages 18-21 were losing their adipogenic capacity and greater heterogeneity was noted between aliquots of cells.

Expression of a number of other transcripts related to adipocyte function was determined in the Pt2 primary pre-adipocytes and passage 8-9 cell lines (Figure 7.2.E-J). Expression of fatty acid synthetase (*FASN*) and perilipin 1 (*PLIN1*) through differentiation in the low passage cell lines mirrored that in the primary cells. The Pt2 cell lines also upregulated mRNA expression of the adipokines leptin (*LEP)* and adiponectin (*ADIPOQ*). There was a marked depot difference in *LEP* expression in the cell line, with higher expression in Pt2 Glut cells, which was not present in the primary Pt2 cells. In remains unclear whether there is a difference in leptin release from ASAT and GSAT *in vivo,* but serum leptin concentrations correlate negatively with WHR in obesity [412] and interstitial leptin has been reported to be higher in femoral subcutaneous AT than ASAT [413]. In line with previous reports [414] expression of adrenoreceptor β1 was higher in Pt2 primary pre-adipocytes derived from ASAT and in the Pt2 Abdo low passage cell line compared to pre-adipocytes from GSAT.

7.3.1.3 miR196a expression

MiR-196a expression increased during differentiation in Pt2 cell line in both depots at low and higher passages (Figure 7.3). Pt2 cell lines at passages 8-9 retained depot-specific expression of miR-196a and of *HOXA5* and *HOXB8* (as illustrated in Chapter 3). At higher passages the depot difference in miR-196a expression in pre-adipocytes was lost. Because the higher passage Pt2 cells did not differentiate consistently well and did not mirror primary pre-adipocytes in miR-196a expression, a decision was taken to use Pt2 cells at as low a passage as practical for subsequent experiments.

Figure 7.1: Rates of proliferation A. of Pt2 cell lines and primary pre-adipocytes from the Pt2 donor derived from both ASAT and GSAT B. for primary pre-adipocytes only C. for the Pt2 cell lines only. Data represent the average of four separate experiments. Error bars indicate standard deviations.

A.

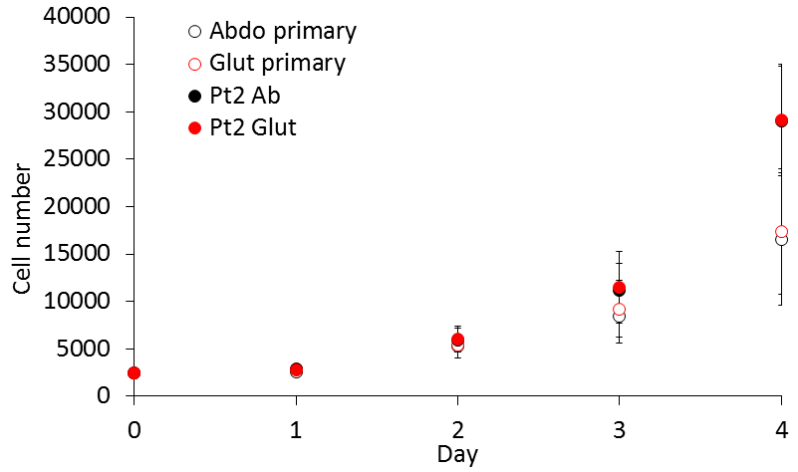

B.

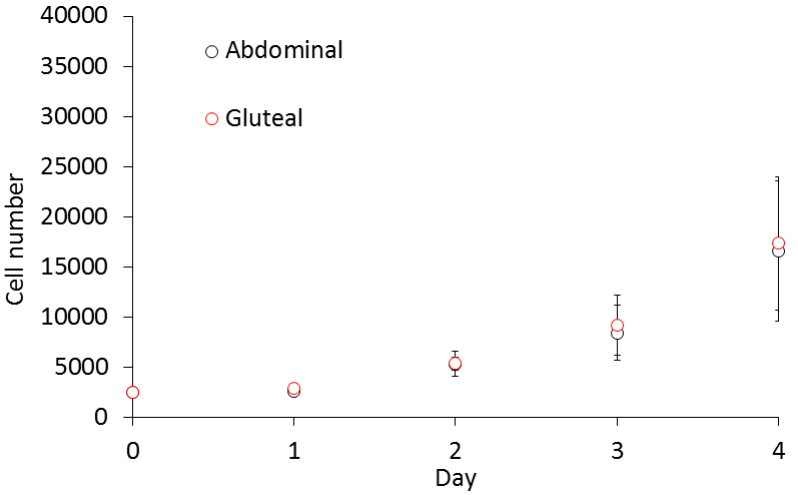

C.

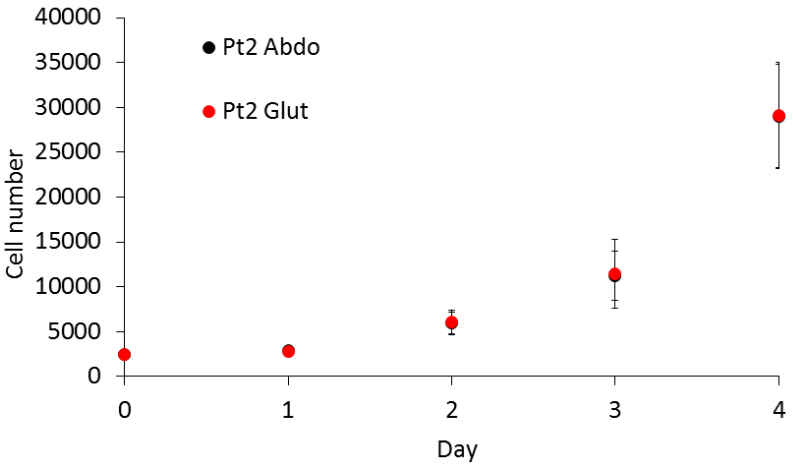

Figure 7.2 Differentiation capacity of the Pt2 Abdo and Pt2 Glut cell lines. Figure A shows microscopy of abdominal subcutaneous Pt2 pre-adipocytes after a 14 day differentiation protocol. Figure B shows microscopy of gluteal Pt2 pre-adipocytes after a 14 day differentiation protocol. Figure C-J show expression of mRNAs relating to adipogenesis and adipocyte function throughout differentiation. Error bars represent standard errors.

Primary **Passages 8-9** **Passages 18-21**

A. Abdominal subcutaneous pre-adipocytes on day 14 of differentiation.

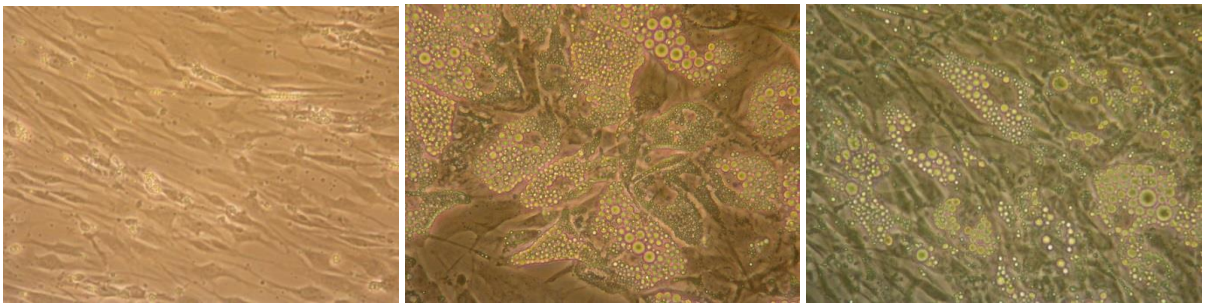

B. Gluteal pre-adipocytes on day 14 of differentiation

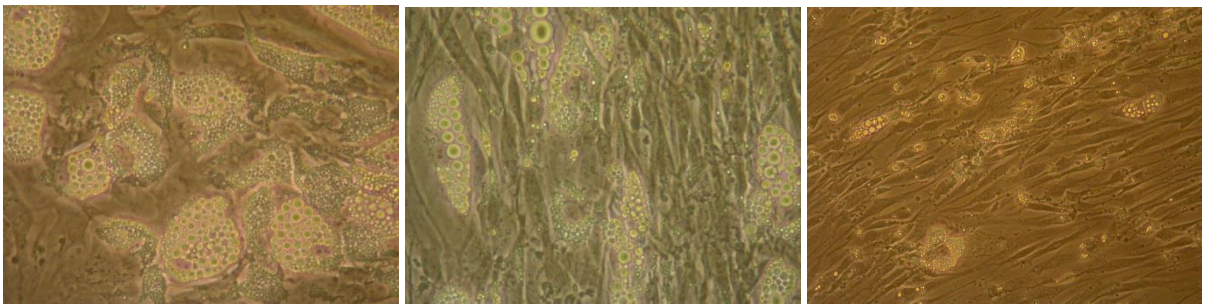

C. *PPARγ2* mRNA expression

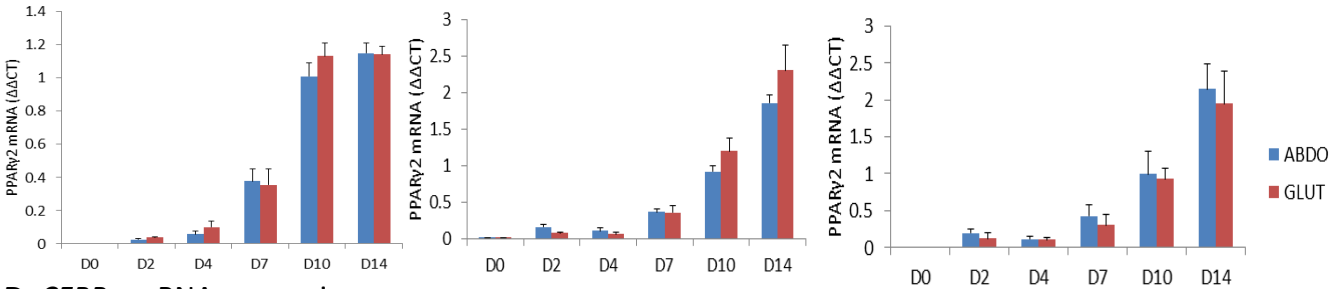

D. *CEBPα* mRNA expression

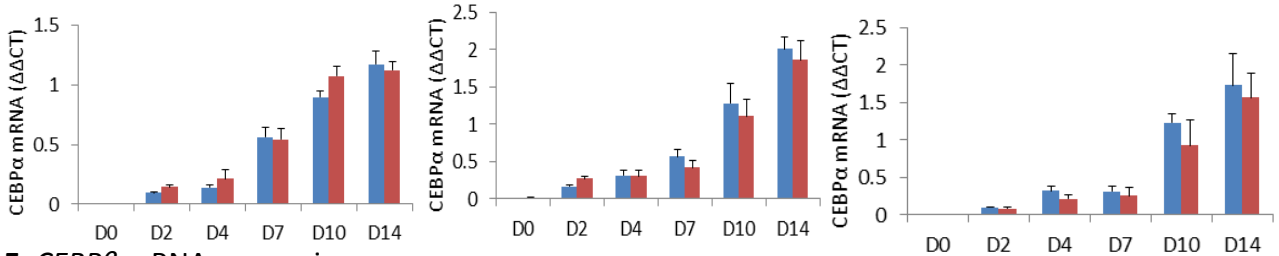

E. *CEBPβ* mRNA expression

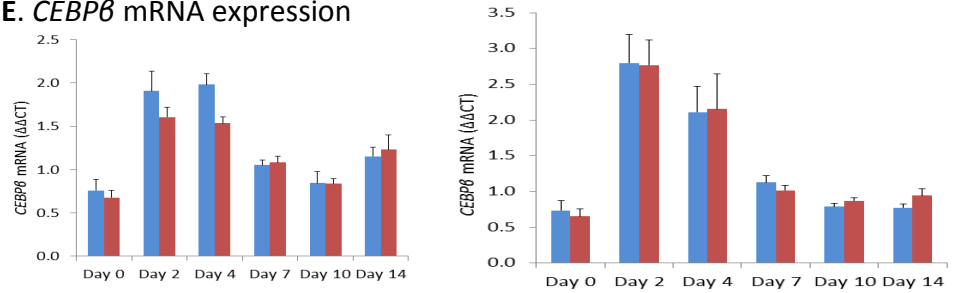

F. *FASN* mRNA expression

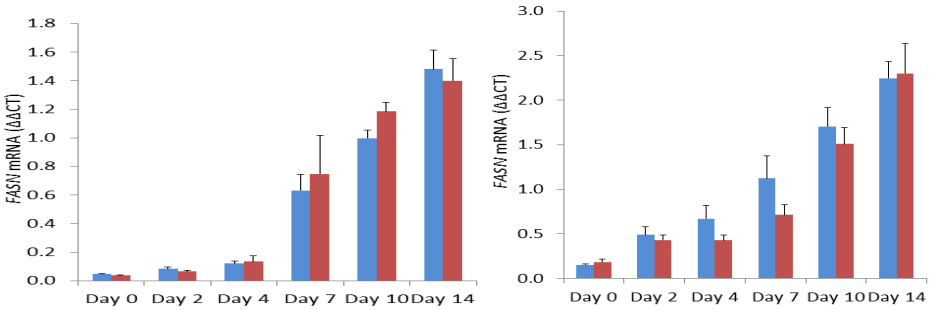

G. *LEPTIN* mRNA expression

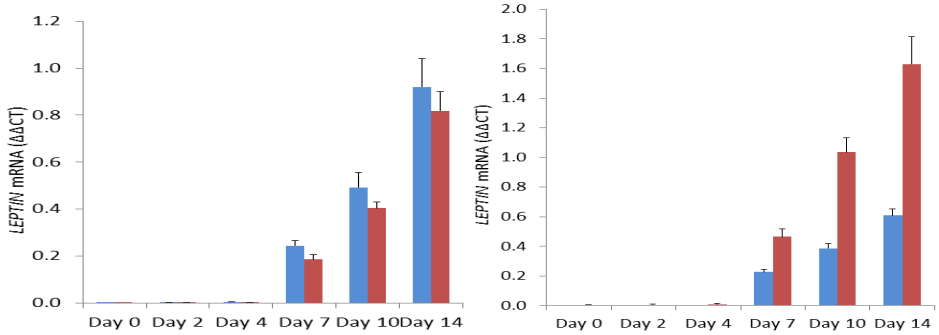

H. *ADIPOQ* mRNA expression

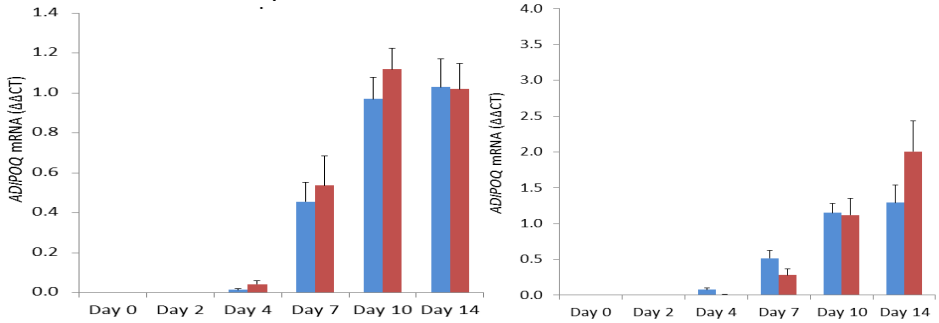

I. *ADRB1* mRNA expression

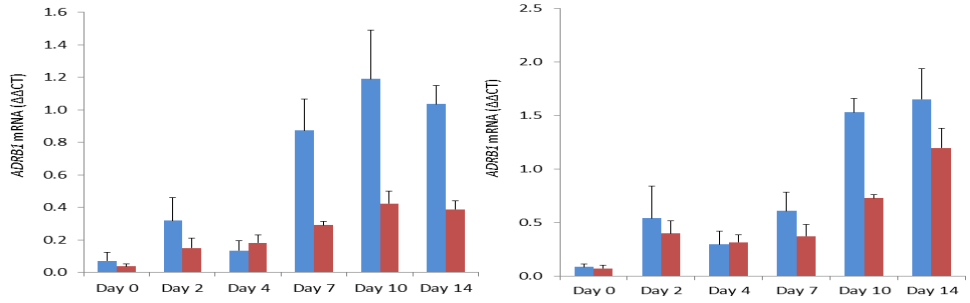

J. *PLIN1* mRNA expression

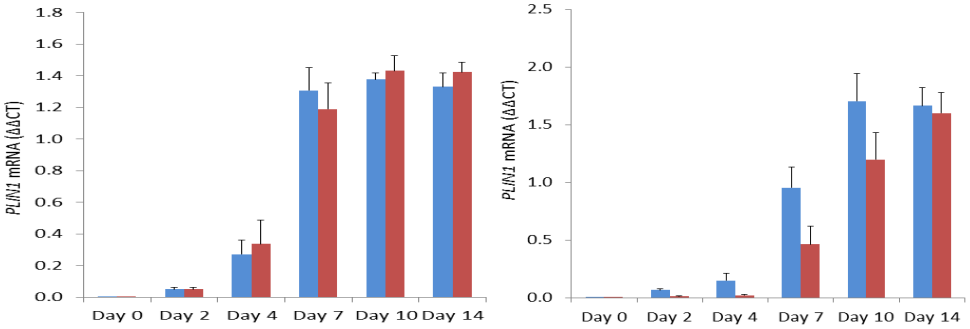

Figure 7.3: miR-196a expression in A. primary pre-adipocytes from the Pt2 donor and in B. passage 8-9 and C. passage 18-21 Pt2 Abdo and Pt2 Glut cell lines during a 14 day differentiation time-course. Error bars represent standard errors.

A. Primary pre-adipocytes from the Pt2 donor. N=6.

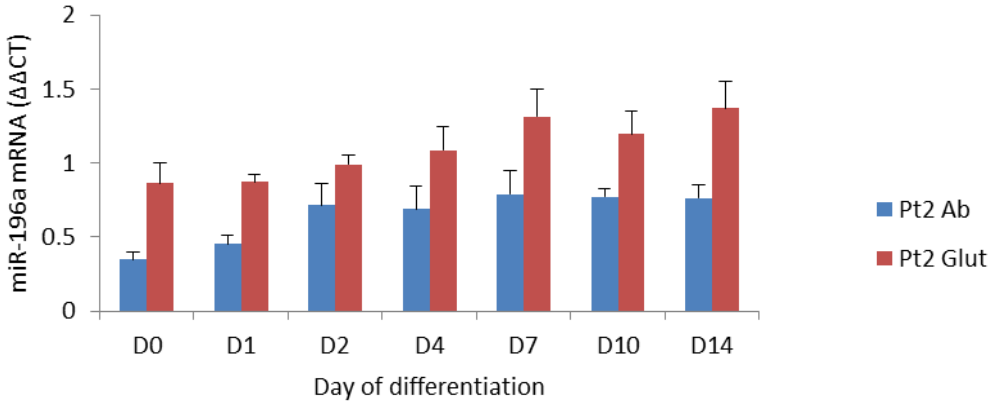

B. Passage 8-9 Pt2 Abdo and Pt2 Glut cell lines. N=6.

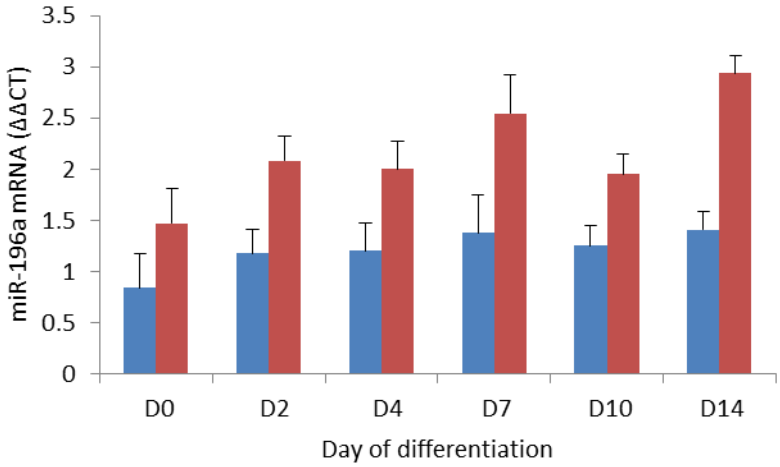

C. Passage 18-21 Pt2 Abdo and Pt2 Glut cell lines. N=3.

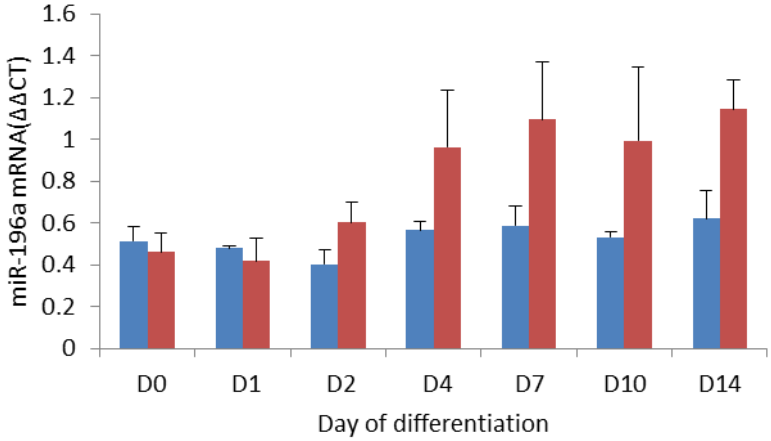

7.3.2 Development of an *in vitro* cell culture model for functional investigation of miR-196a

7.3.2.1 Transient transfection model

Initially a transient transfection system for miR-196a overexpression and inhibition was trialled. In an optimisation experiment sub-confluent Pt2 Abdo pre-adipocytes were transfected with 10 nM miR-196a mimic or scrambled control (Figure 7.4). MiR-196a expression in mimic-transfected wells was several hundred-fold higher than in control wells, even 5 days after transfection.

Figure 7.4 Expression of miR-196a in Pt2 Abdo pre-adipocytes transiently transfected with 10 nM miR-196a mimic or scrambled control construct. MiR-196a expression was determined 24 hours and 5 days following transfection. Data represent three replicate wells of one experimental replicate.

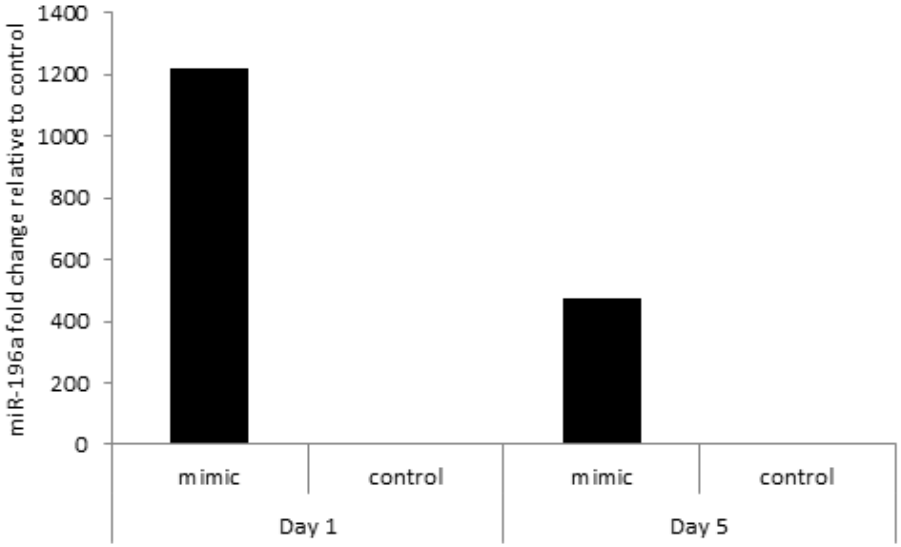

In a separate experiment, Pt2 Abdo and Glut pre-adipocytes were plated in 6-well plates at a density of 200,000 cells/well. The following day cells were transfected with varying concentrations of miR-196a mimic or inhibitor and expression of miR-196a *HOXA5*, *HOXB8* and *HOXC8* were determined after 24 hours. Although there are numerous predicted and established targets of miR-196a (as discussed in 4.3.4) these were selected to assess

transfection efficiency because they were proven targets and because it was suggested that miR-196a might be regulating adipocyte function through its targeting of the HOX genes. Again, miR-196a levels were several hundred-fold higher in cells transfected with mimic (Figure 7.5.A). There was no significant reduction in levels of *HOXA5*, *HOXB8* and *HOXC8* mRNA, although there were non-significant trends in this direction. Following transfection of a miR-196a inhibitor no change in miR-196a was detectable, although there was a trend towards increased detection of *HOXC8* with miR-196a inhibition.

Although a greater effect might be expected at the protein level than at the mRNA level, reduction in the *HOX* genes mRNA was modest given the massively increased miR-196a levels in mimic-transfected cells. Furthermore, miR-196a was not affected by transfection of the miR-196a inhibitor and increase in *HOXA5, HOXB8 and HOXC8* mRNA in response to miR-196a inhibition was unconvincing. Several explanations were considered. Firstly, the *HOX* genes might not be targeted by miR-196a in pre-adipocytes, or mRNA degradation might be minimal compared to modulation of protein expression. Secondly, the miR-196a inhibitor might inactivate miR-196a but not degrade it. If they then separated during the qPCR reaction miR-196a would still be detectable. Finally, it was postulated that the inhibitor and mimic might not have been reaching the appropriate compartment within cells; that is, they were not present in the compartment where miR-196a would usually be active. This last hypothesis was supported by the observation that numerous small vesicles were visible in the cells by light microscopy following transfection (Figure 7.7). To investigate this further Pt2 Glut pre-adipocytes were plated on glass cover slips and transfected with 10 nM of a scrambled control. The control was the same size as the miRNA mimic and emitted fluourence at 480nm. As illustrated in Figure 7.7 the construct appeared to be sequestered in vesicles corresponding with those observed on light

microscopy. Subsequent to these experiments Thomson *et al.* [415] published a report noting the tendency for exogenous miRNA mimics and inhibitors to be detected in vesicles following transfection. They demonstrated that the majority of miRNA mimic was not loaded into the Argonaute complex, and therefore was not functional.

There were therefore several reasons why attempts to modulate miR-196a by transient transfection were abandoned. There were concerns that the mimic and inhibitor constructs were sequestered within vesicles following transfection and were not biologically active. The degree of miR-196a up-regulation did not represent an accurate surrogate for physiological variations in miR-196a expression. In addition, the massive overexpression of observed in these experiments increases the risk of non-specific effects due to saturation of miRNA processing apparatus or targeting of mRNAs that would not be targeted at physiological concentrations.

Figure 7.5 Change in expression in A. miR-196a, B. *HOXA5*, C. *HOXB8* and D. *HOXC8* 24 hours after transient transfection of miR-196a mimic into Pt2 Abdo and Glut pre-adipocytes.

A.

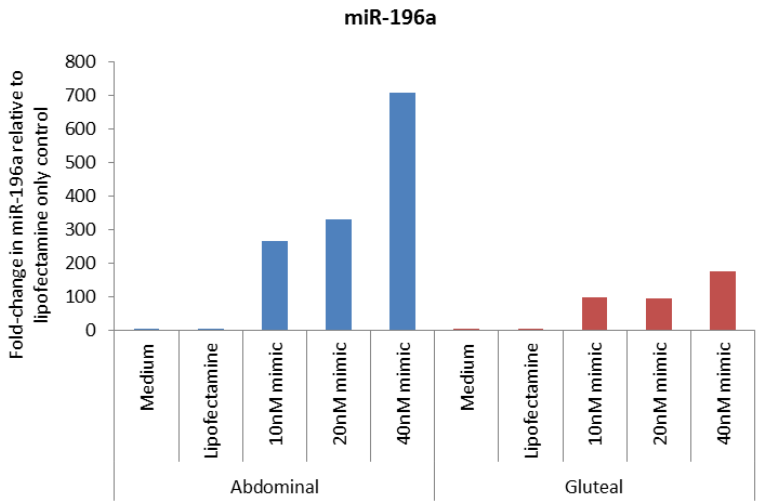

B.

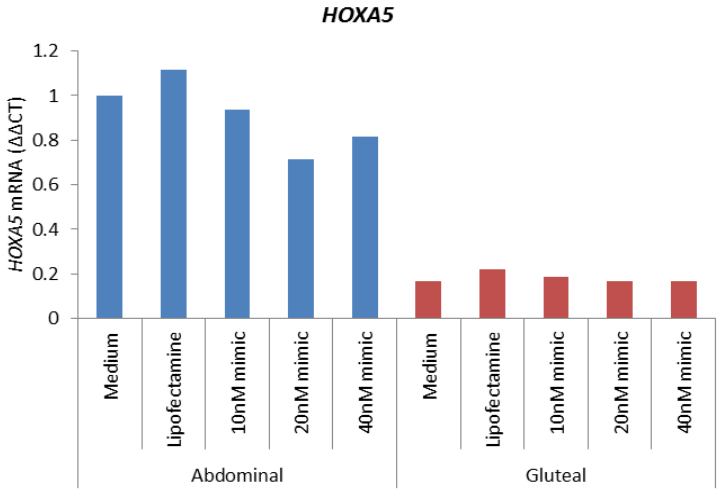

C.

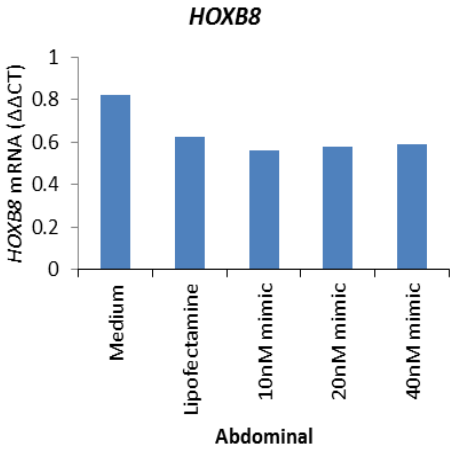

D.

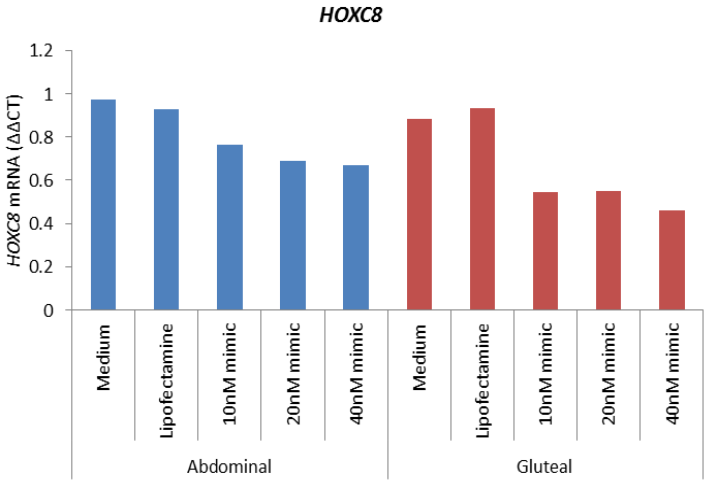

Figure 7.6 Change in expression in A. miR-196a, B. *HOXA5*, C. *HOXB8* and D. *HOXC8* 24 hours after transient transfection of a miR-196a inhibitor into Pt2 Abdo and Glut pre-adipocytes.

A.

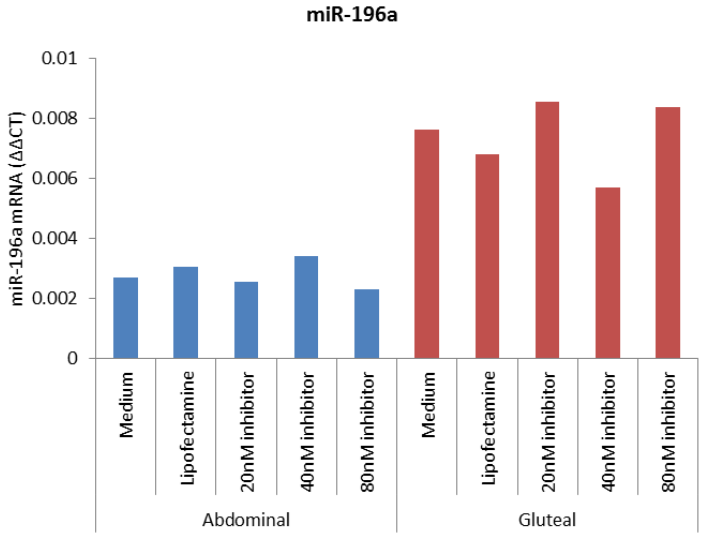

B.

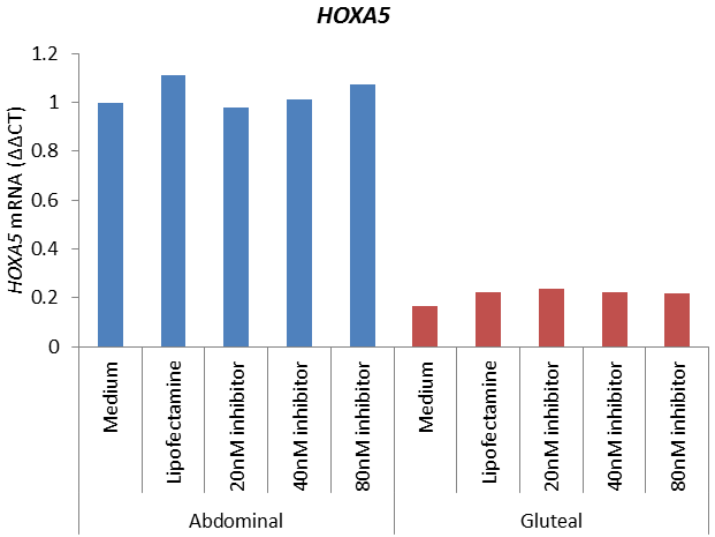

C.

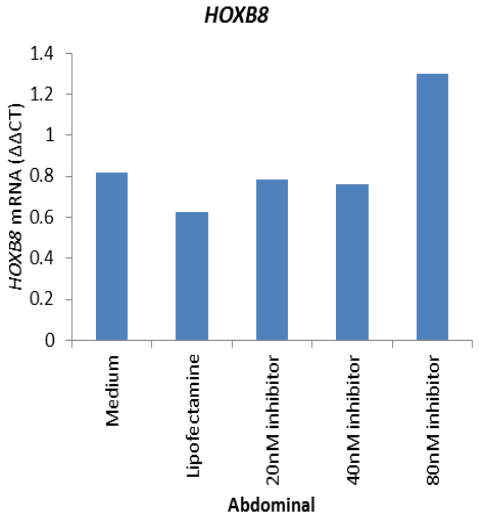

D.

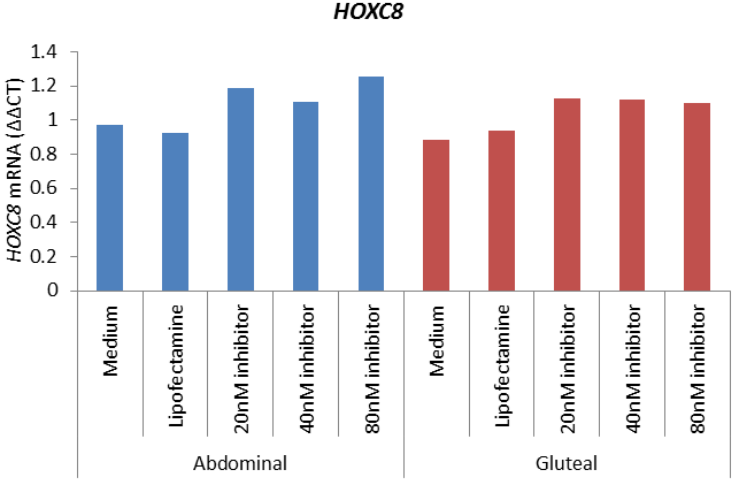

Figure 7.7: Microscopy of pre-adipocytes following transient transfection with a fluorescent scrambled control. A. Light microscopy of Pt2 Glut pre-adipocytes following transfection showing vesicles (10x magnification). B. Control Pt2 Glut pre-adipocytes incubated for 24 hours with Lipofectamine™ according to the transfection protocol but without fluorescent construct (x40 magnification). Nuclei are blue. C. Pt2 Glut pre-adipocytes 24hours post transfection with a fluorescent scrambled control (x40 magnification), demonstrated concentration of the fluorescent signal from within vesicles in the cytoplasm. D. As for C., at x100 magnification.

A. **B.** **C.** **D.**

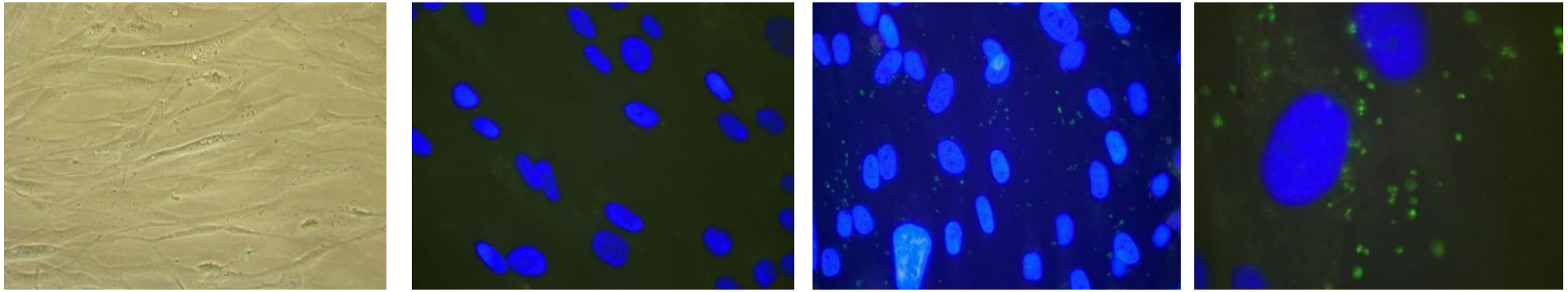

7.3.2.2 Development of a cell line with stable miR-196a inhibition

In Chapter 4, by using rs11614913 as a tool to study miR-196a function I found that the T-allele was associated with reduced mature miR-196a levels detectable in ASAT and with a body fat distribution phenotype, making modelling miR-196a reduction more physiologically relevant. I also had concerns about whether it would be possible to achieve a modest and stable increase in miR-196a expression. Therefore, I opted to develop Pt2 Abdo and Pt2 Glut cell lines with miR-196a inhibition. A HEK293 cell line with stable miR-196a inhibition was also generated for optimisation of the knock-down.

Stable inhibition of miR-196a was achieved by infection of cells with a TRC2-pLKO-puro vector expressing a miR-196a inhibitor. Standard mRNA inhibition is often achieved using siRNA or shRNA that generally cause cleavage and ultimately mRNA degradation [416]. Because of their size, inhibitors for miRNAs tend to bind the miRNA, rendering it non-functional, but may not cleave the miRNA and may not enhance miRNA degradation [417, 418]. It is therefore challenging to accurately quantify miRNA inhibition, and inhibition detected by qPCR is likely to be an underestimate.

A number of secondary endpoints were therefore used to evaluate miR-196a inhibition (Figure 7.8). qPCR for miR-196a showed a decrease in detectable miR-196a in inhibitor cell lines of both HEK293 cells and the Pt2 cell lines (abdo: $p<0.005$, glut $p<0.05$) (Figure 7.8.A). There was a reciprocal but non-significant increase in *HOXB8* mRNA and a statistically significant increase in *HOXC8* mRNA in the Pt2 Abdo ($p<0.05$) and Glut ($p<0.05$) cell lines, with similar patterns seen in the HEK293 cell lines (Figure 7.8.B-C). Regulation of target mRNA is likely to be modest in comparison to protein regulation. Protein extracts were probed for HOXC8 (Figure 7.8.D). Although HOXC8 was almost undetectable in the control HEK293 cell line and in control Pt2 cell lines it increased measurably with miR-196a

inhibition. Total protein per well was determined using the ChemiDoc MP after transfer of proteins onto the PVDF membrane and is shown in Figure 7.8.E. Normalisation and relative quantification of protein was not attempted because the very low expression in some conditions made this meaningless.

Taken together these data demonstrate that effective functional inhibition of miR-196a was achieved.

Figure 7.8: Evaluation of miR-196a inhibition in the HEK293 cell line and in Pt2 Abdo and Pt2 Glut cell lines, infected with either miR-196aKO vector or control. A. miR-196a B. *HOXB8* mRNA C. *HOXC8* mRNA D. HOXC8 protein expression as determined by Western blotting. E. Relative total protein per lane for Western blot. For HEK293 data represent 6 replicate wells of one experiment and data were normalized to PGK1 or to the mean of miR-103, miR-331 and miR-24. For Pt2 cell lines data represent the mean of 6 separate experiments. Bars represent standard errors.

A. **HEK293** **Pt2 cell lines**

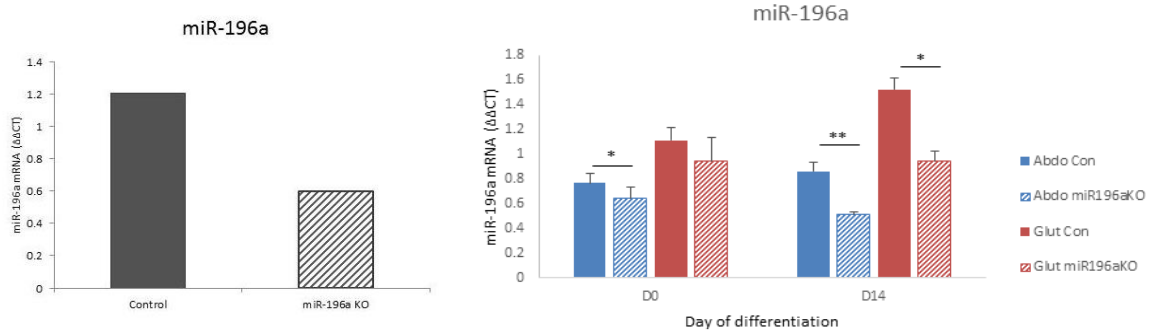

B.

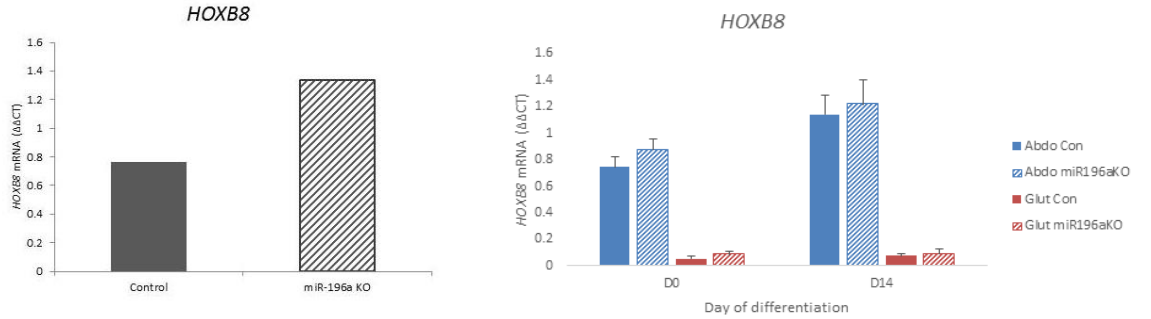

C.

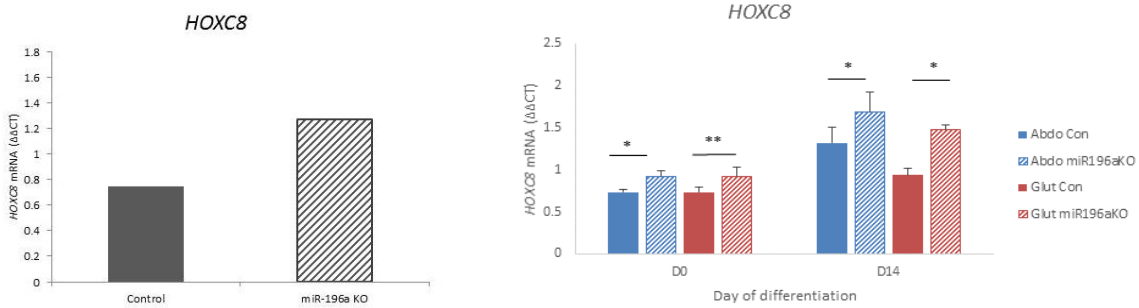

D.

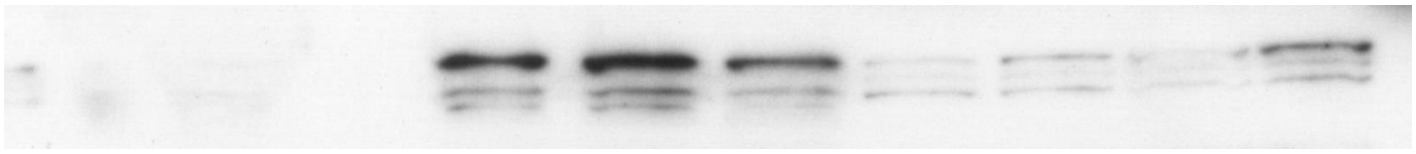

E. Relative total protein per lane

1	0.92	0.88	0.95	0.98	0.76	1.04	1.16	1.11	0.94

7.3.3 *In vitro* functional experiments

7.3.3.1 miR-196a is a negative regulator of proliferation of both abdominal subcutaneous and gluteal pre-adipocytes

Having established cell lines with stable miR-196a inhibition, and because of the *in vivo* phenotype of expanded ASAT associated with lower miR-196a expression, I next investigated proliferation of the Pt2 pre-adipocyte cell lines. There was an increase in doubling time of pre-adipocytes of both ASAT and GSAT origin (Figure 7.9). This equated to a reduction in proliferation of 9.5% in Pt2 Abdo miR-196a pre-adipocytes compared to their control counterparts (p=0.002), and a reduction of 12.3% in the Pt2 Glut miR-196a cell line (p=0.002) compared to Pt2 GlutCon.

Figure 7.9: Doubling time in the Pt2 cell line with miR-196a inhibition. N=14, bars represent standard errors.

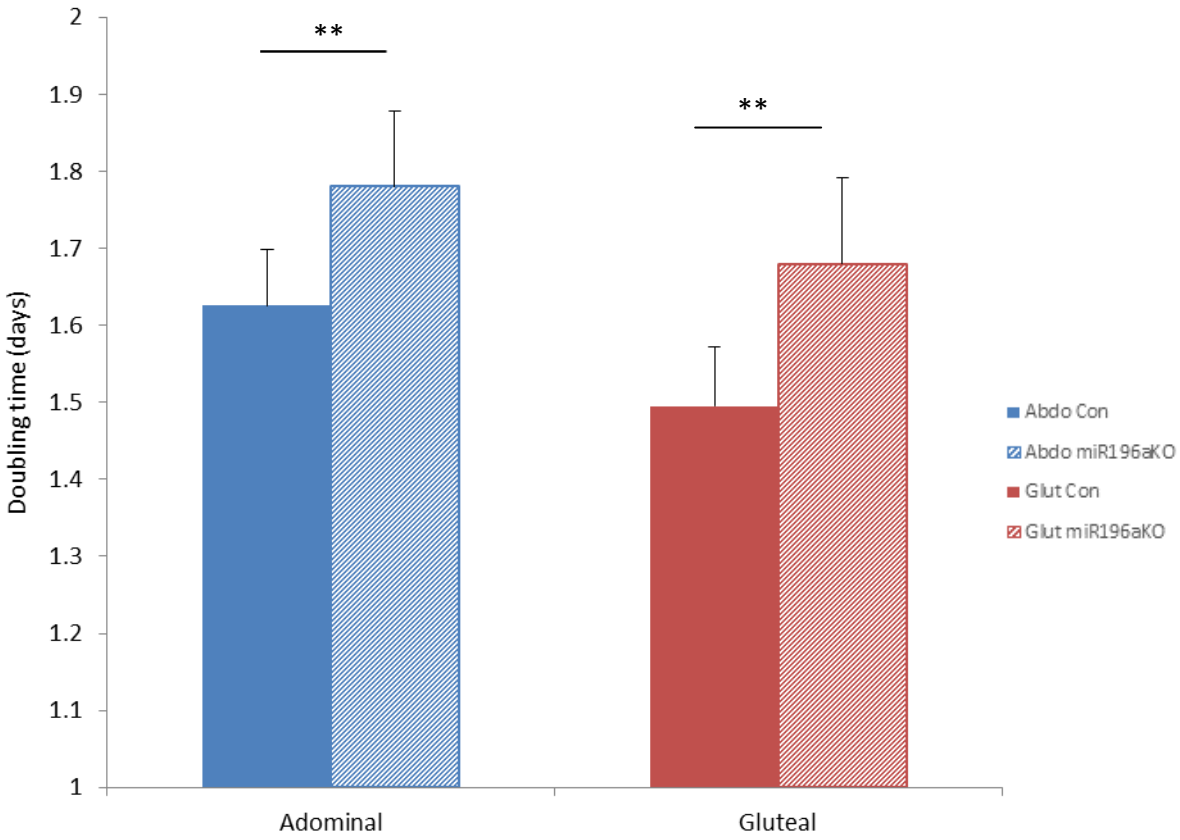

7.3.3.2 miR-196a does not regulate adipogenesis in abdominal subcutaneous or gluteal pre-adipocytes

Next, I evaluated whether miR-196a inhibition affected adipogenesis in a depot-specific manner. Consistent with the results of experiments in 7.3.1.2, there was no marked difference in adipogenic capacity between AbdoCon and GlutCon pre-adipocytes. There was no difference in adipogenesis of miR-196a KO pre-adipocytes compared to control pre-adipocytes as determined by light microscopy or qPCR of *PPARγ2* or *CEBPα*.

Figure 7.10: Adipogenic capacity of miR-196a KO and control Pt2 Abdo and Glut cell lines. A. light microscopy (x10 magnification) **B.** mRNA expression of *PPARγ2* and *CEBPα* throughout the 14 day differentiation time-course

A.

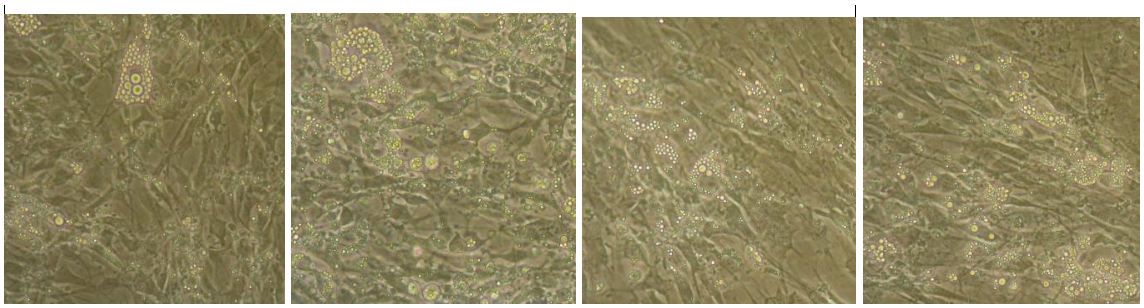

Abdo Con | Abdo miR-196aKO | Glut Con | Glut miR-196aKO

B.

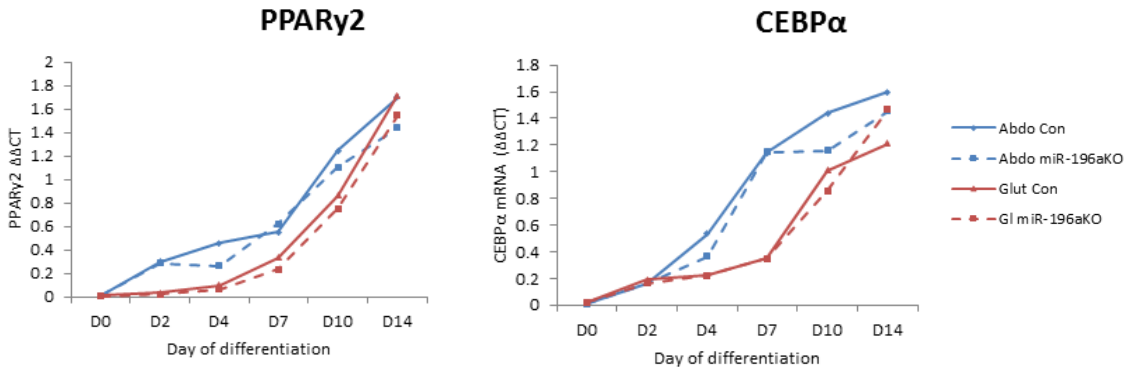

7.3.4 Transcriptomic analysis of pre-adipocytes from abdominal subcutaneous and gluteal adipose tissue with miR-196a inhibition

7.3.4.1 Background correction

There is no formal recommendation for what constitutes background intensity on the Affymetrix ST2.1 arrays. The array contains 'negative control' probes based on putative introns from housekeeping genes. As some of these putative intronic regions may be transcribed the true background level is somewhat lower than this. The array also contains unlabelled polyA spikes that are added to the RNA sample prior to cDNA synthesis, amplification and labelling. Since these are not included in the standard assay they effectively represent negative controls. Microarray probe intensities are routinely expressed on a logarithmic scale to normalise data distribution and make statistical handling more straightforward. In our dataset the average $\log_2$ intensity of the 'negative controls' was 3.16. The mean of the three unlabelled polyA spike controls was 1.606, and the highest of these three probe intensities was 1.783. Because this represented the highest of the 'true' background controls this was selected as the background cut off.

Transcripts were excluded from analysis if expression was below background intensity in both conditions being compared. A transcript that is not expressed in one depot or condition but is highly expressed in another might be very biologically relevant. Therefore, if a transcript was expressed at below background level in one condition and with an intensity of below 2.0 in the comparison condition it was removed; however, if the expression in the comparison tissue was above 2.0 then the transcript was retained for analysis. Table 7.2 indicates the number of transcripts that were removed from analysis for each comparison. Importantly, although around 20% of transcripts were removed

overall, of those that were significantly different according to depot of origin or with miR-196aKO a smaller proportion were excluded, indicating that false positives due to low expression were not making a substantial contribution to significant transcripts.

Table 7.2: Number of transcripts removed from each comparison analysis, including the number of transcripts that were significantly differently expressed before and after adjustment for multiple testing.

Comparison	Number of transcripts <1.783 in both conditions	Number of transcripts removed	Number of significant transcripts removed	
			Unadjusted p<0.05	Adjusted p<0.05
GlutCon vs AbdoCon	9,051	11,013 (20.5%)	516 (6.4%)	29 (0.9%)
Glut miR196aKO vs GlutCon	8,802	11,184 (20.9%)	675 (12.4%)	11 (1.8%)
Abdo miR-196aKO vs AbdoCon	9,105	11,387 (21.2%)	550 (20.1%)	0 (0%)

Table 7.3: Number of significantly changing transcripts with each comparison, before and after multiple testing correction, out of the 54,617 probe sets included on the microarray and after removal of transcripts falling below background expression.

Comparison	ΔmiR-196a (qPCR)	Number of significantly changing transcripts	
		Unadjusted p<0.05	Adjusted p<0.05
GlutCon vs AbdoCon	+86%, p=0.02	7,554	3,300
Glut miR-196aKO vs GlutCon	-47%, p=0.001	4,693	591
Abdo miR-196aKO vs AbdoCon	-15.8%, p=0.244	2,077	24

7.3.4.2 MicroRNA-196a expression in samples submitted for microarray profiling

The degree of miR-196a inhibition for samples used in the microarray experiment mirrored that seen in previous experiments (Figure 7.11). Importantly, miR-196a

expression in Glut miR-196aKO cell line was similar to that in the AbdoCon cell line, and the degree of miR-196a reduction in the Abdo miR-196aKO pre-adipocytes compared with the AbdoCon pre-adipocytes mirrored the difference in miR-196a in ASAT in TT rs11614913 homozygotes. The differences in miR-196a expression in samples submitted for transcriptomic profiling were therefore biologically relevant.

Figure 7.11: miR-196a as detected by qPCR in samples submitted for microarray analysis. n=8. Error bars represent standard errors.

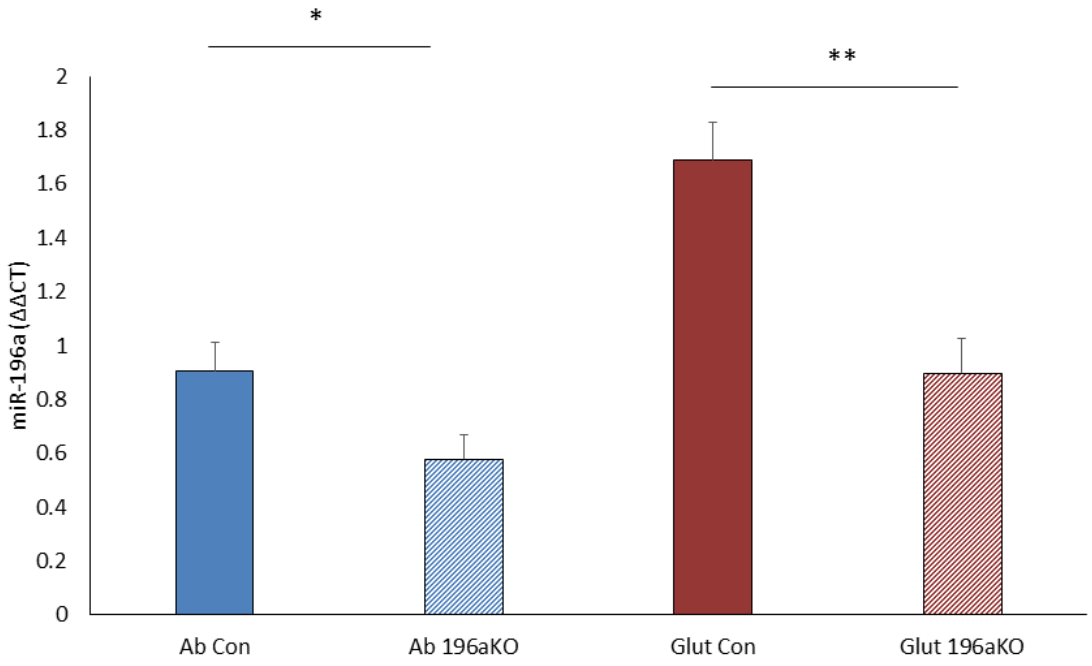

7.3.4.3 Distribution of fold-changes for significantly changing transcripts

Figure 7.12 shows the distribution of $\log_2$ fold-changes for comparisons between GlutCon and AbdoCon and between Glut miR196aKO and GlutCon. The majority of differently expressed transcripts had modest fold-changes (less than 2-fold). Comparisons between Abdo miR-196aKO and AbdoCon were not included because of the small number of significant results.

Figure 7.12: Distribution of log2 fold-changes for significantly different transcripts between Glut miR-196aKO compared to GlutCon cell line and in GlutCon as compared to AbdoCon cell lines.

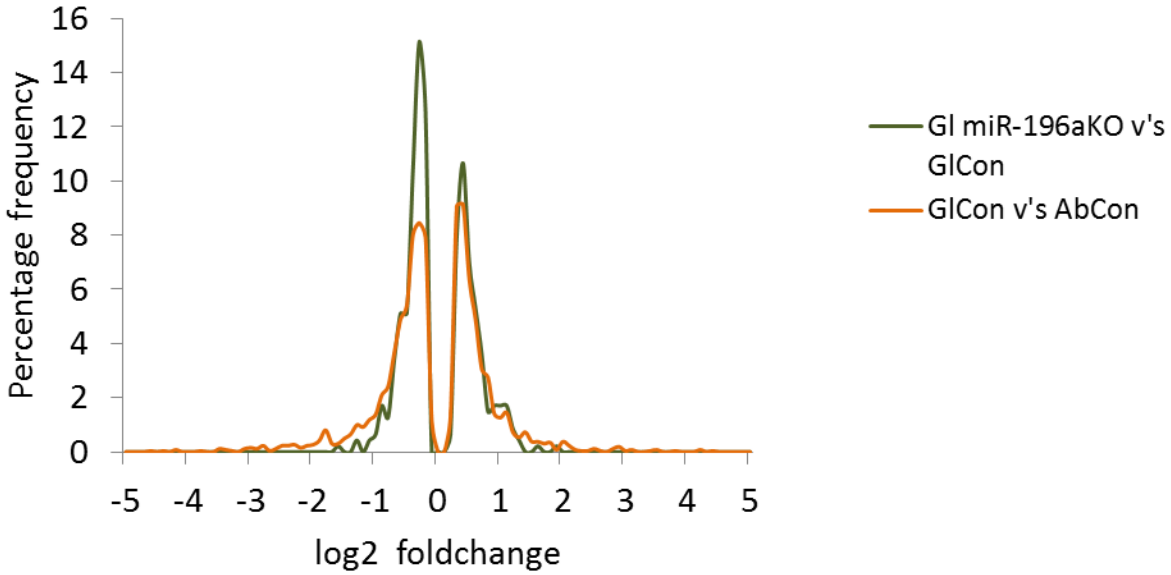

7.3.4.4 Principal Component Analysis

I hypothesized that because expression of miR-196a in the Glut miR-196aKO cells was comparable to that in the AbdoCon cell line this would act to shift the gluteal pre-adipocytes towards a more 'abdominal' transcriptomic profile.

With this in mind principal component analysis (PCA) was performed during the initial bioinformatics analysis at the Wellcome Trust Centre for Human Genetics. PCA aims to reduce a complex set of variables to a simpler set of principle components which represent most of the variance in the original variables. In Figure 7.13 the two axes represent the main directions of variance in the dataset and individual samples are plotted according to their contribution to the variance. Pre-adipocytes of ASAT and GSAT origin are seen to clearly separate on the plot. Some separation can be seen between GlutCon and Glut miR-196aKO, but there is no discernable difference between AbdoCon and Abdo miR-196aKO samples. Therefore, the cell line depot of origin had the most substantial impact on transcriptomic profile. This data did not support the hypothesis that inhibiting

miR-196a in gluteal pre-adipocytes makes them more closely resemble pre-adipocytes derived from ASAT. PCA is weighted towards detecting global shifts in transcriptional profile. Therefore, if the number of transcripts changing in the hypothesized manner compared to the total number of transcripts analysed is small then an overall shift in the direction hypothesised may be hard to detect.

Figure 7.13 Principal component analysis plot demonstrating variance of the samples included in the microarray experiment.

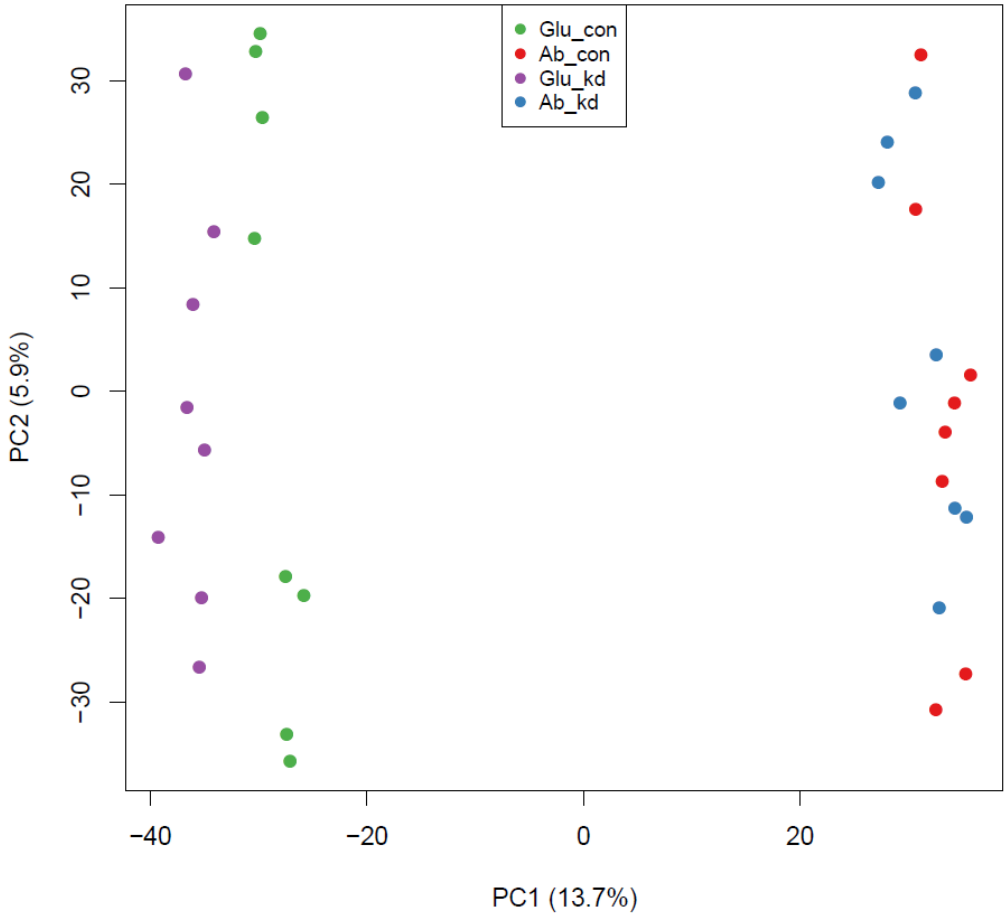

7.3.4.5 Identification of enriched gene ontology term clusters

7.3.4.5.1 Pt2 cells lines retain depot-of-origin memory

The Pt2 cell lines were derived from polyclonal pre-adipocytes from paired ASAT and GSAT. Earlier experiments had confirmed that the Pt2 cell lines retained the properties of primary pre-adipocytes in terms of differentiation capacity and expression of miR-196a

(7.3.1*)* and expression of depot-specific *HOX* genes (4.3.5). Transcriptomic profiling from Pt2 AbdoCon and Pt2 GlutCon was compared to whole ASAT and GSAT transcriptomic profiling from a separate experiment to investigate the extent to which the Pt2 cell lines retained 'depot memory'.

Whole ASAT and GSAT transcriptomic profiling by microarray analysis was performed by Dr Katherine Pinnick (OCDEM, University of Oxford) and bioinformatics analysis was performed by Dr George Nicolson (Department of Statistics, University of Oxford) [40]. Forty-nine paired ASAT and GSAT biopsies from individuals from the OBB were interrogated using Affymetrix HGU133 Plus 2 arrays. Of the 18,122 probe sets annotated to autosomal genes, 942 reached significance for different expression between ASAT and GSAT using a multiple testing corrected significance cutoff of $p<5x10^{-4}$.

In my experiment, a total of 3,300 transcripts were significantly differently expressed between Pt2 GlutCon and AbdoCon cell lines after adjustment for multiple testing. Of these, 2,558 corresponded to annotated genes.

In the comparison between whole ASAT and GSAT a key finding had been enrichment of genes in the GO terms 'sequence-specific DNA binding', 'anterior/posterior pattern specification', 'embryonic skeletal system morphogenesis' and 'sequence-specific DNA-binding transcription factor activity': in other words, processes related to transcription factor activity, body patterning and embryogenesis. In whole AT 70 of the transcripts significantly differently expressed in ASAT and GSAT related to developmental processes. In the experiment comparing transcriptomic profiles of the AbdoCon and GlutCon Pt2 cell lines, 27 of these 70 transcripts were also significantly differently expressed. The Pt2 cell lines were derived from a male donor. If transcriptomic profiling was considered for whole

ASAT and GSAT from men only then 56 genes were related to developmental processes, of which 26 were also significantly different with depot of origin of the Pt2 cell lines.

Next, lists of significantly different annotated transcripts for whole AT and Pt2 cell lines were compared. A total of 213 transcripts were common to both experiments. Of these, 120 transcripts were more highly expressed in the same depot and 93 had opposite expression patterns. GO enrichment analysis was performed in DAVID (http://www.david.niaid.nih.gov/ [410, 411] as described on p.194 for the 120 annotated transcripts with the same direction of change in both datasets. As shown in Table 7.4, GO term clusters were significantly overrepresented relating to embryogenesis and body patterning. Therefore, the Pt2 cell lines retain transcriptomic depot-of-origin memory and mirror whole AT in their depot-specific expression of development related transcripts.

Annotated transcripts significantly different between GSAT and ASAT but not between the Pt2 cell lines were most significantly enriched for GO terms associated with the immune response (Enrichment Score=2.07). This suggests that at least some of the difference in transcriptomic profile between whole AT and the Pt2 cell lines is due to non-adipocyte cell populations in whole AT.

Table 7.4: Gene ontology term clusters significantly enriched for transcripts significantly differently expressed both between whole abdominal subcutaneous adipose tissue and whole gluteal subcutaneous adipose tissue and between the Pt2 AbdoCon and GlutCon cell lines.

Gene ontology terms relating to	Enrichment score
Embryonic skeletal and organ morphogenesis	6.14
Anterior/posterior pattern formation and Homeobox proteins	5.72
Skeletal system morphogenesis	4.55
Homeobox and regional localisation	4.42
Negative regulation of cell migration	2.37
Pleckstrin homology	2.26
Regulation of cell motion	2.21
Limb and appendage morphogenesis	1.76
Protein kinase activity and phosphorylation	1.74
Positive regulation of gene transcription	1.46

7.3.4.5.2 Pathways regulated by miR-196a inhibition in Pt2 pre-adipocyte cell lines derived from gluteal adipose tissue

Comparison of Glut miR-196aKO and GlutCon transcriptional profiles revealed 441 annotated transcripts that were significantly regulated (187 up-regulated in Glut miR-196aKO pre-adipocytes and 254 down-regulated). GO enrichment analysis in DAVID demonstrated significant enrichment for GO term clusters related to extracellular matrix and vascular development (Table 7.5), suggesting that miR-196a might have a role in AT structure and remodeling.

As illustrated in Figure 7.12, transcript regulation was generally modest. Furthermore, DAVID performs enrichment analysis on user-specified lists of genes but does not take into account magnitude of effect. Therefore, to assess the processes that were enriched for transcripts with the largest fold-changes, annotated gene transcripts were selected if they

changed by more than 50% with miR-196a modulation (unadjusted p<0.01). This confirmed that GO terms relating to extracellular development and vascular development, as well as being enriched for significantly regulated genes, were also enriched for those transcripts with the most substantial fold-changes (Table 7.6). Other GO term clusters identified were related to inflammatory response and apoptosis.

Table 7.5: Gene ontology terms with significant enrichment for annotated transcripts differently expressed between Glut miR-196aKO and GlutCon Pt2 cell lines, after correction for multiple testing.

Gene ontology terms relating to	Enrichment score
Extracellular matrix	9.14
Vasculature development	6.98
EGF-like region	6.48
EGF-calcium binding	5.36
Cell migration	5.17
Insoluble/membrane fraction	4.59
Polysaccharide and carbohydrate binding	4.1
Fibrinectin	3.2
Positive regulation of transcription	3.05
Regulation of apoptosis	2.53

Table 7.6: Gene ontology terms with significant enrichment for annotated transcripts differently expressed between Glut miR-196aKO and GlutCon Pt2 cell lines with a fold-change of greater than 50% and significance of p<0.01.

Gene ontology terms relating to	Enrichment score
Extracellular matrix	4.2
Inflammatory response	3.68
Chemokine signalling and chemotaxis	3.34
Leukocyte and neutrophil chemotaxis	3.31
negative regulation of apoptosis	2.9
Cell motility	2.76
Plasma membrane	2.69
Vascular development	2.49

7.3.4.6 Pathways regulated by miR-196a inhibition in pre-adipocyte cell lines derived from abdominal subcutaneous adipose tissue

After correction for multiple testing 21 annotated transcripts were significantly different with miR-196a inhibition in the abdominal Pt2 cell line. Of these, eleven were increased by miR-196a inhibition and 11 were decreased. These transcripts were significantly enriched for GO term clusters relating to inflammation, macromolecule synthesis and angiogenesis (Table 7.7). To evaluate the processes associated with those transcripts with the most marked fold-changes data were filtered to give transcripts that changed by greater than 50% with miR-196a inhibition with an uncorrected significance of $p<0.01$ (Table 7.8) (n=225; 107 up-regulated and 118 down-regulated with miR-196a inhibition). A total of 47 transcripts were identified of which 21 were downregulated with miR-196a inhibition and 26 up-regulated. Mirroring the effect of miR-196a downregulation in the gluteal Pt2 cell line, these were enriched for GO terms relating to extracellular matrix.

Table 7.7: Gene ontology terms with significant enrichment for annotated transcripts differently expressed between Abdo miR-196aKO and AbdoCon Pt2 cell lines, after correction for multiple testing.

Gene ontology terms relating to	Enrichment score
Inflammation and immune response	2.92
Interleukin 1	1.85
Positive regulation of macromolecule biosynthetic process	1.76
Acute inflammatory response	1.74
Leucine rich repeat	1.67
Angiogenesis	1.58

Table 7.8: Gene ontology terms with significant enrichment for annotated transcripts differently expressed between Abdo miR-196aKO and AbdoCon Pt2 cell lines with a fold-change of greater than 50% and significance of p<0.01.

Gene ontology terms relating to	Enrichment score
Extracellular region	3.26
Hormone, amidation	2
Extracellular matrix	1.83
Cell motility	1.42
Negative regulation of transcription	1.41

7.3.4.6.1 Investigation of putative miR-196a targets using significant gene lists generated by the microarray experiment

In Chapter 4 miR-196a mRNA targets were predicted using PicTar, DIANA microT and TargetScan. A total of 621 mRNAs were predicted to be miR-196a targets by at least one of these algorithms. Only 16 of the 441 annotated transcripts differently expressed between GlutCon and Glut miR-196aKO pre-adipocytes were predicted miR-196a targets (Table 7.9). Direct target transcripts were enriched for GO term clusters related to extracellular matrix and embryonic development, in addition to signalling peptides. None of the 22 transcripts significantly regulated in abdominal Pt2 pre-adipocytes with miR-196a inhibition were predicted to be direct targets.

Table 7.9: Predicted miR-196a targets that were significantly regulated at the mRNA level by miR-196a inhibition in gluteal Pt2 pre-adipocytes. Targets of miR-196a were predicted by PicTar, DIANA microT and TargetScan. Enriched GO term clusters (as predicted in DAVID) and the transcripts related to each GO term cluster are indicated.

	Signal peptide/ glycoprotein	Extracellular matrix	Embryonic development/ tissue morphogenesis
Enrichment Score	2.79	1.58	1.50
ARSJ	*		
BNC2			
COL11A1	*	*	*
COL3A1	*	*	
KCNQ5			
NLGN1	*		
NTN4	*	*	
OPCML	*		
PAPPA	*		
PBX1			*
PORCN			
RASGRP1			
SERPINE1	*		
SLC38A4	*		
STEAP2			
TGFBR3	*		*

7.3.4.7 Confirmation of key targets by qPCR

Expression patterns of fourteen transcripts from key GO terms were confirmed by qPCR (Table 7.10). As shown in Figure 7.14 and Figure 7.15 fold-changes in microarray and qPCR datasets were generally in agreement, although there were a number of transcripts for which qPCR data did not reach significance for differential expression. Of note several transcripts relating to inflammation and apoptosis, including *IL1β, IL1α, CCL2* and *CCL5* did not replicate in the qPCR dataset, implying that there may have been a spurious inflammation-related effect in the samples submitted for microarray analysis.

Table 7.10: Agreement between fold-changes calculated using microarray and qPCR data. Transcripts predicted to be direct miR-196a targets are indicated by underlining. Results that were significant both in the microarray and the qPCR experiments, with the same direction of effect, are indicated in bold.

	DEPOT (Gluteal/Abdominal)				Abdo miR-196aKO vs AbdoCon				Glut miR-196aKO vs GlutCon			
	Microarray experiment		qPCR experiment		Microarray experiment		qPCR experiment		Microarray experiment		qPCR experiment	
Transcript	**Fold-change**	**p-value**	**Fold-change**	**p-value**	**Fold-change**	**p-value**	**Fold-change**	**p-value**	**Fold-change**	**p-value**	**Fold-change**	**p-value**
miR196a	1.00	0.99	1.86	0.02	0.90	1.00	0.64	0.13	0.81	0.41	0.53	0.001
CCL2	1.19	0.03	1.74	0.15	1.02	1.00	0.72	0.18	1.61	7.2×10^{-11}	0.82	0.21
CCL5	1.28	0.05	1.25	0.38	1.11	1.00	0.85	0.41	**1.56**	**0.0009**	**0.76**	**0.07**
COL11A1	**0.88**	**0.09**	**0.55**	**0.002**	0.96	1.00	1.10	0.74	**0.78**	**3.1×10^{-6}**	**0.89**	**0.07**
COL3A1	1.04	0.67	1.26	0.009	1	0.99	1.24	0.063	1.23	8.4×10^{-4}	1.08	0.5
COMP	2.55	1.4×10^{-10}	2.11	0.74	0.76	0.88	0.97	0.40	**0.40**	**7.2×10^{-9}**	**0.51**	**0.03**
FOXC2	**0.26**	**4.7×10^{-15}**	**0.23**	**0.02**	0.90	1.00	0.98	0.74	0.73	0.03	0.97	0.87
HOXB9	**0.78**	**0.01**	**0.67**	**0.02**	1.08	1.00	1.27	0.50	1.29	0.04	1.02	0.87
IL1A	0.94	0.68	1.42	0.14	1.45	0.002	1.08	0.54	2.04	5.0×10^{-10}	0.95	0.68
IL1B	**1.78**	**8.9×10^{-10}**	**3.08**	**0.01**	1.35	0.02	1.23	0.74	2.29	1.0×10^{-11}	0.99	0.96
IL1R1	2.45	2.5×10^{-6}	0.94	0.31	0.80	0.01	0.75	0.31	**0.73**	**3.1×10^{-6}**	**0.79**	**0.06**
KLF10	**0.47**	**2.3×10^{-12}**	**0.64**	**0.003**	0.70	0.002	1.22	0.24	1.05	0.82	1.01	1.00
MMP1	**0.07**	**5.8×10^{-24}**	**0.49**	**0.029**	1.22	0.71	1.14	0.29	2.06	2.4×10^{-8}	1.19	0.45
MMP3	**7.41**	**8.3×10^{-21}**	**12.26**	**0.018**	0.82	0.030	1.04	0.86	**2.28**	**1.7×10^{-9}**	**1.49**	**0.047**
PBX1	**1.34**	**0.00**	**1.42**	**0.001**	0.78	0.01	1.65	0.12	0.81	0.03	0.90	0.34
SERPINE1	0.97	0.77	0.98	0.92	0.99	1.00	0.98	0.82	1.18	0.003	0.90	0.53

Figure 7.14: Agreement between log_{10} fold-changes in transcript expression between GlutCon and AbdoCon, as detected by microarray and qPCR.

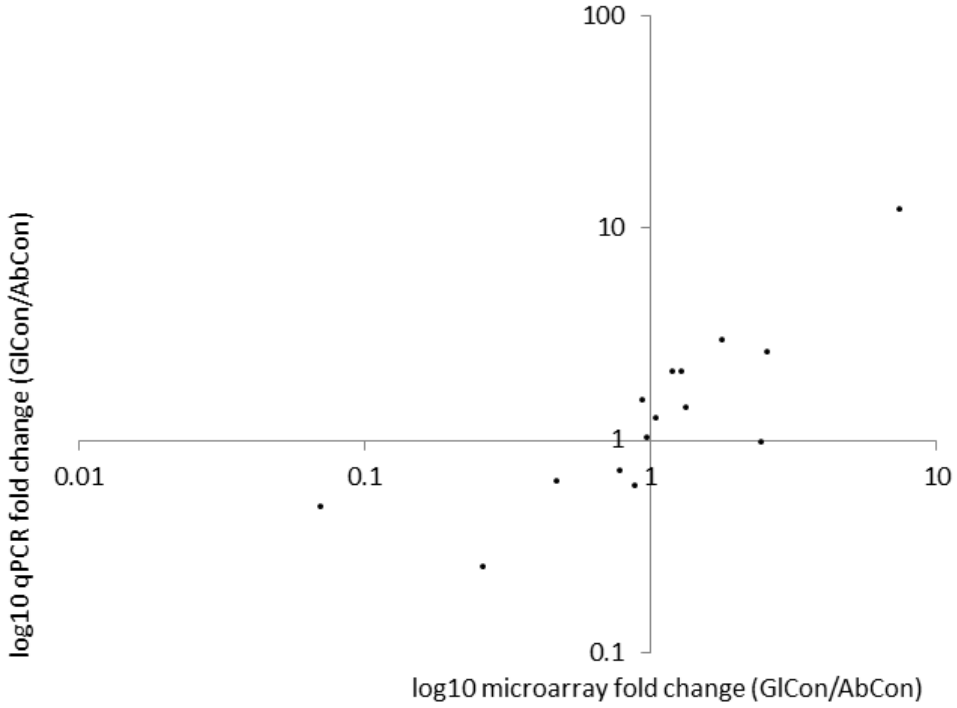

Figure 7.15: Agreement between fold-changes in transcript expression between Glut miR-196aKO and GlutCon, as detected by microarray and qPCR.

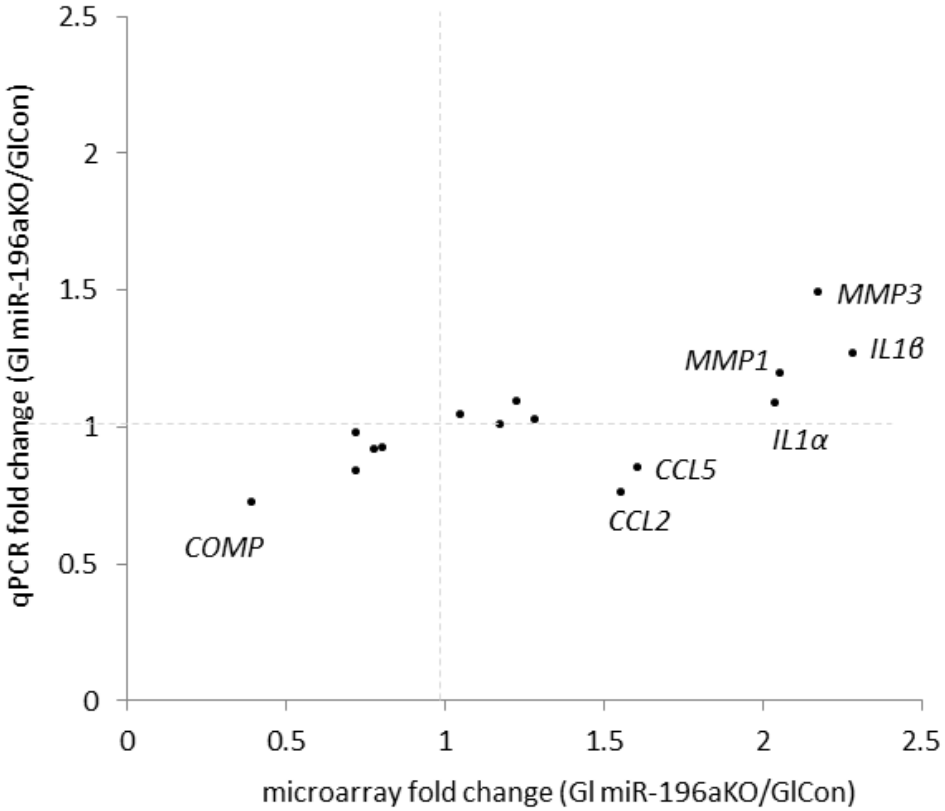

7.3.5 Relating microarray findings to pre-adipocytes and whole adipose tissue

7.3.5.1 Immunocytology for Caspase 3

In 7.2.1.1 I observed an increase in pre-adipocyte doubling time as detected by cell counting in both the Pt2 Abdo miR-196aKO and Pt2 Glut miR-196aKO pre-adipocytes compared to control. This could have been modulated by a true decrease in proliferation, i.e., in decrease in the rate of division, or by an increase in apoptosis. It was noted that transcripts relating to apoptosis were enriched with miR-196a inhibition in the Pt2 Glut pre-adipocytes (Table 7.4). In addition, a number of well-recognised apoptosis associated transcripts were up-regulated in the Pt2 Glut miR-196aKO vs Pt2 GlutCon analysis (Table 7.11), although none of these were significant after multiple testing correction. Caspase 3 (CASP3) is a key regulator of the human apoptosis cascade. Although *CASP3* was not up-regulated in the microarray analysis, mRNA levels underestimate changes in CASP3 activity and do not always correspond well to level of the activated protein [419, 420]. To clarify whether there was an increase in apoptosis relating to miR-196a inhibition, Pt2 miR-196a and Con pre-adipocytes from both depots were grown on cover slips, fixed and then immunostained for activated CASP3. Activated CASP3 was detected in a small proportion of pre-adipocytes (Figure 7.16) but the numbers of positive cells were too small to permit detection of differences between conditions.

Table 7.11: Apoptosis-related transcripts altered by miR-196a inhibition in Pt2 Glut pre-adipocytes as detected by microarray analysis. Significant results are indicated in bold.

Gene ID	Gene name	Fold-change	p-value	Adjusted p-value
CASP3	caspase 3, apoptosis-related cysteine peptidase	1.00	0.94	0.99
BAX	BCL2-associated X protein	1.18	**0.0022**	0.12
BCL2A1	BCL2-related protein A1	1.28	**0.029**	0.41
BCL2	B-cell CLL/lymphoma 2	1.13	0.19	0.73
DDIT3	DNA-damage-inducible transcript 3	1.18	0.09	0.60
HSPA5	heat shock 70kDa protein 5	1.07	**0.059**	0.53

Figure 7.16: Immunocytochemistry of Pt2 Glut miR-196aKO pre-adipocytes showing a pre-adipocyte immunostaining for activated Caspase 3 at A. 20x magnification B. 60x magnification.

A. **B.**

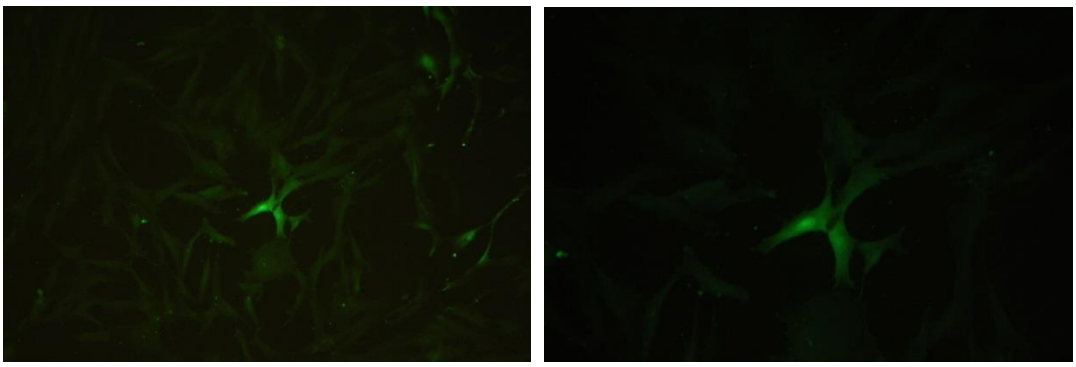

7.3.6 Discussion

In this chapter I have used an *in vitro* model of miR-196a inhibition to investigate depot-specific actions of miR-196a. Previous experiments revealed an association between rs11614913 genotype and ASAT adipocyte volume. Proliferation and adipogenesis of Pt2 miR-196aKO pre-adipocytes were evaluated in order to identify a mechanism for this. I had hypothesised that there would be a depot-specific functional effect of miR-196a. In fact, I observed a negative effect on pre-adipocyte proliferation in pre-adipocytes derived

from both depots. It seems initially counterintuitive that reduced pre-adipocyte proliferation might lead to expansion of WAT. However, it may be that miR-196a directs AT towards a phenotype of expanding by hypertrophy rather than hyperplasia. Unfortunately we do not have data relating GSAT adipocyte size to rs11614913, making it difficult to speculate on whether this is likely to be a mechanism by which body fat distribution is regulated. These findings might also reflect the difficulties in extrapolating in vitro observations in adipocytes to the development of whole tissue, the latter of which makes use of poorly characterized triggers for both proliferation and adipocyte differentiation.

Microarray profiling of pre-adipocytes with miR-196aKO revealed another possible regulatory mechanism for WAT expansion. MiR-196a inhibition led to modest regulation of a large number of transcripts. Interestingly, transcripts differentially expressed with miR-196aKO in pre-adipocytes from both depots were enriched for GO term clusters relating to ECM and angiogenesis, suggesting that these findings are real. It is also supported by previous literature on miR-196a. MiR-196a dysregulation has been noted in scleroderma [262, 263] and keloid scarring [264], both pathologies underpinned by ECM abnormalities. Functional studies have shown that miR-196a inhibits production of type I [262-264] and type III collagen [264].

The Pt2 cell lines are a unique resource. To our knowledge they represent the only paired pre-adipocyte cell lines derived from ASAT and GSAT in existence. There is a limited supply of primary pre-adipocytes, as obtaining them relies on an OBB participant attending for a biopsy, it takes some weeks to expand enough material for experiments, and they lose differentiation capacity at around passage 6. By contrast the use of the Pt2 cell lines allows for comparatively rapid expansion of large numbers of pre-adipocytes, as well as

minimising biological variation in experiments. The proliferation capacity of the Pt2 Abdo and Glut cell lines had previously been validated. In the experiments contained in this chapter I have also validated the Pt2 cell lines as a model for adipogenesis and have demonstrated that they retain depot-of-origin memory.

MiR-196a was successfully inhibited in the Pt2 Abdo and Pt2 Glut cell lines. Importantly for functional experiments the degree of miR-196a reduction reflected that seen between rs11614913 genotypes and between depots. MiR-196a inhibition was more potent in pre-adipocytes of GSAT origin, perhaps reflecting the higher baseline expression of miR-196a in these cells.

As evidenced by the microarray data, miR-196a inhibition had a far more marked impact in pre-adipocytes of GSAT origin than ASAT origin, even allowing for the greater miR-196a inhibition in Pt2 Glut miR-196aKO. This may suggest that miR-196a has a more active regulatory role in GSAT. This at first seems counterintuitive, given that lower miR-196a is associated with ASAT, but not GSAT, expansion. An increase in ECM proteins may represent an ability of ECM to expand and to accommodate adipocyte expansion or proliferation. Equally, ECM can be dysfunctional, causing AT fibrosis in GSAT which might limit its expansion. Therefore, increased fat storage in ASAT may represent 'overflow' storage as a result of GSAT being less able to expand, rather than a primary effect of miR-196a on ASAT. Obviously, these results derived from a cell culture model where pre-adipocytes were grown in a monolayer. It will be of crucial importance for future studies to relate the microarray findings back to whole AT by examining the ECM in ASAT and GSAT in relation to rs11614913 genotype.

Of note, GO-term clusters related to developmental and body patterning processes were not enriched in the miR-196aKO microarray experiment. MiR-196a is expressed from

within the *HOX* gene clusters, there is a body of literature relating miR-196a functionally to the *HOX* genes and indeed I observed regulation of HOXC8 in miR196aKO pre-adipocytes. The transcriptional profiles of the cell lines, however, might suggest that the importance of miR-196a's regulation of the HOX genes in AT is less important than I had hypothesised. However, the HOX proteins are transcription factors: if they were regulated at the protein level but not the mRNA level then even a small difference in HOX protein expression might have marked down-stream effects on other transcripts. It would be useful for future work to clarify whether there is enrichment for transcripts with HOX binding sites in their promoter regions within the subset of regulated transcripts identified by microarray.

Previous reports have noted that miR-196a has a negative effect on proliferation of cells from a number of different lineages [235-240]. Other studies have identified it as a positive regulator of proliferation in other cell types [226, 241-244] and some studies have found no effect [245, 246]. Contrary to our findings, the one study to examine the effect of miR-196a in hASCs observed a positive effect on proliferation [206]. The disparity in our findings may be due to differences in experimental protocols or may be the result of using an immortalised pre-adipocyte model instead of primary pre-adipocytes. It will be necessary for future experiments to repeat these experiments with miR-196aKO in primary abdominal and gluteal pre-adipocytes in order to clarify this. Studies examining the effect of miR-196a on adipogenesis have reported conflicting results [206, 208, 273]. In our experiments there was no evidence to support a pro-adipogenic role for miR-196a.

There were several limitations to the methodologies used in these studies. WAT is a complex tissue and the effect of a microRNA will depend on the density, contact and interaction between cells and tissue innervation and vasculature. It is not possible to

model these complexities adequately in a cell culture environment and this limits the processes that can be investigated, particularly with regards to ECM and angiogenesis. An experimental design was considered where whole biopsies from individuals of CC or TT rs11614913 would be interrogated by microarray. The variability between people is such that a large number of arrays and experimental replicates would be required to produce meaningful results. The use of a cell lines minimised biological variability and allowed us to detect small effects. In future work it will be necessary to relate these findings back to whole AT in order to confirm their relevance *in vivo.*

8 Discussion and conclusions

The associations between body fat distribution and metabolic disease are well established, with android and gluteofemoral adiposity conferring different metabolic risk profiles [73]. WAT depots are complex and heterogeneous organs. GSAT and ASAT are distinct in terms of their transcriptomic signatures [40], histology [47], adipokine and cytokine release [40, 54] and their mechanisms of remodeling [69]. The strong genetic influence on body fat distribution has been recognised [85, 86] but the mechanisms underlying this are poorly understood.

MiRNA regulation is necessary for healthy AT function (Table 1.1) but to date there is a lack of research into their role in determining upper- vs lower- body AT deposition and function in humans. With this in mind, this thesis aimed to describe miRNA expression in human ASAT and GSAT and to understand their potential role in determining fat distribution and the different properties of the tissues.

In order to identify miRNAs which were different between the depots we first conducted a genome-wide microarray screen of human whole ASAT and GSAT. I then validated a selection of miRNAs with qPCR. This represents a comprehensive reference atlas of miRNA expression in human AT according to depot (ASAT vs GSAT), obesity and sex. As outlined in Table 1.1 and Table 1.2 a number of investigators have used genome-wide techniques to identify miRNAs regulated in obesity and have then sought to characterise their roles in human or murine WAT. Only one other published study has described miRNA profiles in human ASAT and GSAT [134] . Rantalainen *et al.* used a more rigorous statistical threshold but without filtering for effect sizes [134] whilst I opted to select miRNA only if they had fold changes between depots of greater than 20% in an attempt to select 'biologically significant' miRNAs. Reassuringly though, the strongest candidates identified were common to both studies.

Men and women exhibit marked sexual dimorphism in their body fat distribution [96] with sex hormones having, to some extent, a causal role in this [97]. Despite this, the differences in miRNA regulation in WAT between men and women has been neglected in the literature. In this thesis I have identified 19 miRNAs that show sex-specific expression patterns, often in only either ASAT or GSAT. Further investigation into these may identify miRNAs that regulate sex-specific fat deposition and, perhaps more importantly, depot- and sex-specific metabolic pathways in WAT that contribute to the different metabolic risk profiles of men and women [421, 422].

A handful of researchers have sought to identify functional roles for miRNAs in determining depot-differences between ASAT and VAT [162, 176] but there have been virtually no published efforts to functionally characterise miRNAs contributing to the depot-specific properties of ASAT and GSAT. MiR-196a was one of the most different miRNAs between ASAT and GSAT. The literature relating it to adipocyte biology and the *HOX* genes made it an interesting candidate for further study. In addition, the presence of a SNP in pre-mir-196a-2 presented an opportunity to interrogate its function in humans *in vivo*. Expression profiling of miR-196a confirmed that it was highly expressed within WAT compared to other tissues, and that its expression was highest within the adipocyte fraction of WAT. Depot-specific miR-196a expression patterns were maintained in *in vitro* cultured primary and immortalised preadipocytes, implying that its expression is intrinsic to preadipocytes and not a function of *in vivo* environment. Importantly, investigation of expression of the miR-196a precursors suggested that miR-196a-2 was the predominant paralogue in human WAT.

Pre-miR-196a-2 contains a SNP, rs11614913, which is predicted to alter the folding and stability of the precursor hairpin, potentially altering the efficiency of its processing. In line

with this, expression of mature miR-196a, but not the precursor pre-miR-196a-2, was reduced in TT-homozygotes. Within the OBB cohort the T-allele was associated with expanded central adiposity, with the suggestion from DXA imaging data that this was mediated through an increase in ASAT rather than VAT. The association between rs11614913 and WHR was convincingly replicated in the GIANT consortium meta-analysis.

It should be noted that this thesis is limited by its use of almost exclusively Caucasian populations, both in primary studies (the OBB cohort) and in replication studies (the GIANT consortium [90]). Studying the impact of a SNP in a population of similar genetic ancestry reduces genetic variation and makes it more straightforward to dissect the effects of the variant. However, these findings cannot necessarily be extrapolated to other populations, particularly considering that rs11614913 MAF and associations have already been shown to differ according to ethnicity [332]. Patterns of body fat distribution are well recognised to differ according to race [423-425]. It follows that studies into miRNA regulation of body fat distribution in different populations might not replicate the findings presented in this thesis. Indeed, it is likely that different patterns of miRNA expression in AT play at least some role in determining the different body shapes of different populations.

In order to establish a causal relationship between miR-196a and body fat distribution it was necessary to identify a mechanism of action. Evidence to suggest a potential mechanism came from further genotyping studies (in collaboration with Professor Arner's group) and from functional experiments. Immortalised pre-adipocytes with miR-196a were generated in which the degree of miR-196a inhibition mirrored that associated with the TT-allele of rs11614913 and between ASAT and GSAT.

Genotyping of a cohort of individuals for whom adipocyte size data was available revealed that the TT-genotype of rs11614913 was associated with larger mean adipocyte size in men. *In vitro* experiments demonstrated that lower levels of miR-196a were associated with reduced rates of proliferation in preadipocytes from both ASAT and GSAT. This may suggest that miR-196a has a role in determining whether AT expands by hyperplasia or hypertrophy. Ideally further work will demonstrate whether the association between rs11614913 and adipocyte size is also seen in GSAT. Transcriptomic profiling of preadipocytes with miR-196a inhibition identified regulation of processes relating to extracellular matrix and angiogenesis, suggesting that miR-196a may regulate structural changes in AT that effect the ability of adipocytes to increase in volume.

AT ECM modulation effects adiposity in murine models [401] and in humans a polymorphism near MMP1 has been associated with BMI [426]. Rosiglitazone (a thiazolidinedione) is well documented to cause redistribution of AT, with expansion of ASAT [427, 428]. Interestingly, work from our group has shown that after a 3 month course of rosiglitazone the most strongly regulated transcripts in whole ASAT relate to ECM (unpublished data, Dr Matt Neville). MiR-196a might regulate depot-specific WAT expansion by directly regulating ECM deposition in ASAT. Equally, it may be that miR-196a regulates ECM in GSAT in a way that limits adipocyte expansion. This might then indirectly lead to increased fat storage centrally. The modest improvements in various metabolic parameters associated with higher miR-196a levels (Figure 4.8) suggest that alterations in body fat distribution with miR-196a expression might also be associated with metabolic phenotype.

During the generation of this thesis I have become aware of the limitations of *in vivo* experiments in attempting to replicate the complex environment of *in vivo* AT. I have also

discovered the difficulties in targeting experiments to a particular question, and the time and effort required to complete a single experiment. If I could change one thing about this project, I would conduct microarray analysis earlier, so that functional experiments could be targeted towards confirming hypotheses generated by the transcriptomic data.

The experiments in this thesis have shed light on the role that miRNAs, in particular miR-196a, play in the regulation of human body fat distribution. The project began by generating hypotheses based on profiling of miRNAs in ASAT and GSAT. Genotype associations and functional experiments have suggested mechanisms by which miR-196a might regulate AT expansion; the next step in the project should now be to take these observations back to whole AT to validate their relevance *in vivo*. Future work should focus on identifying histological differences in ASAT and GSAT from rs11614913 homozygotes, particularly relating to ECM, adipocyte size and angiogenesis. A traditional approach to dissecting the role of a transcript is to assess the phenotype of a transgenic murine model. Indeed, a mouse with AT-specific miR-196a overexpression has previously been generated [207] but due to the marked differences between mice and humans with regards to the WAT depots and fat distribution this approach would not be relevant to this question.

Whilst this thesis set out to examine the role of miRNA in body fat distribution, it became apparent during the course of the project that miR-196a might also be involved with bone metabolism. The complex relationship between AT and BMD is well recognized [357] and indeed miR-196a has been implicated in osteogenesis [206]. In Chapter 6 I make the novel observation that rs11614913 is associated with BMD, and demonstrated through analysis of the OBB dataset that it unlikely that the association between rs11614913 and body fat

distribution is confounding its relationship with BMD, or *vice versa*. The role of miR-196a in bone metabolism is unclear and certainly warrants further research.

In summary, this thesis has confirmed the importance of miRNA regulation to AT biology and has identified a role for miR-196a in the regulation of human body fat distribution. This adds a small piece of information to our understanding of what determines human body fat distribution and the distinct properties ASAT and GSAT and, ultimately, of how human WAT could be manipulated to improve metabolic health.

9 Appendix

Table 9.1: miRNAs differentially expressed in abdominal and gluteal adipose depots. P-values reaching the Bonferroni adjusted significance threshold (p=0.00125) are indicated in bold.

miRNA	Mean expression in ASAT (SEM)	Mean expression in GSAT (SEM)	Fold-change	Higher in ASAT or GSAT	p-value
mir-335	0.73 (0.05)	0.58 (0.05)	0.9	Abdominal	0.012
mir-320	0.51 (0.03)	0.42 (0.03)	0.9	Abdominal	0.009
mir-204	0.26 (0.03)	0.60 (0.07)	2.3	Gluteal	**<0.001**
mir-196a	0.48 (0.04)	0.99 (0.06)	2.1	Gluteal	**<0.001**
mir-27b	0.73 (0.05)	0.97 (0.06)	1.3	Gluteal	**<0.001**
mir-21	0.46 (0.04)	0.61 (0.05)	1.3	Gluteal	**0.001**
mir-146b	0.61 (0.09)	0.78 (0.11)	1.3	Gluteal	0.002
mir-1225	0.99 (0.07)	1.23 (0.09)	1.2	Gluteal	0.002
mir-572	1.58 (0.11)	1.93 (0.11)	1.2	Gluteal	0.002
mir-23b	0.58 (0.03)	0.70 (0.04)	1.2	Gluteal	0.008
mir-221	0.20 (0.03)	0.24 (0.03)	1.2	Gluteal	0.042
mir-221	0.37 (0.03)	0.44 (0.03)	1.2	Gluteal	0.005
mir-335	0.73 (0.05)	0.58 (0.05)	0.9	Abdominal	0.012

Table 9.2: miRNAs differentially expressed in lean and obese subjects in abdominal adipose tissue. P-values reaching the Bonferroni adjusted significance threshold (p=0.00125) are indicated in bold.

miRNA	Mean expression in lean (SEM)	Mean expression in obese (SEM)	Fold-change	p-value
miR-146b	0.34 (0.09)	0.87 (0.12)	2.5	**<0.001**
miR-221	0.12 (0.02)	0.28 (0.06)	2.3	0.045
miR-204	0.20 (0.03)	0.33 (0.04)	1.7	0.009
miR-146a	0.32 (0.03)	0.50 (0.04)	1.6	0.002
miR-21	0.42 (0.06)	0.51 (0.04)	1.2	0.027
miR-143	0.89 (0.06)	0.70 (0.06)	0.8	0.02
miR-27b	0.83 (0.07)	0.63 (0.05)	0.8	0.027
miR-23b	0.66 (0.05)	0.50 (0.04)	0.8	0.013
let-7g	0.62 (0.07)	0.44 (0.05)	0.7	0.045
miR-551b	1.09 (0.12)	0.74 (0.07)	0.7	0.03
miR-122a	0.58 (0.08)	0.38 (0.03)	0.7	0.034
miR-335	0.89 (0.08)	0.58 (0.05)	0.7	0.009
miR-378	1.96 (0.19)	1.34 (0.10)	0.7	0.013
miR-145	1.00 (0.07)	0.63 (0.04)	0.6	**<0.001**

Table 9.3: miRNAs differentially expressed in lean and obese subjects in gluteal adipose tissue. P-values reaching the Bonferroni adjusted significance threshold (p=0.00125) are indicated in bold.

miRNA	Mean expression in lean (SEM)	Mean expression in obese (SEM)	Fold-change (obese/lean)	p-value
mir-146b	0.47 (0.09)	1.09 (0.17)	2.3	**0.001**
mir-21	0.47 (0.04)	0.75 (0.07)	1.6	**<0.001**
mir-146a	0.37 (0.03)	0.57 (0.06)	1.6	0.01
mir-335	0.71 (0.07)	0.44 (0.05)	1.6	0.003
mir-551b	1.05 (0.09)	0.76 (0.08)	1.4	0.02
mir-143	0.89 (0.06)	0.70 (0.06)	1.3	0.05
miR-1225-5p	1.01 (0.10)	1.38 (0.13)	1.2	0.05
miR-23b	0.66 (0.05)	0.50 (0.04)	0.9	0.013
miR-378	1.78 (0.14)	1.52 (0.12)	0.85	0.12
mir-145	0.89 (0.05)	0.62 (0.05)	0.7	**<0.001**

Table 9.4: miRNAs differentially expressed between men and women in gluteal and abdominal subcutaneous adipose tissue. P-values reaching the Bonferroni adjusted significance threshold (p=0.00125) are indicated in bold.

	Abdominal				Gluteal			
	Men	Women	Fold-change	p-value	Men	Women	Fold-change	p-value
	Mean (SEM)	Mean (SEM)			Mean (SEM)	Mean (SEM)		
miR-424	0.28 (0.04)	0.56 (0.07)	2.0	<0.001	0.32 (0.05)	0.69 (0.08)	2.1	**<0.001**
miR-551b	0.72 (0.07)	1.09 (0.11)	1.5	0.01	0.85 (0.08)	0.95 (0.10)	1.1	0.45
miR-27b	0.59 (0.06)	0.87 (0.06)	1.5	0.001	0.83 (0.07)	1.10 (0.08)	1.3	0.014
miR-23b	0.47 (0.03)	0.69 (0.05)	1.5	0.001	0.64 (0.05)	0.76 (0.05)	1.2	0.17
miR-122a	0.39 (0.05)	0.57 (0.08)	1.4	0.03	0.47 (0.06)	0.50 (0.04)	1.1	0.433
miR-551b	0.67 (0.05)	0.91 (0.06)	1.4	0.007	0.73 (0.07)	0.86 (0.06)	1.2	0.19
miR-335	0.63 (0.08)	0.84 (0.07)	1.3	0.03	0.49 (0.05)	0.67 (0.08)	1.4	0.11
miR-145	0.70 (0.07)	0.93 (0.07)	1.3	0.02	0.69 (0.06)	0.82 (0.06)	1.2	0.32
miR-125b	0.71 (0.05)	0.92 (0.06)	1.3	0.02	0.76 (0.08)	0.82 (0.06)	1.1	0.48
let-7c	0.93 (0.08)	1.15 (0.05)	1.2	0.01	0.87 (0.08)	0.93 (0.05)	1.1	0.36
miR-939	1.31 (0.09)	1.61 (0.08)	1.2	0.02	1.32 (0.07)	1.40 (0.07)	1.1	0.49
miR-575	0.81 (0.06)	1.01 (0.06)	1.2	0.03	0.95 (0.09)	1.15 (0.08)	1.2	0.10
miR-99	0.81 (0.08)	0.98 (0.04)	1.2	0.023	0.81 (0.07)	0.87 (0.05)	1.1	0.37
miR-10b	1.05 (0.07)	1.24 (0.05)	1.2	0.01	0.89 (0.10)	1.11 (0.04)	1.2	**0.001**
miR-132	0.98 (0.06)	1.05 (0.04)	1.1	0.3	0.96 (0.06)	1.20 (0.07)	1.2	0.02
miR-195	0.42 (0.06)	0.29 (0.03)	0.7	0.3	0.43 (0.07)	0.25 (0.05)	0.6	0.04
miR-210	0.64 (0.03)	0.51 (0.02)	0.8	0.005	0.65 (0.04)	0.55 (0.02)	0.8	0.03
miR-378	1.27 (0.10)	2.02 (0.18)	0.6	0.002	1.35 (0.13)	1.94 (0.11)	0.7	0.002
miR-15b	0.27 (0.07)	0.13 (0.02)	0.5	0.2	0.28 (0.07)	0.10 (0.02)	0.4	0.03

Table 9.5: Associations between body fat distribution and BMD in men in the OBB cohort.

	Total BMD		Total BMD Adjusted for HOMA-IR		LS BMD		Pelvic BMD		Arm BMD	
	Standardised β	p-value	Standardised β	p-value	Standardised β	p-value	Standardised β	p-value	Standardised β	p-value
Lean mass†	0.475	$2.70x10^{-33}$	0.439	$1.8x10^{-28}$	0.395	$1.2x10^{-23}$	0.561	$3.3x10^{-41}$	0.347	$1.8x10^{-16}$
Android-to-gynoid AT ratio‡	0.018	0.58	0.028	0.025	0.104	0.001	0.052	0.13	-0.028	0.40
VAT mass‡	-0.017	0.12	-0.0.37	0.64	0.036	0.47	0.009	0.86	-0.122	0.02
Android SAT mass‡	-0.038	0.41	-0.058	0.21	-0.072	0.12	-0.055	0.25	-0.66	0.16
VAT-to-android SAT ratio‡	0.004	0.85	0.340	0.73	0.022	0.34	0.009	0.72	0.006	0.83
Gynoid AT mass‡	-0.139	0.068	-0.201	0.021	-0.243	0.001	-0.111	0.16	-0.220	0.005

†Adjusted for age at study visit, weight and height

‡Adjusted for age at study visit, height and total body fat mass

Table 9.6: Associations between body fat distribution and BMD in women in the OBB cohort.

	Total BMD		Total BMD Adjusted for HOMA-IR		Spine BMD		Pelvic BMD		Arm BMD	
	Standardised β	p-value	Standardised β	p-value	Standardised β	p-value	Standardised β	p-value	Standardised β	p-value
Lean mass†	0.398	$1.7x10^{-28}$	0.408	$2.7x10^{-29}$	0.293	$9.6x10^{-17}$	0.474	$7.7x10^{-38}$	0.185	$8.3x10^{-7}$
Android-to-gynoid AT ratio‡	0.041	0.15	0.060	0.045	0.159	$1.7x10^{-8}$	0.106	$3.2x10^{-4}$	-0.037	0.21
VAT mass‡	-0.153	$2.7x10^{-5}$	-0.132	0.001	-0.002	0.95	-0.059	0.18	-0.185	$4.7x10^{-7}$
Android SAT mass‡	0.263	$4.9x10^{-5}$	0.265	$5.3x10^{-5}$	0.260	$4.2x10^{-5}$	0.290	$1.1x10^{-5}$	0.073	0.27
VAT-to-android SAT ratio §	-0.116	$5.2x10^{-8}$	-0.08	$1.4x10^{-4}$	-0.013	0.53	-0.090	$3.8x10^{-5}$	-0.089	$4.9x10^{-5}$
Gynoid AT mass‡	-0.109	0.07	-0.121	0.058	-0.210	$3.7x10^{-4}$	-0.183	0.003	-0.022	0.72

†Adjusted for age at study visit, weight, height, use of hormonal contraceptives and menopause status.
‡Adjusted for age at study visit, height, total body fat mass, use of hormonal contraceptives and menopause status.
§Adjusted for age at study visit, height, weight, use of hormonal contraceptives and menopause status.

References

1. *Obesity: preventing and managing the global epidemic. Report of a WHO consultation.* World Health Organ Tech Rep Ser, 2000. **894**: p. i-xii, 1-253.
2. Cinti, S., *The adipose organ at a glance.* Dis Model Mech, 2012. **5**(5): p. 588-94.
3. Petrovic, N., et al., *Chronic peroxisome proliferator-activated receptor gamma (PPARgamma) activation of epididymally derived white adipocyte cultures reveals a population of thermogenically competent, UCP1-containing adipocytes molecularly distinct from classic brown adipocytes.* J Biol Chem, 2010. **285**(10): p. 7153-64.
4. Schulz, T.J., et al., *Identification of inducible brown adipocyte progenitors residing in skeletal muscle and white fat.* Proc Natl Acad Sci U S A, 2011. **108**(1): p. 143-8.
5. Gesta, S., Y.H. Tseng, and C.R. Kahn, *Developmental origin of fat: tracking obesity to its source.* Cell, 2007. **131**(2): p. 242-56.
6. Wronska, A. and Z. Kmiec, *Structural and biochemical characteristics of various white adipose tissue depots.* Acta Physiol (Oxf), 2012. **205**(2): p. 194-208.
7. Galic, S., J.S. Oakhill, and G.R. Steinberg, *Adipose tissue as an endocrine organ.* Molecular and Cellular Endocrinology, 2010. **316**(2): p. 129-139.
8. Zuk, P.A., et al., *Human adipose tissue is a source of multipotent stem cells.* Mol Biol Cell, 2002. **13**(12): p. 4279-95.
9. Weisberg, S.P., et al., *Obesity is associated with macrophage accumulation in adipose tissue.* J Clin Invest, 2003. **112**(12): p. 1796-808.
10. Elgazar-Carmon, V., et al., *Neutrophils transiently infiltrate intra-abdominal fat early in the course of high-fat feeding.* J Lipid Res, 2008. **49**(9): p. 1894-903.
11. Wu, H., et al., *T-cell accumulation and regulated on activation, normal T cell expressed and secreted upregulation in adipose tissue in obesity.* Circulation, 2007. **115**(8): p. 1029-38.
12. Winer, D.A., et al., *B cells promote insulin resistance through modulation of T cells and production of pathogenic IgG antibodies.* Nat Med, 2011. **17**(5): p. 610-7.
13. Nedergaard, J., T. Bengtsson, and B. Cannon, *Unexpected evidence for active brown adipose tissue in adult humans.* Am J Physiol Endocrinol Metab, 2007. **293**(2): p. E444-52.
14. Cypess, A.M., et al., *Identification and importance of brown adipose tissue in adult humans.* N Engl J Med, 2009. **360**(15): p. 1509-17.
15. Cannon, B. and J. Nedergaard, *Brown adipose tissue: function and physiological significance.* Physiol Rev, 2004. **84**(1): p. 277-359.
16. van Marken Lichtenbelt, W.D., et al., *Cold-activated brown adipose tissue in healthy men.* N Engl J Med, 2009. **360**(15): p. 1500-8.

17. Ouellet, V., et al., *Outdoor temperature, age, sex, body mass index, and diabetic status determine the prevalence, mass, and glucose-uptake activity of 18F-FDG-detected BAT in humans.* J Clin Endocrinol Metab, 2011. **96**(1): p. 192-9.

18. Lee, P., et al., *A critical appraisal of the prevalence and metabolic significance of brown adipose tissue in adult humans.* Am J Physiol Endocrinol Metab, 2010. **299**(4): p. E601-6.

19. Huttunen, P., J. Hirvonen, and V. Kinnula, *The occurrence of brown adipose tissue in outdoor workers.* Eur J Appl Physiol Occup Physiol, 1981. **46**(4): p. 339-45.

20. Yoneshiro, T., et al., *Recruited brown adipose tissue as an antiobesity agent in humans.* J Clin Invest, 2013. **123**(8): p. 3404-8.

21. Cousin, B., et al., *Occurrence of brown adipocytes in rat white adipose tissue: molecular and morphological characterization.* J Cell Sci, 1992. **103 (Pt 4)**: p. 931-42.

22. Wu, J., et al., *Beige adipocytes are a distinct type of thermogenic fat cell in mouse and human.* Cell, 2012. **150**(2): p. 366-76.

23. Owens, B., *Cell physiology: The changing colour of fat.* Nature, 2014. **508**(7496): p. S52-3.

24. Cohen, P., et al., *Ablation of PRDM16 and beige adipose causes metabolic dysfunction and a subcutaneous to visceral fat switch.* Cell, 2014. **156**(1-2): p. 304-16.

25. Seale, P., et al., *Prdm16 determines the thermogenic program of subcutaneous white adipose tissue in mice.* J Clin Invest, 2011. **121**(1): p. 96-105.

26. Sharp, L.Z., et al., *Human BAT Possesses Molecular Signatures That Resemble Beige/Brite Cells.* PLoS One, 2012. **7**(11): p. e49452.

27. Hilton, C., F. Karpe, and K.E. Pinnick, *Role of developmental transcription factors in white, brown and beige adipose tissues.* Biochimica Et Biophysica Acta-Molecular and Cell Biology of Lipids, 2015. **1851**(5): p. 686-696.

28. Billon, N., et al., *The generation of adipocytes by the neural crest.* Development, 2007. **134**(12): p. 2283-92.

29. Billon, N. and C. Dani, *Developmental origins of the adipocyte lineage: new insights from genetics and genomics studies.* Stem Cell Rev, 2012. **8**(1): p. 55-66.

30. Chau, Y.Y., et al., *Visceral and subcutaneous fat have different origins and evidence supports a mesothelial source.* Nat Cell Biol, 2014. **16**(4): p. 367-75.

31. Cantile, M., et al., *HOX gene network is involved in the transcriptional regulation of in vivo human adipogenesis.* J Cell Physiol, 2003. **194**(2): p. 225-36.

32. Yamamoto, Y., et al., *Adipose depots possess unique developmental gene signatures.* Obesity (Silver Spring), 2010. **18**(5): p. 872-8.

33. Cheung, L., et al., *Human mediastinal adipose tissue displays certain characteristics of brown fat.* Nutr Diabetes, 2013. **3**: p. e66.

34. Vohl, M.C., et al., *A survey of genes differentially expressed in subcutaneous and visceral adipose tissue in men.* Obes Res, 2004. **12**(8): p. 1217-22.

35. Gesta, S., et al., *Evidence for a role of developmental genes in the origin of obesity and body fat distribution.* Proc Natl Acad Sci U S A, 2006. **103**(17): p. 6676-81.

36. Levi, B., et al., *Depot-specific variation in the osteogenic and adipogenic potential of human adipose-derived stromal cells.* Plast Reconstr Surg, 2010. **126**(3): p. 822-34.

37. Tchkonia, T., et al., *Identification of depot-specific human fat cell progenitors through distinct expression profiles and developmental gene patterns.* Am J Physiol Endocrinol Metab, 2007. **292**(1): p. E298-307.

38. Macotela, Y., et al., *Intrinsic differences in adipocyte precursor cells from different white fat depots.* Diabetes, 2012. **61**(7): p. 1691-9.

39. Karastergiou, K., et al., *Distinct developmental signatures of human abdominal and gluteal subcutaneous adipose tissue depots.* J Clin Endocrinol Metab, 2013. **98**(1): p. 362-71.

40. Pinnick, K.E., et al., *Distinct Developmental Profile of Lower-Body Adipose Tissue Defines Resistance Against Obesity-Associated Metabolic Complications.* Diabetes, 2014.

41. Frontini, A. and S. Cinti, *Distribution and development of brown adipocytes in the murine and human adipose organ.* Cell Metab, 2010. **11**(4): p. 253-6.

42. Van Harmelen, V., et al., *Leptin secretion from subcutaneous and visceral adipose tissue in women.* Diabetes, 1998. **47**(6): p. 913-7.

43. O'Connell, J., et al., *The relationship of omental and subcutaneous adipocyte size to metabolic disease in severe obesity.* PLoS One, 2010. **5**(4): p. e9997.

44. Zhang, Y., et al., *Fat cell size and adipokine expression in relation to gender, depot, and metabolic risk factors in morbidly obese adolescents.* Obesity (Silver Spring), 2014. **22**(3): p. 691-7.

45. Boivin, A., et al., *Regional differences in adipose tissue metabolism in obese men.* Metabolism, 2007. **56**(4): p. 533-40.

46. Maslowska, M.H., et al., *Regional differences in triacylglycerol synthesis in adipose tissue and in cultured preadipocytes.* J Lipid Res, 1993. **34**(2): p. 219-28.

47. Sbarbati, A., et al., *Subcutaneous adipose tissue classification.* Eur J Histochem, 2010. **54**(4): p. e48.

48. Johnson, D., A.K. Dixon, and P.H. Abrahams, *The abdominal subcutaneous tissue: computed tomographic, magnetic resonance, and anatomical observations.* Clin Anat, 1996. **9**(1): p. 19-24.

49. Marinou, K., et al., *Structural and functional properties of deep abdominal subcutaneous adipose tissue explain its association with insulin resistance and cardiovascular risk in men.* Diabetes Care, 2014. **37**(3): p. 821-9.

50. Tordjman, J., et al., *Structural and inflammatory heterogeneity in subcutaneous adipose tissue: relation with liver histopathology in morbid obesity.* J Hepatol, 2012. **56**(5): p. 1152-8.

51. Kadowaki, T., et al., *Adiponectin and adiponectin receptors in insulin resistance, diabetes, and the metabolic syndrome.* J Clin Invest, 2006. **116**(7): p. 1784-92.

52. Lihn, A.S., et al., *Lower expression of adiponectin mRNA in visceral adipose tissue in lean and obese subjects.* Mol Cell Endocrinol, 2004. **219**(1-2): p. 9-15.

53. Fried, S.K., D.A. Bunkin, and A.S. Greenberg, *Omental and subcutaneous adipose tissues of obese subjects release interleukin-6: depot difference and regulation by glucocorticoid.* J Clin Endocrinol Metab, 1998. **83**(3): p. 847-50.

54. Pinnick, K.E., et al., *Gluteofemoral adipose tissue plays a major role in production of the lipokine palmitoleate in humans.* Diabetes, 2012. **61**(6): p. 1399-403.

55. Martin, M.L. and M.D. Jensen, *Effects of body fat distribution on regional lipolysis in obesity.* J Clin Invest, 1991. **88**(2): p. 609-13.

56. Tan, G.D., et al., *Upper and lower body adipose tissue function: a direct comparison of fat mobilization in humans.* Obes Res, 2004. **12**(1): p. 114-8.

57. Manolopoulos, K.N., F. Karpe, and K.N. Frayn, *Marked resistance of femoral adipose tissue blood flow and lipolysis to adrenaline in vivo.* Diabetologia, 2012. **55**(11): p. 3029-37.

58. Wahrenberg, H., F. Lonnqvist, and P. Arner, *Mechanisms underlying regional differences in lipolysis in human adipose tissue.* J Clin Invest, 1989. **84**(2): p. 458-67.

59. Arner, P., *Differences in lipolysis between human subcutaneous and omental adipose tissues.* Ann Med, 1995. **27**(4): p. 435-8.

60. Jensen, M.D., et al., *Regional uptake of meal fatty acids in humans.* Am J Physiol Endocrinol Metab, 2003. **285**(6): p. E1282-8.

61. Malcom, G.T., et al., *Fatty acid composition of adipose tissue in humans: differences between subcutaneous sites.* Am J Clin Nutr, 1989. **50**(2): p. 288-91.

62. Guo, Z., et al., *Regional postprandial fatty acid metabolism in different obesity phenotypes.* Diabetes, 1999. **48**(8): p. 1586-92.

63. McQuaid, S.E., et al., *Femoral adipose tissue may accumulate the fat that has been recycled as VLDL and nonesterified fatty acids.* Diabetes, 2010. **59**(10): p. 2465-73.

64. Yim, J.E., et al., *Femoral-gluteal subcutaneous and intermuscular adipose tissues have independent and opposing relationships with CVD risk.* J Appl Physiol (1985), 2008. **104**(3): p. 700-7.

65. Johnson, J.A., et al., *Impaired insulin action in subcutaneous adipocytes from women with visceral obesity.* Am J Physiol Endocrinol Metab, 2001. **280**(1): p. E40-9.

66. Richelsen, B., et al., *Regional differences in triglyceride breakdown in human adipose tissue: effects of catecholamines, insulin, and prostaglandin E2.* Metabolism, 1991. **40**(9): p. 990-6.

67. Tchkonia, T., et al., *Fat depot-specific characteristics are retained in strains derived from single human preadipocytes.* Diabetes, 2006. **55**(9): p. 2571-8.

68. Tchkonia, T., et al., *Abundance of two human preadipocyte subtypes with distinct capacities for replication, adipogenesis, and apoptosis varies among fat depots.* Am J Physiol Endocrinol Metab, 2005. **288**(1): p. E267-77.

69. Tchoukalova, Y.D., et al., *Regional differences in cellular mechanisms of adipose tissue gain with overfeeding.* Proc Natl Acad Sci U S A, 2010. **107**(42): p. 18226-31.

70. Tchoukalova, Y.D., et al., *Subcutaneous adipocyte size and body fat distribution.* American Journal of Clinical Nutrition, 2008. **87**(1): p. 56-63.

71. Haslam, D.W. and W.P. James, *Obesity.* Lancet, 2005. **366**(9492): p. 1197-209.

72. van Vliet-Ostaptchouk, J.V., et al., *The prevalence of metabolic syndrome and metabolically healthy obesity in Europe: a collaborative analysis of ten large cohort studies.* BMC Endocr Disord, 2014. **14**(1): p. 9.

73. Yusuf, S., et al., *Obesity and the risk of myocardial infarction in 27,000 participants from 52 countries: a case-control study.* Lancet, 2005. **366**(9497): p. 1640-9.

74. Puder, J.J., et al., *Central fat excess in polycystic ovary syndrome: relation to low-grade inflammation and insulin resistance.* J Clin Endocrinol Metab, 2005. **90**(11): p. 6014-21.

75. Kirchengast, S. and J. Huber, *Body composition characteristics and body fat distribution in lean women with polycystic ovary syndrome.* Hum Reprod, 2001. **16**(6): p. 1255-60.

76. Horejsi, R., et al., *Android subcutaneous adipose tissue topography in lean and obese women suffering from PCOS: comparison with type 2 diabetic women.* Am J Phys Anthropol, 2004. **124**(3): p. 275-81.

77. Snijder, M.B., et al., *Low subcutaneous thigh fat is a risk factor for unfavourable glucose and lipid levels, independently of high abdominal fat. The Health ABC Study.* Diabetologia, 2005. **48**(2): p. 301-8.

78. Smith, S.R., et al., *Contributions of total body fat, abdominal subcutaneous adipose tissue compartments, and visceral adipose tissue to the metabolic complications of obesity.* Metabolism, 2001. **50**(4): p. 425-35.

79. Fox, C.S., et al., *Abdominal visceral and subcutaneous adipose tissue compartments: association with metabolic risk factors in the Framingham Heart Study.* Circulation, 2007. **116**(1): p. 39-48.

80. Kaess, B.M., et al., *The ratio of visceral to subcutaneous fat, a metric of body fat distribution, is a unique correlate of cardiometabolic risk.* Diabetologia, 2012. **55**(10): p. 2622-30.

81. Frayn, K.N., *Visceral fat and insulin resistance--causative or correlative?* Br J Nutr, 2000. **83 Suppl 1**: p. S71-7.

82. Manolopoulos, K.N., F. Karpe, and K.N. Frayn, *Gluteofemoral body fat as a determinant of metabolic health.* International Journal of Obesity, 2010. **34**(6): p. 949-959.

83. White, U.A. and Y.D. Tchoukalova, *Sex dimorphism and depot differences in adipose tissue function.* Biochim Biophys Acta, 2014. **1842**(3): p. 377-92.

84. Despres, J.P., *Body fat distribution and risk of cardiovascular disease: an update.* Circulation, 2012. **126**(10): p. 1301-13.

85. Pausova, Z., et al., *Heritability estimates of obesity measures in siblings with and without hypertension.* Hypertension, 2001. **38**(1): p. 41-7.

86. Souren, N.Y., et al., *Anthropometry, carbohydrate and lipid metabolism in the East Flanders Prospective Twin Survey: heritabilities.* Diabetologia, 2007. **50**(10): p. 2107-16.

87. Garg, A., *Clinical review#: Lipodystrophies: genetic and acquired body fat disorders.* J Clin Endocrinol Metab, 2011. **96**(11): p. 3313-25.

88. Vigouroux, C., et al., *Molecular mechanisms of human lipodystrophies: from adipocyte lipid droplet to oxidative stress and lipotoxicity.* Int J Biochem Cell Biol, 2011. **43**(6): p. 862-76.

89. Wagner, R., et al., *The genetic influence on body fat distribution.* Drug Discovery Today: Disease Mechanisms, 2013. **10**(1–2): p. e5-e13.

90. Shungin, D., et al., *New genetic loci link adipose and insulin biology to body fat distribution.* Nature, 2015. **518**(7538): p. 187-96.

91. Ukkola, O., et al., *Interactions among the alpha2-, beta2-, and beta3-adrenergic receptor genes and obesity-related phenotypes in the Quebec Family Study.* Metabolism, 2000. **49**(8): p. 1063-70.

92. Kim, K.S., et al., *Effects of peroxisome proliferator-activated receptor-gamma 2 Pro12Ala polymorphism on body fat distribution in female Korean subjects.* Metabolism, 2004. **53**(12): p. 1538-43.

93. Syed, A.A., et al., *Association of glucocorticoid receptor polymorphism A3669G in exon 9beta with reduced central adiposity in women.* Obesity (Silver Spring), 2006. **14**(5): p. 759-64.

94. Gallagher, C.J., et al., *Association of the estrogen receptor-alpha gene with the metabolic syndrome and its component traits in African-American families: the Insulin Resistance Atherosclerosis Family Study.* Diabetes, 2007. **56**(8): p. 2135-41.

95. Bjorntorp, P., *Hormonal control of regional fat distribution.* Hum Reprod, 1997. **12 Suppl 1**: p. 21-5.

96. Goodman-Gruen, D. and E. Barrett-Connor, *Sex differences in measures of body fat and body fat distribution in the elderly.* Am J Epidemiol, 1996. **143**(9): p. 898-906.

97. Elbers, J.M., et al., *Effects of sex steroid hormones on regional fat depots as assessed by magnetic resonance imaging in transsexuals.* Am J Physiol, 1999. **276**(2 Pt 1): p. E317-25.

98. Wajchenberg, B.L., et al., *Estimation of body fat and lean tissue distribution by dual energy X-ray absorptiometry and abdominal body fat evaluation by computed tomography in Cushing's disease.* J Clin Endocrinol Metab, 1995. **80**(9): p. 2791-4.

99. Kuk, J.L., et al., *Age-related changes in total and regional fat distribution.* Ageing Res Rev, 2009. **8**(4): p. 339-48.

100. Lovejoy, J.C., et al., *Increased visceral fat and decreased energy expenditure during the menopausal transition.* Int J Obes (Lond), 2008. **32**(6): p. 949-58.

101. Villarroya, F., P. Domingo, and M. Giralt, *Drug-induced lipotoxicity: lipodystrophy associated with HIV-1 infection and antiretroviral treatment.* Biochim Biophys Acta, 2010. **1801**(3): p. 392-9.

102. Tran, T.T., et al., *Beneficial effects of subcutaneous fat transplantation on metabolism.* Cell Metab, 2008. **7**(5): p. 410-20.

103. Hocking, S.L., D.J. Chisholm, and D.E. James, *Studies of regional adipose transplantation reveal a unique and beneficial interaction between subcutaneous adipose tissue and the intra-abdominal compartment.* Diabetologia, 2008. **51**(5): p. 900-2.

104. van Harmelen, V., et al., *Increased lipolysis and decreased leptin production by human omental as compared with subcutaneous preadipocytes.* Diabetes, 2002. **51**(7): p. 2029-36.

105. Hocking, S.L., et al., *Intrinsic depot-specific differences in the secretome of adipose tissue, preadipocytes, and adipose tissue-derived microvascular endothelial cells.* Diabetes, 2010. **59**(12): p. 3008-16.

106. Caserta, F., et al., *Fat depot origin affects fatty acid handling in cultured rat and human preadipocytes.* Am J Physiol Endocrinol Metab, 2001. **280**(2): p. E238-47.

107. Niesler, C.U., K. Siddle, and J.B. Prins, *Human preadipocytes display a depot-specific susceptibility to apoptosis.* Diabetes, 1998. **47**(8): p. 1365-8.

108. Friedman, R.C., et al., *Most mammalian mRNAs are conserved targets of microRNAs.* Genome Res, 2009. **19**(1): p. 92-105.

109. Jansson, M.D. and A.H. Lund, *MicroRNA and cancer.* Mol Oncol, 2012. **6**(6): p. 590-610.

110. Quiat, D. and E.N. Olson, *MicroRNAs in cardiovascular disease: from pathogenesis to prevention and treatment.* J Clin Invest, 2013. **123**(1): p. 11-8.

111. Krutzfeldt, J., et al., *Silencing of microRNAs in vivo with 'antagomirs'.* Nature, 2005. **438**(7068): p. 685-9.

112. Elmen, J., et al., *LNA-mediated microRNA silencing in non-human primates.* Nature, 2008. **452**(7189): p. 896-9.

113. Ling, H., M. Fabbri, and G.A. Calin, *MicroRNAs and other non-coding RNAs as targets for anticancer drug development.* Nat Rev Drug Discov, 2013. **12**(11): p. 847-65.

114. Yang, W.J., et al., *Dicer is required for embryonic angiogenesis during mouse development.* J Biol Chem, 2005. **280**(10): p. 9330-5.

115. Kim, V.N., J. Han, and M.C. Siomi, *Biogenesis of small RNAs in animals.* Nat Rev Mol Cell Biol, 2009. **10**(2): p. 126-39.

116. Krol, J., I. Loedige, and W. Filipowicz, *The widespread regulation of microRNA biogenesis, function and decay.* Nat Rev Genet, 2010. **11**(9): p. 597-610.

117. Lee, Y., et al., *The nuclear RNase III Drosha initiates microRNA processing.* Nature, 2003. **425**(6956): p. 415-9.

118. Yang, J.S., et al., *Widespread regulatory activity of vertebrate microRNA* species.* RNA, 2011. **17**(2): p. 312-26.

119. Griffiths-Jones, S., et al., *MicroRNA evolution by arm switching.* EMBO Rep, 2011. **12**(2): p. 172-7.

120. Orom, U.A., F.C. Nielsen, and A.H. Lund, *MicroRNA-10a binds the 5'UTR of ribosomal protein mRNAs and enhances their translation.* Mol Cell, 2008. **30**(4): p. 460-71.

121. Fang, Z. and N. Rajewsky, *The impact of miRNA target sites in coding sequences and in 3'UTRs.* PLoS One, 2011. **6**(3): p. e18067.

122. Vasudevan, S., Y. Tong, and J.A. Steitz, *Switching from repression to activation: microRNAs can up-regulate translation.* Science, 2007. **318**(5858): p. 1931-4.

123. Selbach, M., et al., *Widespread changes in protein synthesis induced by microRNAs.* Nature, 2008. **455**(7209): p. 58-63.

124. Baek, D., et al., *The impact of microRNAs on protein output.* Nature, 2008. **455**(7209): p. 64-71.

125. Mukherji, S., et al., *MicroRNAs can generate thresholds in target gene expression.* Nat Genet, 2011. **43**(9): p. 854-9.

126. Hornstein, E., et al., *The microRNA miR-196 acts upstream of Hoxb8 and Shh in limb development.* Nature, 2005. **438**(7068): p. 671-4.

127. Lim, L.P., et al., *Microarray analysis shows that some microRNAs downregulate large numbers of target mRNAs.* Nature, 2005. **433**(7027): p. 769-73.

128. Oskowitz, A.Z., et al., *Human multipotent stromal cells from bone marrow and microRNA: regulation of differentiation and leukemia inhibitory factor expression.* Proc Natl Acad Sci U S A, 2008. **105**(47): p. 18372-7.

129. Wang, Q., et al., *miR-17-92 cluster accelerates adipocyte differentiation by negatively regulating tumor-suppressor Rb2/p130.* Proc Natl Acad Sci U S A, 2008. **105**(8): p. 2889-94.

130. Mudhasani, R., et al., *Dicer is required for the formation of white but not brown adipose tissue.* J Cell Physiol, 2011. **226**(5): p. 1399-406.

131. Xu, P., et al., *The Drosophila microRNA Mir-14 suppresses cell death and is required for normal fat metabolism.* Curr Biol, 2003. **13**(9): p. 790-5.

132. Teleman, A.A., S. Maitra, and S.M. Cohen, *Drosophila lacking microRNA miR-278 are defective in energy homeostasis.* Genes Dev, 2006. **20**(4): p. 417-22.

133. Hyun, S., et al., *Conserved MicroRNA miR-8/miR-200 and its target USH/FOG2 control growth by regulating PI3K.* Cell, 2009. **139**(6): p. 1096-108.

134. Rantalainen, M., et al., *MicroRNA Expression in Abdominal and Gluteal Adipose Tissue Is Associated with mRNA Expression Levels and Partly Genetically Driven.* PLoS One, 2011. **6**(11): p. e27338.

135. Karolina, D.S., et al., *Circulating miRNA profiles in patients with metabolic syndrome.* J Clin Endocrinol Metab, 2012. **97**(12): p. E2271-6.

136. Mouse Genome Sequencing, C., et al., *Initial sequencing and comparative analysis of the mouse genome.* Nature, 2002. **420**(6915): p. 520-62.

137. Lin, S., et al., *Comparison of the transcriptional landscapes between human and mouse tissues.* Proceedings of the National Academy of Sciences of the United States of America, 2014. **111**(48): p. 17224-17229.

138. Parts, L., et al., *Extent, causes, and consequences of small RNA expression variation in human adipose tissue.* PLoS Genet, 2012. **8**(5): p. e1002704.

139. Civelek, M., et al., *Genetic regulation of human adipose microRNA expression and its consequences for metabolic traits.* Hum Mol Genet, 2013. **22**(15): p. 3023-37.

140. Prats-Puig, A., et al., *Changes in circulating microRNAs are associated with childhood obesity.* J Clin Endocrinol Metab, 2013. **98**(10): p. E1655-60.

141. Heneghan, H.M., et al., *Differential miRNA expression in omental adipose tissue and in the circulation of obese patients identifies novel metabolic biomarkers.* J Clin Endocrinol Metab, 2011. **96**(5): p. E846-50.

142. Ortega, F.J., et al., *MiRNA expression profile of human subcutaneous adipose and during adipocyte differentiation.* PLoS One, 2010. **5**(2): p. e9022.

143. Sun, T., et al., *MicroRNA let-7 regulates 3T3-L1 adipogenesis.* Mol Endocrinol, 2009. **23**(6): p. 925-31.

144. Kajimoto, K., H. Naraba, and N. Iwai, *MicroRNA and 3T3-L1 pre-adipocyte differentiation.* Rna-A Publication of the Rna Society, 2006. **12**(9): p. 1626-32.

145. Esau, C., et al., *MicroRNA-143 regulates adipocyte differentiation.* J Biol Chem, 2004. **279**(50): p. 52361-5.

146. Xie, H., B. Lim, and H.F. Lodish, *MicroRNAs induced during adipogenesis that accelerate fat cell development are downregulated in obesity.* Diabetes, 2009. **58**(5): p. 1050-7.

147. Gerin, I., et al., *Roles for miRNA-378/378* in adipocyte gene expression and lipogenesis.* Am J Physiol Endocrinol Metab, 2010. **299**(2): p. E198-206.

148. Neville, M.J., et al., *Comprehensive human adipose tissue mRNA and microRNA endogenous control selection for quantitative real-time-PCR normalization.* Obesity (Silver Spring), 2011. **19**(4): p. 888-92.

149. Trajkovski, M., et al., *MicroRNAs 103 and 107 regulate insulin sensitivity.* Nature, 2011. **474**(7353): p. 649-53.

150. Herrera, B.M., et al., *MicroRNA-125a is over-expressed in insulin target tissues in a spontaneous rat model of Type 2 Diabetes.* BMC Med Genomics, 2009. **2**: p. 54.

151. Yeh, C.L., et al., *MicroRNA-125a-3p expression in abdominal adipose tissues is associated with insulin signalling gene expressions in morbid obesity: observations in Taiwanese.* Asia Pacific Journal of Clinical Nutrition, 2014. **23**(2): p. 331-337.

152. Ji, H.L., et al., *miR-125a inhibits porcine preadipocytes differentiation by targeting ERRalpha.* Mol Cell Biochem, 2014. **395**(1-2): p. 155-65.

153. Mi, L., et al., *MicroRNA-139-5p Suppresses 3T3-L1 Preadipocyte Differentiation Through Notch and IRS1/PI3K/Akt Insulin Signaling Pathways.* J Cell Biochem, 2015. **116**(7): p. 1195-204.

154. Chen, C., et al., *miR-135a-5p inhibits 3T3-L1 adipogenesis through activation of canonical Wnt/beta-catenin signaling.* Journal of Molecular Endocrinology, 2014. **52**(3): p. 311-320.

155. Yang, Z., et al., *MicroRNA hsa-miR-138 inhibits adipogenic differentiation of human adipose tissue-derived mesenchymal stem cells through adenovirus EID-1.* Stem Cells Dev, 2011. **20**(2): p. 259-67.

156. Mi, L., et al., *MicroRNA-139-5p Suppresses 3T3-L1 Preadipocyte Differentiation Through Notch and IRS1/PI3K/Akt Insulin Signaling Pathways.* Journal of Cellular Biochemistry, 2015. **116**(7): p. 1195-1204.

157. Keller, P., et al., *Gene-chip studies of adipogenesis-regulated microRNAs in mouse primary adipocytes and human obesity.* BMC Endocr Disord, 2011. **11**: p. 7.

158. Kilic, I.D., et al., *MicroRNA -143 and -223 in obesity.* Gene, 2015. **560**(2): p. 140-2.

159. Takanabe, R., et al., *Up-regulated expression of microRNA-143 in association with obesity in adipose tissue of mice fed high-fat diet.* Biochem Biophys Res Commun, 2008. **376**(4): p. 728-32.

160. Guo, Y., et al., *Up-regulated miR-145 expression inhibits porcine preadipocytes differentiation by targeting IRS1.* Int J Biol Sci, 2012. **8**(10): p. 1408-17.

161. Lin, Y.Y., et al., *KSRP and MicroRNA 145 Are Negative Regulators of Lipolysis in White Adipose Tissue.* Molecular and Cellular Biology, 2014. **34**(12): p. 2339-2349.

162. Chen, L., et al., *MiR-146b is a regulator of human visceral preadipocyte proliferation and differentiation and its expression is altered in human obesity.* Molecular and Cellular Endocrinology, 2014. **393**(1-2): p. 65-74.

163. Chartoumpekis, D.V., et al., *Differential expression of microRNAs in adipose tissue after long-term high-fat diet-induced obesity in mice.* PLoS One, 2012. **7**(4): p. e34872.

164. Ahn, J., et al., *MicroRNA-146b promotes adipogenesis by suppressing the SIRT1-FOXO1 cascade.* Embo Molecular Medicine, 2013. **5**(10): p. 1602-1612.

165. Shi, C.M., et al., *miR-148a is Associated with Obesity and Modulates Adipocyte Differentiation of Mesenchymal Stem Cells through Wnt Signaling.* Scientific Reports, 2015. **5**.

166. Andersen, D.C., et al., *MicroRNA-15a fine-tunes the level of Delta-like 1 homolog (DLK1) in proliferating 3T3-L1 preadipocytes.* Exp Cell Res, 2010. **316**(10): p. 1681-91.

167. Belarbi, Y., et al., *MicroRNA-193b controls adiponectin production in human white adipose tissue.* J Clin Endocrinol Metab, 2015: p. jc20151530.

168. Yun, U.J., et al., *MiR-195a Inhibits Adipocyte Differentiation by Targeting the Preadipogenic Determinator Zfp423.* J Cell Biochem, 2015.

169. Kim, Y.J., et al., *MiR-21 regulates adipogenic differentiation through the modulation of TGF-beta signaling in mesenchymal stem cells derived from human adipose tissue.* Stem Cells, 2009. **27**(12): p. 3093-102.

170. Kim, Y.J., et al., *MicroRNA 21 regulates the proliferation of human adipose tissue-derived mesenchymal stem cells and high-fat diet-induced obesity alters microRNA 21.* J Cell Physiol, 2011.

171. He, H., et al., *miR-204-5p promotes the adipogenic differentiation of human adipose-derived mesenchymal stem cells by modulating DVL3 expression and suppressing Wnt/beta-catenin signaling.* Int J Mol Med, 2015. **35**(6): p. 1587-95.

172. Qin, L., et al., *A deep investigation into the adipogenesis mechanism: profile of microRNAs regulating adipogenesis by modulating the canonical Wnt/beta-catenin signaling pathway.* BMC Genomics, 2010. **11**: p. 320.

173. Meerson, A., et al., *Human adipose microRNA-221 is upregulated in obesity and affects fat metabolism downstream of leptin and TNF-alpha.* Diabetologia, 2013. **56**(9): p. 1971-9.

174. Herrera, B.M., et al., *Global microRNA expression profiles in insulin target tissues in a spontaneous rat model of type 2 diabetes.* Diabetologia, 2010. **53**(6): p. 1099-109.

175. Shi, Z.H., et al., *Differential Expression of MicroRNAs in Omental Adipose Tissue From Gestational Diabetes Mellitus Subjects Reveals miR-222 as a Regulator of ER alpha Expression in Estrogen-Induced Insulin Resistance.* Endocrinology, 2014. **155**(5): p. 1982-1990.

176. Xu, G., et al., *MiR-26b modulates insulin sensitivity in adipocytes by interrupting the PTEN/PI3K/AKT pathway.* Int J Obes (Lond), 2015.

177. Karbiener, M., et al., *MicroRNA-26 Family Is Required for Human Adipogenesis and Drives Characteristics of Brown Adipocytes.* Stem Cells, 2014. **32**(6): p. 1578-1590.

178. Lin, Q., et al., *A role of miR-27 in the regulation of adipogenesis.* FEBS J, 2009. **276**(8): p. 2348-58.

179. Kim, S.Y., et al., *miR-27a is a negative regulator of adipocyte differentiation via suppressing PPARgamma expression.* Biochem Biophys Res Commun, 2010. **392**(3): p. 323-8.

180. Karbiener, M., et al., *microRNA miR-27b impairs human adipocyte differentiation and targets PPARgamma.* Biochem Biophys Res Commun, 2009. **390**(2): p. 247-51.

181. Kang, T., et al., *MicroRNA-27 (miR-27) Targets Prohibitin and Impairs Adipocyte Differentiation and Mitochondria! Function in Human Adipose-derived Stem Cells.* Journal of Biological Chemistry, 2013. **288**(48): p. 34394-34402.

182. He, A., et al., *Overexpression of micro ribonucleic acid 29, highly up-regulated in diabetic rats, leads to insulin resistance in 3T3-L1 adipocytes.* Mol Endocrinol, 2007. **21**(11): p. 2785-94.

183. Zaragosi, L.E., et al., *Small RNA sequencing reveals miR-642a-3p as a novel adipocyte-specific microRNA and miR-30 as a key regulator of human adipogenesis.* Genome Biol, 2011. **12**(7): p. R64.

184. Karbiener, M., et al., *MicroRNA-30c promotes human adipocyte differentiation and co-represses PAI-1 and ALK2.* RNA Biol, 2011. **8**(5).

185. Ling, H.Y., et al., *Changes in microRNA profile and effects of miR-320 in insulin-resistant 3T3-L1 adipocytes.* Clin Exp Pharmacol Physiol, 2009.

186. Nakanishi, N., et al., *The up-regulation of microRNA-335 is associated with lipid metabolism in liver and white adipose tissue of genetically obese mice.* Biochem Biophys Res Commun, 2009. **385**(4): p. 492-6.

187. Huang, N., et al., *MiR-378a-3p enhances adipogenesis by targeting mitogen-activated protein kinase 1.* Biochem Biophys Res Commun, 2015. **457**(1): p. 37-42.

188. Liu, S.Y., et al., *MiR-378 Plays an Important Role in the Differentiation of Bovine Preadipocytes.* Cell Physiol Biochem, 2015. **36**(4): p. 1552-1562.

189. Kulyte, A., et al., *MicroRNA profiling links miR-378 to enhanced adipocyte lipolysis in human cancer cachexia.* American Journal of Physiology-Endocrinology and Metabolism, 2014. **306**(3): p. E267-E274.

190. Ishida, M., et al., *MicroRNA-378 Regulates Adiponectin Expression in Adipose Tissue: A New Plausible Mechanism.* Plos One, 2014. **9**(11).

191. Martinelli, R., et al., *miR-519d overexpression is associated with human obesity.* Obesity (Silver Spring), 2010. **18**(11): p. 2170-6.

192. Kloting, N., et al., *MicroRNA expression in human omental and subcutaneous adipose tissue.* PLoS One, 2009. **4**(3): p. e4699.

193. Matthews, D.R., et al., *Homeostasis model assessment: insulin resistance and beta-cell function from fasting plasma glucose and insulin concentrations in man.* Diabetologia, 1985. **28**(7): p. 412-9.

194. Darimont, C., et al., *Reconstitution of telomerase activity combined with HPV-E7 expression allow human preadipocytes to preserve their differentiation capacity after immortalization.* Cell Death Differ, 2003. **10**(9): p. 1025-31.

195. Pfaffl, M.W., *A new mathematical model for relative quantification in real-time RT-PCR.* Nucleic Acids Research, 2001. **29**(9).

196. Ng, M., et al., *Global, regional, and national prevalence of overweight and obesity in children and adults during 1980-2013: a systematic analysis for the Global Burden of Disease Study 2013.* Lancet, 2014. **384**(9945): p. 766-81.

197. Chen, Y., et al., *Reproducibility of quantitative RT-PCR array in miRNA expression profiling and comparison with microarray analysis.* BMC Genomics, 2009. **10**: p. 407.

198. R Development Core Team, *R: A language and environment for statistical computing.* R Foundation for Statistical Computing: Vienna, Austria, 2015.

199. Lopez-Romero, P., *AgiMicroRna: Processing and Differential Expression Analysis of Agilent microRNA chips.* R package version 1.0.0., 2015.

200. Davalos, A., et al., *miR-33a/b contribute to the regulation of fatty acid metabolism and insulin signaling.* Proc Natl Acad Sci U S A, 2011. **108**(22): p. 9232-7.

201. Wu, W., et al., *Characterization and comparative profiling of MicroRNAs in a sexual dimorphism insect, Eupolyphaga sinensis Walker.* PLoS One, 2013. **8**(4): p. e59016.

202. Ciaudo, C., et al., *Highly dynamic and sex-specific expression of microRNAs during early ES cell differentiation.* PLoS Genet, 2009. **5**(8): p. e1000620.

203. Feng, J., et al., *Evidence for X-chromosomal schizophrenia associated with microRNA alterations.* PLoS One, 2009. **4**(7): p. e6121.

204. Zhang, Y., et al., *Protective role of estrogen-induced miRNA-29 expression in carbon tetrachloride-induced mouse liver injury.* J Biol Chem, 2012. **287**(18): p. 14851-62.

205. Siegel, C., et al., *miR-23a regulation of X-linked inhibitor of apoptosis (XIAP) contributes to sex differences in the response to cerebral ischemia.* Proc Natl Acad Sci U S A, 2011. **108**(28): p. 11662-7.

206. Kim, Y.J., et al., *miR-196a regulates proliferation and osteogenic differentiation in mesenchymal stem cells derived from human adipose tissue.* J Bone Miner Res, 2009. **24**(5): p. 816-25.

207. Mori, M., et al., *Essential role for miR-196a in brown adipogenesis of white fat progenitor cells.* PLoS Biol, 2012. **10**(4): p. e1001314.

208. Mori, M., H. Nakagaml, and Y. Kaneda, *Homeobox C8 Suppresses Adipogenesis of Human Adipose Tissue-Derived Stem.* Circulation, 2008. **118**(18): p. S279-S279.

209. He, H., et al., *miR204-5p promotes the adipogenic differentiation of human adipose-derived mesenchymal stem cells by modulating DVL3 expression and suppressing Wnt/beta-catenin signaling.* Int J Mol Med, 2015. **35**(6): p. 1587-95.

210. Huang, J., et al., *MicroRNA-204 Regulates Runx2 Protein Expression and Mesenchymal Progenitor Cell Differentiation.* Stem Cells, 2010. **28**(2): p. 357-364.

211. Hamam, D., et al., *microRNA-320/RUNX2 axis regulates adipocytic differentiation of human mesenchymal (skeletal) stem cells.* Cell Death Dis, 2014. **5**: p. e1499.

212. Zhu, L., et al., *MiR-335, an Adipogenesis-Related MicroRNA, is Involved in Adipose Tissue Inflammation.* Cell Biochemistry and Biophysics, 2014. **68**(2): p. 283-290.

213. Vlachos, I.S., et al., *DIANA miRPath v.2.0: investigating the combinatorial effect of microRNAs in pathways.* Nucleic Acids Research, 2012. **40**(W1): p. W498-W504.

214. Godard, P. and J. van Eyll, *Pathway analysis from lists of microRNAs: common pitfalls and alternative strategy.* Nucleic Acids Res, 2015. **43**(7): p. 3490-7.

215. Mori, M.A., et al., *Altered miRNA processing disrupts brown/white adipocyte determination and associates with lipodystrophy.* J Clin Invest, 2014. **124**(8): p. 3339-51.

216. Bhaumik, D., et al., *MicroRNAs miR-146a/b negatively modulate the senescence-associated inflammatory mediators IL-6 and IL.* Aging (Albany NY), 2009. **1**(4): p. 402-11.

217. Perry, M.M., et al., *Divergent intracellular pathways regulate interleukin-1beta-induced miR-146a and miR-146b expression and chemokine release in human alveolar epithelial cells.* FEBS Lett, 2009. **583**(20): p. 3349-55.

218. Olefsky, J.M. and C.K. Glass, *Macrophages, inflammation, and insulin resistance.* Annu Rev Physiol, 2010. **72**: p. 219-46.

219. Hotamisligil, G.S., *Inflammation and metabolic disorders.* Nature, 2006. **444**(7121): p. 860-7.

220. Taganov, K.D., et al., *NF-kappaB-dependent induction of microRNA miR-146, an inhibitor targeted to signaling proteins of innate immune responses.* Proc Natl Acad Sci U S A, 2006. **103**(33): p. 12481-6.

221. Bhaumik, D., et al., *Expression of microRNA-146 suppresses NF-kappaB activity with reduction of metastatic potential in breast cancer cells.* Oncogene, 2008.

222. Talebizadeh, Z., S.D. Simon, and M.G. Butler, *X chromosome gene expression in human tissues: male and female comparisons.* Genomics, 2006. **88**(6): p. 675-81.

223. Johnston, C.M., et al., *Large-scale population study of human cell lines indicates that dosage compensation is virtually complete.* Plos Genetics, 2008. **4**(1).

224. Git, A., et al., *Systematic comparison of microarray profiling, real-time PCR, and next-generation sequencing technologies for measuring differential microRNA expression.* RNA, 2010. **16**(5): p. 991-1006.

225. Ach, R.A., H. Wang, and B. Curry, *Measuring microRNAs: comparisons of microarray and quantitative PCR measurements, and of different total RNA prep methods.* BMC Biotechnol, 2008. **8**: p. 69.

226. Liu, X.H., et al., *MicroRNA-196a promotes non-small cell lung cancer cell proliferation and invasion through targeting HOXA5.* BMC Cancer, 2012. **12**: p. 348.

227. Mansfield, J.H., et al., *MicroRNA-responsive 'sensor' transgenes uncover Hox-like and other developmentally regulated patterns of vertebrate microRNA expression.* Nat Genet, 2004. **36**(10): p. 1079-83.

228. Yekta, S., I.H. Shih, and D.P. Bartel, *MicroRNA-directed cleavage of HOXB8 mRNA.* Science, 2004. **304**(5670): p. 594-6.

229. Mueller, D.W. and A.K. Bosserhoff, *MicroRNA miR-196a controls melanoma-associated genes by regulating HOX-C8 expression.* Int J Cancer, 2011. **129**(5): p. 1064-74.

230. Tanzer, A., et al., *Evolution of microRNAs located within Hox gene clusters.* J Exp Zool B Mol Dev Evol, 2005. **304**(1): p. 75-85.

231. He, X., et al., *miR-196 regulates axial patterning and pectoral appendage initiation.* Dev Biol, 2011. **357**(2): p. 463-77.

232. Ohnishi, Y., et al., *Enhancement of Allele Discrimination by Introduction of Nucleotide Mismatches into siRNA in Allele-Specific Gene Silencing by RNAi.* Plos One, 2008. **3**(5).

233. Qiu, R., et al., *Misexpression of miR-196a induces eye anomaly in Xenopus laevis.* Brain Res Bull, 2009. **79**(1): p. 26-31.

234. McGlinn, E., et al., *In ovo application of antagomiRs indicates a role for miR-196 in patterning the chick axial skeleton through Hox gene regulation.* Proc Natl Acad Sci U S A, 2009. **106**(44): p. 18610-5.

235. Filkova, M., et al., *MiR-196a Is An Important Regulator of Synovial Fibroblasts In the Pathogenesis of Rheumatoid Arthritis.* Arthritis and Rheumatism, 2011. **63**(10): p. S986-S986.

236. Hou, T., et al., *MicroRNA-196a promotes cervical cancer proliferation through the regulation of FOXO1 and p27Kip1.* Br J Cancer, 2014. **110**(5): p. 1260-8.

237. Liu, C., et al., *HPV16 early gene E5 specifically reduces miRNA-196a in cervical cancer cells.* Sci Rep, 2015. **5**: p. 7653.

238. Zhang, J., et al., *miR-196a targets netrin 4 and regulates cell proliferation and migration of cervical cancer cells.* Biochem Biophys Res Commun, 2013. **440**(4): p. 582-8.

239. Severino, P., et al., *MicroRNA expression profile in head and neck cancer: HOX-cluster embedded microRNA-196a and microRNA-10b dysregulation implicated in cell proliferation.* BMC Cancer, 2013. **13**: p. 533.

240. Pazzaglia, L., et al., *miR-196a expression in human and canine osteosarcomas: A comparative study.* Res Vet Sci, 2014.

241. Yang, G., et al., *MiR-196a exerts its oncogenic effect in glioblastoma multiforme by inhibition of IkappaBalpha both in vitro and in vivo.* Neuro Oncol, 2014. **16**(5): p. 652-61.

242. Huang, F., et al., *MiR-196a promotes pancreatic cancer progression by targeting nuclear factor kappa-B-inhibitor alpha.* PLoS One, 2014. **9**(2): p. e87897.

243. Liu, M., et al., *Aberrant expression miR-196a is associated with abnormal apoptosis, invasion, and proliferation of pancreatic cancer cells.* Pancreas, 2013. **42**(7): p. 1169-81.

244. Sun, M., et al., *MiR-196a Is Upregulated in Gastric Cancer and Promotes Cell Proliferation by Downregulating p27(kip1).* Molecular Cancer Therapeutics, 2012. **11**(4): p. 842-852.

245. Schimanski, C.C., et al., *High miR-196a levels promote the oncogenic phenotype of colorectal cancer cells.* World J Gastroenterol, 2009. **15**(17): p. 2089-96.

246. Lu, Y.C., et al., *OncomiR-196 promotes an invasive phenotype in oral cancer through the NME4-JNK-TIMP1-MMP signaling pathway.* Mol Cancer, 2014. **13**: p. 218.

247. Kawasaki, H. and K. Taira, *MicroRNA-196 inhibits HOXB8 expression in myeloid differentiation of HL60 cells.* Nucleic Acids Symp Ser (Oxf), 2004(48): p. 211-2.

248. Niinuma, T., et al., *Upregulation of miR-196a and HOTAIR drive malignant character in gastrointestinal stromal tumors.* Cancer Res, 2012. **72**(5): p. 1126-36.

249. Szafranska, A.E., et al., *Analysis of microRNAs in pancreatic fine-needle aspirates can classify benign and malignant tissues.* Clinical Chemistry, 2008. **54**(10): p. 1716-1724.

250. Ge, J., et al., *Upregulation of microRNA-196a and microRNA-196b cooperatively correlate with aggressive progression and unfavorable prognosis in patients with colorectal cancer.* Cancer Cell Int, 2014. **14**(1): p. 128.

251. Li, J., et al., *Analysis of microRNA expression profiles in human hepatitis B virus-related hepatocellular carcinoma.* Clin Lab, 2013. **59**(9-10): p. 1009-15.

252. Danen-van Oorschot, A.A., et al., *Differentially expressed miRNAs in cytogenetic and molecular subtypes of pediatric acute myeloid leukemia.* Pediatr Blood Cancer, 2012. **58**(5): p. 715-21.

253. Coskun, E., et al., *The role of microRNA-196a and microRNA-196b as ERG regulators in acute myeloid leukemia and acute T-lymphoblastic leukemia.* Leuk Res, 2011. **35**(2): p. 208-13.

254. Revilla-Nuin, B., et al., *Predictive value of MicroRNAs in the progression of barrett esophagus to adenocarcinoma in a long-term follow-up study.* Ann Surg, 2013. **257**(5): p. 886-93.

255. Wang, J., et al., *MicroRNAs in plasma of pancreatic ductal adenocarcinoma patients as novel blood-based biomarkers of disease.* Cancer Prev Res (Phila), 2009. **2**(9): p. 807-13.

256. Liu, C.J., et al., *miR-196a overexpression and miR-196a2 gene polymorphism are prognostic predictors of oral carcinomas.* Ann Surg Oncol, 2013. **20 Suppl 3**: p. S406-14.

257. Lu, Y.C., et al., *Combined determination of circulating miR-196a and miR-196b levels produces high sensitivity and specificity for early detection of oral cancer.* Clin Biochem, 2015. **48**(3): p. 115-21.

258. Tsai, M.M., et al., *MicroRNA-196a/-196b promote cell metastasis via negative regulation of radixin in human gastric cancer.* Cancer Lett, 2014. **351**(2): p. 222-31.

259. Braig, S., et al., *MicroRNA miR-196a is a central regulator of HOX-B7 and BMP4 expression in malignant melanoma.* Cell Mol Life Sci, 2010. **67**(20): p. 3535-48.

260. Xiong, H., et al., *Integrated microRNA and mRNA transcriptome sequencing reveals the potential roles of miRNAs in stage I endometrioid endometrial carcinoma.* PLoS One, 2014. **9**(10): p. e110163.

261. Li, Y., et al., *Ratio of miR-196s to HOXC8 messenger RNA correlates with breast cancer cell migration and metastasis.* Cancer Res, 2010. **70**(20): p. 7894-904.

262. Honda, N., et al., *TGF-beta-Mediated Downregulation of MicroRNA-196a Contributes to the Constitutive Upregulated Type I Collagen Expression in Scleroderma Dermal Fibroblasts.* J Immunol, 2012. **188**(7): p. 3323-31.

263. Makino, T., et al., *Down-regulation of microRNA-196a in the sera and involved skin of localized scleroderma patients.* Eur J Dermatol, 2014. **24**(4): p. 470-6.

264. Kashiyama, K., et al., *miR-196a Downregulation Increases the Expression of Type I and III Collagens in Keloid Fibroblasts.* J Invest Dermatol, 2012.

265. Hoss, A.G., et al., *MicroRNAs located in the Hox gene clusters are implicated in huntington's disease pathogenesis.* PLoS Genet, 2014. **10**(2): p. e1004188.

266. Cheng, P.H., et al., *miR-196a ameliorates phenotypes of Huntington disease in cell, transgenic mouse, and induced pluripotent stem cell models.* Am J Hum Genet, 2013. **93**(2): p. 306-12.

267. Pedersen, I.M., et al., *Interferon modulation of cellular microRNAs as an antiviral mechanism.* Nature, 2007. **449**(7164): p. 919-22.

268. Bruni, R., et al., *An integrated approach identifies IFN-regulated microRNAs and targeted mRNAs modulated by different HCV replicon clones.* BMC Genomics, 2011. **12**: p. 485.

269. Hou, W., et al., *MicroRNA-196 represses Bach1 protein and hepatitis C virus gene expression in human hepatoma cells expressing hepatitis C viral proteins.* Hepatology, 2010. **51**(5): p. 1494-504.

270. Brest, P., et al., *A synonymous variant in IRGM alters a binding site for miR-196 and causes deregulation of IRGM-dependent xenophagy in Crohn's disease.* Nat Genet, 2011. **43**(3): p. 242-5.

271. Pin, A.L., et al., *Annexin-1-mediated endothelial cell migration and angiogenesis are regulated by vascular endothelial growth factor (VEGF)-induced inhibition of miR-196a expression.* J Biol Chem, 2012. **287**(36): p. 30541-51.

272. Miyazaki, Y., et al., *Viral delivery of miR-196a ameliorates the SBMA phenotype via the silencing of CELF2.* Nat Med, 2012. **18**(7): p. 1136-41.

273. XiaoMin, N., L. GuoXi, and Y. GongShe, *Expression and function of miR-196a-1 during 3T3-L1 adipocyte differentiation.* Journal of Agricultural Biotechnology, 2011. **19**(1): p. 135-141.

274. Liao, Y.H., et al., *Osteogenic differentiation of adipose-derived stem cells and calvarial defect repair using baculovirus-mediated co-expression of BMP-2 and miR-148b.* Biomaterials, 2014. **35**(18): p. 4901-10.

275. Candini, O., et al., *Mesenchymal progenitors aging highlights a miR-196 switch targeting HOXB7 as master regulator of proliferation and osteogenesis.* Stem Cells, 2015.

276. Billon, N., et al., *Comprehensive transcriptome analysis of mouse embryonic stem cell adipogenesis unravels new processes of adipocyte development.* Genome Biol, 2010. **11**(8): p. R80.

277. Apiou, F., et al., *Fine mapping of human HOX gene clusters.* Cytogenet Cell Genet, 1996. **73**(1-2): p. 114-5.

278. Pearson, J.C., D. Lemons, and W. McGinnis, *Modulating Hox gene functions during animal body patterning.* Nat Rev Genet, 2005. **6**(12): p. 893-904.

279. Gonzalez-Reyes, A. and G. Morata, *The developmental effect of overexpressing a Ubx product in Drosophila embryos is dependent on its interactions with other homeotic products.* Cell, 1990. **61**(3): p. 515-22.

280. Gorfinkiel, N., G. Morata, and I. Guerrero, *The homeobox gene Distal-less induces ventral appendage development in Drosophila.* Genes Dev, 1997. **11**(17): p. 2259-71.

281. Condie, B.G. and M.R. Capecchi, *Mice with targeted disruptions in the paralogous genes hoxa-3 and hoxd-3 reveal synergistic interactions.* Nature, 1994. **370**(6487): p. 304-7.

282. Davis, A.P., et al., *Absence of radius and ulna in mice lacking hoxa-11 and hoxd-11.* Nature, 1995. **375**(6534): p. 791-5.

283. Jeannotte, L., et al., *Specification of axial identity in the mouse: role of the Hoxa-5 (Hox1.3) gene.* Genes Dev, 1993. **7**(11): p. 2085-96.

284. Quinonez, S.C. and J.W. Innis, *Human HOX gene disorders.* Mol Genet Metab, 2014. **111**(1): p. 4-15.

285. Abe, M., et al., *Disordered expression of HOX genes in human non-small cell lung cancer.* Oncol Rep, 2006. **15**(4): p. 797-802.

286. Alami, Y., et al., *HOXC5 and HOXC8 expression are selectively turned on in human cervical cancer cells compared to normal keratinocytes.* Biochem Biophys Res Commun, 1999. **257**(3): p. 738-45.

287. Wang, Z., et al., *The prognostic biomarkers HOXB13, IL17BR, and CHDH are regulated by estrogen in breast cancer.* Clin Cancer Res, 2007. **13**(21): p. 6327-34.

288. Kikugawa, T., et al., *PLZF regulates Pbx1 transcription and Pbx1-HoxC8 complex leads to androgen-independent prostate cancer proliferation.* Prostate, 2006. **66**(10): p. 1092-9.

289. Chen, H., et al., *Hoxb7 inhibits transgenic HER-2/neu-induced mouse mammary tumor onset but promotes progression and lung metastasis.* Cancer Res, 2008. **68**(10): p. 3637-44.

290. Salser, S.J. and C. Kenyon, *A C. elegans Hox gene switches on, off, on and off again to regulate proliferation, differentiation and morphogenesis.* Development, 1996. **122**(5): p. 1651-61.

291. Yokouchi, Y., et al., *Misexpression of Hoxa-13 induces cartilage homeotic transformation and changes cell adhesiveness in chick limb buds.* Genes Dev, 1995. **9**(20): p. 2509-22.

292. Salser, S.J. and C. Kenyon, *Activation of a C. elegans Antennapedia homologue in migrating cells controls their direction of migration.* Nature, 1992. **355**(6357): p. 255-8.

293. Lohmann, I., et al., *The Drosophila Hox gene deformed sculpts head morphology via direct regulation of the apoptosis activator reaper.* Cell, 2002. **110**(4): p. 457-66.

294. Slattery, M., et al., *Genome-wide tissue-specific occupancy of the Hox protein Ultrabithorax and Hox cofactor Homothorax in Drosophila.* PLoS One, 2011. **6**(4): p. e14686.

295. Pavlopoulos, A. and M. Akam, *Hox gene Ultrabithorax regulates distinct sets of target genes at successive stages of Drosophila haltere morphogenesis.* Proc Natl Acad Sci U S A, 2011. **108**(7): p. 2855-60.

296. Sevastianova, K., et al., *Comparison of dorsocervical with abdominal subcutaneous adipose tissue in patients with and without antiretroviral therapy-associated lipodystrophy.* Diabetes, 2011. **60**(7): p. 1894-900.

297. Heid, I.M., et al., *Meta-analysis identifies 13 new loci associated with waist-hip ratio and reveals sexual dimorphism in the genetic basis of fat distribution.* Nat Genet, 2010. **42**(11): p. 949-60.

298. Bradfield, J.P., et al., *A genome-wide association meta-analysis identifies new childhood obesity loci.* Nat Genet, 2012. **44**(5): p. 526-31.

299. Dankel, S.N., et al., *Switch from stress response to homeobox transcription factors in adipose tissue after profound fat loss.* PLoS One, 2010. **5**(6): p. e11033.

300. Gehrke, S., et al., *Epigenetic regulation of depot-specific gene expression in adipose tissue.* PLoS One, 2013. **8**(12): p. e82516.

301. Timmons, J.A., et al., *Myogenic gene expression signature establishes that brown and white adipocytes originate from distinct cell lineages.* Proc Natl Acad Sci U S A, 2007. **104**(11): p. 4401-6.

302. Walden, T.B., et al., *Recruited vs. nonrecruited molecular signatures of brown, "brite," and white adipose tissues.* Am J Physiol Endocrinol Metab, 2012. **302**(1): p. E19-31.

303. Cowherd, R.M., et al., *Developmental profile of homeobox gene expression during 3T3-L1 adipogenesis.* Biochem Biophys Res Commun, 1997. **237**(2): p. 470-5.

304. Lee, K.Y., et al., *Shox2 is a molecular determinant of depot-specific adipocyte function.* Proc Natl Acad Sci U S A, 2013. **110**(28): p. 11409-14.

305. Moens, C.B. and L. Selleri, *Hox cofactors in vertebrate development.* Dev Biol, 2006. **291**(2): p. 193-206.

306. Selleri, L., et al., *Requirement for Pbx1 in skeletal patterning and programming chondrocyte proliferation and differentiation.* Development, 2001. **128**(18): p. 3543-57.

307. Monteiro, M.C., et al., *PBX1: a novel stage-specific regulator of adipocyte development.* Stem Cells, 2011. **29**(11): p. 1837-48.

308. Gordon, J.A., et al., *Pbx1 represses osteoblastogenesis by blocking Hoxa10-mediated recruitment of chromatin remodeling factors.* Mol Cell Biol, 2010. **30**(14): p. 3531-41.

309. Liotti, A., et al., *The transcription factor Prep1 impairs adipose tissue differentiation.* Diabetologia, 2013. **56**: p. S21-S21.

310. Lempradl, A. and L. Ringrose, *How does noncoding transcription regulate Hox genes?* Bioessays, 2008. **30**(2): p. 110-21.

311. Pollock, R.A., et al., *Gain of function mutations for paralogous Hox genes: implications for the evolution of Hox gene function.* Proc Natl Acad Sci U S A, 1995. **92**(10): p. 4492-6.

312. Yekta, S., C.J. Tabin, and D.P. Bartel, *MicroRNAs in the Hox network: an apparent link to posterior prevalence.* Nat Rev Genet, 2008. **9**(10): p. 789-96.

313. Tsuchiya, S., et al., *Establishment and characterization of a human acute monocytic leukemia cell line (THP-1).* Int J Cancer, 1980. **26**(2): p. 171-6.

314. Maragkakis, M., et al., *DIANA-microT web server: elucidating microRNA functions through target prediction.* Nucleic Acids Research, 2009. **37**: p. W273-W276.

315. Lewis, B.P., et al., *Prediction of mammalian microRNA targets.* Cell, 2003. **115**(7): p. 787-98.

316. Grun, D., et al., *microRNA target predictions across seven Drosophila species and comparison to mammalian targets.* PLoS Comput Biol, 2005. **1**(1): p. e13.

317. Hsu, S.D., et al., *miRTarBase update 2014: an information resource for experimentally validated miRNA-target interactions.* Nucleic Acids Research, 2014. **42**(D1): p. D78-D85.

318. Liang, Y., et al., *Characterization of microRNA expression profiles in normal human tissues.* BMC Genomics, 2007. **8**: p. 166.

319. Mestdagh, P., et al., *The microRNA body map: dissecting microRNA function through integrative genomics.* Nucleic Acids Research, 2011. **39**(20).

320. Lee, E.J., et al., *Systematic evaluation of microRNA processing patterns in tissues, cell lines, and tumors.* RNA, 2008. **14**(1): p. 35-42.

321. Fan, X. and L. Kurgan, *Comprehensive overview and assessment of computational prediction of microRNA targets in animals.* Brief Bioinform, 2014.

322. Grimson, A., et al., *MicroRNA targeting specificity in mammals: determinants beyond seed pairing.* Mol Cell, 2007. **27**(1): p. 91-105.

323. Bartel, D.P., *MicroRNAs: target recognition and regulatory functions.* Cell, 2009. **136**(2): p. 215-33.

324. Cancello, R., et al., *Increased infiltration of macrophages in omental adipose tissue is associated with marked hepatic lesions in morbid human obesity.* Diabetes, 2006. **55**(6): p. 1554-61.

325. Hindorff, L.A., et al., *Potential etiologic and functional implications of genome-wide association loci for human diseases and traits.* Proc Natl Acad Sci U S A, 2009. **106**(23): p. 9362-7.

326. Li, M.J., et al., *GWASdb: a database for human genetic variants identified by genome-wide association studies.* Nucleic Acids Res, 2012. **40**(Database issue): p. D1047-54.

327. Han, M. and Y. Zheng, *Comprehensive analysis of single nucleotide polymorphisms in human microRNAs.* PLoS One, 2013. **8**(11): p. e78028.

328. Gong, J., et al., *Genome-Wide Identification of SNPs in MicroRNA Genes and the SNP Effects on MicroRNA Target Binding and Biogenesis.* Human Mutation, 2012. **33**(1): p. 254-263.

329. Sun, G., et al., *SNPs in human miRNA genes affect biogenesis and function.* RNA, 2009. **15**(9): p. 1640-51.

330. Lee, H.C., et al., *Single point mutation of microRNA may cause butterfly effect on alteration of global gene expression.* Biochemical and Biophysical Research Communications, 2011. **404**(4): p. 1065-1069.

331. Randall, J.C., et al., *Sex-stratified genome-wide association studies including 270,000 individuals show sexual dimorphism in genetic loci for anthropometric traits.* PLoS Genet, 2013. **9**(6): p. e1003500.

332. Yuan, Z., et al., *Effects of common polymorphism rs11614913 in Hsa-miR-196a2 on lung cancer risk.* PLoS One, 2013. **8**(4): p. e61047.

333. Peng, S., et al., *Association of microRNA-196a-2 gene polymorphism with gastric cancer risk in a Chinese population.* Dig Dis Sci, 2010. **55**(8): p. 2288-93.

334. Xu, W., et al., *Effects of common polymorphisms rs11614913 in miR-196a2 and rs2910164 in miR-146a on cancer susceptibility: a meta-analysis.* PLoS One, 2011. **6**(5): p. e20471.

335. Akkiz, H., et al., *A functional polymorphism in pre-microRNA-196a-2 contributes to the susceptibility of hepatocellular carcinoma in a Turkish population: a case-control study.* J Viral Hepat, 2011. **18**(7): p. e399-407.

336. Hu, Z., et al., *Genetic variants of miRNA sequences and non-small cell lung cancer survival.* J Clin Invest, 2008. **118**(7): p. 2600-8.

337. Zhan, J.F., et al., *A functional variant in microRNA-196a2 is associated with susceptibility of colorectal cancer in a Chinese population.* Arch Med Res, 2011. **42**(2): p. 144-8.

338. Hoffman, A.E., et al., *microRNA miR-196a-2 and breast cancer: a genetic and epigenetic association study and functional analysis.* Cancer Res, 2009. **69**(14): p. 5970-7.

339. Christensen, B.C., et al., *Mature microRNA sequence polymorphism in MIR196A2 is associated with risk and prognosis of head and neck cancer.* Clin Cancer Res, 2010. **16**(14): p. 3713-20.

340. Gerrits, A., et al., *Expression quantitative trait loci are highly sensitive to cellular differentiation state.* PLoS Genet, 2009. **5**(10): p. e1000692.

341. Flutre, T., et al., *A statistical framework for joint eQTL analysis in multiple tissues.* PLoS Genet, 2013. **9**(5): p. e1003486.

342. McKenzie, M., et al., *Overlap of expression quantitative trait loci (eQTL) in human brain and blood.* BMC Med Genomics, 2014. **7**: p. 31.

343. Dimas, A.S., et al., *Common regulatory variation impacts gene expression in a cell type-dependent manner.* Science, 2009. **325**(5945): p. 1246-50.

344. Gu, S., et al., *The Loop Position of shRNAs and Pre-miRNAs Is Critical for the Accuracy of Dicer Processing In Vivo.* Cell, 2012. **151**(4): p. 900-911.

345. Lund, E. and J.E. Dahlberg, *Substrate selectivity of exportin 5 and Dicer in the biogenesis of microRNAs.* Cold Spring Harb Symp Quant Biol, 2006. **71**: p. 59-66.

346. Macrae, I.J., et al., *Structural basis for double-stranded RNA processing by Dicer.* Science, 2006. **311**(5758): p. 195-8.

347. Tsutsumi, A., et al., *Recognition of the pre-miRNA structure by Drosophila Dicer-1.* Nat Struct Mol Biol, 2011. **18**(10): p. 1153-8.

348. Zhang, X. and Y. Zeng, *The terminal loop region controls microRNA processing by Drosha and Dicer.* Nucleic Acids Res, 2010. **38**(21): p. 7689-97.

349. Park, J.E., et al., *Dicer recognizes the 5' end of RNA for efficient and accurate processing.* Nature, 2011. **475**(7355): p. 201-5.

350. Gu, S., et al., *The loop position of shRNAs and pre-miRNAs is critical for the accuracy of dicer processing in vivo.* Cell, 2012. **151**(4): p. 900-11.

351. Soifer, H.S., et al., *A role for the Dicer helicase domain in the processing of thermodynamically unstable hairpin RNAs.* Nucleic Acids Res, 2008. **36**(20): p. 6511-22.

352. Estrada, K., et al., *Genome-wide meta-analysis identifies 56 bone mineral density loci and reveals 14 loci associated with risk of fracture.* Nature Genetics, 2012. **44**(5): p. 491-+.

353. Hirsch, J. and E. Gallian, *Methods for the determination of adipose cell size in man and animals.* J Lipid Res, 1968. **9**(1): p. 110-9.

354. Grundberg, E., et al., *Mapping cis- and trans-regulatory effects across multiple tissues in twins.* Nat Genet, 2012. **44**(10): p. 1084-9.

355. Yang, T.P., et al., *Genevar: a database and Java application for the analysis and visualization of SNP-gene associations in eQTL studies.* Bioinformatics, 2010. **26**(19): p. 2474-6.

356. Pruim, R.J., et al., *LocusZoom: regional visualization of genome-wide association scan results.* Bioinformatics, 2010. **26**(18): p. 2336-7.

357. Naot, D. and J. Cornish, *Cytokines and Hormones That Contribute to the Positive Association between Fat and Bone.* Front Endocrinol (Lausanne), 2014. **5**: p. 70.

358. Pittenger, M.F., et al., *Multilineage potential of adult human mesenchymal stem cells.* Science, 1999. **284**(5411): p. 143-7.

359. Loh, N.Y., et al., *LRP5 regulates human body fat distribution by modulating adipose progenitor biology in a dose- and depot-specific fashion.* Cell Metab, 2015. **21**(2): p. 262-72.

360. Akune, T., et al., *PPAR gamma insufficiency enhances osteogenesis through osteoblast formation from bone marrow progenitors.* Journal of Clinical Investigation, 2004. **113**(6): p. 846-855.

361. Horan, G.S., et al., *Mutations in paralogous Hox genes result in overlapping homeotic transformations of the axial skeleton: evidence for unique and redundant function.* Dev Biol, 1995. **169**(1): p. 359-72.

362. Fromental-Ramain, C., et al., *Specific and redundant functions of the paralogous Hoxa-9 and Hoxd-9 genes in forelimb and axial skeleton patterning.* Development, 1996. **122**(2): p. 461-72.

363. Robledo, R.F., et al., *The Dlx5 and Dlx6 homeobox genes are essential for craniofacial, axial, and appendicular skeletal development.* Genes Dev, 2002. **16**(9): p. 1089-101.

364. van den Akker, E., et al., *Axial skeletal patterning in mice lacking all paralogous group 8 Hox genes.* Development, 2001. **128**(10): p. 1911-21.

365. Kang, D., et al., *Relationship of body composition with bone mineral density in northern Chinese men by body mass index levels.* Journal of Endocrinological Investigation, 2014. **37**(4): p. 359-367.

366. Zhu, K., et al., *Associations between body mass index, lean and fat body mass and bone mineral density in middle-aged Australians: The Busselton Healthy Ageing Study.* Bone, 2015. **74**: p. 146-52.

367. George, J.A., et al., *The Association Between Body Composition, 25(OH)D, and PTH and Bone Mineral Density in Black African and Asian Indian Population Groups.* Journal of Clinical Endocrinology & Metabolism, 2014. **99**(6): p. 2146-2154.

368. Yang, P.L.S., et al., *Associations Between Ethnicity, Body Composition, and Bone Mineral Density in a Southeast Asian Population.* The Journal of Clinical Endocrinology & Metabolism, 2013. **98**(11): p. 4516-4523.

369. Marwaha, R.K., et al., *Relationship of body fat and its distribution with bone mineral density in Indian population.* J Clin Densitom, 2013. **16**(3): p. 353-9.

370. Cui, L.H., et al., *Sex-related differences in the association between waist circumference and bone mineral density in a Korean population.* Bmc Musculoskeletal Disorders, 2014. **15**.

371. Zhang, J., et al., *Associations of fat mass and fat distribution with bone mineral density in Chinese obese population.* J Clin Densitom, 2015. **18**(1): p. 44-9.

372. Blaauw, R., E.C. Albertse, and S. Hough, *Body fat distribution as a risk factor for osteoporosis.* S Afr Med J, 1996. **86**(9): p. 1081-4.

373. Zhang, W., et al., *Associations between fat distribution and volumetric bone mineral density in Chinese adults.* Endocrine, 2014. **47**(3): p. 862-868.

374. Tarquini, B., et al., *Evidence for bone mass and body fat distribution relationship in postmenopausal obese women.* Arch Gerontol Geriatr, 1997. **24**(1): p. 15-21.

375. Matsuo, T., et al., *Relationship of upper body fat distribution to higher regional lean mass and bone mineral density.* J Bone Miner Metab, 2003. **21**(3): p. 179-83.

376. Liu, Y.H., et al., *Association of weight-adjusted body fat and fat distribution with bone mineral density in middle-aged chinese adults: a cross-sectional study.* PLoS One, 2013. **8**(5): p. e63339.

377. Cohen, A., et al., *Abdominal Fat Is Associated With Lower Bone Formation and Inferior Bone Quality in Healthy Premenopausal Women: A Transiliac Bone Biopsy Study.* Journal of Clinical Endocrinology & Metabolism, 2013. **98**(6): p. 2562-2572.

378. Freitas, I.F., et al., *The relationship between visceral fat thickness and bone mineral density in sedentary obese children and adolescents.* Bmc Pediatrics, 2013. **13**.

379. Ng, A.C., et al., *Relationship of adiposity to bone volumetric density and microstructure in men and women across the adult lifespan.* Bone, 2013. **55**(1): p. 119-25.

380. Purcell, S., et al., *PLINK: a tool set for whole-genome association and population-based linkage analyses.* Am J Hum Genet, 2007. **81**(3): p. 559-75.

381. Berenson, A.B., et al., *A prospective, controlled study of the effects of hormonal contraception on bone mineral density.* Obstet Gynecol, 2001. **98**(4): p. 576-82.

382. Prior, J.C., et al., *Oral contraceptive use and bone mineral density in premenopausal women: cross-sectional, population-based data from the Canadian Multicentre Osteoporosis Study.* CMAJ, 2001. **165**(8): p. 1023-9.

383. Gonnelli, S., et al., *The associations of body composition and fat distribution with bone mineral density in elderly Italian men and women.* J Clin Densitom, 2013. **16**(2): p. 168-77.

384. Buchanan, C.C., et al., *A comparison of cataloged variation between International HapMap Consortium and 1000 Genomes Project data.* J Am Med Inform Assoc, 2012. **19**(2): p. 289-94.

385. Garcia-Gasca, A. and D.D. Spyropoulos, *Differential mammary morphogenesis along the anteroposterior axis in Hoxc6 gene targeted mice.* Dev Dyn, 2000. **219**(2): p. 261-76.

386. Genomes Project, C., et al., *An integrated map of genetic variation from 1,092 human genomes.* Nature, 2012. **491**(7422): p. 56-65.

387. Cornish, J., K.E. Callon, and I.R. Reid, *Insulin increases histomorphometric indices of bone formation In vivo.* Calcif Tissue Int, 1996. **59**(6): p. 492-5.

388. Khosla, S., et al., *Relationship of serum sex steroid levels and bone turnover markers with bone mineral density in men and women: a key role for bioavailable estrogen.* J Clin Endocrinol Metab, 1998. **83**(7): p. 2266-74.

389. Mohamed-Ali, V., et al., *Subcutaneous adipose tissue releases interleukin-6, but not tumor necrosis factor-alpha, in vivo.* J Clin Endocrinol Metab, 1997. **82**(12): p. 4196-200.

390. Schett, G., *Effects of inflammatory and anti-inflammatory cytokines on the bone.* Eur J Clin Invest, 2011. **41**(12): p. 1361-6.

391. Yang, J., et al., *Conditional and joint multiple-SNP analysis of GWAS summary statistics identifies additional variants influencing complex traits.* Nat Genet, 2012. **44**(4): p. 369-75, S1-3.

392. Heinonen, S., et al., *Adipocyte morphology and implications for metabolic derangements in acquired obesity.* Int J Obes (Lond), 2014. **38**(11): p. 1423-31.

393. Spalding, K.L., et al., *Dynamics of fat cell turnover in humans.* Nature, 2008. **453**(7196): p. 783-7.

394. Salans, L.B., E.S. Horton, and E.A. Sims, *Experimental obesity in man: cellular character of the adipose tissue.* J Clin Invest, 1971. **50**(5): p. 1005-11.

395. Hirsch, J. and B. Batchelor, *Adipose tissue cellularity in human obesity.* Clin Endocrinol Metab, 1976. **5**(2): p. 299-311.

396. Iwen, K.A., et al., *Gluteal and abdominal subcutaneous adipose tissue depots as stroma cell source: gluteal cells display increased adipogenic and osteogenic differentiation potentials.* Experimental Dermatology, 2014. **23**(6): p. 395-400.

397. Joe, A.W.B., et al., *Depot-Specific Differences in Adipogenic Progenitor Abundance and Proliferative Response to High-Fat Diet.* Stem Cells, 2009. **27**(10): p. 2563-2570.

398. Rosen, E.D. and O.A. MacDougald, *Adipocyte differentiation from the inside out.* Nat Rev Mol Cell Biol, 2006. **7**(12): p. 885-96.

399. Adams, M., et al., *Activators of peroxisome proliferator-activated receptor gamma have depot-specific effects on human preadipocyte differentiation.* J Clin Invest, 1997. **100**(12): p. 3149-53.

400. Rodeheffer, M.S., K. Birsoy, and J.M. Friedman, *Identification of white adipocyte progenitor cells in vivo.* Cell, 2008. **135**(2): p. 240-9.

401. Khan, T., et al., *Metabolic Dysregulation and Adipose Tissue Fibrosis: Role of Collagen VI.* Molecular and Cellular Biology, 2009. **29**(6): p. 1575-1591.

402. Chun, T.H., et al., *A pericellular collagenase directs the 3-dimensional development of white adipose tissue.* Cell, 2006. **125**(3): p. 577-591.

403. Strissel, K.J., et al., *Adipocyte death, adipose tissue remodeling, and obesity complications.* Diabetes, 2007. **56**(12): p. 2910-8.

404. Nishimura, S., et al., *Adipogenesis in obesity requires close interplay between differentiating adipocytes, stromal cells, and blood vessels.* Diabetes, 2007. **56**(6): p. 1517-26.

405. Rupnick, M.A., et al., *Adipose tissue mass can be regulated through the vasculature.* Proceedings of the National Academy of Sciences of the United States of America, 2002. **99**(16): p. 10730-10735.

406. Sun, K., et al., *Selective inhibition of hypoxia-inducible factor 1alpha ameliorates adipose tissue dysfunction.* Mol Cell Biol, 2013. **33**(5): p. 904-17.

407. Madri, J.A. and M. Marx, *Matrix composition, organization and soluble factors: modulators of microvascular cell differentiation in vitro.* Kidney Int, 1992. **41**(3): p. 560-5.

408. Kosteli, A., et al., *Weight loss and lipolysis promote a dynamic immune response in murine adipose tissue.* J Clin Invest, 2010. **120**(10): p. 3466-79.

409. Nishimura, S., et al., *In vivo imaging in mice reveals local cell dynamics and inflammation in obese adipose tissue.* J Clin Invest, 2008. **118**(2): p. 710-21.

410. Huang, D.W., B.T. Sherman, and R.A. Lempicki, *Systematic and integrative analysis of large gene lists using DAVID bioinformatics resources.* Nature Protocols, 2009. **4**(1): p. 44-57.

411. Huang, D.W., B.T. Sherman, and R.A. Lempicki, *Bioinformatics enrichment tools: paths toward the comprehensive functional analysis of large gene lists.* Nucleic Acids Research, 2009. **37**(1): p. 1-13.

412. Lonnqvist, F., A. Wennlund, and P. Arner, *Relationship between circulating leptin and peripheral fat distribution in obese subjects.* International Journal of Obesity, 1997. **21**(4): p. 255-260.

413. Nielsen, N.B., et al., *Interstitial concentrations of adipokines in subcutaneous abdominal and femoral adipose tissue.* Regul Pept, 2009. **155**(1-3): p. 39-45.

414. Arner, P., et al., *Beta-adrenoceptor expression in human fat cells from different regions.* J Clin Invest, 1990. **86**(5): p. 1595-600.

415. Thomson, D.W., et al., *On measuring miRNAs after transient transfection of mimics or antisense inhibitors.* PLoS One, 2013. **8**(1): p. e55214.

416. Rao, D.D., et al., *siRNA vs. shRNA: similarities and differences.* Adv Drug Deliv Rev, 2009. **61**(9): p. 746-59.

417. Torres, A.G., et al., *MicroRNA fate upon targeting with anti-miRNA oligonucleotides as revealed by an improved Northern-blot-based method for miRNA detection.* RNA, 2011. **17**(5): p. 933-43.

418. Davis, S., et al., *Potent inhibition of microRNA in vivo without degradation.* Nucleic Acids Res, 2009. **37**(1): p. 70-7.

419. Yang, B., et al., *Caspase-3 and apoptosis in experimental chronic renal scarring.* Kidney Int, 2001. **60**(5): p. 1765-76.

420. O'Donovan, N., et al., *Caspase 3 in breast cancer.* Clin Cancer Res, 2003. **9**(2): p. 738-42.

421. Hubert, H.B., et al., *Obesity as an Independent Risk Factor for Cardiovascular-Disease - a 26-Year Follow-up of Participants in the Framingham Heart-Study.* Circulation, 1983. **67**(5): p. 968-977.

422. Jousilahti, P., et al., *Sex, age, cardiovascular risk factors, and coronary heart disease - A prospective follow-up study of 14 786 middle-aged men and women in Finland.* Circulation, 1999. **99**(9): p. 1165-1172.

423. Lovejoy, J.C., et al., *Abdominal fat distribution and metabolic risk factors: effects of race.* Metabolism, 1996. **45**(9): p. 1119-24.

424. Raji, A., et al., *Body fat distribution and insulin resistance in healthy Asian Indians and Caucasians.* J Clin Endocrinol Metab, 2001. **86**(11): p. 5366-71.

425. Lear, S.A., et al., *The use of BMI and waist circumference as surrogates of body fat differs by ethnicity.* Obesity, 2007. **15**(11): p. 2817-2824.

426. Nho, Y.K., et al., *Matrix metalloproteinase-1 promoter is associated with body mass index in Korean population with aged greater or equal to 50 years.* Clinica Chimica Acta, 2008. **396**(1-2): p. 14-17.

427. Soo-Kyung, K., et al., *The increase in abdominal subcutaneous fat depot is an independent factor to determine the glycemic control after rosiglitazone treatment.* European Journal of Endocrinology, 2007. **157**(2): p. 167-174.

428. Kelly, I.E., et al., *Effects of a thiazolidinedione compound on body fat and fat distribution of patients with type 2 diabetes (vol 22, pg 288, 1999).* Diabetes Care, 1999. **22**(3): p. 536-536.